



A University of Sussex DPhil thesis

Available online via Sussex Research Online:

<http://sro.sussex.ac.uk/>

This thesis is protected by copyright which belongs to the author.

This thesis cannot be reproduced or quoted extensively from without first obtaining permission in writing from the Author

The content must not be changed in any way or sold commercially in any format or medium without the formal permission of the Author

When referring to this work, full bibliographic details including the author, title, awarding institution and date of the thesis must be given

Please visit Sussex Research Online for more information and further details

UNIVERSITY OF



SUSSEX
AT BRIGHTON

**Bimetallic Complexes of
d- and *f*-Block Metals
with Pentalene Ligands**

by

Alexander F. R. Kilpatrick

Submitted for the degree of Doctor of Philosophy

September 2014

ACKNOWLEDGEMENTS

With thanks to:

Prof. F. G. N. Cloke FRS

The members of Lab 14 past and present

Dr J. F. C. Turner

Prof. J. C. Green

Drs A. S. & J. A. Frey

Dr N. Tsoureas

Dr Abdul-Sada

Dr I. J. Day

Dr S. M. Roe

Dr G. Wildgoose

Dr A. E. Ashley

Dr F. Tuna

Dr T. Pugh

Dr B. M. Day

Dr R. A. Layfield

Prof. K. Meyer and his working group at FAU Erlangen

EPSRC EPR Facility, University of Manchester

UK National Crystallography Service, University of Southampton

Rachel Kahan for help with proof reading this when it was in a sketchy state.

Many thanks to my family and friends who have have come to visit during my years in academic exile, and to Rosie for all the miles & getting me there *just* in the nick of time.

Special thanks go to AMD, I could not have done it without you schatz. X

ABSTRACT

Bimetallic Complexes of *d*- and *f*-Block Metals with Pentalene Ligands

Alexander F. R. Kilpatrick

Ph.D Thesis

The focus of this thesis is the synthesis and characterisation of organometallic complexes incorporating the silylated pentalene ligand, $[\text{C}_8\text{H}_4\{\text{Si}^i\text{Pr}_{3-1,4}\}_2]^{2-}$ ($= \text{Pn}^\dagger$), bound to more than one metal centre. In general, metals in low oxidation states from the *d*- and *f*-block of the periodic table have been selected for these bimetallic complexes, as they are potentially reactive with small molecule substrates.

Chapter One introduces the pentalene molecule and its derivatives, and discusses their use as ligands in organometallic chemistry. Particular emphasis is given to the application of organometallic pentalene complexes, ranging from conducting polymers in materials chemistry to small molecule activation and catalysis.

In **Chapter Two** the silylated pentalene ligand Pn^\dagger is used to bridge two lanthanide(II) centres in *anti*-bimetallic sandwich complexes of the type $[\text{Cp}^*\text{Ln}]_2(\mu\text{-Pn}^\dagger)$ ($\text{Ln} = \text{Yb}$, Eu and Sm). Magnetic measurements and electrochemical methods are used to investigate the extent of intermetallic communication in some of these systems, which show potential for the design of organometallic 'molecular-wires'. Chemical oxidation of $[\text{Cp}^*\text{Yb}]_2(\mu\text{-Pn}^\dagger)$ leads to dissociation into mononuclear fragments $(\eta^8\text{-Pn}^\dagger)\text{YbCp}^*$ and $[\text{Cp}^*\text{Yb}]^+$, and reaction of $[\text{Cp}^*\text{Sm}]_2(\mu\text{-Pn}^\dagger)$ with CO yields $(\eta^8\text{-Pn}^\dagger)\text{SmCp}^*$. Rational synthetic routes to mononuclear mixed-sandwich $\text{Pn}^\dagger/\text{Cp}^*$ compounds with trivalent *f*-block ions (Dy , Tb and U) are also developed, and their magnetic properties are studied by SQUID magnetometry including variable-frequency ac susceptibility measurements. These studies identified $(\eta^8\text{-Pn}^\dagger)\text{DyCp}^*$ as the first known example of a pentalene based single molecule magnet, with a closed-waist hysteresis loop observed up to 2 K.

Chapter Three describes the synthesis of iron(II) complexes with silylated pentalene ligands, and efforts towards incorporating them into extended organometallic arrays and heteronuclear *anti*-bimetallic complexes. Six complexes have been structurally

characterised including the triple-decker homobimetallic $[\text{Cp}^*\text{Fe}]_2(\mu\text{-Pn}^\dagger)$, and the potassium salt $[\text{Cp}^*\text{Fe}(\eta^5\text{-Pn}^\dagger)][\text{K}]$ which is an organometallic polymer in the solid state.

Chapter Four documents efforts towards the synthesis of *syn*-bimetallic pentalene complexes, including the first row d-block metals V, Ti and Sc. A novel synthetic route to the di-titanium bis(pentalene) 'double-sandwich' complex $(\text{Pn}^\dagger)_2\text{Ti}_2$ is developed, *via* chloride-bridged dimers $[(\eta^8\text{-Pn}^\dagger)\text{Ti}]_2(\mu\text{-Cl})_x$ ($x = 2$ and 3). The electronic and magnetic properties of the latter are investigated using EPR spectroscopy and SQUID magnetometry, and the structure and bonding in $(\text{Pn}^\dagger)_2\text{Ti}_2$ is examined using spectroscopic, crystallographic, electrochemical and computational techniques. Preliminary studies toward the synthesis of an analogous di-scandium complex were unsuccessful, however three novel complexes have been synthesised including $(\eta^8\text{-Pn}^\dagger)\text{ScCp}^*$ which is first example of a Sc complex bearing a Pn^\dagger ligand to be characterised by X-ray diffraction.

Chapter Five explores the reactivity of the double-sandwich compound $(\text{Pn}^\dagger)_2\text{Ti}_2$ prepared in Chapter Four, with small molecules which are of industrial and environmental importance. The relatively open structure of $(\text{Pn}^\dagger)_2\text{Ti}_2$ allows the formation of adducts with unsaturated small molecules CO, MeNC and CO₂. In the latter case the adduct formed is unstable at room temperature and the coordinated CO₂ molecule is reduced to give a bis(oxo) bridged dimer and a di-carbonyl complex. This provides the first example of small molecule activation by a di-metal bis(pentalene) double-sandwich complex.

The reactivity survey of $(\text{Pn}^\dagger)_2\text{Ti}_2$ is extended in **Chapter Six** to other substrates; including unsaturated heteroallenes as model molecules for CO₂. In the case of non-polar heteroallenes CS₂ and carbodiimide, thermally stable adducts are isolated and have been structurally characterised. Polar heteroallenes COS and organic isocyanates undergo reductive transformations to give sulfide- and carbonimidate-bridged complexes respectively. The reactivity of $(\text{Pn}^\dagger)_2\text{Ti}_2$ with organic molecules containing heteroatom-heteroatom bonds is also described; the reactions with diphenyldichalcogenides and azobenzene show the ability of the double-sandwich complex to act as a 2e⁻ and 4e⁻ reducing agent respectively. The rich and varied chemistry shown by $(\text{Pn}^\dagger)_2\text{Ti}_2$ is evaluated and future work is suggested.

LIST OF ABBREVIATIONS USED IN THE TEXT

General

[A] ⁻	generic anion
Å	Angstrom
ac	alternating current
ADF	Amsterdam Density Functional
acac	acetylacetonate
atm	atmosphere
Ar	generic aryl group
Bn	benzyl, (CH ₂ C ₆ H ₅)
ⁿ Bu, ^t Bu	<i>n</i> -butyl, <i>tert</i> -butyl
<i>ca.</i>	<i>circa</i> , about
cat	catalyst
°C	degrees Celsius
χ	magnetic susceptibility
cm ⁻¹	wavenumber
COD	cycloocta-1,4-diene
COT	cyclooctatetraene
Cp, Cp*	cyclopentadienide, pentamethylcyclopentadienide
CSD	Cambridge Structural Database
Ct	centroid
CV	cyclic voltammetry/cyclic voltammogram
Cy	cyclohexyl
°	degrees
d	day(s)
dc	direct current
ΔH	enthalpy change
ΔG	Gibbs free energy change
DFT	density functional theory
Dip	2,6-di-isopropylphenyl
DMAP	dimethylaminopyridine
DME	1,2-dimethoxyethane
E	generic heteroatom
<i>E</i> [°]	electrode potential
EI-MS	electron impact mass spectrometry

EPR	electron paramagnetic resonance
ESD	estimated standard deviation
Et	ethyl
η^n	hapticity of degree n
FVP	flash vacuum pyrolysis
g	gram(s)
HOMO	highest occupied molecular orbital
h	hour(s)
i	current
+I	electron donating inductive effect
IVCT	inter-valence charge transfer
K	degrees Kelvin
kJ	kilojoule
kcal	kilocalorie
L	generic ligand
Ln	lanthanide
LUMO	lowest unoccupied molecular orbital
m	<i>meta</i>
M	generic metal
MAO	methylaluminoxane
Me	methyl
Mes	mesityl (2,4,6-Me ₃ C ₆ H ₂)
mg	milligram(s)
mL	millilitre(s)
MO	molecular orbital
min	minute(s)
mmol	millimoles(s)
ms	millisecond(s)
mV	millivolt(s)
μmol	micromole(s)
μ_{eff}	effective magnetic moment
μ_{B}	Bohr magneton
MV	mixed-valence
m/z	mass to charge ratio
NHC	<i>N</i> -heterocyclic carbene

NIR	near infra-red
<i>o</i>	<i>ortho</i>
Oe	Oersted
OTf	triflate
ORTEP	Oak Ridge Thermal Ellipsoid Plot
<i>p</i>	<i>para</i>
PE	polyethylene
Ph	phenyl
Pn, Pn*	pentalene, permethylpentalene,
Pn [†]	1,4-bis(triisopropylsilyl)pentalene
ⁱ Pr	isopropyl
<i>p</i> -Tol	<i>para</i> -tolyl (4-MeC ₆ H ₄)
<i>p</i> -TCD	1,3- <i>N,N'</i> -di- <i>p</i> -tolylcarbodiimide
QTM	quantum tunnelling of magnetisation
R	generic alkyl group
RT	room temperature
s	second(s)
SCF	self-consistent field
SCE	saturated calomel electrode
SOC	spin-orbit coupling
SOMO	singly-occupied molecular orbital
SMM	single molecule magnet
SQUID	superconducting quantum interference device
<i>T</i>	temperature
<i>t</i>	time
THF	tetrahydrofuran
TMEDA	<i>N,N,N',N'</i> -tetramethyl-ethane-1,2-diamine
UV	ultraviolet
V	Volt
VE	valence electron
vs	versus
XRD	X-ray diffraction
X	halide or non-coordinating anion
Xyl	xylyl (2,6-Me ₂ C ₆ H ₃)

Nuclear Magnetic Resonance spectroscopic data

COSY	2D correlation spectroscopy
d	doublet
δ	chemical shift in ppm
EXSY	exchange spectroscopy
xJ	coupling constant over x bonds
HMBC	heteronuclear multiple bond correlation
HSQC	heteronuclear single-quantum correlation spectroscopy
Hz	Hertz
m	multiplet
MHz	megahertz
NMR	nuclear magnetic resonance
ppm	parts per million
$\{^1\text{H}\}$	proton decoupled
s	singlet
t	triplet
$\Delta\nu_{1/2}$	peak width at half-height

TABLE OF CONTENTS

CHAPTER ONE: Introduction	1
1.1 Fundamentals of Pentalene Chemistry	1
1.1.1 Nomenclature.....	1
1.1.2 Synthesis of pentalene derivatives.....	2
1.1.3 Bonding in pentalene complexes.....	6
1.2 Applications of Organometallic Complexes with Pentalene Ligands	9
1.2.1 Studying interactions in bimetallic complexes.....	9
1.2.2 Electronic delocalisation in pentalene-bridged complexes	11
1.2.3 Synthesis of metal-metal bonded complexes	16
1.2.4 Magnetic interactions and spin transport.....	19
1.2.5 Small molecule activation	22
1.2.6 Catalysis.....	25
1.3 Aims of This Thesis.....	28
1.4 References for Chapter One.....	28
CHAPTER TWO: Electrochemical and Magnetic Studies of f-Block Pentalene Complexes.....	34
2.1 Introduction.....	34
2.2 Anti-Bimetallic Complexes of the f-Block Metals	35
2.2.1 Synthesis of $[Cp^*Ln]_2(\mu-Pn^{\dagger})$ complexes.....	36
2.2.2 Characterisation of $[Cp^*Yb]_2(\mu:\eta^5, \eta^5-Pn^{\dagger})$ (2.1)	37
2.2.3 Characterisation of $[Cp^*Eu]_2(\mu-Pn^{\dagger})$ (2.2)	39
2.2.4 Characterisation of $[Cp^*Sm]_2(\mu:\eta^5, \eta^5-Pn^{\dagger})$ (2.3).....	41
2.2.5 X-ray crystallographic studies of 2.1, 2.2 and 2.3	44
2.2.6 Solvation of 2.1, 2.2 and 2.3	48
2.2.7 Electrochemical studies of 2.1, 2.2 and 2.3	50
2.2.8 Redox reactions of 2.1; Synthesis and characterisation of $[Cp^*Yb(OEt_2)_3][B(C_6F_5)_4]$ (2.4)	52
2.2.9 Synthesis and characterisation of $[(\eta^8-Pn^{\dagger})_2Yb][K]$ (2.5).....	55
2.2.10 Reaction of 2.3 with carbon monoxide.....	56
2.2.11 Attempted synthesis of a pentalene bridged uranium bimetallic	57
2.3 Mononuclear Lanthanide(III) Complexes as Single Ion Magnets.....	59
2.3.1 Background	59
2.3.2 Synthesis and characterisation of $(\eta^8-Pn^{\dagger})LnCp^*$ complexes for $Ln = Dy$ (2.6), Tb (2.7) and Y (2.8)..	60
2.3.3 Magnetic studies	61
2.4 Conclusions.....	66
2.5 Experimental Details for Chapter Two.....	68
2.5.1 Synthesis of $[Cp^*Yb]_2(\mu:\eta^5, \eta^5-Pn^{\dagger})$ (2.1).....	68
2.5.2 Synthesis of $[Cp^*Eu]_2(\mu-Pn^{\dagger})$ (2.2)	69
2.5.3 Synthesis of $[Cp^*Sm]_2(\mu:\eta^5, \eta^5-Pn^{\dagger})$ (2.3)	69
2.5.4 Synthesis of $[Cp^*Yb(OEt_2)_3][B(C_6F_5)_4]$ (2.4)	70
2.5.5 Synthesis of $[(\eta^8-Pn^{\dagger})Yb][K]$ (2.5)	71
2.5.6 Synthesis of $(\eta^8-Pn^{\dagger})UCp^*$	72

2.5.7	Synthesis of $(\eta^8\text{-Pn}^\dagger)\text{DyCp}^*$ (2.6)	72
2.5.8	Synthesis of $(\eta^8\text{-Pn}^\dagger)\text{TbCp}^*$ (2.7)	73
2.5.9	Synthesis of $(\eta^8\text{-Pn}^\dagger)\text{YCp}^*$ (2.8)	73
2.6	References for Chapter Two	74

CHAPTER THREE: Towards Oligomeric and Heteronuclear Pentalene-Bridged Iron

Complexes.....	78
3.1 Introduction.....	78
3.2 Iron Bis(Pentalene) Complexes	79
3.2.1 Synthesis and characterisation of $\text{Fe}(\eta^5\text{-Pn}^\dagger\text{H})_2$ (3.1)	79
3.2.2 Synthesis and characterisation of $(\eta^5\text{-Pn}^\dagger\text{H})\text{Fe}[\eta^5\text{-Pn}^\dagger(\eta^5\text{-K}\{\text{THF}\}_2)]$ (3.2)	83
3.2.3 X-ray crystallographic studies of 3.1 and 3.2.....	84
3.2.4 Reactions of 3.2.....	87
3.3 Mixed-Sandwich Iron Complexes	88
3.3.1 Synthesis and characterisation of $\text{Cp}^*\text{Fe}(\eta^5\text{-Pn}^\dagger\text{H})$ (3.3).....	88
3.3.2 Synthesis and characterisation of $[\text{FeCp}^*(\mu\text{-}\eta^5\text{:}\eta^5\text{-Pn}^\dagger)][\text{K}]$ (3.4)	88
3.3.3 X-ray crystallographic studies of 3.3, 3.4 and 3.5.....	90
3.3.4 Synthesis and characterisation of $[\text{FeCp}^*]_2(\mu\text{:}\eta^5\text{:}\eta^5\text{-Pn}^\dagger)$ (3.6)	93
3.3.5 Towards oligomeric and heteronuclear pentalene-bridged complexes.....	96
3.4 Electrochemical Studies.....	97
3.5 Conclusions.....	102
3.6 Experimental Details for Chapter Three.....	103
3.6.1 Synthesis of $\text{Fe}(\eta^5\text{-Pn}^\dagger\text{H})_2$ (3.1)	103
3.6.2 Synthesis of $(\eta^5\text{-Pn}^\dagger\text{H})\text{Fe}[\eta^5\text{-Pn}^\dagger(\eta^5\text{-K}\{\text{THF}\}_2)]$ (3.2)	104
3.6.3 Synthesis of $\text{Cp}^*\text{Fe}(\eta^5\text{-Pn}^\dagger\text{H})$ (3.3)	105
3.6.4 Synthesis of $[\text{Cp}^*\text{Fe}(\eta^5\text{-Pn}^\dagger)][\text{K}]$ (3.4)	106
3.6.5 Characterisation of double bond isomer $\text{Cp}^*\text{Fe}(\eta^5\text{-Pn}^\dagger\text{H})$ (3.5)	107
3.6.6 Synthesis of $[\text{Cp}^*\text{Fe}]_2(\mu\text{:}\eta^5\text{:}\eta^5\text{-Pn}^\dagger)$ (3.6)	107
3.7 References for Chapter Three.....	109

CHAPTER FOUR: Double-Sandwich Complexes of the d-Block Elements

4.1	Introduction	111
4.2	Vanadium	112
4.2.1	Synthesis and characterisation of $(\mu\text{-}\eta^5\text{-}\eta^5\text{-Pn}^\dagger)_2\text{V}_2$	112
4.3	Titanium	114
4.3.1	Synthesis and characterisation of $[(\eta^8\text{-Pn}^\dagger)\text{Ti}]_2(\mu\text{-Cl})_3$ (4.1)	114
4.3.2	Electronic and magnetic studies of 4.1	116
4.3.3	Synthesis and characterisation of $[(\eta^8\text{-Pn}^\dagger)\text{Ti}(\text{py})(\mu\text{-Cl})]_2$ (4.2(py) ₂)	119
4.3.4	Synthesis and characterisation of $(\mu\text{-}\eta^5\text{-}\eta^5\text{-Pn}^\dagger)_2\text{Ti}_2$ (4.3)	122
4.3.5	Electrochemical studies; synthesis and characterisation of $[(\mu\text{-}\eta^5\text{-}\eta^5\text{-Pn}^\dagger)_2\text{Ti}_2][\text{B}(\text{C}_6\text{F}_5)_4]$ (4.4)	126
4.4	Scandium	129
4.4.1	Synthesis and characterisation of $[(\eta^8\text{-Pn}^\dagger)\text{Sc}(\text{THF})(\mu\text{-Cl})]_2$ (4.5)	129
4.4.2	Reactivity studies of 4.5	131
4.4.3	Synthesis and characterisation of $(\eta^8\text{-Pn}^\dagger)\text{ScCp}^*$ (4.7)	132

4.5	Experimental Details for Chapter Four.....	135
4.5.1	Synthesis of $[(\eta^8\text{-Pn}^\dagger)\text{Ti}]_2(\mu\text{-Cl})_3$ (4.1)	135
4.5.2	Synthesis of $[(\eta^8\text{-Pn}^\dagger)\text{Ti}\{\text{py}\}]_2(\mu\text{-Cl})_2$ (4.2)(py) ₂	136
4.5.3	Synthesis of $(\mu\text{:}\eta^5, \eta^5\text{-Pn}^\dagger)_2\text{Ti}_2$ (4.3)	137
4.5.4	Synthesis of $[(\mu\text{:}\eta^5, \eta^5\text{-Pn}^\dagger)_2\text{Ti}_2] [\text{B}(\text{C}_6\text{F}_5)_4]$ (4.4)	138
4.5.5	Synthesis of $[(\eta^8\text{-Pn}^\dagger)\text{Sc}(\text{THF})(\mu\text{-Cl})]_2$ (4.5)	138
4.5.6	Synthesis of $[(\eta^8\text{-Pn}^\dagger)\text{Sc}(\text{C}_3\text{H}_5)\{\text{THF}\}]_x$ (4.6)	139
4.5.7	Synthesis of $(\eta^8\text{-Pn}^\dagger)\text{ScCp}^*$ (4.7)	140
4.6	References for Chapter Four.....	141

CHAPTER FIVE: Reactivity of $(\mu\text{:}\eta^5, \eta^5\text{-Pn}^\dagger)_2\text{Ti}_2$ with Carbon Monoxide and Carbon

Dioxide	144
5.1 Introduction.....	144
5.1.1 Carbon monoxide.....	144
5.1.2 Isocyanides.....	148
5.1.3 Carbon dioxide.....	150
5.2 Reactivity of 4.3 with CO and Related Molecules	153
5.2.1 Synthesis and characterisation of $(\mu:\eta^5, \eta^5\text{-Pn}^\dagger)_2\text{Ti}_2(\text{CO})$ (5.1).....	153
5.2.2 Synthesis and characterisation of $(\mu:\eta^5, \eta^5\text{-Pn}^\dagger)_2[\text{Ti}(\text{CO})]_2$ (5.2).	155
5.2.3 Synthesis and characterisation of $(\mu:\eta^5, \eta^5\text{-Pn}^\dagger)_2[\text{Ti}(\text{CO})]_2(\mu\text{-CO})$ (5.3).....	156
5.2.4 Reactivity of 4.3 with isocyanides	159
5.2.5 X-ray crystallographic studies of 5.1, 5.2 and 5.4.....	161
5.2.6 DFT studies of 5.1, 5.2 and 5.3.....	165
5.3 Reactivity of 4.3 with CO ₂	168
5.3.1 Reaction of 4.3 with CO ₂ at room temperature.....	168
5.3.2 Synthesis and characterisation of $(\mu:\eta^5, \eta^5\text{-Pn}^\dagger)_2\text{Ti}_2(\text{CO}_2)$ (5.7).	170
5.3.3 Synthesis and characterisation of mono(μ -oxo) complexes 5.8 and 5.9.....	172
5.3.4 Mechanistic investigation of reaction of 4.3 with CO ₂	176
5.4 Experimental Details for Chapter Five	180
5.4.1 Synthesis of $(\mu:\eta^5, \eta^5\text{-Pn}^\dagger)_2\text{Ti}_2(\text{CO})$ (5.1).....	180
5.4.2 Synthesis of $(\mu:\eta^5, \eta^5\text{-Pn}^\dagger)_2\text{Ti}_2(\text{CO})_2$ (5.2).....	181
5.4.3 Synthesis of $(\mu:\eta^5, \eta^5\text{-Pn}^\dagger)_2\text{Ti}_2(\text{CO})_3$ (5.3).....	182
5.4.4 Synthesis of $(\mu:\eta^5, \eta^5\text{-Pn}^\dagger)_2\text{Ti}_2(\mu:\eta^2\text{-CNMe})$ (5.4).	183
5.4.5 Synthesis of $[(\eta^8\text{-Pn}^\dagger)\text{Ti}(\mu\text{-O})]_2$ (5.5).	184
5.4.6 Synthesis of $[(\eta^5\text{-Pn}^\dagger)\text{Ti}(\mu\text{-O})(\text{py})]_2$ (5.6).	184
5.4.7 Synthesis of $(\mu:\eta^5, \eta^5\text{-Pn}^\dagger)_2\text{Ti}_2(\text{CO}_2)$ (5.7).....	185
5.4.8 Synthesis of $(\mu:\eta^5, \eta^5\text{-Pn}^\dagger)_2\text{Ti}_2(\mu\text{-O})$ (5.8).	186
5.4.9 Synthesis of $[(\eta^8\text{-Pn}^\dagger)\text{Ti}]_2(\mu\text{-O})$ (5.9).	187
5.5 References for Chapter Five	188

CHAPTER SIX: Reactivity of $(\mu\text{:}\eta^5, \eta^5\text{-Pn}^\dagger)_2\text{Ti}_2$ with Heteroallenes and E–E Bonds 193

6.1	Introduction.....	193
6.1.1	Carbon disulfide and carbonyl sulfide.....	193
6.1.2	Carbodiimides.....	195

6.1.3	Organic Isocyanates	197
6.1.4	Homonuclear E–E bonds; Organic dichalcogenides and azobenzene.....	199
6.2	Reactivity of 4.3 with Heteroallenes	201
6.2.1	Synthesis and characterisation of $(\mu:\eta^5, \eta^5\text{-Pn}^\dagger)_2\text{Ti}_2(\mu:\eta^2, \eta^2\text{-CS}_2)$ (6.1).....	201
6.2.2	Reactivity studies with COS.....	204
6.2.3	Synthesis and characterisation of $(\mu:\eta^5, \eta^5\text{-Pn}^\dagger)_2\text{Ti}_2(\mu\text{-S})$ (6.4).....	206
6.2.4	Synthesis and characterisation of $[(\eta^8\text{-Pn}^\dagger)\text{Ti}(\mu\text{-S})]_2$ (6.5).....	208
6.2.5	Synthesis and characterisation of $(\mu:\eta^5, \eta^5\text{-Pn}^\dagger)_2\text{Ti}_2(\mu\text{-C}\{N(4\text{-C}_6\text{H}_4\text{CH}_3)\}_2)$ (6.6).....	210
6.2.6	Synthesis and characterisation of $[(\eta^8\text{-Pn}^\dagger)\text{Ti}]_2(\mu\text{-}\kappa^2:\kappa^2\text{-O}_2\text{CNPh})$ (6.7).....	213
6.3	Reactivity of 4.3 with Homonuclear E–E Bonds	217
6.3.1	Synthesis and characterisation of $(\mu:\eta^5, \eta^5\text{-Pn}^\dagger)_2[\text{Ti}(\text{EPh})]_2$, for E = S (6.8), Se (6.9) and Te (6.10).	217
6.3.2	Synthesis and characterisation of $[(\eta^8\text{-Pn}^\dagger)\text{Ti}]_2(\mu\text{-NPh})_2$ (6.11).	222
6.4	Conclusions on Reactivity of 4.3	224
6.5	Experimental Details for Chapter Six.....	226
6.5.1	Synthesis of $(\mu:\eta^5, \eta^5\text{-Pn}^\dagger)_2\text{Ti}_2(\mu:\eta^2, \eta^2\text{-CS}_2)$ (6.1).	226
6.5.2	Synthesis of $(\mu:\eta^5, \eta^5\text{-Pn}^\dagger)_2\text{Ti}_2(\text{COS})$ (6.2).	227
6.5.3	Synthesis of $(\mu:\eta^5, \eta^5\text{-Pn}^\dagger)_2\text{Ti}_2(\mu\text{-S})(\text{CO})$ (6.3).	227
6.5.4	Synthesis of $(\mu:\eta^5, \eta^5\text{-Pn}^\dagger)_2\text{Ti}_2(\mu\text{-S})$ (6.4).	228
6.5.5	Synthesis of $[(\eta^8\text{-Pn}^\dagger)\text{Ti}(\mu\text{-S})]_2$ (6.5).	229
6.5.6	Synthesis of $(\mu:\eta^5, \eta^5\text{-Pn}^\dagger)_2\text{Ti}_2(\mu\text{-C}\{N(4\text{-C}_6\text{H}_4\text{CH}_3)\}_2)$ (6.6).	230
6.5.7	Synthesis of $[(\eta^8\text{-Pn}^\dagger)\text{Ti}]_2(\mu\text{-}\kappa^2:\kappa^2\text{-O}_2\text{CNPh})$ (6.7).	231
6.5.8	Synthesis of $(\mu:\eta^5, \eta^5\text{-Pn}^\dagger)_2[\text{Ti}(\text{SPh})]_2$ (6.8).	232
6.5.9	Synthesis of $(\mu:\eta^5, \eta^5\text{-Pn}^\dagger)_2[\text{Ti}(\text{SePh})]_2$ (6.9).	233
6.5.10	Synthesis of $(\mu:\eta^5, \eta^5\text{-Pn}^\dagger)_2[\text{Ti}(\text{TePh})]_2$ (6.10).	234
6.5.11	Synthesis of $[(\eta^8\text{-Pn}^\dagger)\text{Ti}]_2(\mu\text{-NPh})_2$ (6.11).....	235
6.6	References for Chapter Six.....	236
	APPENDIX ONE: EXPERIMENTAL DETAILS.....	242
A1.1	General Procedures.....	242
A1.2	Purification of Solvents	242
A1.3	Instrumentation.....	242
A1.3.1	NMR spectroscopy.....	242
A1.3.2	EPR spectroscopy.....	243
A1.3.3	IR spectroscopy.....	243
A1.3.4	Mass spectrometry.....	243
A1.3.5	Elemental analysis.....	243
A1.3.6	Magnetic measurements.....	244
A1.3.7	Cyclic voltammetry	245
A1.3.8	X-ray crystallography.....	245
A1.3.9	DFT calculations	246
A1.4	Commercially Supplied Reagents	247
A1.5	Synthesis of Starting Materials.....	247
A1.6	References for Appendix One	248
	APPENDIX 2: SUPPLEMENTARY DATA.....	CD Attached

"We construct and keep on constructing, yet intuition is a good thing. You can do a good deal without it, but not everything. Where intuition is combined with exact research it speeds up the progress of research. Exactitude winged by intuition is at times best. But because exact research is exact research, it gets ahead even without intuition, though perhaps not very quickly."

Paul Klee, 'Exact Experiments in the Realm of Art', 1928.

1 CHAPTER ONE: Introduction

1.1 Fundamentals of Pentalene Chemistry

The pentalene molecule has fascinated chemists for over 50 years and has sparked much debate and occasional controversy: from the time its existence was first hypothesised, through the practical difficulties in achieving its synthesis, and ultimately to speculation as to its potential applications in materials chemistry.

The use of pentalene as a versatile ligand in coordination chemistry has been extensively reviewed.¹⁻⁴ This chapter serves to briefly introduce the fundamentals of pentalene chemistry, its nomenclature, synthesis and bonding modes, and draw attention to the areas in which pentalene complexes have been applied in the frontiers of modern organometallic chemistry.

1.1.1 Nomenclature

In this work, the term 'pentalene' is used to refer to any generic pentalene derivative, neutral or charged. Specific fragments which are referred to include 'dihydropentalene' [C_8H_8], 'hydropentalenyl' [C_8H_7]⁻ and 'pentalenyl' [C_8H_6]²⁻.

The numbering system for the carbon framework, used for naming substituted pentalenes, is shown in Figure 1.1. Carbon atom 7 and 8 are referred to as the 'bridgehead' carbons, and 1, 2, 3, 4, 5 and 6 as the 'wing' carbons. The latter group are sub-categorised as follows; carbons 2 and 5 are the 'wing-tip' positions, carbons 1, 3, 4 and 6 are the 'wing-side' positions. Pentalene shows a variety of coordination modes in its organometallic complexes (*vide infra*), hence the coordination mode will be stated unless in reference to a complex which has not been structurally authenticated, a series of related complexes, or if the binding mode is otherwise unambiguous.

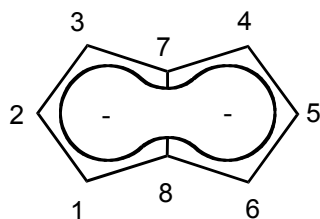
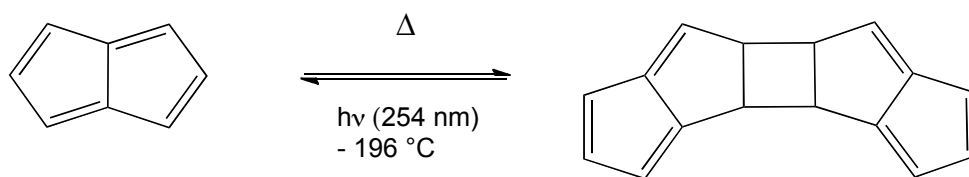


Figure 1.1 Numbering system for pentalene.

1.1.2 Synthesis of pentalene derivatives

Pentalene, C_8H_6 , is an eight carbon molecule that can be considered as the double-ring fused relative of cyclopentadiene, or as cyclooctatetraene with a 1,5-transannular bond. The neutral species is an 8π Huckel anti-aromatic hydrocarbon with a double-bond alternant C_{2h} structure, and the molecule has only been isolated in matrices at very low temperatures.⁵ Neutral pentalene is unstable above $-196\text{ }^\circ\text{C}$ and undergoes a rapid Diels-Alder reaction to the [2+2] dimer (Scheme 1.1).⁶

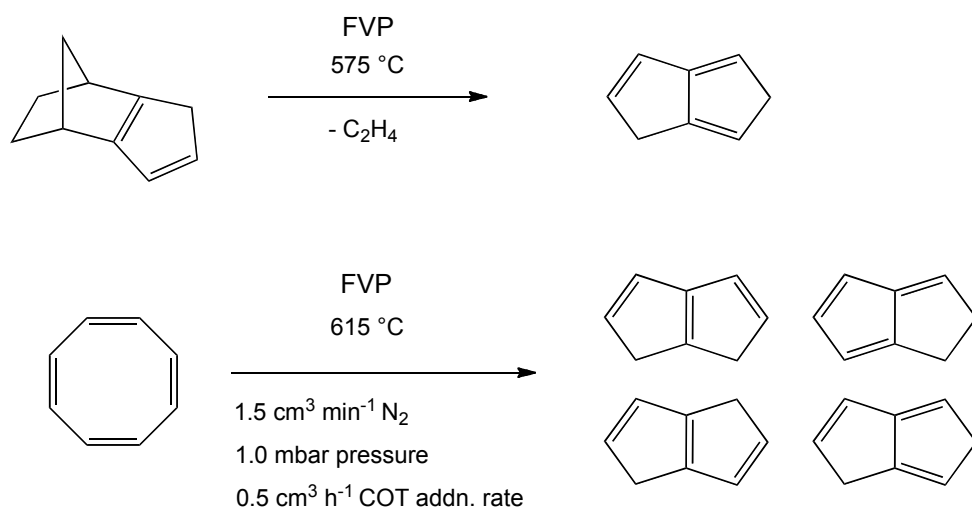


Scheme 1.1 Dimerisation of neutral pentalene.⁶

In contrast the dianionic form, $[C_8H_6]^{2-}$ ($= Pn$), is a 10π aromatic species and is consequently thermally stable at room temperature. The pentalenyl dianion has been crystallographically characterised as a dilithiated dimethoxyethane (DME) adduct $[Li(DME)]_2Pn$,⁶ and the carbocycle shows D_{2h} symmetry, with lithium ions in an η^5, η^5 -coordination mode on opposite faces of the planar pentalene ring. Naphthalene, which is structurally related to benzene as pentalene is to cyclopentadiene, also shows an *anti* geometry of alkali metal atoms in its dilithium salt.⁷ Alkali metal salts of the ligand are presumed to have ionic, carbanion-like character and provide the most accessible source of the Pn moiety in organometallic synthesis, in a similar fashion to the use of $[C_5H_5]^-$ ($= Cp$). This analogy is evident in the initial synthesis of $[Li]_2Pn$, which was achieved by Katz *et al.* by double deprotonation of 1,5-dihydropentalene (PnH_2) with two mole equivalents of nBuLi in THF, a preparation which parallels the facile synthesis of $LiCp$ from cyclopentadiene (CpH).⁸

Dihydropentalenes may be prepared by various synthetic routes. Katz *et al.* reported the pyrolysis of iso-dicyclopentadiene at $575\text{ }^\circ\text{C}$ under a dinitrogen stream, to afford PnH_2 in 33% yield (Scheme 1.2, top).⁹ The reaction proceeds *via* a 1,2-hydrogen shift followed by a retro Diels-Alder reaction, and product was assigned a single isomer, 1,5- PnH_2 , on the basis of (UV and 1H NMR) spectroscopic evidence.

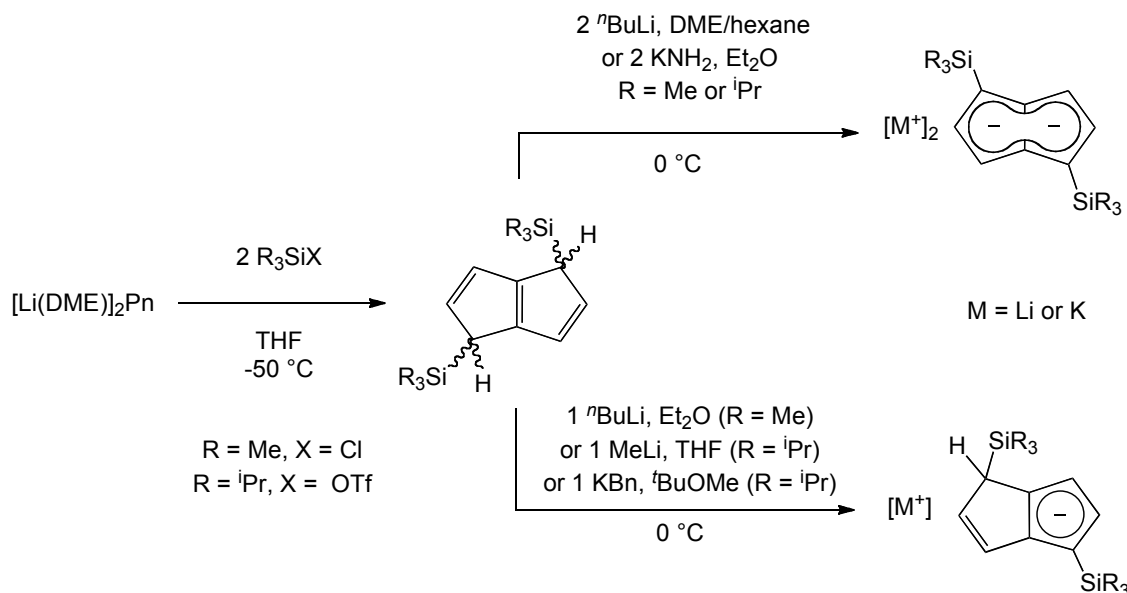
An alternative procedure, as first demonstrated by Jones and Schwab,¹⁰ involves the flash vacuum pyrolysis (FVP) of COT which produces PnH₂ as a mixture of four isomers. This procedure was later optimised by Cloke *et al.* using careful control of conditions including flow rate, pressure, COT addition rate and temperature to produce various isomers of PnH₂ (Scheme 1.2, bottom).¹¹ These isomers are condensed at -78 °C and then collectively deprotonated with ⁿBuLi in DME/hexane to afford [Li(DME)]₂Pn on a 25 g scale in *ca.* 90% yield.



Scheme 1.2 Pyrolytic routes to dihydropentalenes.⁹⁻¹¹

Research into the organometallic chemistry of pentalene has gradually increased as the number of reliable synthetic routes to substituted pentalene ligands has developed. Cloke *et al.* have reported that trialkylsilyl substituents (SiR₃) can be installed regiospecifically into the 1 and 4 positions of the pentalene ring, by reaction of the nucleophilic pentalene dianion with the appropriate silyl electrophile.¹¹ For example, reaction of [Li(DME)]₂Pn with two equivalents of Me₃SiCl affords C₈H₆{SiMe₃-1,4}₂ (= Pn^HH₂) as a mixture of racemic and *meso* isomers in *ca.* 90% purity by ¹H NMR spectroscopy. Reaction of [Li(DME)]₂Pn with two equivalents of triisopropylsilyl triflate, produces C₈H₆{SiⁱPr-1,4}₂ (= Pn[†]H₂), isolated as an off-white crystalline solid which is thermally unstable above -30 °C. Pn[†]H₂ was identified as a single diastereomer by NMR spectroscopy, which was structurally verified by a single crystal X-ray diffraction (XRD) study showing the bulky SiR₃ (R = ⁱPr) groups arranged in an anti configuration.

By careful control of stoichiometry and reaction conditions, the appropriate basic lithium or potassium reagent may be selected to furnish the mono- or di-alkali metal salts, which are used as transfer agents for the silylated hydropentalenyl (Pn^{H} and Pn^{H}) or pentalenyl (Pn' and Pn^{H}) moieties (Scheme 1.3).^{2,11-13}

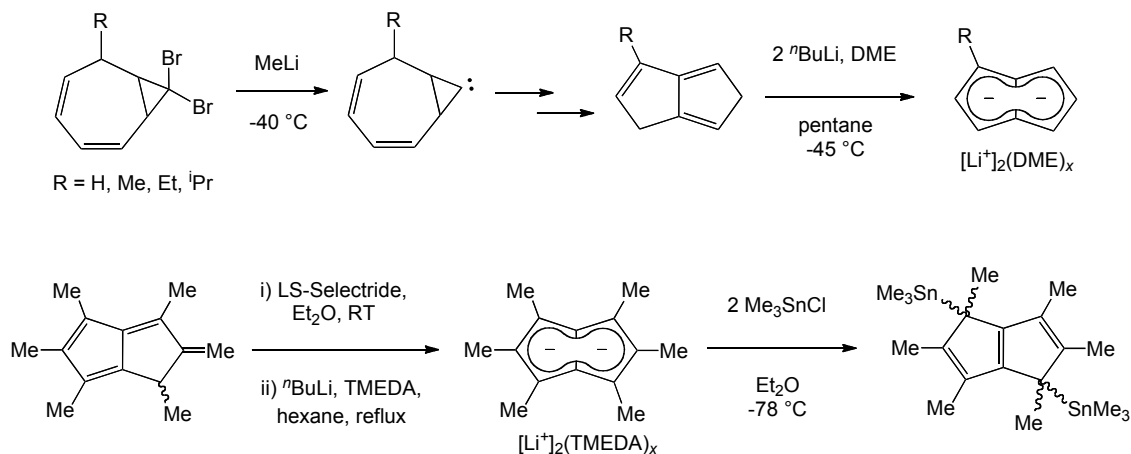


Scheme 1.3 Synthesis of silylated pentalenes.¹¹

Non-pyrolytic routes to $[\text{Li}]_2\text{Pn}$ have been reported, in particular the Skattebøl rearrangement of a geminal dibromocyclopropane-fused cycloheptatriene.¹⁴ This method provides a convenient method for incorporating alkyl substituents into the ring, *via* the use of the 7-alkyl substituted cycloheptatrienes, to afford the dilithium/DME salts of $[\text{C}_8\text{H}_6\{1\text{-R}\}]^{2-}$ ($= \text{Pn}^{\text{R}}$, $\text{R} = \text{Me}, \text{Et}, \text{iPr}$) in *ca.* 40% yields (Scheme 1.4, top).¹⁵ The organometallic complexes derived from Pn^{R} ligands showed increased solubility with respect to their unsubstituted analogues, however their purification is often hampered by complex mixtures of diastereomers forming, which may be attributed to the significant asymmetry in the mono-substituted ligand.¹⁶

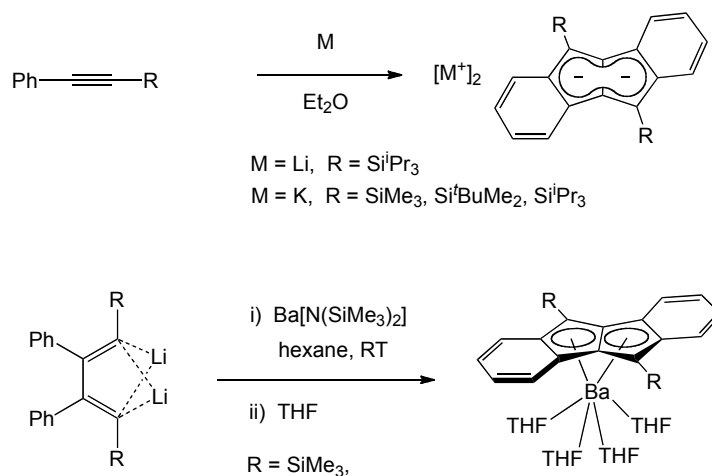
The total synthesis of an organic precursor and its conversion into the dilithium salt of permethylpentalene $[\text{C}_8\text{Me}_6]^{2-}$ ($= \text{Pn}^*$) have been reported by O'Hare *et al.* (Scheme 1.4, bottom).^{17,18} Furthermore these researchers have utilised the organotin(IV) complexes, *cis*- and *trans*-(SnMe_3) $_2\text{Pn}^*$, as 'softer' transfer agents for the Pn^* fragment.^{19,20} Permethylation of the pentalene ring confers enhanced stability, solubility and crystallinity on its metal complexes, in a fashion that resembles the widespread

replacement of Cp with permethylcyclopentadienyl (Cp*) ligands in organometallic chemistry.²¹⁻²⁶



Scheme 1.4 Solution-phase synthesis of alkylated pentalenes.^{15,17}

The benzannulated dibenzo[*a,e*]pentalene dianion, $[C_{16}H_{10}]^{2-}$, has attracted renewed attention in recent years as a potential π -extended ligand.^{27,28} Saito *et al.* reported in a communication that the reduction of phenyl silyl acetylenes with lithium led to the unexpected formation of a dilithium dibenzopentalene derivative in 8% yield (Scheme 1.5, top).²⁹ An improved procedure to furnish the analogous dipotassium salts (35 - 89% yields) was the subject of a subsequent full report by these researchers,³⁰ which also included the synthesis of the first transition metal dibenzopentalene complex. The synthesis of barium dibenzopentalene, the first example of main-group metal bound in an η^8 -coordination mode, was recently reported by Xi *et al.* by reaction of phenyl substituted 1,4-dilithio-1,3-butadiene with $Ba[N(SiMe_3)_2]_2$ (Scheme 1.5, bottom).³¹



Scheme 1.5 Synthetic routes to silylated dibenzopentalene salts.²⁹⁻³¹

1.1.3 Bonding in pentalene complexes

When acting as a ligand with transition metals pentalene has a maximum of 8 bonding electrons, L_3X_2 function in a neutral counting scheme,³² and shows a variety of multihaptic bonding modes (Figure 1.2).

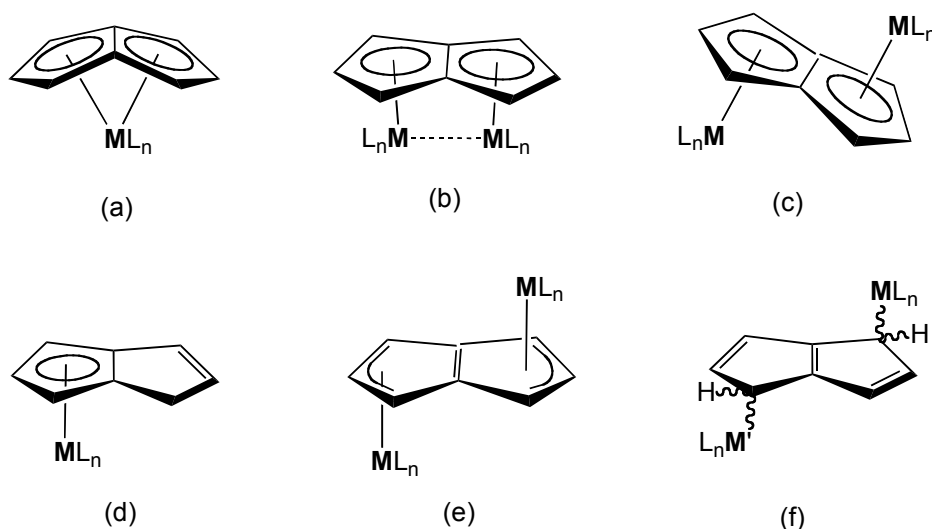


Figure 1.2 Examples of the coordination modes of pentalene ligands.

The η^8 -mode, in which all eight carbons are involved in bonding to the metal (Figure 1.2 (a)), leads to a folding of the ligand about its C–C bridgehead bond towards the metal centre. This is commonly encountered in pentalene complexes with f- and early d-block elements, as the 'umbrella'-like effect of the folded ligand aids the steric stabilisation of the metal centres.¹ This distortion from planarity is accompanied by a loss of aromaticity, and is quantified by the 'fold angle' (Figure 1.3), which is dependent on both steric and electronic factors.

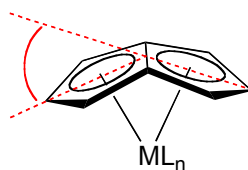


Figure 1.3 Fold angle for an η^8 -bound pentalene complex.

In general, for complexes with a given ligand set the fold angle may be simply related inversely to the size of the central metal.¹ For example, (η^8 -Pn)MCp complexes reported by Jonas *et al.* show a marked increase in fold angle from M = Ti (37.0°) to V (43.0°) in accordance with the decreasing ionic radii (0.670 vs 0.640 Å respectively for 6-coordinate M^{3+} ions).³³ However comparing the series of group 4 permethylpentalene complexes Pn^*MCpCl and Pn^*MCp_2 for M = Ti, Zr, Hf,³⁴ the titanium and hafnium species have near identical fold angles, despite the considerably larger size of Hf^{4+} (0.71 Å) relative to Ti^{4+} (0.605 Å).³³ O'Hare *et al.* attributed this to the more diffuse nature of the atomic orbitals for the 3rd row transition metal leading to better orbital overlap with Pn^* , which compensates for the loss in aromaticity as the ligand folds away from planarity.³⁴ Within a series of complexes bearing the same metal and pentalene ligand, the fold angles increase as electron deficiency at the metal centre increases. For example, Cloke *et al.* reported the mononuclear tantalum(V) complexes (η^8 - Pn^+) $TaCl_xMe_{3-x}$ for $x = 0-3$, which show a small but discernable increase in fold angle as the number of electron withdrawing chloride ligands increases.³⁵ Furthermore, the electronic properties of the pentalene ligand itself have an effect on fold angle, as first shown by comparison of the fold angles for (η^8 -Pn)ZrCpCl (33.0°)³⁶ and (η^8 - Pn^*)ZrCpCl (30.7°),^{34,37} which provides evidence for the enhanced donor ability of the permethylated ligand.

The η^5 -mode of pentalene most closely resembles that of Cp metallocenes, with donation of 5 bonding electrons (L_2X function) to each metal centre by virtue of the fact that the bridgehead double bond in the 'bis(allyl)' resonance form of Pn (Figure 1.4) can act as an μ -L donor. This mode is commonly encountered in bimetallic complexes, with the metal centres either bound to the same (*syn*) or opposite (*anti*) faces of the ligand (Figure 1.2 (b) and (c)).

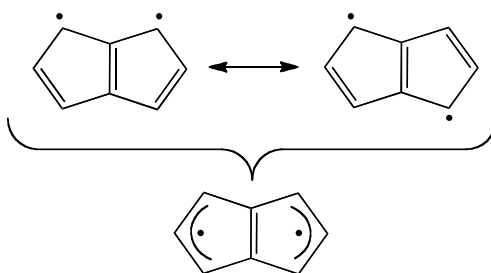


Figure 1.4 Representation of the 'bis(allyl)' (L_3X_2) resonance form of pentalene.³⁸

For instance in the anti-bimetallic complex $[\text{Cp}^*\text{Fe}]_2(\mu\text{-}\eta^5\text{:}\eta^5\text{-Pn})$ (Figure 1.5 (a)), pentalene can be viewed as an L_2X donor to each metal centre, providing a bonding description in which each iron centre achieves a valence electron (VE) count of 18 (ML_4X_2).³⁸ The neutral compound $[\text{Cp}^*\text{Fe}]_2(\mu\text{-}\eta^5\text{:}\eta^5\text{-Pn})$ is diamagnetic, and its dication $[[\text{Cp}^*\text{Fe}]_2(\mu\text{-}\eta^5\text{:}\eta^5\text{-Pn})]^{2+}$ has two unpaired electrons, consistent with this bonding picture. Extended Hückel calculations by Garland *et al.*³⁹ on the model anti-bimetallic system $[\text{CpFe}]_2(\mu\text{-}\eta^5\text{:}\eta^5\text{-Pn})$, revealed bonding interactions which increase significantly if the two CpFe units are allowed to slip to the edges of the Pn rings. This description is in good agreement with X-ray structural data for $[\text{Cp}^*\text{Fe}]_2(\mu\text{-}\eta^5\text{:}\eta^5\text{-Pn})$ and other anti-bimetallic complexes.^{40,41} Hence, slippage of the metal from the bridgehead towards the 'wing-tip' positions may be quantified by a geometric parameter, Δ (Figure 1.5 (b)).

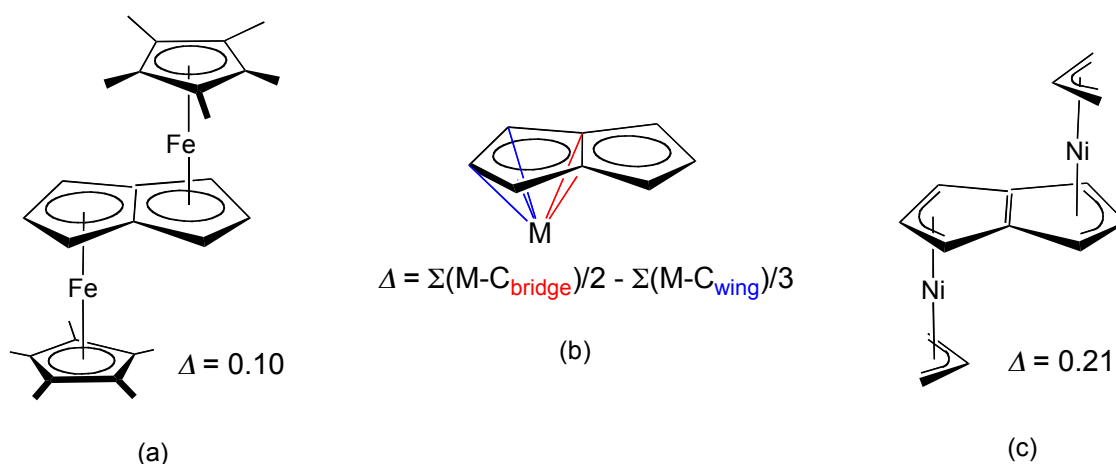


Figure 1.5 Examples of anti-bimetallic pentalene complexes, and a definition of Δ .

In more extreme cases ($\Delta > ca. 0.2$) this ring slippage leads to an η^3 -coordination mode in preference to η^5 , akin to the 'ene-allyl' distortion found in indenyl and other Cp complexes.⁴² The first structurally characterised complex of this class was $[(\text{allyl})\text{Ni}]_2(\mu\text{-}\eta^3\text{:}\eta^3\text{-Pn})$ (Figure 1.5 (c)), prepared by Kanai *et al.*⁴³ In η^3 -mode the 'allyl-like' fragment of the pentalene ligand donates 3 electrons (LX function) to a metal centre. However caution must be taken with this bonding description, given the fact that the 'allyl' unit is electronically linked to the remainder of the Pn dianion.

η^5 -binding is not exclusive to bimetallics, and is commonly found in the monomeric complexes bearing the hydropentalenyl ligand (Figure 1.6 (a)),^{15,44-46} which may be considered as a substituted Cp ligand (L_2X function). Rare examples of η^5 -binding are also found in monometallic complexes such as $Cp^*Co(\eta^5-Pn)$ (Figure 1.6(b)), where the pentalene ligand is planar and aromatic but one ring is uncoordinated due to a saturation of the metal's steric/electronic requirements. This may be represented as a zwitterionic structure in which the metal has a formal positive charge and there is a formal negative charge on the uncoordinated part of the aromatic Pn. The simplest metal-pentalene bonding mode is η^1 -‘allyl-like’ coordination (X function), and is most common for $Sn(IV)$ complexes (Figure 1.6 (c)).^{17,19,20,47,48}

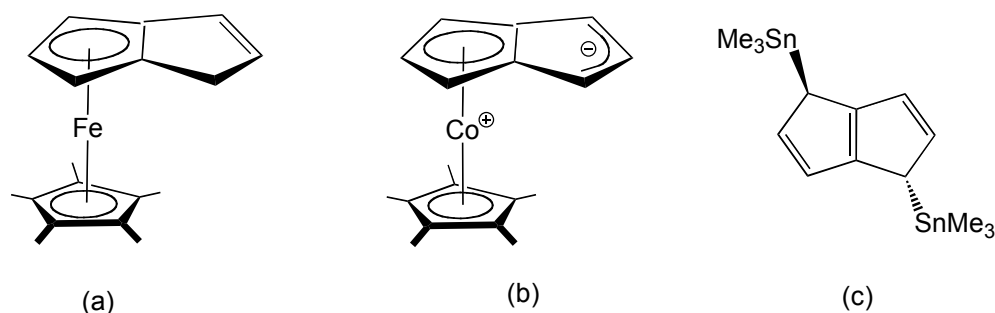


Figure 1.6 Examples of η^5 and η^1 -coordinated pentalene complexes.

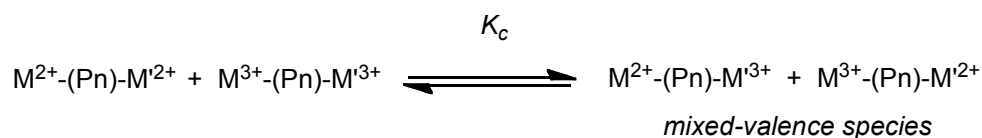
1.2 Applications of Organometallic Complexes with Pentalene Ligands

1.2.1 Studying interactions in bimetallic complexes

Molecules containing more than one metal centre can exhibit profoundly different physical properties and reactivity to monometallic complexes, particularly where there is a strong interaction between the metal centres.⁴⁹⁻⁵² The synthesis of polymers which contain metallocene units in close proximity are highly desirable as they should allow extended metal–metal interactions throughout the chain. In such cases, polymers with interesting electrical, magnetic or other physical properties might be envisaged.⁵³ A brief overview of the classification of the mixed-valence (MV) state with a particular focus on pentalene bridged bimetallics is presented herein.

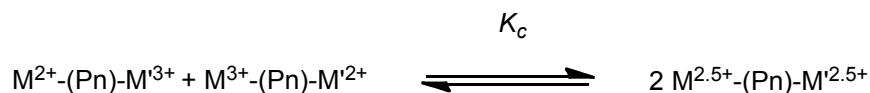
In a complex with two redox centres that are electronically coupled to some extent, e.g. a generic pentalene bridged bimetallic $L_nM(\mu-Pn)M'L_n$ (where M and M' are divalent in the reduced form), removal of an electron creates a so-called MV system, with two formally different oxidation states. Depending on the strength of the electronic coupling, the unpaired electron is either concentrated on one of the redox centres, or it is symmetrically delocalised between the two sites. These are the extreme situations (I and III respectively) of the Robin-Day classification for a MV species.^{54,55} Class I bimetallic compounds show no metal-metal interactions and have electronic properties corresponding to the separate sites M^{n+} and $M'^{(n+1)+}$, Class III systems have very strong metal-metal interactions and are obvious candidates for use as 'molecular wires' in the field of molecular electronics.^{56,57} Between these two extremes are Class II complexes, which exhibit intermediate metal-metal interactions. Where a bimetallic complex lies in this classification depends on the strength of electronic coupling, and can be investigated using a number of physical techniques.

Electrochemical methods, particularly cyclic voltammetry (CV), provide a convenient way of inferring the extent of delocalisation in MV state. In the case of a homobimetallic compound ($M = M'$) two redox processes ($E^{(1)}$ and $E^{(2)}$) should be observed. The potential difference between two *reversible* electrochemical processes, $\Delta E_{1/2} = |E_{1/2}^{(1)} - E_{1/2}^{(2)}|$, is indicative of the thermodynamic stability of the MV state with respect to other redox states. $\Delta E_{1/2}$ separations close to zero are characteristic of non-interacting metal sites (Class I), either due to large distance between them or because the ligand does not provide an electronic coupling pathway. Small values of $\Delta E_{1/2}$ suggest weak electronic coupling, corresponding to a small comproportionation constant K_c (Scheme 1.6) and a MV state involving so-called 'trapped' valence metal centres (Class II).



Scheme 1.6 Formation of Class I and II mixed-valence pentalene bridged bimetallics, where K_c = comproportionation equilibrium constant.

Large $\Delta E_{1/2}$ separations (above *ca.* 200 mV, corresponding to $K_c \geq 10^4$, Scheme 1.7) are commonly cited as evidence for a highly delocalised system with a strong degree of thermodynamic stabilisation of the MV state (Class III).



Scheme 1.7 Fully delocalised Class III bimetallics with large K_c .

In the case of heteronuclear complexes ($M \neq M'$) a non-zero $\Delta E_{1/2}$ is expected even in the absence of any metal-metal interactions, due to the different redox properties of metal centres present in the molecule.

Assigning Robin-Day classification to electronic interaction in a MV species should not be based on $\Delta E_{1/2}$ alone, since it is purely a measure of thermodynamic stabilisation of the MV state for which other energetic terms such as through-space electrostatics, solvation or entropy may also make a significant contribution.⁵⁸ However electrochemical methods such as CV are a useful screening technique for bimetallic complexes, which may exhibit other interesting interactions. For example MV species can exhibit strong intervalence charge transfer (IVCT) bands in the near-infrared (NIR). Other techniques commonly used include EPR and ^{57}Fe Mössbauer spectroscopy to study the electronic and nuclear interactions respectively, SQUID magnetometry for magnetic interactions, and NMR spectroscopy and X-ray crystallography to provide structural information in the solution and solid state.

1.2.2 Electronic delocalisation in pentalene-bridged complexes

The aromatic nature of the pentalene ligand has been shown to induce very strong electronic delocalisation in anti-bimetallic complexes and promote coupling effects through the planar π -system.² Metal-metal interactions have been studied extensively by Manriquez *et al.* for the capped triple decker-complexes $[\text{Cp}^*\text{M}(\mu\text{-}\eta^5\text{:}\eta^5\text{-Pn})\text{MCp}^*]^{n+}$ with transition metals (Figure 1.7 (a), $M = \text{Fe, Co, Ni, Ru}$) using a variety of physical techniques.^{40,59-61}

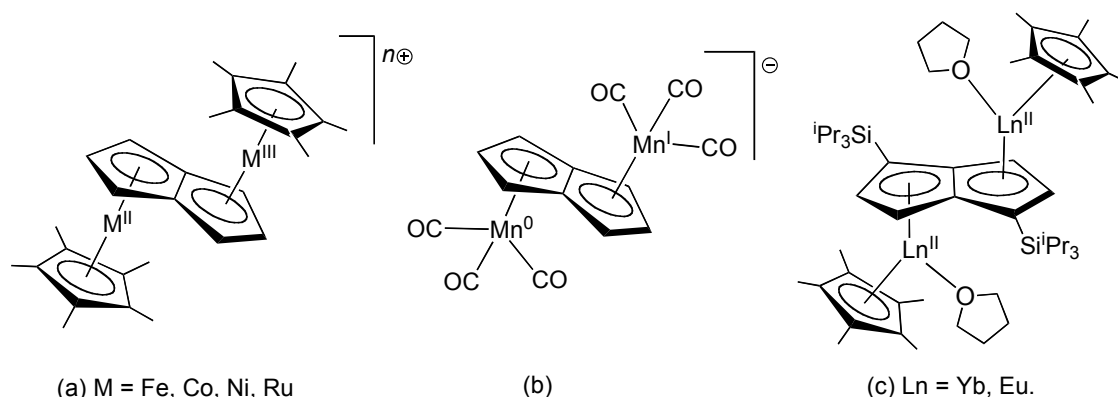


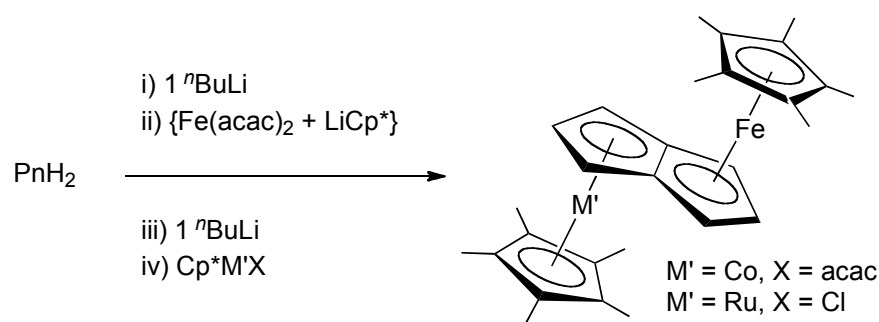
Figure 1.7 Examples of anti-bimetallic complexes studied for metal-metal interactions.

Cyclic voltammetry shows that these compounds undergo two successive one-electron transfers, with large potential separations between successive oxidations (decreasing in the order $\text{Fe} > \text{Co} > \text{Ni} > \text{Ru}$). Oxidation to the cationic forms ($n = +1$ and $+2$) was achieved for each complex, of which the MV forms ($n = +1$) show IVCT bands in the NIR spectrum that are not observed in the neutral or di-cationic forms. ^{57}Fe Mössbauer spectroscopy (timescale $\approx 10^{-7}$ s) studies of the cationic $[\text{Cp}^*\text{Fe}(\mu\text{-}\eta^5\text{:}\eta^5\text{-Pn})\text{FeCp}^*]^+$ species found the iron environment to be fully averaged down to 1.5 K, indicative of a strong electronic interaction between the metal centres and extensive delocalisation in the MV state.

Bimetallic complexes of group 7 metal carbonyls, $[\text{M}(\text{CO})_3]_2(\mu\text{-}\eta^5\text{:}\eta^5\text{-Pn})$ for $M = \text{Mn}$ and Re , were synthesised by O'Hare *et al.* by treatment of $[\text{Li}(\text{DME})]_2\text{Pn}$ with two equivalents of $\text{Mn}(\text{CO})_3(\text{py})_2\text{Br}$ or one equivalent of $[\text{Re}(\text{CO})_3(\text{THF})\text{Br}]_2$ respectively.⁶² The manganese(I) complex, formed as an exclusively anti-bimetallic, is particularly noteworthy. $[\text{Mn}(\text{CO})_3]_2(\mu\text{-}\eta^5\text{:}\eta^5\text{-Pn})$ may be reduced by electrochemical or chemical methods to yield both the dianion as a dilithium salt, or the mono-anion stabilised by a $[\text{FeCp}(\text{C}_6\text{Me}_6)]^+$ counterion (Figure 1.7 (b)). The latter is formally a Mn(I)/Mn(0) mixed-valence complex and shows hyperfine coupling with the two equivalent ^{55}Mn ($I = 5/2$) centres in the EPR spectrum, consistent with a Robin-Day class III system.⁵⁴ This MV anion remains one of the most delocalised organometallic systems reported to date.

Anti-bimetallic complexes of the divalent lanthanides with silylated pentalene ligands, $[\text{Cp}^*\text{Ln}(\text{THF})]_2(\mu\text{:}\eta^5, \eta^5\text{-Pn}^\dagger)$ for $\text{Ln} = \text{Eu}$ and Yb (Figure 1.7 (c)), were prepared by Cloke *et al.* from the one-pot reaction of $\text{LnI}_2(\text{THF})_x$ and KCp^* and the subsequent addition of half an equivalent of $[\text{K}]_2\text{Pn}^\dagger$.⁶³ These complexes are of interest as molecular models for lanthanide-based polymers,^{64,65} which have potential applications as magnetic materials,⁶⁶⁻⁶⁹ molecular catalysis,^{70,71} and luminescent devices.⁷²⁻⁷⁴ CV studies indicated that $[\text{Cp}^*\text{Eu}(\text{THF})]_2(\mu\text{:}\eta^5, \eta^5\text{-Pn}^\dagger)$ decomposes readily upon oxidation but the $[[\text{Cp}^*\text{Yb}(\text{THF})]_2(\mu\text{:}\eta^5, \eta^5\text{-Pn}^\dagger)]^+$ mono-cation appeared to be stable under the conditions and timescale of the experiment. Furthermore through-ligand Yb–Yb coupling was suggested by the electrochemical data for $[\text{Cp}^*\text{Yb}(\text{THF})]_2(\mu\text{:}\eta^5, \eta^5\text{-Pn}^\dagger)$, of magnitude similar to that of its transition metal analogues.

Despite the number of pentalene-bridged homobimetallic compounds of the general formula $\text{L}_n\text{M}(\mu\text{:}\eta^5, \eta^5\text{-Pn})\text{M}'\text{L}_n'$ ($\text{M} = \text{M}'$) that have been synthesised, comparatively few heterobimetallic ($\text{M} \neq \text{M}'$) examples are known. The main synthetic challenge is selective coordination of two different metal centres to the pentalene bridge to give a mixed-metal complex, whilst preventing formation of homobimetallic species. Strategies for the rational synthesis of such materials were pioneered by Manriquez *et al.* starting with dihydropentalene *via* successive deprotonation and incorporation of the appropriate metal ‘half-sandwich’ synthon (Scheme 1.8).⁵⁹



Scheme 1.8 ‘Building block’ synthetic route to heterobimetallics.⁵⁹

The heterobimetallic complex $[\text{Cp}^*\text{Ru}(\mu\text{:}\eta^5, \eta^5\text{-Pn})\text{FeCp}^*]^+$ was studied by ^{57}Fe Mössbauer spectroscopy, which indicates full delocalisation and a unique Fe environment for the mono-cation over the entire temperature range 1.5–300 K.^{75,76}

It has been suggested that the pentalene ligand allows an extent of electronic communication between the Fe/Ru centres which is not observed between these metal centres with other unsaturated bridging ligands such as fulvalene.⁷⁷ The MV form of both heteronuclear complexes $[\text{Cp}^*\text{M}'(\mu\text{-}\eta^5\text{:}\eta^5\text{-Pn})\text{FeCp}^*]^+$ $\text{M}' = \text{Ru}$ and Co , exhibit IVCT bands in the NIR region not observed in the neutral and di-cationic species, and were classified as Class III and Class II respectively.

In a modification of the ‘building block’ synthetic route, $\text{Fe}(\eta^5\text{-PnH})_2$ was lithiated *in situ* and used to incorporate a Cp^*Co unit into the chain, forming $\text{Cp}^*\text{Co}(\mu\text{-}\eta^5\text{:}\eta^5\text{-Pn})\text{Fe}(\eta^5\text{-PnH})$ (Figure 1.8, left), classified as an *asymmetric* anti-bimetallic due to the different ligand environments of the two metals ($\text{L}_n \neq \text{L}_n'$).⁶⁰ Interestingly the introduction of asymmetry in the ligand environment in $[\text{Cp}^*\text{Co}(\mu\text{-}\eta^5\text{:}\eta^5\text{-Pn})\text{Fe}(\eta^5\text{-PnH})]^+$ leads to Class I behavior based on the electrochemical (CV) and spectroscopic (NIR, Mössbauer) evidence,⁶¹ whereas the symmetric congener $[\text{Cp}^*\text{Co}(\mu\text{-}\eta^5\text{:}\eta^5\text{-Pn})\text{FeCp}^*]^+$ is Class II. It was suggested that ligand asymmetry in general introduces a barrier for electron transfer and as a result decreases the extent of electronic interaction. This has a larger impact for heteronuclear complexes which already have an built-in barrier for electron transfer from the different electronic nature of the metal centres, and the subtle effect of changing the terminal ligand in this case can cause a complete loss of electronic communication.

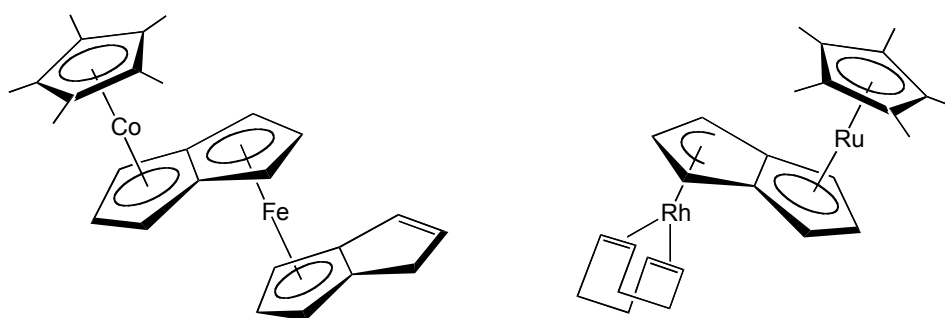
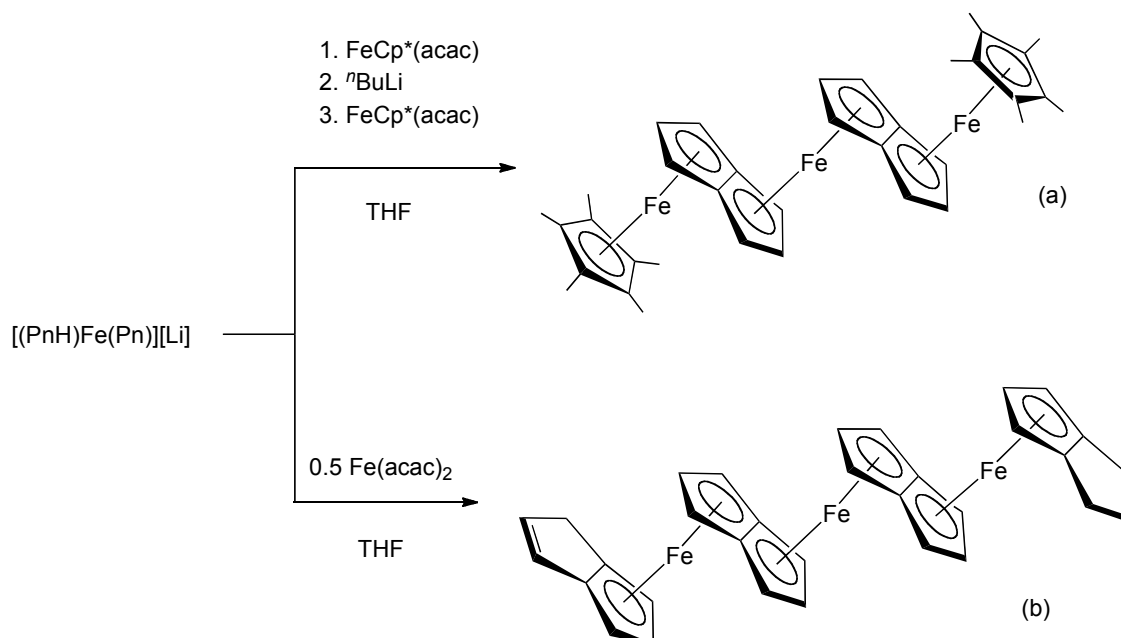


Figure 1.8 Examples of hetero-bimetallics with asymmetric ligand environments.

The synthesis of oligomeric or polymeric materials consisting of alternating metal atoms and fused-ring ligands is expected to offer a range of interesting delocalised properties.⁴⁹ Strategies for the rational synthesis of such materials were pioneered by

Manriquez *et al.* who extended work on bimetallic pentalene systems described above to incorporate further organometallic fragments into the chain.⁶⁰



Scheme 1.9 Synthetic routes to trimetallic pentalene complexes.⁶⁰

The fully capped trimetallic complex $(\text{Cp}^*\text{Fe})_2[\text{Pn}_2\text{Fe}]$ was synthesised from $\text{Fe}(\eta^5\text{-PnH})_2$ by lithiation with $n\text{BuLi}$ followed by addition of $\text{FeCp}^*(\text{acac})$ in two successive iterations (Scheme 1.9 (a)). A potentially iterative process to higher chain oligomers was presented in the synthesis of a novel quadruple decker iron-pentalene complex from reaction of $[\text{Li}][\text{PnFe}(\eta^5\text{-PnH})]$ with 0.5 equivalents of $\text{Fe}(\text{acac})_2$ in THF (Scheme 1.9 (b)). The quadruple-decker complex $(\{\eta^5\text{-PnH}\}\text{Fe})_2[\text{Pn}_2\text{Fe}]$ was characterised by mass spectrometry and IR spectroscopy, however NMR and structural characterisation by single crystal XRD were hampered by its low solubility in hydrocarbon solvents (400 mg L^{-1} of boiling toluene), and this has prevented synthesis of higher chain oligomers.

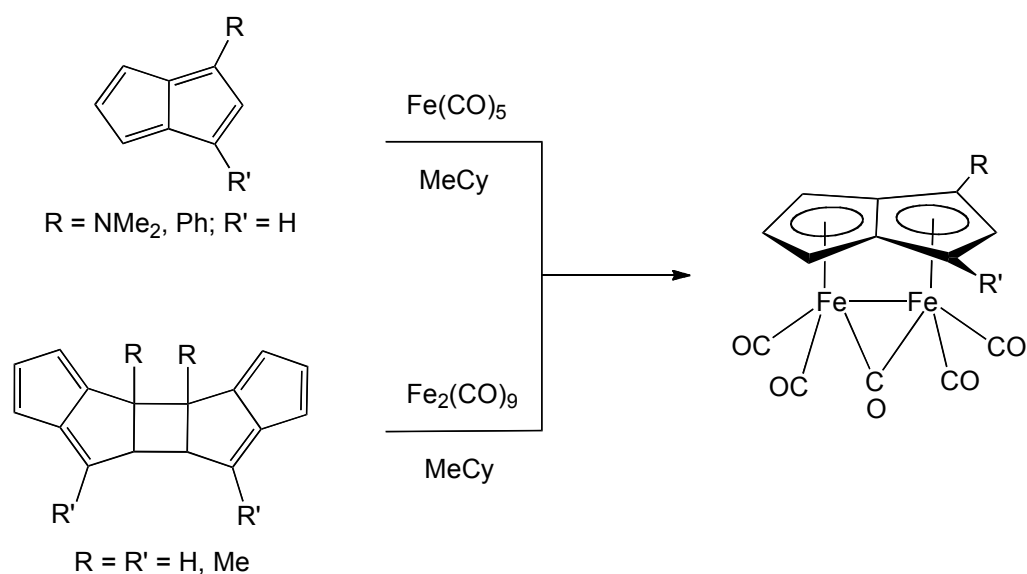
Subsequent investigations employing alkylated (Pn^{R}) or silylated (Pn^{Si}) pentalene ligands have successfully introduced greater degree of solubility in hydrocarbons to the resulting iron(II) complexes.^{12,16} However due to the lack of symmetry in these ligands, a mixture of isomeric multi-decker species were isolated as oils which could not be purified, and precluded full characterisation. The formation of multiple isomers also

prevented unambiguous assignment of the electrochemical data obtained, and their potential as delocalised organometallic polymers could not be fully determined.

1.2.3 Synthesis of metal-metal bonded complexes

The ability of pentalene to coordinate two metals on the same side of the ligand can facilitate direct bonding interactions between the metals. The feature of metal-metal bonds is often cited as the reason for bimetallic pentalene complexes to adopt a syn disposition as opposed to the sterically favourable anti conformation. However the existence of syn-bimetallics containing a *bona fide* metal-metal bond as opposed to merely a close proximity of metal centres has been the subject of some debate, and is best clarified using a combination of spectroscopic, structural and theoretical evidence.

Dinuclear iron pentacarbonyl complexes, *syn*-(μ - η^5 : η^5 -Pn^{1,3-RR'})[Fe(CO)₂]₂(μ -CO), have been synthesised by reaction of substituted dihydropentalenes with Fe(CO)₅,⁷⁸ and also by fission of neutral pentalene dimers with excess Fe₂(CO)₉ (Scheme 1.10).⁷⁹ IR spectroscopy of these complexes revealed a bridging carbonyl stretch between 1750-1785 cm⁻¹, as well as ν (CO) bands for the terminal carbonyl ligands. The structure shown in Scheme 1.10 featuring a M–M single bond was inferred by analogy with the isoelectronic *syn*-(μ -COT)[Fe(CO)₂]₂(μ -CO),⁸⁰ however this has not been confirmed in the pentalene complex by XRD methods.



Scheme 1.10 Synthesis of iron carbonyl syn-bimetallics.^{78,79}

Recently Green *et al.* have shown that the ability of pentalene to act as an L_2X donor to each metal centre provides a simple structure-bonding representation that requires no Fe–Fe bond for each to achieve an 18 VE configuration (Figure 1.9, left).³⁸ This description was consistent with theoretical calculations on the permethylated analogue $\text{syn}-(\mu-\eta^5:\eta^5\text{-Pn}^*)[\text{Fe}(\text{CO})_2]_2(\mu\text{-CO})$;⁸¹ the intermetallic distance in the latter (2.6869(5) Å) does not necessarily imply an Fe–Fe bond, since the metal centres are held at close length as a requirement of the pentalene ligand framework.

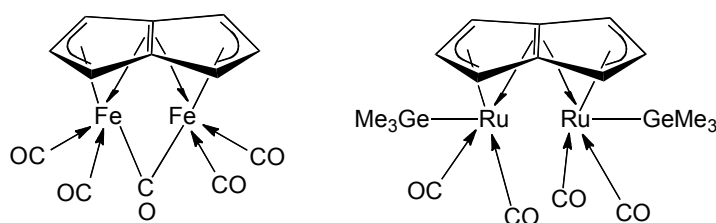
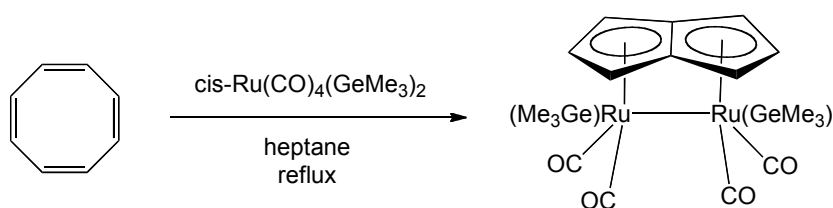


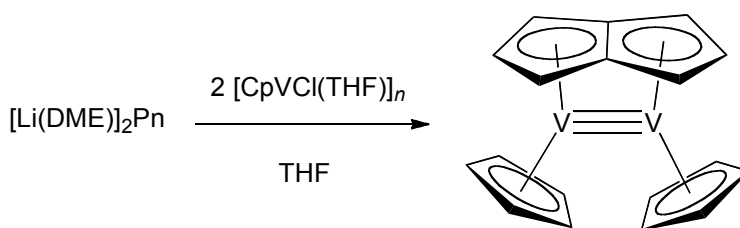
Figure 1.9 Structure-bonding representations of $\text{syn}-(\mu-\eta^5:\eta^5\text{-Pn})[\text{Fe}(\text{CO})_2]_2(\mu\text{-CO})$ and $\text{syn}-(\mu-\eta^5:\eta^5\text{-Pn})[\text{Ru}(\text{CO})_2(\text{GeMe}_3)]_2$.³⁸

An alternative route to syn-bimetallic pentalene complexes was pioneered by Knox and Stone,⁸² who showed that the dehydrogenative transannular ring closure of unsubstituted, alkylated, and silylated COT derivatives is facilitated by ruthenium carbonyls in boiling heptane.^{83–85} This allowed for the first structural characterisation of a syn-bimetallic pentalene complex by X-ray methods, $\text{syn}-(\mu-\eta^5:\eta^5\text{-Pn})[\text{Ru}(\text{CO})_2(\text{GeMe}_3)]_2$ (Scheme 1.11),⁸³ which revealed a short distance between the ruthenium atoms (3.05 Å). The pentalene ring is non-planar in this complex, with a fold angle of 7° in the direction away from the Ru_2 core, in order to hold the metals in close enough proximity. However $\text{syn}-(\mu-\eta^5:\eta^5\text{-Pn})[\text{Ru}(\text{CO})_2(\text{GeMe}_3)]_2$ is another example of a complex that according to DFT calculations does not have a metal-metal bond,⁸⁶ and is consistent with a structure-bonding representation that invokes the pentalene ligand as an L_2X donor to each ruthenium (Figure 1.9, right).



Scheme 1.11 Synthesis of ruthenium carbonyl syn-bimetallics.⁸³

Salt metathesis routes are typically used to synthesise syn-bimetallics with multiple metal-metal bonds. For example O'Hare *et al.* reported reaction of $[\text{Li}(\text{DME})]_2\text{Pn}$ with two equivalents of the half-sandwich V(II) complex $[\text{CpVCl}(\text{THF})]_n$, to produce *syn*- $[\text{Cp}_2\text{V}]_2\text{Pn}$ (Scheme 1.12).⁸⁷ The X-ray structure shows a fold angle of 13° and an intermetallic distance of $2.5380(5) \text{ \AA}$, described with support of DFT calculations as a V–V triple bond. Multiple bonds between vanadium atoms are very rare in comparison to wealth of examples in di-chromium complexes.⁸⁸



Scheme 1.12 Synthesis of a $\text{V}\equiv\text{V}$ bonded syn-bimetallic.⁸⁷

Of the $(\text{Pn})_2\text{M}_2$ ‘double-sandwich’ complexes that have been synthesised (Figure 1.10), multiple metal-metal bonding interactions are well described by X-ray and DFT methods for $\text{M} = \text{Cr}, \text{Mo}$, with Pn^+ (Figure 1.10 (b)),⁸⁹⁻⁹¹ and $\text{M} = \text{V}, \text{Cr}$ with Pn^* (Figure 1.10 (c)).¹⁹

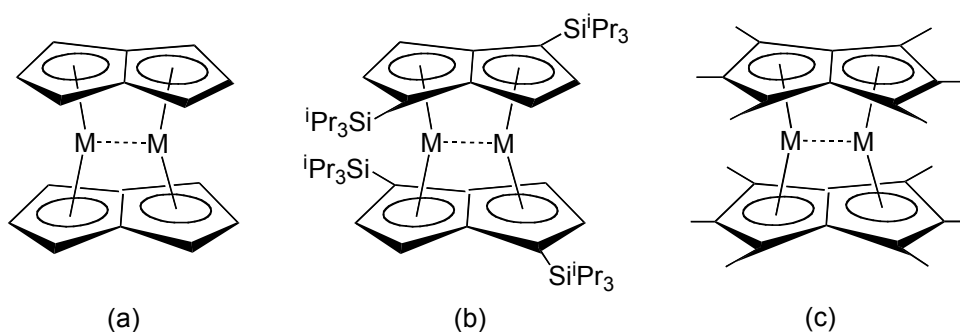
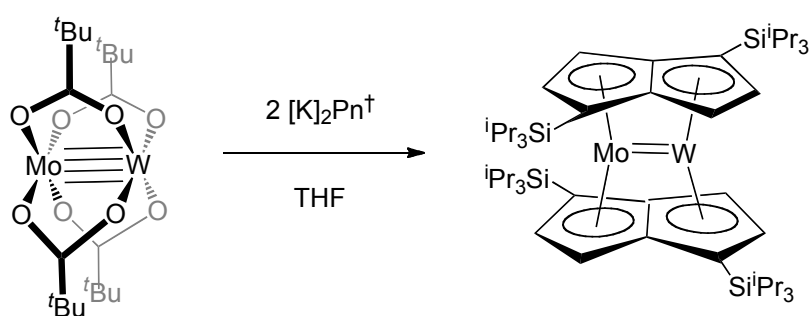


Figure 1.10 Examples of di-metal bis(pentalene) double-sandwich complexes.

The most successful synthetic route to multiple M–M bonded complexes of this type involves a metathesis reaction with a divalent metal salt that already contains a degree of metal-metal interaction. For example the choice of $\text{VCl}_2(\text{DME})$ as a V(II) precursor

with all-bridging chlorides, proved critical in the first synthesis of a di-vanadium double-sandwich complex, $(\mu:\eta^5, \eta^5\text{-Pn}^*)_2\text{V}_2$ by O'Hare *et al.*¹⁹ This strategy was recently extended by Cloke *et al.* for the synthesis of the heteronuclear double-sandwich complex, $(\mu:\eta^5, \eta^5\text{-Pn}^\dagger)_2\text{MoW}$, by reaction of $\text{MoW}(\text{}^t\text{BuCO}_2)_4$ with two equivalents of $[\text{K}_2]\text{Pn}^\dagger$ (Scheme 1.3),⁹² in which the Pn^\dagger dianion serves to 'trap' the M–M' multiple bond present in the 'paddlewheel' carboxylate precursor.⁹³



Scheme 1.13 Synthesis of a heteronuclear double-sandwich complex.⁹²

XRD studies revealed a distance of 2.3638(3) Å between Mo and W atoms, which are disordered over two identical sites. This was described as a molybdenum-tungsten double bond by analogy with the isoelectronic di-molybdenum analogue.⁹⁰ Compounds containing heteronuclear metal-metal bonds have sustained interest in the field of small molecule activation, as M–M' bond polarity can have a profound influence on reactivity.⁹⁴⁻¹⁰⁰

1.2.4 Magnetic interactions and spin transport

There is growing research interest in metallocene based charge-transfer complexes as models for magnetic materials,¹⁰¹⁻¹⁰⁴ which have potential applications in information storage devices and molecular spintronics.¹⁰⁵⁻¹⁰⁸ The ability of the pentalene ligand to promote spin-spin interactions was first reported by Katz *et al.* in the double-sandwich complexes $(\text{Pn})_2\text{M}_2$ for M = Co and Ni (Figure 1.11 (a)).^{109,110} These complexes are diamagnetic in contrast to their mononuclear cyclopentadienyl counterparts, Cp_2Co and Cp_2Ni (Figure 1.11 (b)) which are paramagnetic,^{111,112} with one and two unpaired electrons respectively (Table 1.1).

Table 1.1 Solid state effective magnetic moments (μ_{eff}) for selected sandwich and double-sandwich compounds.

Compound	$\mu_{\text{eff}} / \mu_{\text{B}}^a$	temp range / K	ref
(Cp ^{1,3-<i>t</i>Bu}) ₂ Ti	2.44	5-300	113
(Cp*) ₂ Ti	2.48-2.60	129-298	114
Cp ₂ V	3.78	14-430	115,116
(Cp*) ₂ V	3.68	5-64	117
(Pn*) ₂ V ₂	diamagnetic		19
Cp ₂ Cr	3.20	90-295	115,116
(Cp*) ₂ Cr	1.45	5-130	117
(Pn*) ₂ Cr ₂	1.76 ^b	298	19
(Pn [†]) ₂ Cr ₂	2.12 ^b	298	91
(Cp ^{1,3-{SiMe₃}₂}) ₂ Mn (h.s.)	5.88	5-300	118
(Cp*) ₂ Mn (l.s.)	2.16	4-116	23
(Pn*) ₂ Mn ₂	2.78	4-300	19
(Pn [†]) ₂ Mn	5.15-5.32	4-300	119
Cp ₂ Fe, (Cp*) ₂ Fe	diamagnetic		120,121
Cp ₂ Co	2.04 ^b	83-298	122
Cp* ₂ Co	1.45	5-130	117
(Pn) ₂ Co ₂ , (Pn*) ₂ Co ₂	diamagnetic		19,110
Cp ₂ Ni	2.89	70-300	116
Cp* ₂ Ni	2.93	6-100	117
(Pn) ₂ Ni ₂ , (Pn*) ₂ Ni ₂	diamagnetic		19,109

^a Data obtained from linear section of the Curie-Weiss (χ_{m} vs T) plot.

^b Non-Curie behaviour.

The permethylated analogues $(\text{Pn}^*)_2\text{M}_2$, ($\text{M} = \text{Co}, \text{Ni}$),¹⁹ have been comprehensively characterised, including by XRD studies, and their bonding has been studied by DFT. The X-ray structure of the cobalt complex shows a Co–Co distance of 2.491(2) Å which is in the range of a typical Co–Co single bond, however DFT calculations suggest a π^* -antibonding HOMO and a reduced metal-metal interaction (ground state M–M bond order of -0.59). The nickel complex shows a $\eta^3:\eta^3$ coordination of the metal centres, in a geometry which positions them out of range for metal-metal bonding (Ni–Ni distance = 2.569 Å), supported by DFT calculations (ground state M–M bond order of 0.03). $(\text{Pn}^*)_2\text{Ni}_2$ was also found to have diamagnetic properties, supporting the argument for antiferromagnetic coupling of the d^8 centres *via* ligand orbitals rather than direct metal-metal bonding in this and Katz's unsubstituted double-sandwich complex.

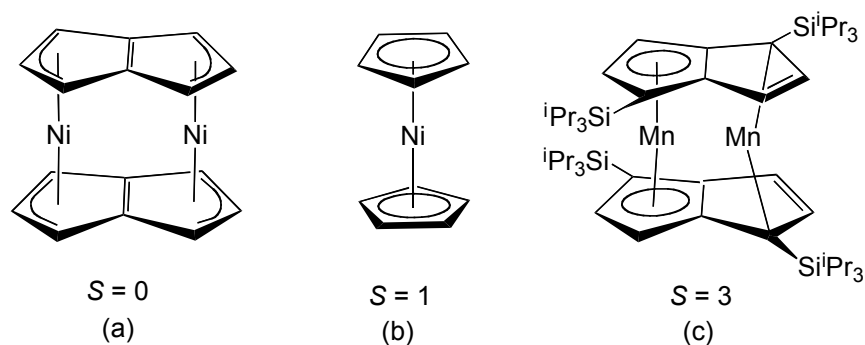


Figure 1.11 Examples of sandwich complexes with different (total) spin angular momentum ($= S$) ground states.

The analogous complexes with silylated pentalene ligands, $(\text{Pn}^\dagger)_2\text{M}_2$, further illustrate the ability of the double-sandwich motif to support metal centres with divergent magnetic properties. Variable temperature magnetic studies on the $\text{M} = \text{Cr}$ complex reveal a spin equilibrium between an $S = 0$ ground state and a thermally populated $S = 1$ excited state.⁹¹ In contrast the $\text{M} = \text{Mn}$ complex (Figure 1.11 (c)) is best described as having an $S = 3$ ground state containing both high spin (h.s.) and low spin (l.s.) manganese.¹¹⁹

Theoretical studies by Zeng *et al.* using the double-sandwich motif in extended 1D organometallic ‘nanowires’ (Figure 1.12, left) have described rich magnetic properties,¹²³ for example the $\text{M} = \text{Mn}$ nanowire is ferromagnetic with strong coupling between M and Pn mainly attributed to a double exchange mechanism.^{124,125}

Molecular spintronic devices, which control the electron current *via* the spin-up and spin-down states in organometallic compounds, require spin signals to be transmitted over long enough distances to allow for spin manipulation.¹⁰⁵ Hence, a ligand that can facilitate through-bond delocalisation of charge and magnetisation would be desirable. Towards these ends, the anti-bimetallic complexes, $\text{Cp}^*\text{M}(\mu\text{-}\eta^5\text{:}\eta^5\text{-Pn})\text{M}'\text{Cp}^*$ were studied by Manriquez *et al.* using SQUID magnetometry.⁵⁹ The hetero-bimetallic $\text{M} = \text{Fe}$, $\text{M}' = \text{Co}$ is paramagnetic at room temperature with an unpaired electron on the cobalt atom, however intermolecular exchange was weak and antiferromagnetically coupled with no cooperative magnetic behavior. In the case of the $\text{Fe}^{\text{III}}\text{-Fe}^{\text{III}}$ di-cation $[\text{Cp}^*\text{Fe}(\mu\text{-}\eta^5\text{:}\eta^5\text{-Pn})\text{FeCp}^*]^{2+}$, an intramolecular ferromagnetic coupling of spins was suggested by variable temperature magnetic data.

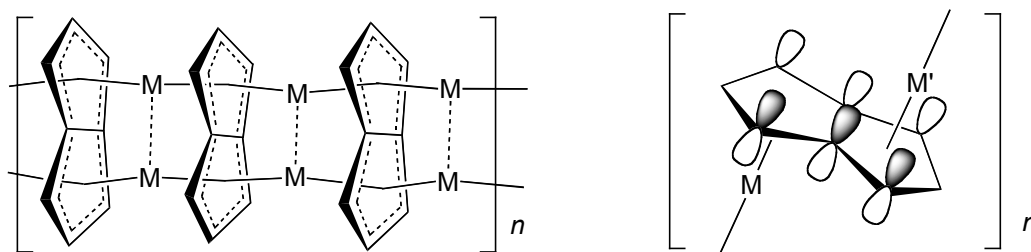


Figure 1.12 Theoretical models for extended organometallic nanowires.

The spin transport properties for anti-bimetallic pentalene complexes have recently been investigated using DFT by Matsuura (Figure 1.12, right),¹²⁶ and it was reported that heterobimetallic systems containing an odd number of electrons exhibit high electronic conduction and good spin filter behavior when sandwiched between two gold electrodes. However experimental evidence to corroborate these theoretical predictions remain lacking, so ultimately the potential applications for these complexes in magnetic materials remain entirely speculative.

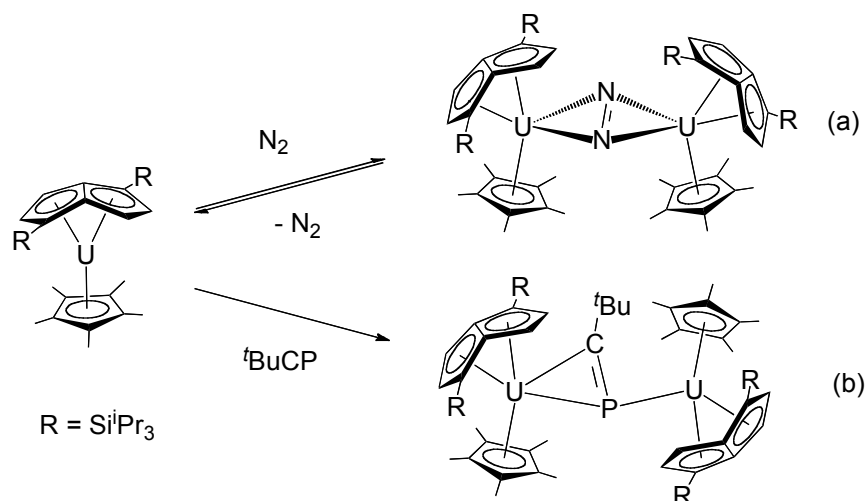
1.2.5 Small molecule activation

In light of global energy demands there is considerable interest in the activation of small molecules (such as CO , CO_2 , N_2 , H_2 and CH_4) for use as chemical feedstocks for industrially important commodity chemicals.¹²⁷⁻¹²⁹ The difficulty in achieving such transformations of small molecules often lies in the kinetic barrier to their activation,

and as a result highly reducing metal complexes are typically employed. Pentalene ligands have shown the ability to stabilise complexes containing highly reactive metal centres, particularly when coordinated in an η^8 -mode to a early transition or f-block metal as previously described.¹ However, reports of small molecule activation in organometallic chemistry of pentalene are limited to a handful of examples.

Cloke *et al.* have reported the reaction of uranium(III) mixed-sandwich complex $(\eta^8\text{-Pn}^\dagger)\text{UCp}^*$ with dinitrogen.¹³⁰ The reaction is reversible and the di-uranium(IV) product, $[(\eta^8\text{-Pn}^\dagger)\text{UCp}^*]_2(\mu\text{-}\eta^2\text{:}\eta^2\text{-N}_2)$, features a 'side-on' bridging N_2 ligand in its molecular structure (Scheme 1.14 (a)). The N–N distance of 1.232(10) Å in this complex is lengthened with respect to free N_2 (1.098 Å)¹³¹ indicating a significant activation resulting in a reduced formal bond order of two, which was supported by a DFT study.

Another example of the reductive capability of $(\eta^8\text{-Pn}^\dagger)\text{UCp}^*$ is found in the recent report of its reaction with the phosphalkyne, $t\text{BuCP}$.¹³² The X-ray structure of the product isolated from this reaction, $[(\eta^8\text{-Pn}^\dagger)\text{UCp}^*]_2(\mu\text{-}\eta^2\text{:}\eta^1\text{-}t\text{BuCP})$, shows a $t\text{BuCP}$ ligand which has been doubly reduced and binds to one of the U(IV) centres in an unprecedented η^2 -mode (Scheme 1.14 (b)).

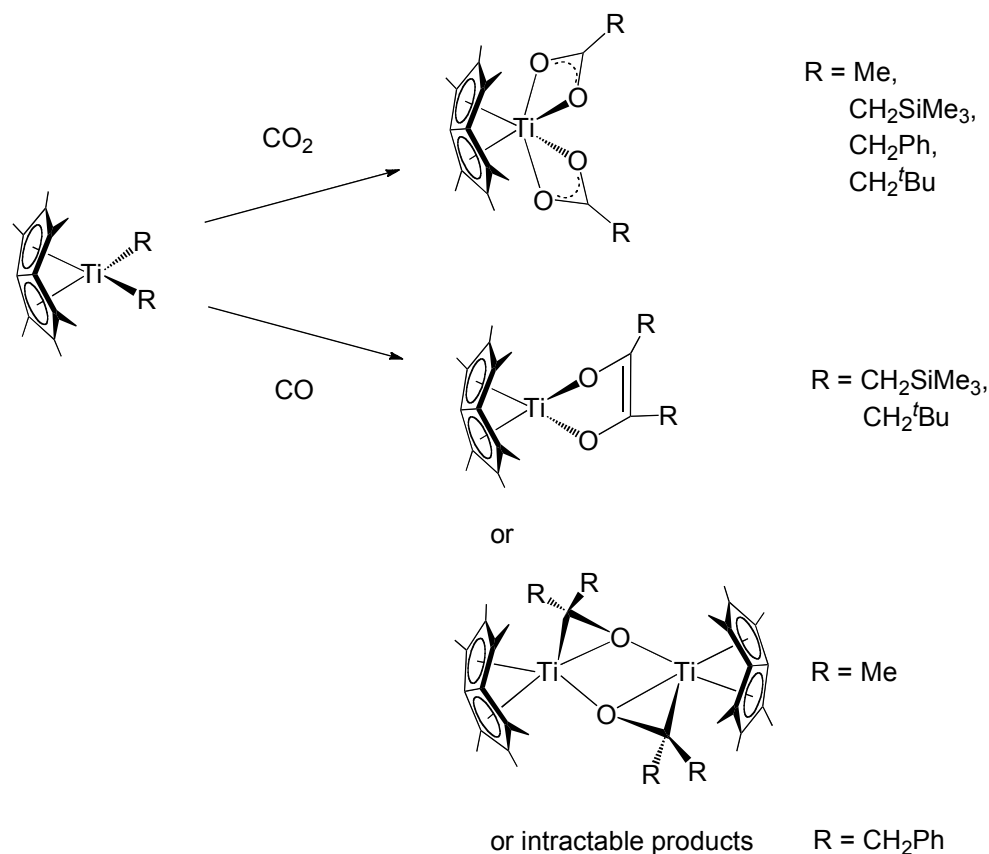


Scheme 1.14 Activation of N_2 and $t\text{BuCP}$ by a U(III) complex.^{130,132}

Recent CV studies by Cloke *et al.* on $(\eta^8\text{-Pn}^\dagger)\text{UCp}^*$ in $[\text{}^n\text{Bu}_4\text{N}][\text{B}(\text{C}_6\text{F}_5)_4]/\text{THF}$ suggest this uranium(III) pentalene complex is *ca.* 0.4 V more reducing than the analogous

complex bearing the isoelectronic 1,4-bis(triisopropylsilyl)cyclooctatetraenyl $[\text{COT}^\dagger]^{2-}$ ligand, $(\eta^8\text{-COT}^\dagger)\text{UCp}^*\{\text{THF}\}$.^{13,133} Furthermore the latter complex shows no reactivity with dinitrogen,^{133,134} consistent with the additional electronic donation provided by the folded η^8 -carbocyclic ligand, Pn^\dagger , as compared with the planar COT^\dagger .

The only other significant contribution to small molecule activation chemistry provided by organometallic pentalene complexes comes from the recent report of the permethylpentalene Ti(IV) dialkyls, $(\eta^8\text{-Pn}^*)\text{TiR}_2$, $\text{R} = \text{Me}$, CH_2Ph , CH_2SiMe_3 and CH_2^tBu , by O'Hare *et al.* and investigations into their reactions with CO_2 , CO and H_2 .⁴ These highly electron deficient 14 VE complexes readily undergo insertion reactions with CO_2 into the Ti–C bond, to yield di-carboxylate complexes, $(\eta^8\text{-Pn}^*)\text{Ti}(\kappa^2\text{-O}_2\text{CR})_2$ which are 18 VE (Scheme 1.15, top). These complexes have been structurally characterised for $\text{R} = \text{Me}$, CH_2Ph and CH_2SiMe_3 , and each show symmetrical bidentate coordination of the RCO_2 units. More interestingly, reactions of these complexes with CO led to direct reductive coupling of CO to give the mono cis-enediolate products, and a rare example of a dimeric titanaoxirane (Scheme 1.15, bottom).



Scheme 1.15 Activation of CO and CO_2 by 14 VE Ti(IV) di-alkyl complexes.⁴

Reactivity of $(\eta^8\text{-Pn}^*)\text{TiR}_2$ with dihydrogen showed more complex results, however reaction of the $\text{R} = \text{CH}_2\text{SiMe}_3$ complex with H_2 led to the isolation of the unusual trimeric cluster, $[(\eta^8\text{-Pn}^*)\text{Ti}(\mu_2\text{-H})]_3(\mu_3\text{-H})$ (Figure 1.13). This intriguing compound was assigned as a formally $\text{Ti}^{\text{III}}/\text{Ti}^{\text{III}}/\text{Ti}^{\text{IV}}$ MV species on the basis of NMR spectroscopy and single crystal XRD evidence.

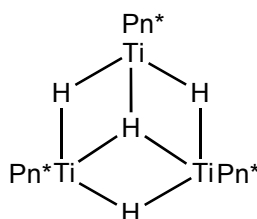


Figure 1.13 Bonding in a $\text{Ti}^{\text{III}}/\text{Ti}^{\text{III}}/\text{Ti}^{\text{IV}}$ mixed-valence hydride cluster.⁴

1.2.6 Catalysis

In over 30 years since Sinn and Kaminsky's discovery that partially hydrolysed Al_2Me_6 , now known as methylaluminoxane (MAO), dramatically improves the activity of group 4 metallocenes for the polymerisation of ethylene and α -olefins,^{135,136} transition metal catalysts bearing cyclopentadienyl ligands have become ubiquitous in homogeneous Ziegler-Natta catalysis research.¹³⁷⁻¹⁴⁰ In light of the intense exploration and commercialisation of new technologies based on single-site olefin polymerisation catalysts and the focus on the design of catalyst precursors, it seems surprising that there are very few catalytic applications of organometallic complexes with pentalene ligands reported in the literature.

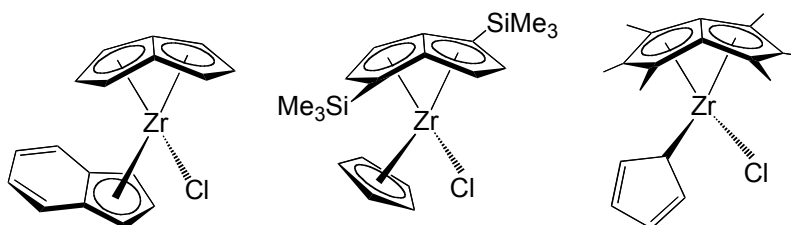
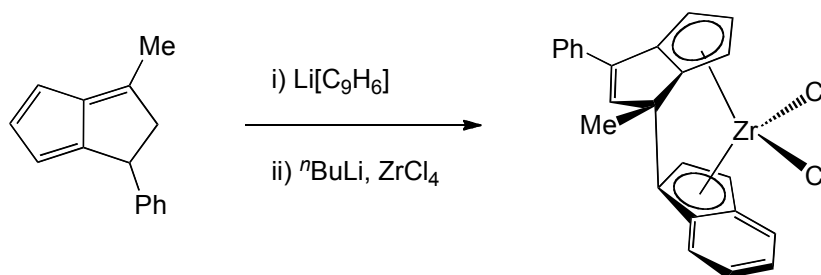


Figure 1.14 Examples of group 4 pentalene complexes tested for olefin polymerisation activity.

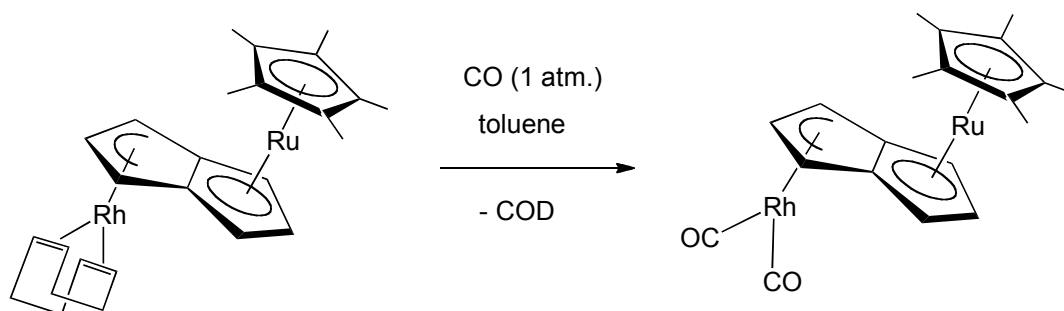
Jonas *et al.* have reported as a patent the ethylene polymerisation activity of $(\eta^8\text{-Pn})\text{-ZrCl}_2$, $(\eta^8\text{-Pn})\text{Zr(allyl)}_2$ and $(\eta^8\text{-Pn})\text{Zr(indenyl)Cl}$,¹⁴¹ and the latter was found to give the best activity of $712.0 \text{ kg(PE) mol(cat)}^{-1} \text{ h}^{-1} \text{ bar}^{-1}$, which is rated as 'high' on the Gibson scale.¹⁴² Cloke *et al.* have also reported patents for the synthesis of group 4 analogues with silylated pentalene ligands, $(\eta^8\text{-Pn}')\text{MCpCl}$ for $\text{M} = \text{Ti, Zr, and } (\eta^8\text{-Pn}')\text{ZrCp}^*\text{Cl}$, and their potential for Ziegler-Natta polymerisation of ethylene in the presence of MAO.¹⁴³ However initial catalytic screenings did not show promising results and were not subsequently optimised. O'Hare *et al.* have tested the aforementioned titanium(IV) permethylpentalene di-alkyl complexes, $(\eta^8\text{-Pn}^*)\text{TiR}_2$ ($\text{R} = \text{Me, CH}_2\text{Ph, CH}_2\text{SiMe}_3$ and CH_2^tBu),⁴ for the homogeneous polymerisation of ethylene in combination with borane and borate activators.¹⁴⁴ Despite the electron deficiency of these 14 VE complexes, the best complex ($\text{R} = \text{CH}_2\text{SiMe}_3$) showed moderate activity on the Gibson scale,¹⁴² with co-catalyst $[\text{Ph}_3\text{C}][\text{B}(\text{C}_6\text{F}_5)_4]$. Recently these researchers have reported the synthesis and characterisation of a series of 18 VE group 4 mixed-ring complexes, $(\eta^8\text{-Pn}^*)\text{MCp}_{2-x}\text{Cl}_x$, ($\text{M} = \text{Ti, Zr, Hf; } x = 0, 1$),³⁴ which are more promising precatalysts for the homogeneous polymerisation of ethylene. The zirconium complexes in the presence of MAO showed very high activity on the Gibson scale,¹⁴² the best performing was $(\eta^8\text{-Pn}^*)\text{ZrCpCl}$ (Figure 1.14, right) which showed activity of $6993 \text{ kg(PE) mol(cat)}^{-1} \text{ h}^{-1} \text{ bar}^{-1}$ at 80°C .

The use of pentalenes in *ansa*-metallocenes has been limited, presumably due to the limited availability of a suitable tethered ligand precursor. However an example of a mixed pentalene-indenyl *ansa*-metallocene has been reported, which was synthesised by reaction of a di-substituted hydropentalene with an indenyl salt to form the annulated ligand *in situ* followed by reaction with ZrCl_4 (Scheme 1.16).^{145,146} This bridged zirconocene has been used in the co-polymerisation of ethylene with cyclic olefins.¹⁴⁷



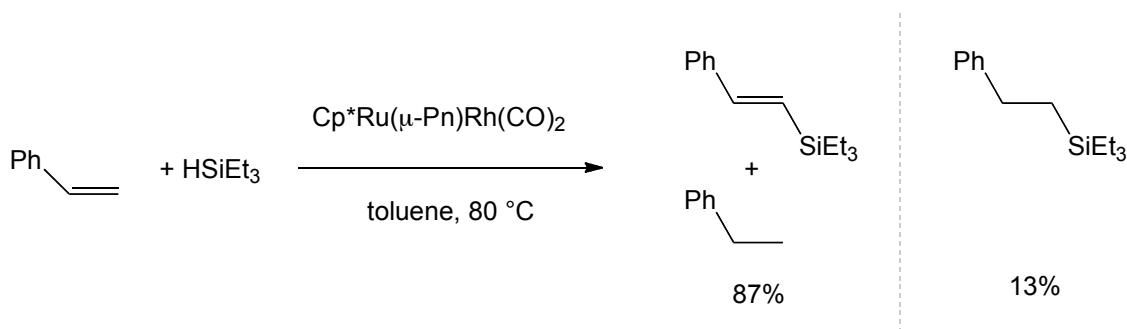
Scheme 1.16 Synthesis of an *ansa*-zirconocene from dihydropentalenes.¹⁴⁵

Outside the field of olefin polymerisation, reports of pentalene complexes with catalytic behavior in the literature are limited to a single case, starting from $\text{Cp}^*\text{Ru}(\mu\text{-}\eta^5\text{:}\eta^3\text{-Pn})\text{-Rh}(\eta^4\text{-COD})$ (COD = 1,5-cyclooctadiene). This asymmetric heterobimetallic complex, was synthesised *via* a stepwise ‘building block’ method from $[\text{Li}][\text{Cp}^*\text{Ru}(\eta^5\text{-Pn})]$ and $[\text{Rh}(\eta^4\text{-COD})\text{Cl}]_2$.^{148,149}



Scheme 1.17 Synthesis of $\text{Cp}^*\text{Ru}(\mu\text{-}\eta^5\text{:}\eta^3\text{-Pn})\text{Rh}(\text{CO})_3$.¹⁴⁸

$\text{Cp}^*\text{Ru}(\mu\text{-}\eta^5\text{:}\eta^3\text{-Pn})\text{Rh}(\eta^4\text{-COD})$ reacts with carbon monoxide, displacing the COD ligand to afford $\text{Cp}^*\text{Ru}(\mu\text{-}\eta^5\text{:}\eta^3\text{-Pn})\text{Rh}(\text{CO})_3$ (Scheme 1.17), which is a relatively unstable species and was characterised solely by IR and NMR spectroscopic methods. This complex is of interest in the context of cooperative interactions between metals, which are known to enhance reactivity in small molecule activation,^{94,150-153} and improve the rate of certain catalytic processes.¹⁵⁴⁻¹⁵⁶ Indeed, $\text{Cp}^*\text{Ru}(\mu\text{-}\eta^5\text{:}\eta^3\text{-Pn})\text{-Rh}(\text{CO})_3$ shows one of the highest activities as a precatalyst for the dehydrogenative silylation of styrene (Scheme 1.18).



Scheme 1.18 Catalytic dehydrogenative silylation of styrene by a Ru/Rh complex.¹⁴⁸

1.3 Aims of This Thesis

This review demonstrates the versatility of the pentalene ligand in its organometallic complexes, which display interesting electronic and magnetic properties and also show novel reactivity. The aim of this thesis is to explore the organometallic chemistry of the 1,4-triisopropylsilyl substituted hydropentalene ($\text{Pn}^{\dagger}\text{H}$) and pentalene ligand (Pn^{\dagger}) with the aforementioned areas of potential application firmly in mind.

1.4 References for Chapter One

1. F. G. N. Cloke, *Pure Appl. Chem.*, 2001, **73**, 233–238.
2. O. T. Summerscales and F. G. N. Cloke, *Coord. Chem. Rev.*, 2006, **250**, 1122–1140.
3. A. E. Ashley, D.Phil Thesis, University of Oxford, 2006.
4. R. T. Cooper, D.Phil Thesis, University of Oxford, 2012.
5. T. Bally, S. Chai, M. Neuenschwander, and Z. Zhu, *J. Am. Chem. Soc.*, 1997, **119**, 1869–1875.
6. P. De Mayo, R. Bloch, and R. A. Marty, *J. Am. Chem. Soc.*, 1971, **93**, 3071–3072.
7. C. Melero, A. Guijarro, and M. Yus, *Dalton Trans.*, 2009, 1286–1289.
8. T. J. Katz and M. Rosenberger, *J. Am. Chem. Soc.*, 1962, **84**, 865–866.
9. T. J. Katz, M. Rosenberger, and R. K. O'Hara, *J. Am. Chem. Soc.*, 1964, **86**, 249–252.
10. M. Jones Jr and L. O. Schwab, *J. Am. Chem. Soc.*, 1968, **90**, 6549–6550.
11. F. G. N. Cloke, M. C. Kuchta, R. M. Harker, P. B. Hitchcock, and J. S. Parry, *Organometallics*, 2000, **19**, 5795–5798.
12. C. J. Rivers, D.Phil Thesis, University of Sussex, 2004.
13. A. Kilpatrick, N. Tsoureas, and F. G. N. Cloke, *Unpublished results*.
14. I. Fleischhauer and U. H. Brinker, *Chem. Ber.*, 1987, **120**, 501–506.
15. S. Jones, P. Roussel, T. Hascall, and D. O'Hare, *Organometallics*, 2006, **25**, 221–229.
16. S. C. Jones, D.Phil Thesis, University of Oxford, 2003.
17. A. E. Ashley, A. R. Cowley, and D. O'Hare, *Chem. Commun.*, 2007, 1512–1514.
18. A. E. Ashley, A. R. Cowley, and D. O'Hare, *Eur. J. Org. Chem.*, 2007, **2007**, 2239–2242.
19. A. E. Ashley, R. T. Cooper, G. G. Wildgoose, J. C. Green, and D. O'Hare, *J. Am. Chem. Soc.*, 2008, **130**, 15662–15677.
20. R. T. Cooper, F. M. Chadwick, A. E. Ashley, and D. O'Hare, *Organometallics*, 2013, **32**, 2228–2233.
21. P. Jutzi, *Comments Inorg. Chem.*, 1987, **6**, 123–144.
22. J. M. Manriquez, D. R. McAlister, E. Rosenberg, A. M. Shiller, K. L. Williamson, S. I. Chan, and J. E. Bercaw, *J. Am. Chem. Soc.*, 1978, **100**, 3078–3083.
23. J. C. Smart and J. L. Robbins, *J. Am. Chem. Soc.*, 1978, **100**, 3936–3937.
24. R. B. King, *Coord. Chem. Rev.*, 1976, **20**, 155–169.

25. J. E. Bercaw, R. H. Marvich, L. G. Bell, and H. H. Brintzinger, *J. Am. Chem. Soc.*, 1972, **94**, 1219–1238.
26. H. Brintzinger and J. E. Bercaw, *J. Am. Chem. Soc.*, 1971, **93**, 2045–2046.
27. I. Willner and M. Rabinovitz, *J. Am. Chem. Soc.*, 1978, **100**, 337–338.
28. I. Willner, J. Y. Becker, and M. Rabinovitz, *J. Am. Chem. Soc.*, 1979, **101**, 395–401.
29. M. Saito, M. Nakamura, T. Tajima, and M. Yoshioka, *Angew. Chem. Int. Ed.*, 2007, **46**, 1504–1507.
30. T. Kuwabara, K. Ishimura, T. Sasamori, N. Tokitoh, and M. Saito, *Chem.–Eur. J.*, 2014, **20**, 7571–7575.
31. H. Li, B. Wei, L. Xu, W.-X. Zhang, and Z. Xi, *Angew. Chem. Int. Ed. Engl.*, 2013, **52**, 10909.
32. M. Green, *J. Organomet. Chem.*, 1995, **500**, 127–148.
33. R. D. Shannon, *Acta. Crystallogr. Sect. A.*, 1976, **32**, 751–767.
34. F. M. Chadwick, R. T. Cooper, A. E. Ashley, J. C. Buffet, and D. M. O'Hare, *Organometallics*, 2014, **33**, 3775–3785.
35. F. G. N. Cloke, P. B. Hitchcock, M. C. Kuchta, and N. A. Morley-Smith, *Polyhedron*, 2004, **23**, 2625–2630.
36. K. Jonas, P. Kolb, G. Kollbach, and B. Gabor, *Angew. Chem. Int. Ed. Engl.*, 1997, **36**, 1714.
37. A. E. Ashley, D.Phil Thesis, University of Oxford, 2006.
38. J. C. Green, M. L. H. Green, and G. Parkin, *Chem. Commun.*, 2012, **48**, 11481–11503.
39. M. T. Garland, J.-Y. Saillard, I. Chavez, B. Oelckers, and J. M. Manriquez, *J. Mol. Struct. Theochem*, 1995, **390**, 199–208.
40. E. E. Bunel, L. Valle, N. L. Jones, P. J. Carroll, C. Barra, M. Gonzalez, N. Munoz, G. Visconti, A. Aizman, and J. M. Manriquez, *J. Am. Chem. Soc.*, 1988, **110**, 6596–6598.
41. A. Alvarez-Larena, J. L. Brianso, J. F. Piniella, J. Farran, J. M. Manriquez, I. Chavez, B. Oelckers, E. Molins, and C. Miravittles, *Acta Crystallogr., Sect. C: Cryst. Struct. Commun.*, 1996, **52**, 2754–2757.
42. J. M. O'Connor and C. P. Casey, *Chem. Rev.*, 1987, **87**, 307–318.
43. A. Miyake and A. Kanai, *Angew. Chem. Int. Ed. Engl.*, 1971, **10**, 801–802.
44. T. J. Katz and M. Rosenberger, *J. Am. Chem. Soc.*, 1963, **85**, 2030–2031.
45. E. Molins, W. Maniukiewicz, C. Miravittles, M. Mas, J. M. Manriquez, I. Chavez, B. Oelckers, J. Farran, and J. L. Brianso, *Acta Crystallogr., Sect. C: Cryst. Struct. Commun.*, 1996, **52**, 2414–2416.
46. O. T. Summerscales, D. R. Johnston, F. G. N. Cloke, and P. B. Hitchcock, *Organometallics*, 2008, **27**, 5612–5618.
47. N. A. Ustynyuk, L. N. Novikova, V. K. Bel'skii, Y. F. Oprunenko, S. G. Malyugina, O. I. Trifonova, and Y. A. Ustynyuk, *J. Organomet. Chem.*, 1985, **294**, 31–44.
48. Y. A. Ustynyuk, A. K. Shestakova, V. A. Chertkov, N. N. Zemlyansky, I. V. Borisova, A. I. Gusev, E. B. Tchuklanova, and E. A. Chernyshev, *J. Organomet. Chem.*, 1987, **335**, 43–57.
49. S. Barlow and D. O'Hare, *Chem. Rev.*, 1997, **97**, 637–667.
50. C. Lapinte, *Coord. Chem. Rev.*, 1998, **178–180**, 431–509.
51. A. Ceccon, S. Santi, L. Orian, and A. Bisello, *Coord. Chem. Rev.*, 2004, **248**, 683–724.
52. P. Aguirre-Etcheverry and D. O'Hare, *Chem. Rev.*, 2010, **110**, 4839–4864.

53. T. J. Peckham, P. Gbmez-Elipe, and I. Manners, in *Metallocenes*, Wiley-VCH Verlag GmbH, 2008, pp. 723–772.
54. M. B. Robin and P. Day, *Mixed Valence Chemistry-A Survey and Classification*, Elsevier, 1968, vol. 10.
55. P. Day, N. S. Hush, and R. J. H. Clark, *Philos. Trans. R. Soc. A*, 2008, **366**, 5–14.
56. P. J. Low, *Dalton Trans.*, 2005, 2821–2824.
57. M. Parthey and M. Kaupp, *Chem. Soc. Rev.*, 2014, **43**, 5067–5088.
58. J. E. Sutton and H. Taube, *Inorg. Chem.*, 1981, **20**, 3125–3134.
59. J. M. Manriquez, M. D. Ward, W. M. Reiff, J. C. Calabrese, N. L. Jones, P. J. Carroll, E. E. Bunel, and J. S. Miller, *J. Am. Chem. Soc.*, 1995, **117**, 6182–6193.
60. B. Oelckers, I. Chávez, J. M. Manriquez, and E. Roman, *Organometallics*, 1993, **12**, 3396–3397.
61. Y. Portilla, I. Chavez, V. Arancibia, B. Loeb, J. M. Manríquez, A. Roig, and E. Molins, *Inorg. Chem.*, 2002, **41**, 1831–1836.
62. S. C. Jones, T. Hascall, S. Barlow, and D. O'Hare, *J. Am. Chem. Soc.*, 2002, **124**, 11610–11611.
63. O. T. Summerscales, S. C. Jones, F. G. N. Cloke, and P. B. Hitchcock, *Organometallics*, 2009, **28**, 5896–5908.
64. T. Tsuji, N. Hosoya, S. Fukazawa, R. Sugiyama, T. Iwasa, H. Tsunoyama, H. Hamaki, N. Tokitoh, and A. Nakajima, *J. Phys. Chem. C*, 2014, **118**, 5896–5907.
65. N. Hosoya, K. Yada, T. Masuda, E. Nakajo, S. Yabushita, and A. Nakajima, *J. Phys. Chem. A*, 2014, **118**, 3051–3060.
66. N. Ishikawa, T. Iino, and Y. Kaizu, *J. Am. Chem. Soc.*, 2002, **124**, 11440–11447.
67. J. J. Le Roy, M. Jeletic, S. I. Gorelsky, I. Korobkov, L. Ungur, L. F. Chibotaru, and M. Murugesu, *J. Am. Chem. Soc.*, 2013, **135**, 3502–3510.
68. N. Magnani, C. Apostolidis, A. Morgenstern, E. Colineau, J.-C. Griveau, H. Bolvin, O. Walter, and R. Caciuffo, *Angew. Chem. Int. Ed. Engl.*, 2011, **50**, 1696–1698.
69. S.-D. Jiang, B.-W. Wang, H.-L. Sun, Z.-M. Wang, and S. Gao, *J. Am. Chem. Soc.*, 2011, **133**, 4730–4733.
70. G. A. Molander and J. A. C. Romero, *Chem. Rev.*, 2002, **102**, 2161–2186.
71. S. Kobayashi, M. Sugiura, H. Kitagawa, and W. W.-L. Lam, *Chem. Rev.*, 2002, **102**, 2227–2302.
72. A. Avdeef, K. Raymond, and K. Hodgson, *Inorg. Chem.*, 1972, **11**, 1083–1088.
73. A. M. Nonat, S. J. Quinn, and T. Gunnlaugsson, *Inorg. Chem.*, 2009, **48**, 4646–4648.
74. S. Marks, J. G. Heck, M. H. Habicht, P. Oña-Burgos, C. Feldmann, and P. W. Roesky, *J. Am. Chem. Soc.*, 2012, **134**, 16983–16986.
75. W. Reiff, J. Manriquez, M. Ward, and J. S. Miller, *Mol. Cryst. Liquid Cryst.*, 1989, **176**, 423–428.
76. W. Reiff, J. Manriquez, and J. S. Miller, *Hyperfine Interact.*, 1990, **53**, 397–402.
77. M. Watanabe and H. Sano, *Bull. Chem. Soc. Jpn. Lett.*, 1998, **63**, 777–784.
78. D. F. Hunt and J. W. Russell, *J. Am. Chem. Soc.*, 1972, **94**, 7198–7199.
79. W. Weidemüller and K. Hafner, *Angew. Chem. Int. Ed. Engl.*, 1973, **12**, 925–925.

80. E. B. Fleischer, A. L. Stone, R. B. K. Dewar, J. D. Wright, C. E. Keller, and R. Pettit, *J. Am. Chem. Soc.*, 1966, **88**, 3158–3159.
81. A. E. Ashley, G. Balazs, A. R. Cowley, J. C. Green, and D. O'Hare, *Organometallics*, 2007, **26**, 5517–5521.
82. S. A. R. Knox and F. G. A. Stone, *Acc. Chem. Res.*, 1974, **7**, 321–328.
83. A. Brookes, J. Howard, S. A. R. Knox, F. G. A. Stone, and P. Woodward, *J. Chem. Soc., Chem. Commun.*, 1973, 587–589.
84. J. A. K. Howard, S. A. R. Knox, F. G. A. Stone, A. C. Szary, and P. Woodward, *J. Chem. Soc., Chem. Commun.*, 1974, 788–789.
85. J. A. K. Howard, S. A. R. Knox, V. Riera, F. G. A. Stone, and P. Woodward, *J. Chem. Soc., Chem. Commun.*, 1974, 452–453.
86. S. Bendjaballah, S. Kahlal, K. Costuas, E. Bévilion, and J.-Y. Saillard, *Chem.–Eur. J.*, 2006, **12**, 2048–2065.
87. S. C. Jones and D. O'Hare, *Chem. Commun.*, 2003, 2208–2209.
88. F. A. Cotton, C. A. Murillo, and R. A. Walton, *Multiple Bonds Between Metal Atoms*, Clarendon Press, 3rd edn. 2005.
89. M. Kuchta and F. G. N. Cloke, *Organometallics*, 1998, **17**, 1934–1936.
90. F. G. N. Cloke, J. C. Green, and C. N. Jardine, *Organometallics*, 1999, **18**, 1087–1090.
91. G. Balazs, F. G. N. Cloke, L. Gagliardi, J. C. Green, A. Harrison, P. B. Hitchcock, A. R. M. Shahi, and O. T. Summerscales, *Organometallics*, 2008, **27**, 2013–2020.
92. A. D. Smith, M.Chem. Dissertation, University of Sussex, 2012.
93. V. Katovic and R. E. McCarley, *J. Am. Chem. Soc.*, 1978, **100**, 5586–5587.
94. D. W. Stephan, *Coord. Chem. Rev.*, 1989, **95**, 41–107.
95. D. G. Dick and D. W. Stephan, *Organometallics*, 1990, **9**, 1910–1916.
96. A. M. Baranger and R. G. Bergman, *J. Am. Chem. Soc.*, 1994, **116**, 3822–3835.
97. T. A. Hanna, A. M. Baranger, and R. G. Bergman, *J. Am. Chem. Soc.*, 1995, **117**, 11363–11364.
98. U. Jayarathne, S. R. Parmelee, and N. P. Mankad, *Inorg. Chem.*, 2014, **53**, 7730–7737.
99. J. P. Krogman, B. M. Foxman, and C. M. Thomas, *J. Am. Chem. Soc.*, 2011, **133**, 14582–14585.
100. C. M. Thomas, J. W. Napoline, G. T. Rowe, and B. M. Foxman, *Chem. Commun.*, 2010, **46**, 5790–5792.
101. J. S. Miller, D. A. Dixon, R. S. McLean, D. M. Groski, R. B. Flippen, J. M. Manriquez, G. T. Yee, K. S. Narayan, and A. J. Epstein, *Adv. Mater.*, 1991, **3**, 309–311.
102. J. S. Miller, C. Vazquez, R. S. McLean, W. M. Reiff, A. Aumüller, and S. Hünig, *Adv. Mater.*, 1993, **5**, 448–450.
103. G. Wang, C. Slebodnick, R. J. Butcher, M. C. Tam, T. D. Crawford, and G. T. Yee, *J. Am. Chem. Soc.*, 2004, **126**, 16890–16895.
104. J. S. Miller and A. J. Epstein, *Angew. Chem. Int. Ed. Engl.*, 1994, **33**, 385–415.
105. L. Bogani and W. Wernsdorfer, *Nat. Mater.*, 2008, **7**, 179–186.
106. C. Felser, G. H. Fecher, and B. Balke, *Angew. Chem. Int. Ed.*, 2007, **46**, 668–699.
107. A. R. Rocha, V. M. García-Suárez, S. W. Bailey, C. J. Lambert, J. Ferrer, and S. Sanvito, *Nat. Mater.*, 2005, **4**, 335–339.
108. S. A. Wolf, *Science*, 2001, **294**, 1488–1495.
109. T. J. Katz and N. Acton, *J. Am. Chem. Soc.*, 1972, **94**, 3281–3283.

110. T. J. Katz, N. Acton, and J. McGinnis, *J. Am. Chem. Soc.*, 1972, **94**, 6205–6206.
111. E. O. Fischer and W. Pfab, *Z. Naturforsch. B*, 1952, **7**, 377–379.
112. C. Elschenbroich and A. Salzer, *Organometallics: a Concise Introduction*, Wiley-VCH, 3rd edn. 1989.
113. M. D. Walter, C. D. Sofield, and R. A. Andersen, *Organometallics*, 2008, **27**, 2959–2970.
114. J. E. Bercaw, *J. Am. Chem. Soc.*, 1974, **96**, 5087–5095.
115. H. Leipfinger, *Z. Naturforsch. B*, 1958, **13**, 53–54.
116. H. P. Fritz and K. E. Schwarzhans, *J. Organomet. Chem.*, 1964, **1**, 208–211.
117. J. L. Robbins, N. Edelstein, B. Spencer, and J. C. Smart, *J. Am. Chem. Soc.*, 1982, **104**, 1882–1893.
118. M. D. Walter, C. D. Sofield, C. H. Booth, and R. A. Andersen, *Organometallics*, 2009, **28**, 2005–2019.
119. G. Balazs, F. G. N. Cloke, A. Harrison, P. B. Hitchcock, J. Green, and O. T. Summerscales, *Chem. Commun.*, 2007, 873–875.
120. T. J. Kealy and P. L. Pauson, *Nature*, 1951, **168**, 1039–1040.
121. R. B. King and M. B. Bisnette, *J. Organomet. Chem.*, 1967, **8**, 287–297.
122. K. R. Gordon and K. D. Warren, *Inorg. Chem.*, 1978, **17**, 987–994.
123. X. Wu and X. C. Zeng, *J. Am. Chem. Soc.*, 2009, **131**, 14246–14248.
124. C. Zener, *Phys. Rev.*, 1951, **82**, 403–405.
125. K. Sato, P. H. Dederichs, H. Katayama-Yoshida, and J. Kudrnovský, *J. Phys.: Condens. Matter*, 2004, **16**, S5491–S5497.
126. Y. Matsuura, *Solid State Commun.*, 2011, **151**, 1877–1880.
127. M. Aresta, *Carbon Dioxide as Chemical Feedstock*, Wiley, 2010.
128. G. A. Olah, *Angew. Chem. Int. Ed. Engl.*, 2005, **44**, 2636–2639.
129. W. B. Tolman, Ed., *Activation of Small Molecules: Organometallic and Bioinorganic Perspectives*, Wiley VCH, 2007.
130. F. G. N. Cloke and P. B. Hitchcock, *J. Am. Chem. Soc.*, 2002, **124**, 9352–9353.
131. K. P. Huber and G. Herzberg, *Molecular Spectra and Molecular Structure. IV. Constants of Diatomic Molecules*, Van Nostrand Reinhold Co., 1979.
132. N. Tsoureas, A. F. R. Kilpatrick, O. T. Summerscales, J. F. Nixon, F. G. N. Cloke, and P. B. Hitchcock, *Eur. J. Inorg. Chem.*, 2013, 4085–4089.
133. O. Summerscales, F. G. N. Cloke, P. Hitchcock, J. Green, and N. Hazari, *Science*, 2006, **311**, 829–831.
134. O. T. Summerscales, D.Phil Thesis, University of Sussex, 2007.
135. A. Andresen, H.-G. Cordes, J. Herwig, W. Kaminsky, A. Merck, R. Mottweiler, J. Pein, H. Sinn, and H.-J. Vollmer, *Angew. Chem.*, 1976, **88**, 689–690.
136. H. Sinn and W. Kaminsky, *Adv. Organomet. Chem.*, 1980, **18**, 99–149.
137. H. G. Alt and A. Köppl, *Chem. Rev.*, 2000, **100**, 1205–1222.
138. G. W. Coates, *J. Chem. Soc., Dalton Trans.*, 2002, 467–475.
139. B. Cornils, W. A. Herrmann, M. Beller, and R. A. Paciello, Eds., *Applied Homogeneous Catalysis with Organometallic Compounds: A Comprehensive Handbook in Three Volumes*, Wiley VCH, 3rd edn. 2012.
140. W. Kaminsky, Ed., *Polyolefins: 50 years after Ziegler and Natta I*, Springer, Berlin, Heidelberg, 2013, vol. 257.
141. K. Jonas, P. Kolb, and G. Kollbach, *US Pat. 5959132 A*, 1999.
142. G. J. Britovsek, V. C. Gibson, and D. F. Wass, *Angew. Chem. Int. Ed. Engl.*, 1999, **38**, 428–447.
143. F. G. N. Cloke and J. S. Parry, *Pat. App. WO1999007716 A1*, 1999.

- 144. E. Y. Chen and T. J. Marks, *Chem. Rev.*, 2000, **100**, 1391–1434.
- 145. G. G. Hlatky, *Coord. Chem. Rev.*, 1999, **181**, 243–296.
- 146. M. Aulbach, F. Kuber, M. Riedel, and F. Helmer-Metzmann, *US Pat. 6063949 A*, 1996.
- 147. F. Helmer-Metzmann, F. Osan, and M. Riedel, *Patent App. CA2179355 A1*, 1996.
- 148. F. Burgos, I. Chavez, and J. Manriquez, *Organometallics*, 2001.
- 149. F. Burgos, V. Arancibia, J. M. Manríquez, and I. Chávez, *Bol. Soc. Chil. Quím.*, 2000, **45**, 621–628.
- 150. R. M. Bullock and C. P. Casey, *Acc. Chem. Res.*, 1987, **20**, 167–173.
- 151. N. Wheatley and P. Kalck, *Chem. Rev.*, 1999, **99**, 3379–3420.
- 152. L. Gade, *Angew. Chem. Int. Ed. Engl.*, 2000, **39**, 2658–2678.
- 153. V. Ritleng and M. J. Chetcuti, *Chem. Rev.*, 2007, **107**, 797–858.
- 154. M. Shibasaki and Y. Yamamoto, *Bimetallic Catalysts in Organic Synthesis Chemistry*, Wiley VCH, 2004.
- 155. J. I. van der Vlugt, *Eur. J. Inorg. Chem.*, 2011, **2012**, 363–375.
- 156. B. G. Cooper, J. W. Napoline, and C. M. Thomas, *Catal. Rev.*, 2012, **54**, 1–40.

2 CHAPTER TWO: Electrochemical and Magnetic Studies of f-Block Pentalene Complexes

2.1 Introduction

This chapter describes studies towards the synthesis and characterisation of triple-decker complexes using the silylated pentalene ligand $[\text{C}_8\text{H}_4\{\text{Si}^i\text{Pr}_{3-1,4}\}_2]^{2-}$ ($= \text{Pn}^\dagger$) to bridge f-block metals in homo-bimetallics capped with $[\text{C}_5\text{Me}_5]$ ($= \text{Cp}^*$) ligands. Magnetic measurements and electrochemical methods are used to investigate the extent of intermetallic communication in these systems, which can be studied as molecular models for organolanthanide based conducting materials^{1,2} and (polynuclear) single molecule magnets.³⁻⁶

Cyclic voltammetry (CV) is a powerful technique for investigating the electronic properties of organometallic complexes.⁷ In f-element chemistry CV is commonly used to rationalise trends in reactivity arising from a different set of ligands on a common metal or vice versa. The thermodynamic trend in $3+/2+$ reduction potentials for Yb and Sm complexes is expected to follow that of the Ln^{3+} ions in acidic aqueous media,⁸ with the latter metal *ca.* 0.5 V more reducing than the former. However, direct observation of the reverse process, i.e. $\text{Ln}^{2+/3+}$ oxidation, is complicated by the high reactivity of $\text{Ln}(\text{II})$ complexes and the fact that the expected redox event lies outside the potential window of many solvent/electrolyte systems commonly used in organotransition metal chemistry. Nonetheless mid-peak potential ($E_{1/2}$) values have been determined by CV in select examples of $\text{Ln}(\text{II})$ metallocenes which show appreciable stability in the chosen electrolytic medium (Table 2.1).

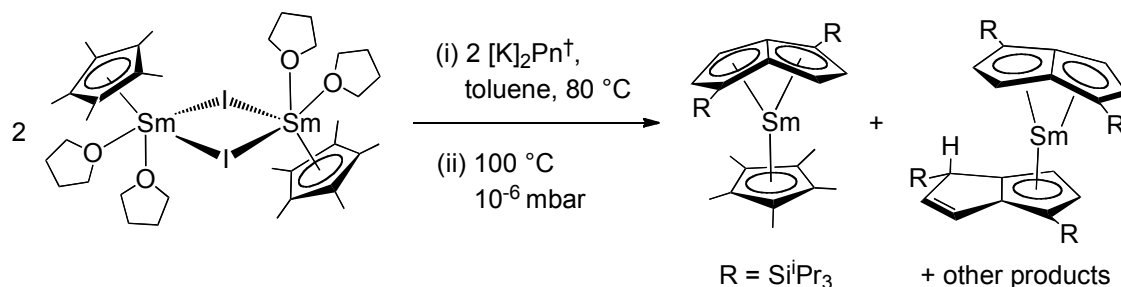
Table 2.1 Mid-peak potentials ($E_{1/2}$) vs $\text{FcCp}_2^{+/0}$ of the $\text{Ln}(\text{III})/\text{Ln}(\text{II})$ couple in divalent lanthanide metallocenes with a $[\text{nBu}_4\text{N}][\text{A}]$ supporting electrolyte.

Compound	$E_{1/2}(\text{Ln}^{3+/2+}) / \text{V}$	solvent	electrolyte $[\text{A}]^-$	ref
Cp^*_2Yb	-1.48	THF	$[\text{B}(\text{C}_6\text{F}_5)_4]$	9
$(\text{Cp}^{\text{Me}_4\text{Et}})_2\text{Sm}$	-2.12	THF	$[\text{B}(\text{C}_6\text{F}_5)_4]$	10
Cp^*_2Yb	-1.78	MeCN	$[\text{PF}_6]$	11
Cp^*_2Eu	-1.22	MeCN	$[\text{PF}_6]$	11
Cp^*_2Sm	-2.41	MeCN	$[\text{PF}_6]$	11

2.2 Anti-Bimetallic Complexes of the f-Block Metals

As described in chapter one, Cloke *et al.* have studied the anti-bimetallic complexes of the divalent lanthanides $[\text{Cp}^*\text{Ln}(\text{THF})]_2(\mu\text{:}\eta^5, \eta^5\text{-Pn}^\dagger)$ $\text{Ln} = \text{Yb}, \text{Eu}$ by CV, which showed some evidence for through ligand Ln–Ln coupling for $\text{Ln} = \text{Yb}$.¹² Attempts to prepare a mixed-valence species chemically were hampered by the poor solubility of $[\text{Cp}^*\text{Yb}(\text{THF})]_2(\mu\text{:}\eta^5, \eta^5\text{-Pn}^\dagger)$, even in strongly coordinating solvents such as THF and DME, a problem that was sought to be remedied by the synthesis of base-free analogues.

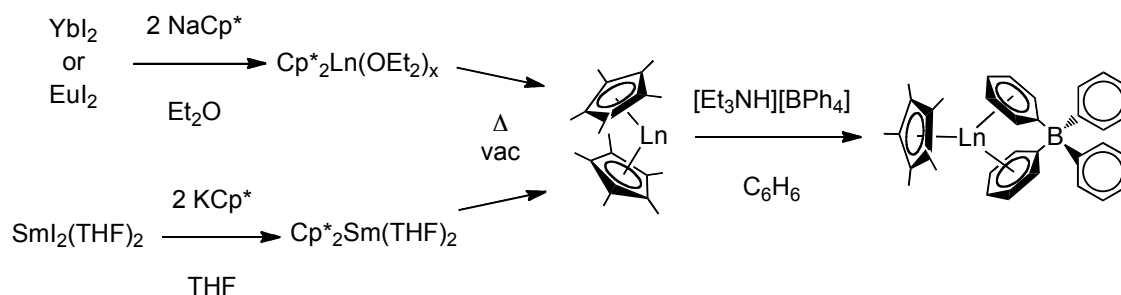
Attempts to prepare the analogous $\text{Ln} = \text{Sm}$ anti-bimetallic by a similar synthetic route, yielded instead the monomeric sandwich complexes $(\eta^8\text{-Pn}^\dagger)\text{SmCp}^*$ and $(\eta^8\text{-Pn}^\dagger)\text{Sm}(\eta^5\text{-Pn}^\dagger\text{H})$ and the mixed-valence cluster $[\text{Cp}^*_6\text{Sm}_6(\text{OMe})_8\text{O}][\text{K}(\text{THF})_6]$ *via* solvent activation of THF (Scheme 2.1).¹² It was suggested that the strongly reducing nature of $\text{Sm}(\text{II})$ and the smaller size of this ion when compared to the larger, less reducing $\text{Eu}(\text{II})$ and $\text{Yb}(\text{II})$, made it better stabilised, electronically and sterically, in the +3 oxidation state with Pn^\dagger . Furthermore, the half-sandwich reagent used in this reaction $[\text{Cp}^*\text{Sm}(\mu\text{-I})(\text{THF})_2]_2$ possesses a coordinated THF molecule which can be non-innocent in reactions with highly reducing metal centres.^{13–15}



Scheme 2.1 Synthesis of samarium(III) pentalene sandwich compounds.¹²

Recently the synthesis of mono- Cp^* lanthanide(II) tetraphenylborate complexes was reported by Evans *et al.* (Scheme 2.2).^{16,17} Complexes of the type $\text{Cp}^*\text{Ln}(\mu\text{-}\eta^6\text{:}\eta^1\text{-Ph})_2\text{-BPh}_2$ ($\text{Ln} = \text{Yb}, \text{Eu}$ and Sm) are base-free and readily soluble in arene solvents, and therefore present alternative half-sandwich precursors to unsolvated $\text{Ln}(\text{II})$ anti-bimetallics *via* salt metathesis elimination of $[\text{M}][\text{BPh}_4]$ (e.g. $\text{M}^+ = \text{K}^+$).¹⁸ The half-sandwich synthons $\text{Cp}^*\text{Ln}(\text{BPh}_4)$, for $\text{Ln} = \text{Yb}$ and Eu , were prepared *via* the

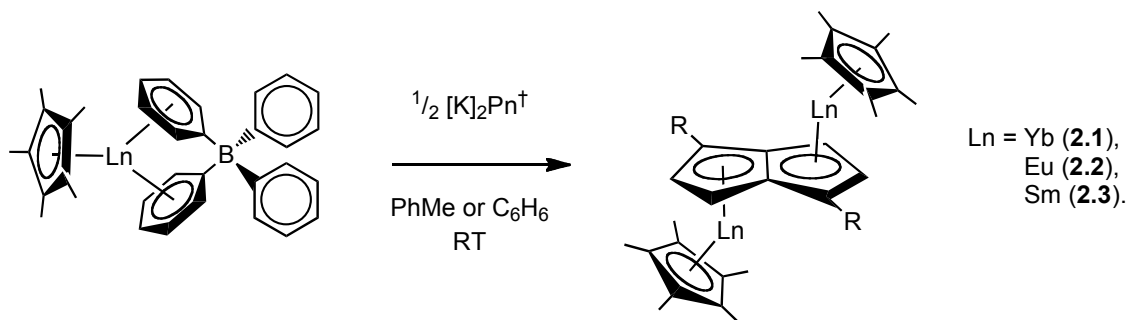
corresponding unsolvated metallocenes,^{19,20} in 46% and 59% overall yield with respect to LnI₂. The Sm(II) analogue, Cp*Sm(BPh₄), was synthesised by a similar route in 31% overall yield with respect to SmI₂(THF)₂.



Scheme 2.2 Synthesis of mono-Cp* Ln(II) tetraphenylborate complexes.^{19,20}

2.2.1 Synthesis of [Cp*Ln]₂(μ-Pn[†]) complexes

The synthesis of the unsolvated triple-decker metallocenes, [Cp*Ln]₂(μ-Pn[†]) (Ln = Yb (**2.1**), Eu (**2.2**) and Sm (**2.3**)), was achieved by reaction of Cp*Ln(BPh₄) with half an equivalent of the pentalene dianion [K]₂Pn[†] in toluene or benzene (Scheme 2.3).



Scheme 2.3 General synthesis of [Cp*Ln]₂(μ-Pn[†]). R = SiⁱPr₃.

This general procedure, and subsequent work-up and recrystallisation from non-coordinating solvents, afforded the base free compounds **2.1**, **2.2** and **2.3** in 61, 68 and 46% yields respectively. The relatively poor yield of the Sm(II) bimetallic may be explained by a secondary product which was isolated in 22% yield, and identified by mass spectrometry (EI) and ¹H NMR spectroscopy as the known mixed-sandwich

complex $(\eta^8\text{-Pn}^\dagger)\text{SmCp}^*$.²¹ An NMR scale reaction of a 2:1 mixture of $\text{Cp}^*\text{Sm}(\text{BPh}_4)$ and $[\text{K}]_2\text{Pn}^\dagger$ in C_6D_6 showed ^1H signals of both **2.2** and $(\eta^8\text{-Pn}^\dagger)\text{SmCp}^*$ after 12 h, indicating that formation of the Sm(III) by-product is inherent in the reaction conditions, rather than through adventitious oxidation. Gratifyingly, the two products can be separated by fractional crystallisation due to the lower solubility of the bimetallic complex **2.3** in pentane. The optimised yield (46%) was obtained by slow addition of the $\text{Cp}^*\text{Sm}(\text{BPh}_4)$ solution to a concentrated solution of $[\text{K}]_2\text{Pn}^\dagger$, and since **2.3** was found to be temperature sensitive, minimising the time the reaction mixture was kept at room temperature (< 12 h) proved beneficial.

2.2.2 Characterisation of $[\text{Cp}^*\text{Yb}]_2(\mu\text{:}\eta^5, \eta^5\text{-Pn}^\dagger)$ (**2.1**)

Compound **2.1** was isolated from tetramethylsilane as a brown crystalline solid, which was characterised by spectroscopic and analytical methods. The co-crystallised solvent in the molecular structure determined by single crystal X-ray diffraction (Section 2.2.5) was lost from the bulk solid after rigorous drying *in vacuo*, as confirmed by microanalysis. Complex **2.1** was found to be diamagnetic, consistent with a ground state $4f^{14}$ configuration for each Yb(II) centre, and displays sharp peaks in its multinuclear (^1H , ^{13}C , ^{29}Si , ^{171}Yb) NMR spectra in C_6D_6 at 303 K. The ^1H NMR spectrum contains two doublet signals assigned to the aromatic Pn^\dagger ring protons, and a singlet due to the Cp^* CH_3 groups. Furthermore the triisopropylsilyl groups appear as a septet and a doublet for the CH and CH_3 groups respectively in the ^1H spectrum, while the $^{29}\text{Si}\{^1\text{H}\}$ spectrum shows a singlet (see Section 2.2.4, Table 2.3). These observations are consistent with a solution structure on the NMR timescale that contains an inversion centre at the midpoint of the Pn^\dagger bridgehead bond and is in agreement with the solid state structure. The $^{13}\text{C}\{^1\text{H}\}$ spectrum was consistent with this interpretation, with full assignment of resonances achieved by HSQC and HMBC experiments.

Ytterbium possesses a spin- $\frac{1}{2}$ isotope (^{171}Yb) of relatively high natural abundance (14.3%) and sensitivity four times greater than that of ^{13}C .²² Its first high resolution direct NMR observation in an organometallic complex was reported in 1989 by Lappert *et al.*²² and exploration of the Yb(II) oxidation state has since been considerably facilitated by high resolution ^{171}Yb NMR spectroscopy.²³⁻²⁸ The $^{171}\text{Yb}\{^1\text{H}\}$ NMR spectrum of **2.1** shows one signal at 59.9 ppm, consistent with two equivalent Yb(II) centres in the symmetrical anti-bimetallic, which is comparable to the other Yb(II)

compounds characterised in this work as well as literature values for unsolvated ytterbocene(II) complexes (Table 2.2). However it should be noted that large variations in ^{171}Yb chemical shift have been reported for Cp^*Yb , thus making a more detailed comparison difficult.^{29,30}

Table 2.2 Solution $^{171}\text{Yb}\{^1\text{H}\}$ NMR spectroscopic chemical shifts (δ_{Yb}) for **2.1** and related ytterbocene(II) complexes.

Compound	δ_{Yb} / ppm (T / K)	solvent	ref
$[\text{Cp}^*\text{Yb}]_2(\mu\text{:}\eta^5, \eta^5\text{-Pn}^\dagger)$ (2.1)	59.9 (303)	benzene	this work
$[\text{Cp}^*\text{Yb}(\text{OEt}_2)_3][\text{B}(\text{C}_6\text{F}_5)_4]$ (2.4)	89.0 (303)	THF	this work
$\text{Yb}(\text{Cp}^{\text{CH}(\text{SiMe}_3)_2})_2$	118.7 (295)	toluene - benzene	27
$\text{Yb}(\text{Cp}^{\text{SiMe}_2\text{tBu-1,3}})_2$	-7.02 (304)	toluene - benzene	27
$[\text{YbCp}^*_2]_\infty$	-3.3 (298)	toluene	31
$(\text{Cp}^*\text{Yb}\{\mu\text{-COT}'''\})_2\text{Yb}$	595, 364 (298)	THF	28

Unfortunately ^{171}Yb NMR data have not been provided for the cyclooctatetrenyl (COT)-bridged bimetallic Yb(II) complexes $[\text{Cp}^*\text{Yb}]_2(\mu\text{-}\eta^8\text{:}\eta^8\text{-COT})$, $[\text{Cp}^*\text{Yb}(\text{THF})](\mu\text{-}\eta^8\text{:}\eta^8\text{-COT})[\text{YbCp}^*]$ and $[\{(\text{Me}_3\text{Si})_2\text{N}\}\text{Yb}(\text{THF})]_2(\mu\text{-}\eta^8\text{:}\eta^8\text{-COT})$,³²⁻³⁴ and multinuclear NMR spectroscopy was not possible for the THF solvate $[\text{Cp}^*\text{Yb}(\text{THF})]_2(\mu\text{:}\eta^5, \eta^5\text{-Pn}^\dagger)$ due to its low solubility. In contrast, the base-free complex **2.1** is highly soluble in hydrocarbon solvents, which spurred interest in studying its reactivity. Specifically, the use of non-polar solvents has been recommended for the precipitation of charged products of redox reactions,³⁵ which may be useful in attempts to synthesise a stable mixed-valence $[\text{Yb}^{\text{II}}\text{-Yb}^{\text{III}}]$ complex (*vide infra*).

2.2.3 Characterisation of $[Cp^*Eu]_2(\mu-Pn^+)$ (**2.2**)

Compound **2.2** was isolated as an orange solid from toluene-pentane solution, and was identified by single crystal XRD studies (Section 2.2.5) as a toluene solvate. Analytical measurements indicated that this solvent molecule remained in powdered samples that had been rigorously dried *in vacuo*, and duplicate microanalysis measurements for **2.2**. $(C_7H_8)_x$ best fit to $x = 1.6$. However, the molecular ion was observed at $m/z = 988$ in the mass spectrum (EI) with an isotopic envelope consistent with the proposed formulation. The paramagnetic nature of **2.2** precludes NMR analysis, giving a broad, unresolved 1H spectrum.

The magnetic susceptibility of **2.2** was studied in solution and the solid state. The magnetic properties of lanthanide ions due to unpaired 4f electrons are generally well described by the coupling of spin (S) and orbital (L) angular momenta in the Russell-Saunders coupling scheme to give a total angular momentum ($J = L + S$). Spin-orbit coupling constants (*ca.* 1000 cm^{-1}) are typically much larger than ligand-field splittings (*ca.* 100 cm^{-1}) so that only the ground J state is thermally populated. Using these assumptions the effective magnetic moment (μ_{eff}) is given by the Landé formula:

$$\mu_{\text{eff}} = g_J \sqrt{J(J+1)} \mu_B \quad \text{Equation 2.1}$$

where, g_J is the Landé g -factor:

$$g_J = \frac{3}{2} + \frac{S(S+1) - L(L+1)}{2J(J+1)} \quad \text{Equation 2.2}$$

Divalent europium ions have a $4f^7$ configuration with term symbol 8S . The effective magnetic moment (μ_{eff}) of **2.2** determined by the Evans method^{36,37} in C_6D_6 solution was $7.64 \mu_B$ per M at 303 K, which is in reasonable agreement with the value for the Eu^{2+} free ion calculated using the Landé formula ($7.94 \mu_B$). The solid state magnetism of powdered crystalline **2.2**. $(C_7H_8)_{1.6}$ was measured as a function of temperature by SQUID magnetometry. The majority of paramagnetic substances have a molar susceptibility (χ_m) that obeys the Curie-Weiss law, that is:

$$\chi_m = \frac{C}{T - \Theta} \quad \text{Equation 2.3}$$

where C is the Curie constant and Θ is the Weiss constant. The plot of χ_m^{-1} vs T for **2.2** (Figure 2.1) follows Curie-Weiss behavior from 16-300 K, with $C = 7.415 \text{ K}^{-1} \text{ mol}^{-1}$ and $\Theta = -1.5 \text{ K}$. This corresponds to a μ_{eff} of $7.68 \mu_B$ per M at 300 K which is comparable with that of monomeric metallocenes Cp_2Eu ($7.63 \mu_B$) and Cp^*_2Eu ($7.70 \mu_B$),²⁰ suggesting that at these temperatures **2.2** behaves as two non-interacting Eu^{2+} centres. The observed intramolecular $\text{Eu}\cdots\text{Eu}$ distance ($5.1605(5) \text{ \AA}$) is relatively long compared with the analogous 1,4-bis(triisopropylsilyl)cyclooctatetraenyl (= COT^\dagger) complex, $[\text{Cp}^*\text{Eu}]_2(\mu\text{-COT}^\dagger)$ ($4.293(5) \text{ \AA}$),¹² and may explain the lack of magnetic interactions. However, long range ferromagnetic f-f interactions have been reported by Fukuda *et al.* in heterobimetallic quadruple-decker phthalocyanine complexes containing $\text{Y}^{3+}/\text{Dy}^{3+}$ or $\text{Y}^{3+}/\text{Er}^{3+}$ ions at distances up to 6.8 \AA .³⁸

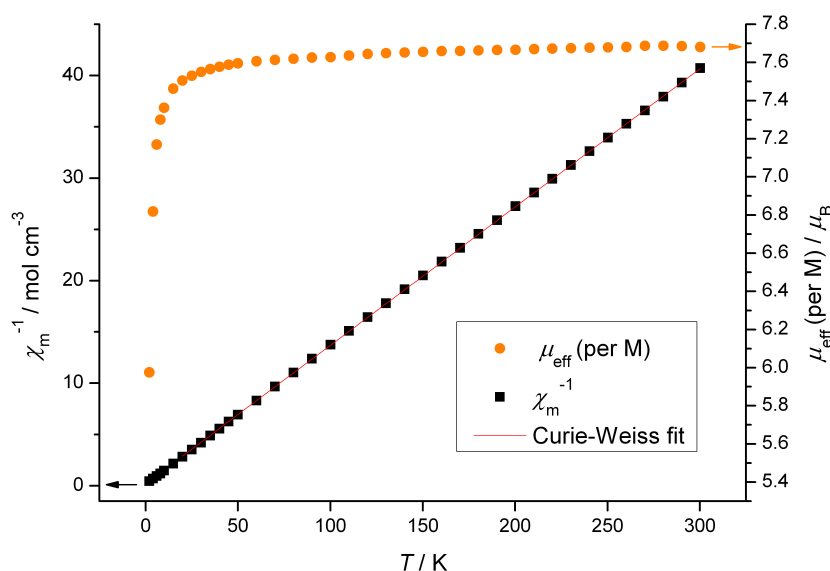


Figure 2.1 Temperature dependence of the solid state μ_{eff} and χ_m^{-1} for **2.2** at 1 Tesla.

Field dependent magnetisation measurements from 0 to 5 Tesla (Figure 2.2) reveal that at 16 K, the magnetisation (M) increases almost linearly with applied field, as expected for a paramagnetic system in which interactions between neighbouring ions are weak. At lower temperatures, M no longer increases linearly with H , and takes the form of a curve described by the Brillouin function.³⁹ The M vs H curve at 2 K approaches a limiting value at 5 Tesla, which is the saturation magnetisation of the sample when all of the spins have aligned.

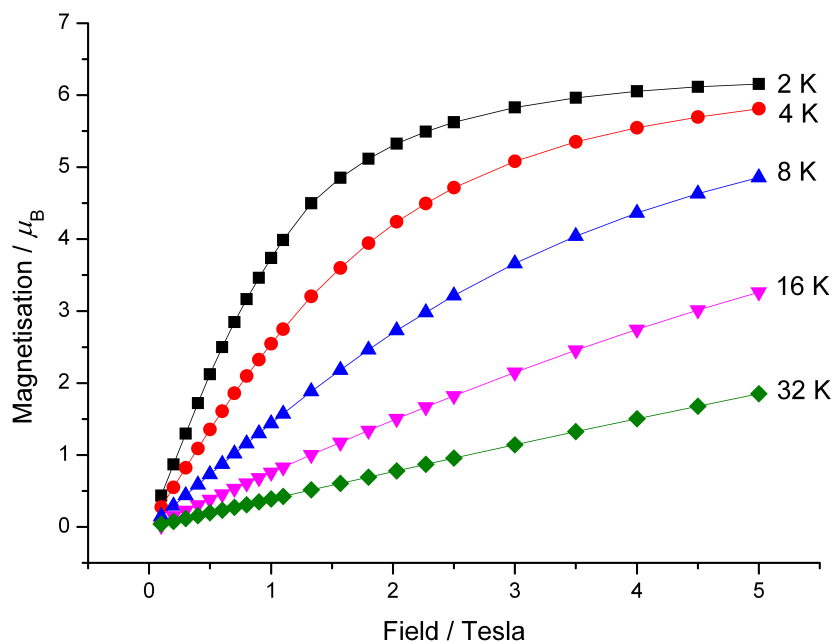


Figure 2.2 Field dependence of the solid state magnetisation for **2.2**.

2.2.4 Characterisation of $[Cp^*Sm]_2(\mu\text{-}\eta^5, \eta^5\text{-}Pn^\dagger)$ (**2.3**)

The Sm^{2+} ion is a $4f^6$ ion with term symbol 7F_0 , which is a special case, in that the Landé formula predicts (incorrectly) a μ_{eff} of zero, hence f^6 ions Sm^{2+} and Eu^{3+} were termed *anomalous* by Van Vleck.³⁹ For these ions the separation of the $J = 0$ and $J = 1$ states is *ca.* 300 cm^{-1} , and the $J = 1$ and $J = 2$ states is *ca.* 200 cm^{-1} , both of which are of the order of $k_B T$.²⁰ This means at normal temperatures there must be a significant population of the excited multiplet states, and this immediately invalidates the Landé formula. Furthermore, the unusually small multiplet intervals suggest the possibility of important second order contributions to μ_{eff} , and complex paramagnetism is anticipated.⁴⁰ As a result, the 1H NMR spectrum of **2.3** in C_6D_6 revealed a set of widely shifted signals with significant line-broadening typical of organometallic $Sm(II)$ complexes. Nonetheless a full assignment of the 1H NMR data was made for the Cp^* and Pn^\dagger ligands of complex **2.3** by the integration of the relevant peaks (Table 2.3). As for **2.1**, the Si^iPr_3 methyl groups were found to be chemically equivalent (i.e. non-diastereotopic) corresponding to a symmetrical bimetallic structure in solution.

Table 2.3. ^1H and $^{29}\text{Si}\{^1\text{H}\}$ NMR chemical shifts of $[\text{Cp}^*\text{M}]_2(\mu\text{-Pn}^\dagger)$ complexes, for $\text{M} = \text{Yb}$ (**2.1**), Sm (**2.3**), and Fe (**3.3**, see chapter three, Section 3.3.4).

Nucleus	Assignment	2.1	2.3	3.3
	$\text{Cp}^* \text{CH}_3$	2.01	-2.71	1.51
δ_{H}	$\text{Pn}^\dagger \text{H}$	6.69, 5.58	10.15, 7.50	4.67, 3.69
	$^i\text{Pr} \text{CH}$	1.28	20.09	2.15
	$^i\text{Pr} \text{CH}_3$	1.13	15.53	1.67, 1.54
δ_{Si}	Si^iPr_3	-2.02	117.7	6.89

The $^{13}\text{C}\{^1\text{H}\}$ NMR spectrum for **2.3** shows the expected number of peaks, again paramagnetically shifted, which could not be assigned unequivocally due to the unsuitability of two dimensional ^{13}C - ^1H correlation experiments for this paramagnetic complex. The molecular ion was observed at $m/z = 985$ in the mass spectrum (EI) with an isotopic envelope in good agreement with the proposed formulation.

The magnetochemistry of **2.3** was studied in solution and the solid state. Complex **2.3** is temperature sensitive, decomposing to $\text{Sm}(\text{III})$ complexes when stored at room temperature, so solution samples were prepared at $-78\text{ }^\circ\text{C}$ and magnetic measurements made in an NMR probe pre-cooled to $-65\text{ }^\circ\text{C}$. At this temperature, the magnetic moment determined by the Evans method^{36,37} in toluene- d_8 was $3.15\text{ }\mu_{\text{B}}$ per M. The solid state magnetism for **2.3** was measured by SQUID magnetometry. The χ_{m}^{-1} vs T plot (Figure 2.3) has a shallow slope below 40 K, suggesting that at these temperatures, when most of the electrons are in the ground state, complex **2.3** behaves as a temperature independent paramagnet. However, as T increases the $J = 1$ and $J = 2$ states become increasingly populated, so that at 200 K μ_{eff} has increased to a value of $3.04\text{ }\mu_{\text{B}}$ per M. The plot of χ_{m}^{-1} vs T for **2.3** is comparable to those for the monomeric samarium metallocenes $\text{Cp}^*_2\text{Sm}(\text{THF})(\text{OEt}_2)$ and Cp^*_2Sm ,²⁰ as well as those found for simple Eu^{3+} salts, which are also f^6 ions.^{41,42} There are no features of the χ_{m}^{-1} vs T plot that indicate intramolecular interactions between the two paramagnetic centres. This is somewhat expected based on the relatively long intramolecular $\text{Sm}\cdots\text{Sm}$ distance (av. $5.336\text{ }\text{\AA}$) found in the molecular structure and the poor radial extension of 4f orbitals, which typically results in weak exchange coupling between lanthanide ions.²

However Murugesu *et al.* have recently shown that the anti-bimetallic complexes, $[\text{COT}'\text{Ln}]_2(\mu\text{:}\eta^8, \eta^8\text{-COT}')$ ($\text{Ln} = \text{Dy}, \text{Er}$; $\text{COT}' = [\text{C}_8\text{H}_6\{\text{SiMe}_3\text{-1,4}\}_2]^{2-}$),^{4,43} have a non-negligible interaction between Ln^{3+} centres which is facilitated by the bridging COT' ligand.

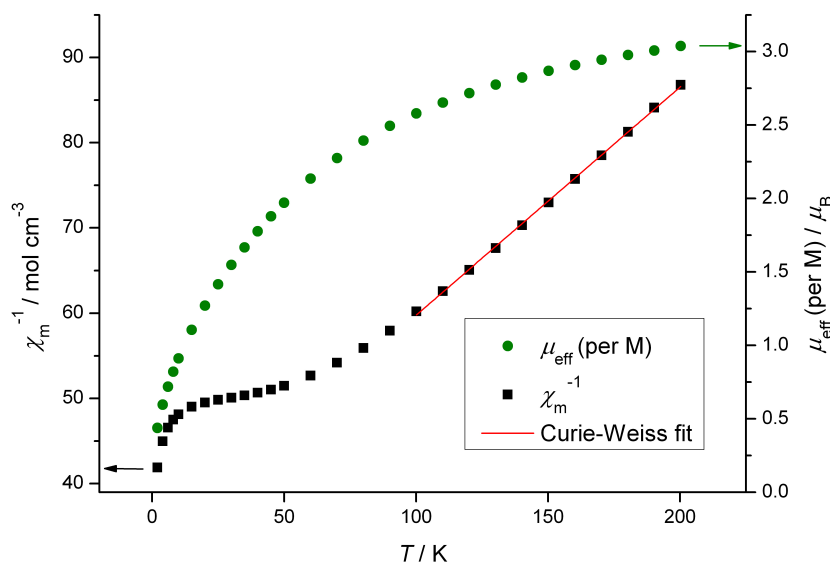


Figure 2.3 Temperature dependence of the solid state μ_{eff} and χ_m^{-1} for **2.3** at 1 Tesla.

Complex **2.3** was found to be extremely thermally sensitive and, despite strict exclusion of air and moisture from the SQUID chamber, samples decomposed to a green paramagnetic solid over the timescale of the SQUID measurement (*ca.* 12 h). Reproducible data for increasing and decreasing temperature scans were obtained only if the sample was kept at 200 K or below, and for this reason only these data are included in Figure 2.3. Fitting a straight line to χ_m^{-1} vs T in the Curie-Weiss regime (between 100-200 K) gives $C = 3.737 \text{ K}^{-1} \text{ mol}^{-1}$, $\Theta = -123.4 \text{ K}$ and an extrapolated μ_{eff} of $3.22 \mu_B$ per M at 282 K, which is comparable with the solid state susceptibility of Cp^*_2Sm ($3.36 \mu_B$) reported at this temperature.²⁰ Field-dependent measurements (Figure 2.4) further illustrate that the magnetisation of **2.3** is temperature independent at 32 K and below. The magnetisation increases almost linearly with applied field, as expected for a paramagnetic system in which intermolecular interactions are weak, confirming that there is no ferromagnetic impurity in the sample.

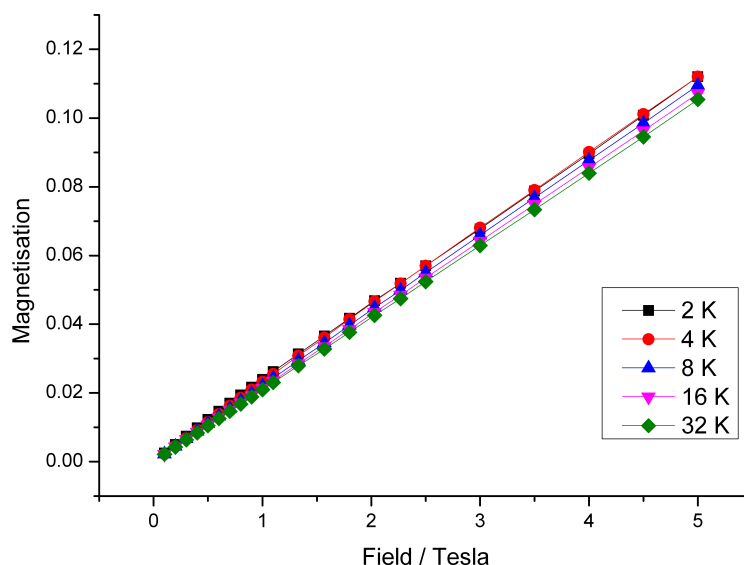


Figure 2.4 Field dependence of the solid state magnetisation for **2.3**.

2.2.5 X-ray crystallographic studies of **2.1**, **2.2** and **2.3**

Anti-bimetallic complexes **2.1**, **2.2** and **2.3** were characterised in the solid state by single crystal X-ray diffraction, and views of their molecular structures are depicted in Figure 2.5. **2.1** crystallises in the monoclinic space group $P2_1/c$ with one half-molecule in the asymmetric unit, whereas **2.3** crystallises in the triclinic space group $P-1$ and contains two independent half-molecules, each with different structural parameters, which are compared in Table 2.4.

Compounds **2.1** and **2.3** are not isomorphous, but are similar in many respects. In the solid state both anti-bimetallics exhibit a slipped triple-decker arrangement and an $\eta^5:\eta^5$ metallocene-like bonding mode. They are symmetrical and possess an inversion centre at the midpoint of the bridgehead carbons, which results in a 180° $\text{Ct}(\text{Cp}^*)\text{--M--M--Ct}(\text{Cp}^*)$ torsional angle. The pentalene and Cp^* ligands are planar but not mutually coplanar, instead adopting a bent arrangement of rings around the metal, as is well-known for the divalent lanthanide metallocenes.^{19,44,45}

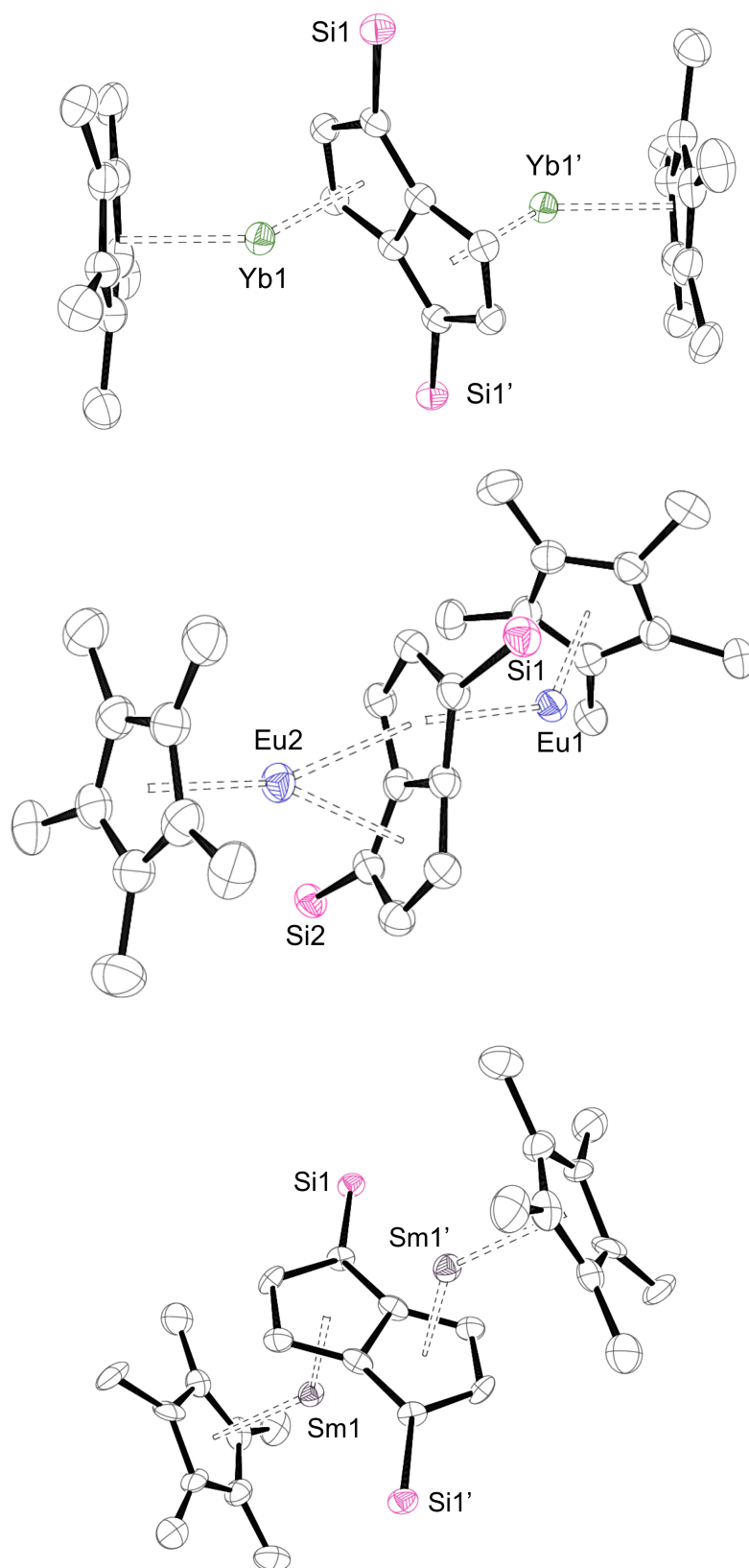


Figure 2.5 Displacement ellipsoid plots (50% probability) of $[\text{Cp}^*\text{Ln}]_2(\mu\text{-Pn}^\dagger)$ (Ln = Yb (**2.1**), Eu (**2.2**), Sm (**2.3**) top to bottom).

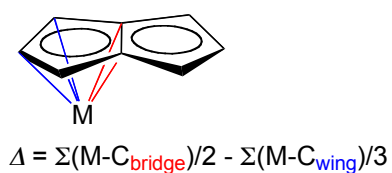
H atoms, ^iPr groups and co-crystallised solvent molecules omitted for clarity.

Table 2.4 Selected distances (Å), angles (°), and parameters (defined in Figure 2.6) for **2.1**, **2.2** and **2.3**. Ct1 and Ct2 correspond to the η^5, η^5 -centroids of the Pn ring. Ct3 and Ct4 correspond to the η^5 -centroids of the Cp* rings.

Parameter	2.1	2.2	2.3
M...M	5.230(2)	5.1605(5)	5.2737(12), 5.3973(6)
M1–Ct1	2.389(3)	2.5689(18)	2.476(4), 2.508(4)
M1–Ct3	2.397(3)	2.516(2)	2.493(5), 2.498(5)
M2–Ct1	-	2.6365(18)	-
M2–Ct2	-	2.5043(16)	-
M2–Ct4	-	2.540(2)	-
Δ_{M1-Ct1}	0.052	0.069	-0.047, 0.006
Δ_{M2-Ct2}	-	-0.268	-
Ct1–M1–Ct3	139.31(8)	131.78(7)	133.711(6), 135.06(9)
Ct1–M2–Ct4	-	157.63	-
Ct2–M2–Ct4	-	153.09	-
av. Pn C–C _{ring}	1.437(7)	1.435(5)	1.435(14), 1.434(14)
M–C _{agostic} ^a	3.1399(5)	3.114(6)	3.278(10), 3.359(11)
Fold angle	0.0	16.1	0.0, 0.0

^a Shortest M–ⁱPr CH₃ distance within each independent molecule.

Ring slippage (Δ)



Fold angle

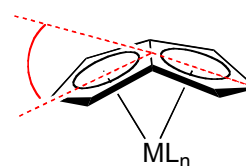


Figure 2.6

The extent of bending in these compounds, as well as their alkaline earth analogues, has been related to metal size.⁴⁶ Complexes of the smallest metals, which have the rings closest together, have the most linear structures. The Ct(Cp*)–M–Ct(Pn) angles for **2.1** and **2.3** follow this trend, reflecting the smaller ionic radius of the Yb²⁺ centre compared with Sm²⁺ ($r_{Ln2+} = 1.02$ and 1.22 Å respectively for 7-coordinate ions).⁴⁷ This angle in **2.1** ($139.31(8)^\circ$) is larger than that in the THF solvated analogue [Cp*Yb(THF)]₂($\mu\text{:}\eta^5\text{:}\eta^5\text{-Pn}^\dagger$) ($138.2(2)^\circ$), just as the Ct(Cp*)–M–Ct(Cp*) angle in Cp*₂Yb (145.0°) is larger than in solvated Cp*₂Yb(THF) ($143.5(3)^\circ$).⁴⁸ For comparison, the Ct(Cp*)–M–Ct(Cp*) angles are 140.1° in unsolvated Cp*₂Sm,⁴⁴ and 136.7° in solvated Cp*₂Sm(THF)₂.⁴⁹

Slight differences between the structures are found in the ligand-metal bonding distances and reflect the variation in metal ionic radii. The smaller Yb(II) centre is found to allow closer coordination of the carbocyclic ligands in **2.1** compared to **2.3**, M–Ct(Pn) = $2.389(3)$ and av. $2.492(4)$ Å, M–Ct(Cp*) = $2.389(3)$ and av. $2.496(5)$ Å, respectively. The average M–C_{ring}(Cp*) distances are comparable to those in the corresponding [Cp*Ln]₂($\mu\text{-}\eta^8\text{:}\eta^8\text{-COT}$), [Cp*Ln]₂($\mu\text{-}\eta^8\text{:}\eta^8\text{-COT}^\dagger$), and Cp*₂Ln complexes.^{12,19,32,50,51} Additionally, all three structures **2.1**, **2.2** and **2.3** show close intermolecular contact between the Ln(II) centres and one of the methyls of the pentalene Si^{*i*}Pr₃ groups, as often occurs in lanthanide complexes with N(SiMe₃)₂ ligands.⁵²⁻⁵⁶

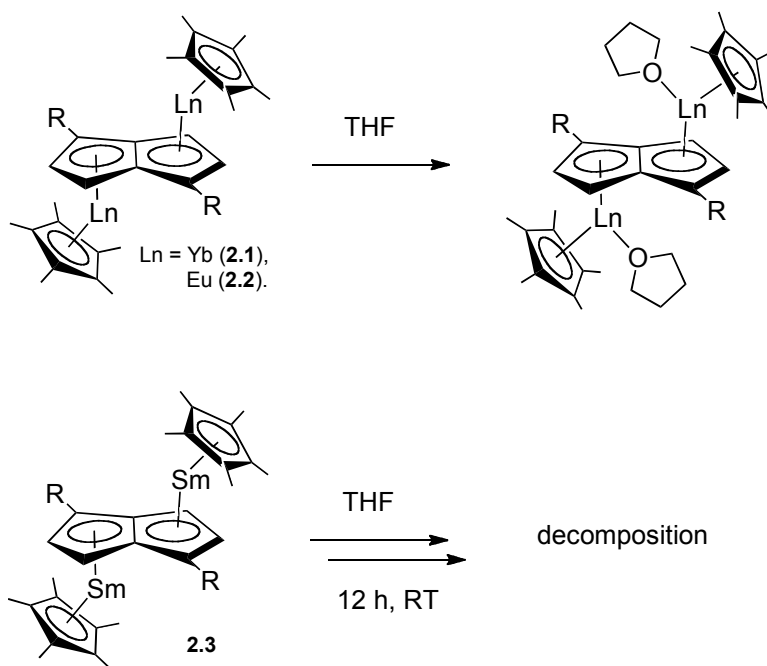
Complex **2.2** has a solid state molecular structure in which the two europium centres occupy radically different coordination environments. Eu1 is in the expected bent $\eta^5\text{:}\eta^5$ -metallocene configuration, with M–Ct(Pn) and Ct(Cp*) distances and angles similar to those found in the THF solvate [Cp*Eu(THF)]₂($\mu\text{:}\eta^5\text{:}\eta^5\text{-Pn}^\dagger$) ($2.502(6)$ Å, $2.477(5)$ Å, and $131.5(2)^\circ$ respectively).¹² However Eu2 interacts with all 8 carbons of the pentalene ring, which folds by 16.1° to accommodate the electropositive centre, as is typical for the structures of *mono* f-element pentalene compounds.^{21,57} This unusual coordination environment for Eu2 is quantified by the ring slippage parameter (-0.268 Å) with its proximal pentalene C₅-centroid (see Figure 2.6 for definition of Δ_{M-Ct}) which is exceptionally large and negative in comparison to this parameter for Eu1 (0.069 Å), and those for **2.1** and **2.3**.

Pentalene is normally considered as a dianionic ligand in the η^8 - bonding mode to a single metal centre, and monoanionic in η^5 - mode,⁵⁸ which would indicate, *prima facie*, a +3 oxidation state for Eu2. However, SQUID magnetometry measurements (Section 2.2.3) are fully consistent with a +2 oxidation state of each Eu centre in **2.2**. Furthermore, addition of THF to **2.2** was shown by IR spectroscopy (*vide infra*) to yield the solvated complex $[\text{Cp}^*\text{Eu}(\text{THF})]_2(\mu\text{-Pn}^\dagger)$ in which the bridging pentalene ligand adopts the expected η^5, η^5 - binding mode in the solid state, leaving no ambiguity in the divalent state for each Eu. The distance between Eu2 and the distal pentalene C₅-centroid in the molecular structure of **2.2** (2.6365(18) Å) is longer than in any Ln–Ct(Pn) formal bonding distance reported to date,⁵⁹ and is thus best considered as a subtle interaction that may be attributed to crystal packing forces. A list of short intermolecular contacts (less than the sum of the van der Waals radii), and an ORTEP view of the unit cell of **2.2** are included in appendix A2.

2.2.6 Solvation of **2.1**, **2.2** and **2.3**

Given the base-free synthetic route to **2.1**, **2.2** and **2.3**, an investigation into the stability of these complexes in polar solvents was required, in order to select a suitable electrolytic medium for subsequent CV studies. This was particularly critical for complex **2.3**, for which the synthesis could not be achieved in the presence of THF,²¹ and the tendency for rapid halide abstraction by Sm(II) complexes in the presence of halogenated solvents.¹¹

Treatment of **2.1** with five drops of THF-*d*₈ resulted in a green solution above a dark green precipitate, suggesting the formation of the sparingly soluble THF adduct $[\text{Cp}^*\text{Yb}(\text{THF})]_2(\mu\text{:}\eta^5, \eta^5\text{-Pn}^\dagger)$,¹² which was confirmed by IR and ¹H NMR spectroscopy (Scheme 2.4, top). Similarly, complex **2.2** reacts with THF to form the orange THF adduct $[\text{Cp}^*\text{Eu}(\text{THF})]_2(\mu\text{:}\eta^5, \eta^5\text{-Pn}^\dagger)$,¹² evidenced by a characteristic band in its IR spectrum at ν 1145 cm⁻¹. Addition of THF to **2.3** resulted in a dark brown solution which after 12 h at room temperature deposited a dark green solid. The ¹H NMR spectrum of the green precipitate contained a plethora of new peaks between -3 and 28 ppm, which could not be assigned unambiguously and it was assumed decomposition had occurred (Scheme 2.4, bottom).



Scheme 2.4 Solvation reactions for **2.1**, **2.2** and **2.3** with THF. R = SiⁱPr₃.

Preliminary trials to determine stability in other common electrochemical solvents were carried out on **2.1** due to its straightforward characterisation by ¹H NMR spectroscopy. If the Yb(II) complex showed appreciable stability in the given solvent, studies were extended to the more reactive Sm(II) complex **2.3**. Addition of DME or CH₂Cl₂ to **2.1** in C₆D₆ in both cases resulted in a colour change from brown to yellow (typical of Yb³⁺ complexes) and only intractable mixtures of different products were observed in the ¹H NMR spectra.

Complex **2.1** was soluble in the presence of 1,2-difluorobenzene, and showed no reaction by ¹H NMR, however with **2.3** disappearance of the Sm(II) complex was observed in the ¹H spectrum, and a new peak at -113.3 ppm was observed in the ¹⁹F spectrum, suggesting fluoride abstraction had taken place. Hence 1,2-difluorobenzene and other aryl fluorides were deemed unsuitable solvents for CV.

Complex **2.1** was sparingly soluble in acetonitrile forming a green solution, which was sufficiently stable for electrochemical studies (*vide infra*). Unfortunately **2.3** was almost insoluble in acetonitrile, such that voltammetric responses were not observed, and the solution appeared very pale yellow in colour. Complexes **2.2** and **2.3** were inert to ethereal solvents ^tBuOMe, and Et₂O, showing no reactivity and very limited solubility.

2.2.7 Electrochemical studies of **2.1**, **2.2** and **2.3**

Complexes **2.1** and **2.2** are readily soluble in hydrocarbon solvents (*ca.* 0.1 mmol cm⁻³ in benzene) with respect to their THF solvated analogues, however finding a suitable solvent/electrolyte system compatible for comparative electrochemical studies for these complexes and **2.3** proved non-trivial. As described in Section 2.2.6, the Sm(II) complex **2.3** reacts with THF over the course of 12 h, however reasonable CV data were obtained in this solvent when measured within a 1 h period after dissolution. Using [ⁿBu₄N][PF₆] supporting electrolyte, two processes were observed within the electrochemical window (Figure 2.7).

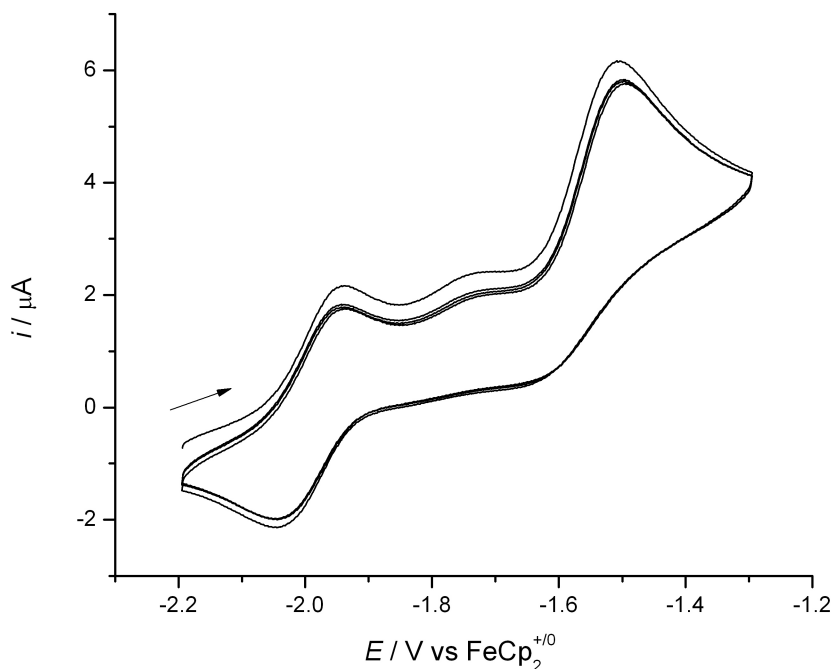


Figure 2.7 Overlaid CV scans (3 cycles) for **2.3** in THF / 0.1 M [ⁿBu₄N][PF₆], scan rate 100 mV s⁻¹.

Process 1, with a mid-peak potential ($E_{1/2} = \{E_{pa} + E_{pc}\}/2$) of -2.0 V vs FeCp₂⁺⁰ (a convention which is assumed for all potentials quoted henceforth), is tentatively assigned to a [Sm^{II}-Sm^{II}]/[Sm^{III}-Sm^{II}] oxidation on the basis of comparable values of the Sm(III/II) couple in this solvent.¹⁰ Repetitive potential cycling over process 1 in isolation using varied scan rates (50 to 500 mV s⁻¹), showed electrochemical behaviour best described as quasi-reversible.⁶⁰ The peak-to-peak separation (ΔE_{pp}) was

comparable to that for ferrocene under the same conditions (*ca.* 150 mV), suggesting that only one electron is being transferred. Process 2 shows an anodic wave with a peak potential (E_{pa}) of -1.5 V in the forward scan, however no associated cathodic wave was observed in the reverse scan. Irreversible behaviour suggests that the product of this second oxidation is not stable under the conditions and timescale of the experiment. It is noted that process 1 shows a lower current response than process 2. Due to the highly negative region of the potential window which at these processes occur, it may be that appreciable oxidation of the Sm(II) species had occurred prior application of the initial potential of the forward scan (-2.2 V). After a period of *ca.* 1 h, the current response of process 1 diminished almost entirely and additional anodic waves appeared upon scanning to more positive potentials. Presumably after this period the Sm(II) species has nearly completely decomposed, consistent with ^1H NMR spectroscopy observations.

The electrochemical behaviour of **2.3** in THF/ $[\text{nBu}_4\text{N}][\text{PF}_6]$, is qualitatively comparable to that previously reported for $[\text{Cp}^*\text{Yb}(\text{THF})_2(\mu\text{:}\eta^5, \eta^5\text{-Pn}^\dagger)]$ in THF/ $[\text{nBu}_4\text{N}][\text{B}(3,5\text{-}\{\text{CF}_3\}_2\text{C}_6\text{H}_3)_4]$,¹² which shows a quasi-reversible oxidation to the mono-cation followed by irreversible behaviour in the second oxidation. For a better comparison, CV studies of **2.3** were attempted using the alternative weakly coordinating electrolyte $[\text{nBu}_4\text{N}][\text{B}(\text{C}_6\text{F}_5)_4]$ in THF,⁶¹ however the voltammograms obtained were distorted due to high solution resistance. Inspection of the gold disc working electrode showed solid deposits on the surface, indicative of electrode fouling.

The CV data for $[\text{Cp}^*\text{Ln}]_2(\mu\text{-Pn}^\dagger)$ complexes **2.1**, **2.2** and **2.3** are given in Table 2.5. The oxidative potentials follow the thermodynamic trend for reducing power $\text{Sm} > \text{Yb} > \text{Eu}$,⁸ although a more in-depth comparison cannot be made due to the different electrolytic media used. Furthermore, the peak separations between the oxidation waves (ΔE) does not represent the difference between mid-peak potentials (hence not designated $\Delta E_{1/2}$), and hence the value does not represent a true thermodynamic measurement of the comproportionation equilibrium constant (K_c , see chapter one) for the mixed-valence mono-cation.

Table 2.5 Electrode potentials vs $\text{FeCp}_2^{+/0}$ in 0.1 M $[\text{nBu}_4\text{N}][\text{A}]$.

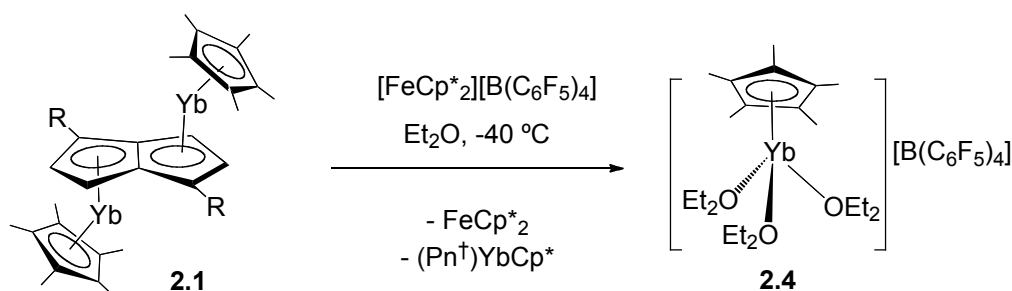
Compound	$E^{(1)} / \text{V}$	$E^{(2)} / \text{V}$	$\Delta E^{(2)-(1)} / \text{V}$	solvent	electrolyte $[\text{A}]^-$	ref
2.1	-1.9	-1.5 ^a	0.4	THF	$[\text{B}(3,5-\{\text{CF}_3\}_2\text{C}_6\text{H}_3)_4]$	¹²
2.1	-1.7 ^a	-1.3	0.5	THF	$[\text{B}(\text{C}_6\text{F}_5)_4]$	this work
2.1	-1.7	-1.5	0.2	MeCN	$[\text{PF}_6]$	this work
2.2	-1.4 ^a	-1.1 ^a	0.3	THF	$[\text{B}(3,5-\{\text{CF}_3\}_2\text{C}_6\text{H}_3)_4]$	¹²
2.3	-2.0	-1.5 ^a	0.5	THF	$[\text{PF}_6]$	this work

^a Anodic peak potentials (E_{pa}) are quoted for irreversible processes.

2.2.8 Redox reactions of **2.1**; Synthesis and characterisation of $[\text{Cp}^*\text{Yb}(\text{OEt}_2)_3][\text{B}(\text{C}_6\text{F}_5)_4]$ (**2.4**)

The CV measurements reveal the potential for oxidation of $[\text{Ln}^{\text{II}}-\text{Ln}^{\text{II}}]$ complexes **2.1**, **2.2** and **2.3**. With this in hand, the synthesis of a mixed-valence $[\text{Ln}^{\text{III}}-\text{Ln}^{\text{II}}]$ complex was attempted on a preparative scale. Complex **2.1** was selected for preliminary reactivity studies for the series. It was envisaged that the milder reducing potential for Yb(II) compared with Sm(II) may result in a stable mixed-valence complex.

Reaction of **2.1** with one equivalent of $[\text{FeCp}^*_2][\text{B}(\text{C}_6\text{F}_5)_4]$ in Et_2O at $-40\text{ }^\circ\text{C}$ resulted in an orange solution. Following evaporation of the solvent and removal of FeCp^*_2 by washing with pentane, the residues were recrystallised from $\text{Et}_2\text{O}/(\text{Me}_3\text{Si})_2\text{O}$ at $-35\text{ }^\circ\text{C}$ yielding $[\text{Cp}^*\text{Yb}(\text{OEt}_2)_3][\text{B}(\text{C}_6\text{F}_5)_4]$ (**2.4**) as a yellow solid. Ion-pair **2.4** was characterised by NMR spectroscopy, elemental analysis and X-ray crystallography.



Scheme 2.5 Oxidation of **2.1** with $[\text{FeCp}^*_2][\text{B}(\text{C}_6\text{F}_5)_4]$. $\text{R} = \text{Si}^i\text{Pr}_3$.

The ^1H NMR spectrum shows resonances for the Cp^* methyl groups at 1.97 ppm, and coordinated Et_2O appears at 3.38 and 1.11 ppm. Relative integration of these peaks indicated the presence of 3 moles of Et_2O per Cp^* ligand. The tetrakis(perfluorophenyl)borate counter anion is easily identified by a sharp singlet in the $^{11}\text{B}\{^1\text{H}\}$ spectrum at -14.7 ppm and three signals at -130, -163.3 and -166.8 ppm in the ^{19}F spectrum for the *o*, *p* and *m*-F respectively.

The molecular structure (Figure 2.8) reveals a mononuclear half-sandwich $\text{Yb}(\text{II})$ cation, $[\text{Cp}^*\text{Yb}(\text{OEt}_2)_3]^+$, and an outer-sphere $[\text{B}(\text{C}_6\text{F}_5)_4]^-$ anion, each displaying a distorted tetrahedral geometry about the central atoms (Yb1 and B1 respectively). The Yb and B atoms of the ion-pair **2.4** are separated by 8.128(6) Å, in contrast to ytterbium(II) tetraphenylborate complexes $[(\text{N}\{\text{SiMe}_3\}_2)\text{Yb}(\text{THF})\text{BPh}_4]$,⁶² $[(^t\text{Bu}_2\text{pz})\text{Yb}(\text{THF})\text{BPh}_4]$,⁶³ and $\text{Cp}^*\text{Yb}(\text{BPh}_4)$ ¹⁶ in which two of the phenyl rings of the anion can bind in an η^6 -mode to the metal centre, resulting in closer Yb...B distances of 3.690(3), 3.636(2) and 3.708(5) Å respectively.

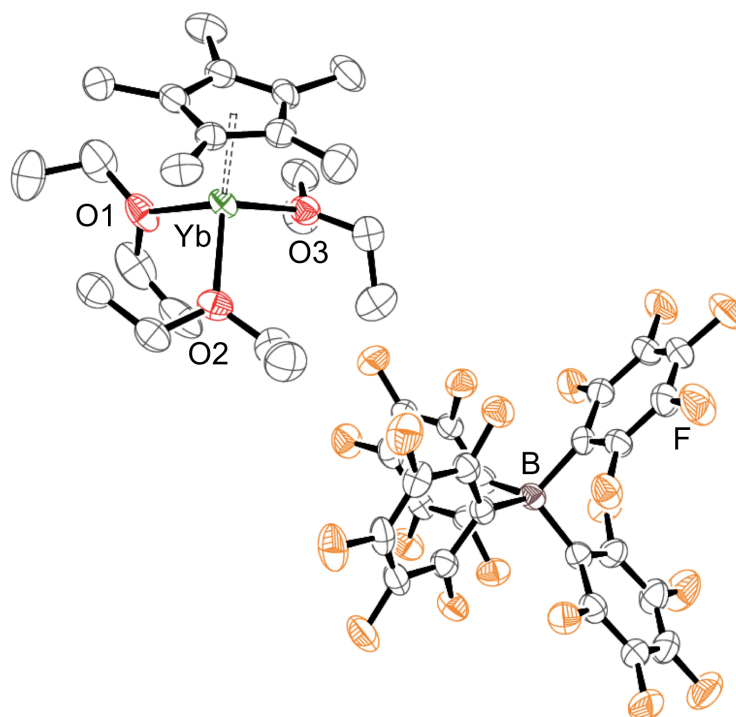


Figure 2.8 ORTEP view of **2.4** (50% probability) with H atoms omitted for clarity.

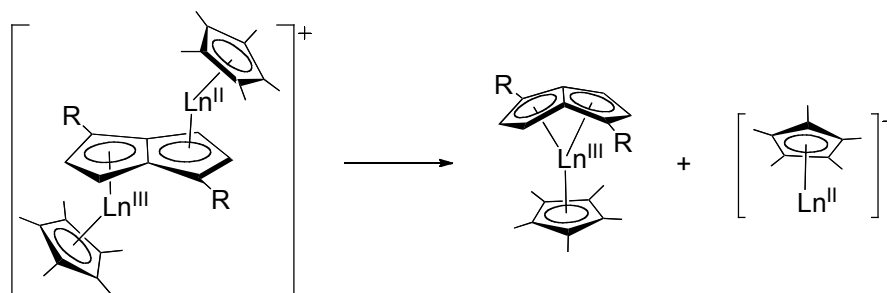
Table 2.6 Selected structural parameters for **2.4**. Ct1 denotes the η^5 -centroid of the Cp* ligand. Ct2 denotes the ring centroid of the proximal C₆F₅ group.

Distances (Å)			
Yb–Ct1	2.369(2)	Yb–O1	2.404(3)
Yb...Ct2	6.769(3)	Yb–O2	2.394(3)
Yb...B	8.128(6)	Yb–O3	2.383(3)
Angles (°)			
O1–Yb–O2	104.43(11)	O1–Yb–O3	90.74(13)
O2–Yb–O3	111.06(12)	O1–Yb–Ct1	122.61(12)
O2–Yb–Ct1	113.62(9)	O3–Yb–Ct1	112.07(9)
C24–B–C30	114.7(4)	C30–B–C42	101.7(4)
C36–B–C42	114.7(3)	C24–B–C36	100.7(4)

Presumably the second Yb-containing product in this reaction is the mixed-sandwich compound (η^8 -Pn[†])YbCp*, which is expected to be readily soluble in pentane, and hence extracted with the decamethylferrocene fraction (Scheme 2.5). Evans *et al.* have reported the synthesis of the related mixed-sandwich compound, (η^8 -COT)YbCp*, by addition of cyclooctatetraene to [Cp*Yb]₂(μ - η^8 : η^8 -COT).³² Repeating the reaction of **2.1** with one equivalent of [FeCp*₂][B(C₆F₅)₄] in Et₂O at -40 °C, followed by removal of the solvent and decamethylferrocene *via* vacuum sublimation resulted in a equimolar mixture of **2.4** and (η^8 -Pn[†])YbCp*, as identified by mass spectrometry and multinuclear (¹H, ¹³C, ¹¹B, ¹⁹F, ²⁹Si, ¹⁷¹Yb) NMR spectroscopy.

Despite the relatively mild oxidising power of the decamethylferrocenium ion (measured as $E_{1/2} = -0.52$ V in THF/0.1 M [ⁿBu₄N][B(C₆F₅)₄]), its reaction with **2.1** leads to dissociation rather than stabilisation of the mixed-valence bimetallic. Previous attempts by Cloke *et al.* using more potent oxidising agents such as [Cp₂Fe][B(3,5-{CF₃})₂C₆H₃)₄] and [Ag][BPh₄] failed to give tractable products.^{12,64-66} This suggests that despite CV evidence in a previous report for a stable mixed-valence pentalene bridged bimetallic, e.g. [Cp*Ln]₂(μ -Pn[†])⁺, its large-scale preparation using available chemical

redox agents is not possible. In this case, the η^5 - and η^8 - bonding modes that are available to the pentalene dianion are detrimental to the formation of bridged bimetallic species such as $[\text{Cp}^*\text{Ln}(\mu\text{-Pn}^\dagger)\text{LnCp}^*]^+$, since the +3 oxidation state is better stabilised, both sterically and electronically, in mononuclear sandwich compounds of the type $(\eta^8\text{-Pn}^\dagger)\text{LnCp}^*$, leading to dissociation (Scheme 2.6).



Scheme 2.6 Possible decomposition pathway of mixed-valence bimetallic. R = Si^iPr_3 .

In principle, this decomposition pathway could be prevented by targeting a heterobimetallic Ln/M complex in which the second metal, M, is pre-disposed to favour η^5, η^5 - metallocene type bonding. Following oxidation, the Ln(III) centre would then be constrained to maintain a bimetallic complex. This synthetic strategy was pursued in further work using M = Fe, and the results are discussed in chapter three.

2.2.9 Synthesis and characterisation of $[(\eta^8\text{-Pn}^\dagger)_2\text{Yb}][\text{K}]$ (**2.5**)

In an attempt to prepare an authentic sample of $(\eta^8\text{-Pn}^\dagger)\text{YbCp}^*$ *via* a direct, one-pot route, YbI_3 was reacted with KCp^* and $[\text{K}]_2\text{Pn}^\dagger$ in THF. Subsequent work-up and recrystallisation from pentane furnished the homoleptic complex $[(\eta^8\text{-Pn}^\dagger)_2\text{Yb}][\text{K}]$ (**2.5**) in 15% yield, as identified by elemental analysis and mass spectrometry. ^1H NMR spectroscopy in $\text{THF-}d_8$ showed broad signals consistent with a paramagnetic Yb(III) (f^{13}) complex which could be assigned to the Pn^\dagger ligand by relative integration ratios. X-ray crystallography established the connectivity of the atoms in **2.5** as the ‘ate’ complex shown in Figure 2.9, however the low quality of the data precluded accurate refinement of metric parameters. There is precedent for such Ln(III) anionic bis(pentalene) sandwich complexes with Ln = Ce,^{64,66} emphasising the steric and electronic stabilisation achieved for the f-elements with the pentalene ligand in η^8 -mode.

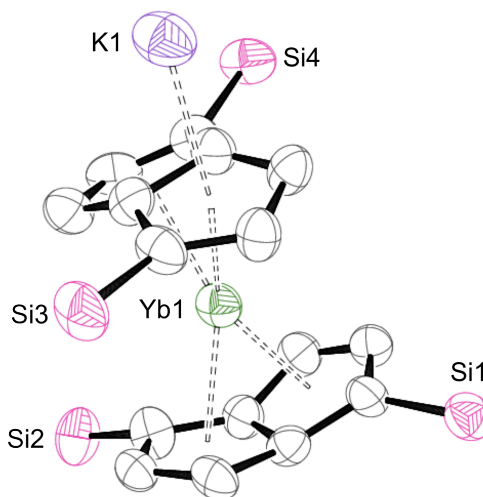
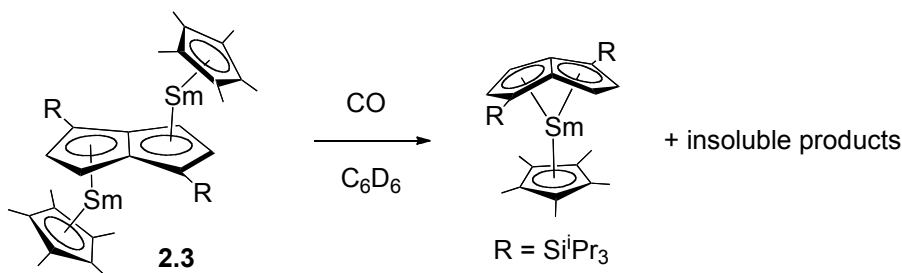


Figure 2.9 ORTEP (30% probability) diagram of partially refined ($R_1 = 12.7\%$) molecular structure of **2.5**. H atoms and ^iPr groups omitted for clarity.

2.2.10 Reaction of **2.3** with carbon monoxide

Since the reductive homologation of carbon monoxide ketene carboxylate by $\text{Cp}^*_2\text{Sm}(\text{THF})_2$ was reported by Evans *et al.*,⁶⁷ there has been considerable interest in the reduction of CO by other soluble Sm(II) reagents.^{55,68} Reaction of **2.3** in C_6D_6 with an excess of ^{13}CO produced a brown solution above a small amount of precipitate. ^1H NMR spectroscopy showed conversion to the mononuclear mixed-sandwich product $(\eta^8\text{-Pn}^\dagger)\text{SmCp}^*$ after 10 mins (Scheme 2.7).



Scheme 2.7 Reaction of **2.3** with CO.

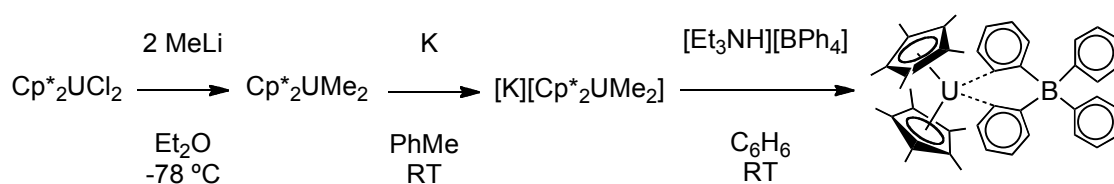
$^{13}\text{C}\{^1\text{H}\}$ NMR spectroscopy of the reaction mixture showed no labelled ^{13}C resonances, and no $\nu(\text{CO})$ stretches were observed in the IR spectrum. As a control experiment, a freeze-thaw degassed solution of **2.3** in C_6D_6 was exposed to excess N_2 (1 atm), and showed no change by ^1H NMR spectroscopy after 24 h. The formation of a trivalent product and an insoluble black solid from Sm(II) complex **2.3** with CO suggests disproportionation. The reactivity of **2.3** with CO to form $(\eta^8\text{-Pn}^\dagger)\text{SmCp}^*$ parallels that

of $(\text{Cp}^{\prime\prime})_2\text{Sm}(\text{THF})$ ($\text{Cp}^{\prime\prime} = \eta^5\text{-}[\text{C}_5\text{H}_3\{1,3\text{-SiMe}_3\}_2]^-$) reported by Evans *et al.*,⁶⁸ in which the tris-ring complex $(\text{Cp}^{\prime\prime})_3\text{Sm}$ was the only isolated product. Indeed, these researchers have suggested that the key feature in the CO reduction chemistry shown by $\text{Cp}^*_2\text{Sm}(\text{THF})_2$, is that the tris-ring complex is not the favoured product due to steric hindrance.⁶⁹

2.2.11 Attempted synthesis of a pentalene bridged uranium bimetallic

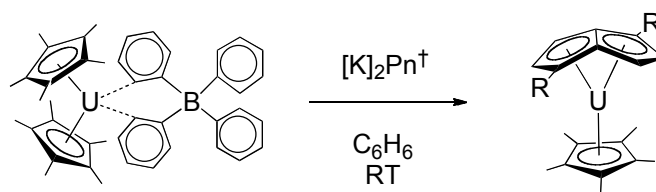
Following on from the successful synthesis of $[\text{Cp}^*\text{Ln}]_2(\mu\text{-Pn}^\dagger)$ complexes, exploiting tetraphenylborate salts of $\text{Cp}^*\text{Ln}(\text{II})$ as precursors, efforts were made towards the synthesis of a uranium anti-bimetallic pentalene complex *via* a similar synthetic route. It was envisaged that a hypothetical $[\text{L}_2\text{U}]_2(\mu\text{:}\eta^5, \eta^5\text{-Pn}^\dagger)$ complex would make for an interesting structural comparison with mononuclear U(III) mixed-sandwich complexes of the type $\text{LU}(\eta^5\text{-Cp}^{\text{Me4R}})$ ($\text{L} = \text{COT}^\dagger$, COT^\ddagger , and Pn^\dagger) for which synthesis and reactivity with small molecules have been extensively studied by Cloke *et al.*^{57,70-74}

Attempts to synthesise a substituted cyclooctatetraene U(III) half-sandwich reagent containing a labile iodide ligand, by reaction of UI_3 with one equivalent of $[\text{K}]_2\text{COT}^\dagger$ in THF or DME, instead resulted in disproportionation, with $\text{U}(\text{COT}^\dagger)_2$ as the sole product identified by ^1H NMR and EI-MS. It was proposed that coordinating solvents may facilitate this redox reaction by stabilisation of charged intermediates, therefore a base-free complex was desirable, which could be utilised in the absence of coordinating solvents. Evans *et al.* have reported the synthesis of $\text{Cp}^*_2\text{U}(\text{BPh}_4)$ (Scheme 2.8) and its subsequent use as a synthon for the preparation of complexes of the type $[\text{Cp}^*_2\text{UX}]$ ($\text{X} = \text{NR}_2$, Cp^*).⁷⁵ These researchers have also demonstrated that the Cp^* ligand can be displaced from $\text{Cp}^*\text{Ln}(\text{BPh}_4)$ by other monoanionic ligands (e.g., NR_2^-) or indeed by bidentate anionic ligands (with co-substitution of $[\text{BPh}_4]^-$).^{18,75-77}



Scheme 2.8 Synthetic route to $\text{Cp}^*_2\text{U}(\text{BPh}_4)$.^{75,76}

Reaction of $\text{Cp}^*_2\text{U}(\text{BPh}_4)$ with half an equivalent of $[\text{K}]_2\text{Pn}^\dagger$ *via* dropwise addition in benzene produced a brown solution. Work up and recrystallisation from pentane furnished the known complex $(\eta^8\text{-Pn}^\dagger)\text{UCp}^*$, as identified by ^1H NMR spectroscopy. Despite the 2:1 stoichiometric ratio of $\text{U}:\text{Pn}^\dagger$ employed in this reaction, the isolation of monomeric U(III) complex $(\eta^8\text{-Pn}^\dagger)\text{UCp}^*$ *via* the substitution of Cp^* and $[\text{BPh}_4]^-$, illustrates the preference of Pn^\dagger for η^8 -hapticity in f-block metal complexes. The original preparation of $(\eta^8\text{-Pn}^\dagger)\text{UCp}^*$ reported by Cloke *et al.*,⁵⁷ can be subject to variable, often very low yields. This is presumably because the mixed-valence trimer $[\text{Cp}^*\text{U}(\mu\text{-I})_2]_3(\mu\text{-O})_3$ is formed from the reaction of UI_3 and KCp^* in Et_2O in the first synthetic step.⁷⁸ The reaction of $\text{Cp}^*_2\text{U}(\text{BPh}_4)$ with $[\text{K}]_2\text{Pn}^\dagger$ in benzene was repeated employing a 1:1 stoichiometry, which afforded $(\eta^8\text{-Pn}^\dagger)\text{UCp}^*$ in 43% optimised yield (Scheme 2.9).



Scheme 2.9 Alternative synthetic route to $(\eta^8\text{-Pn}^\dagger)\text{UCp}^*$. $\text{R} = \text{Si}^i\text{Pr}_3$.

The desired $[\text{L}_2\text{U}]_2(\mu\text{-}\eta^5, \eta^5\text{-Pn}^\dagger)$ complex could not be synthesised *via* this route, and subsequent attempts towards a uranium anti-bimetallic complex were abandoned. However the reaction of $\text{Cp}^*_2\text{U}(\text{BPh}_4)$ with $[\text{K}]_2\text{Pn}^\dagger$ presents a reliable new synthetic route for the preparation of $(\eta^8\text{-Pn}^\dagger)\text{UCp}^*$ and the reactivity of this complex was subsequently investigated by Cloke *et al.* with low coordinate phosphorus compounds, from which the first example of the two-electron reduction of a phosphalkyne was reported.⁷⁹

2.3 Mononuclear Lanthanide(III) Complexes as Single Ion Magnets

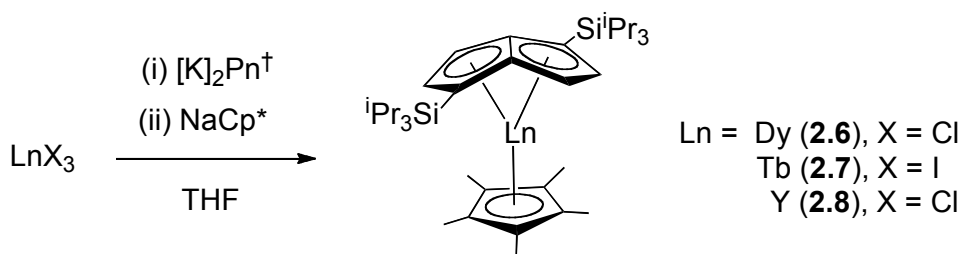
2.3.1 Background

There has been fundamental interest for over a decade in discrete molecules which exhibit slow relaxation of their magnetisation at low temperatures, so-called single molecule magnets (SMMs).⁸⁰⁻⁸² In recent years a more rational synthetic approach has developed in the pursuit of new SMMs with more favourable properties such as higher energy barriers to magnetisation relaxation.^{83,84} To this end, complexes of the f-elements have attracted increased attention,⁸⁵⁻⁸⁸ in particular those of the late lanthanide ions Tb^{3+} , Dy^{3+} , Ho^{3+} and Er^{3+} , due to their large number of unpaired electrons and strong single-ion anisotropy.^{89,90} Long *et al.* have highlighted that a sandwich-type ligand architecture provides the ideal crystal field environment for Ln^{3+} complexes to maximise the anisotropy of oblate ions such as Dy^{3+} ,⁸⁵ since the ligand electron density is concentrated above and below the xy plane. This concept has been practically demonstrated by Ishikawa *et al.* who reported a series of ‘double-decker’ complexes with bis-pthalocyanine (Pc) ligands and a single ion (Dy^{3+} , Ho^{3+} or Yb^{3+}), which display magnetic hysteresis under favourable conditions.^{3,91-96} More recently, it has been shown that strong anisotropy can be harnessed in sandwich complexes of lanthanide centres with axial ligand fields provided by carbocyclic ligands such as COT, COT' and Cp^* .^{4-6,43,97-101} Indeed, these sandwich complexes exhibit some remarkable magnetic properties, with $[(\text{COT})_2\text{Er}]^+$ standing as the current record holder for the highest blocking temperature recorded for a single ion SMM.¹⁰⁰

A noteworthy feature of the mixed-sandwich pentalene/ Cp^* complexes such as $(\eta^8\text{-Pn}^\dagger)\text{SmCp}^*$ encountered previously in this work, is their near axial symmetry ($\text{Ct}(\text{Cp}^*)\text{-M-Ct}(\text{Pn bridgehead})$ angle = 174.56°).^{21,57} This prompted a preliminary investigation into lanthanide Pn^\dagger complexes for comparison with those of COT, with a particular focus on the relative ability of the pentalene ligand to promote crystal field influence on the lanthanide ion's magnetic behaviour.

2.3.2 *Synthesis and characterisation of $(\eta^8\text{-Pn}^\dagger)\text{LnCp}^*$ complexes for Ln = Dy (2.6), Tb (2.7) and Y (2.8)*

The synthesis of the mononuclear mixed-sandwich complexes, $(\eta^8\text{-Pn}^\dagger)\text{LnCp}^*$ (Ln = Dy (2.6), Tb (2.7), Yb (2.8)), was achieved by reaction of LnX_3 with one equivalent of $[\text{K}]_2\text{Pn}^\dagger$ and NaCp^* in THF (Scheme 2.10). Subsequent work-up and recrystallisation from pentane furnished **2.6**, **2.7** and **2.8** as yellow crystals in *ca.* 35% yield, which were identified by elemental analysis and mass spectrometry. The yttrium complex **2.8** was diamagnetic, which allowed for additional characterisation by (^1H , ^{13}C , ^{29}Si) NMR spectroscopy.



Scheme 2.10 Synthesis of $(\eta^8\text{-Pn}^\dagger)\text{LnCp}^*$ complexes.

X-ray diffraction analysis of **2.6**, **2.7** and **2.8** revealed a molecular structure (Figure 2.10) comparable with the f-element mixed sandwich complexes $(\eta^8\text{-Pn}^\dagger)\text{SmCp}^*$ and $(\eta^8\text{-Pn}^\dagger)\text{UCp}^*$ reported by Cloke *et al.*^{21,57} Structures **2.6**, **2.7** and **2.8** are isomorphous and the $\text{Ct}(\text{Cp}^*)\text{--metal--Ct}(\text{Pn bridgehead})$ angle (*ca.* 170°) shows that the mixed-sandwich structure provides a near axial coordination environment for the Ln^{3+} ions.

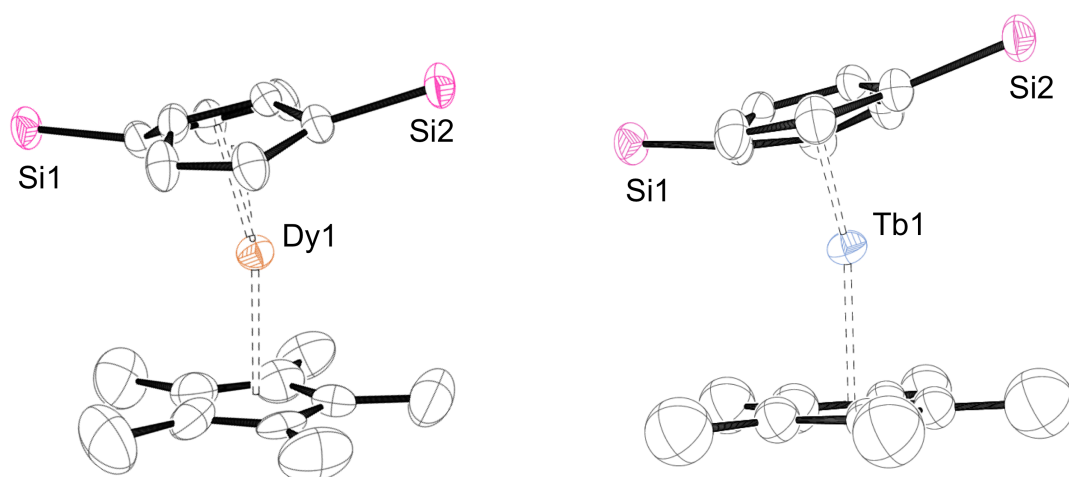


Figure 2.10 ORTEP views of **2.6** and **2.7** (part 1) with ellipsoids at 50% probability. ⁱPr groups and H atoms omitted for clarity. Dynamic disorder in the Cp* ligands was modelled over two positions, with carbon atoms left isotropic for **2.7**.

Table 2.7 Selected distances (Å) and angles (°) for **2.6**, **2.7** (part 1) and **2.8** (part 1). Ct1 and Ct2 are the η^5, η^5 -centroids of the Pn ring and Ct3 is the midpoint of the bridgehead bond. Ct4 is the η^5 -centroid of the Cp* ring.

	2.6	2.7	2.8
M–Ct1(Pn)	2.2361(5)	2.2447(2)	2.2262(13)
M–Ct2(Pn)	2.2426(5)	2.2492(2)	2.2248(14)
M–Ct4(Cp*)	2.3749(5)	2.3862(2)	2.327(4)
Ct3–M–Ct4	170.83(2)	170.78(11)	170.93(9)
Fold angle	26.5(3)	26.8(2)	27.5(2)

2.3.3 Magnetic studies

The magnetic properties of **2.6** were studied by Layfield *et al.*¹⁰² The magnetic susceptibility of **2.6** was measured under an applied field of 0.1 Tesla in the temperature range 1.8 - 300 K (Figure 2.11, left). The room temperature $\chi_m T$ value of 12.14 cm³ K mol⁻¹ is slightly lower than the calculated value for a Dy³⁺ free ion using

the Landé formula ($4f^9$, ground term ${}^6H_{15/2}$, $g_J = 4/3$, $\chi_m T = 14.17 \text{ cm}^3 \text{ K mol}^{-1}$), and a repeat measurement would be required to be confident of the value. The $\chi_m T$ product gradually decreases with decreasing temperature, and reaches a minimum value of $10.00 \text{ cm}^3 \text{ K mol}^{-1}$ at 2 K. The decrease in magnetisation at low temperatures has been attributed to the large inherent magnetic anisotropy of the Dy^{3+} ion,⁴ however depopulation of the excited states in conjunction with weak intermolecular interactions cannot be ruled out as a contributing factor.¹⁰³

Field dependent measurements from 0 to 7 Tesla at low temperatures (Figure 2.11, right) suggest that saturation of the magnetisation occurs in the high field limit, reaching a value of $6.89 \mu_B$ at 7 Tesla for 1.8 K. The M vs H plots recorded at different temperatures are close to superimposition at high field, which is consistent with a well-separated ground state.

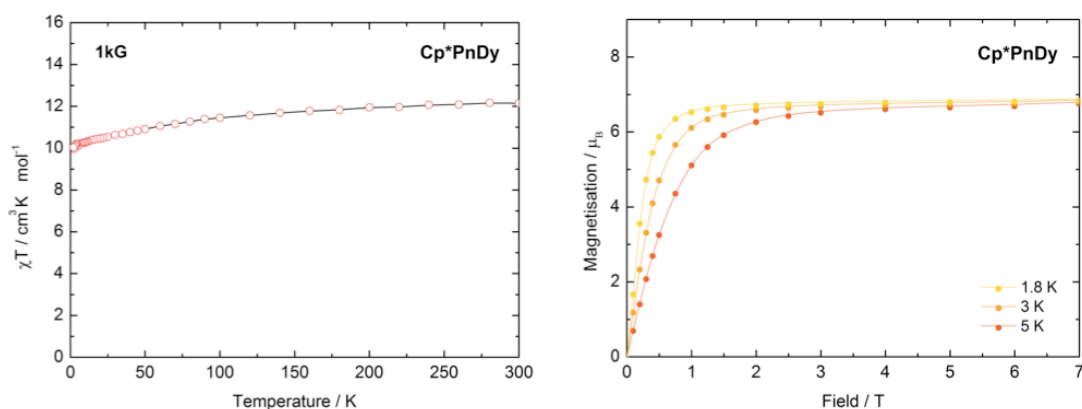


Figure 2.11 Variable temperature (left) and field (right) magnetism of **2.6**.¹⁰²

Variable-frequency alternating current (ac) susceptibility measurements were performed to gain insight into the dynamics of magnetisation relaxation, using an oscillating field of 3.5 Oe. The out-of-phase ac susceptibility (χ'') of **2.6** in the absence of an applied dc field (Figure 2.12, left) shows a frequency dependence in the range of 5 to 39 K, which confirms the SMM nature of complex **2.6**.⁸⁷ At temperatures below *ca.* 20 K the frequency dependence of χ'' is less pronounced, which is typical of efficient quantum tunneling of magnetisation (QTM) due to the mixing of Kramers ground states.^{6,104,105} Above this temperature there is a gradual shift to a second regime, which is more strongly temperature dependent.

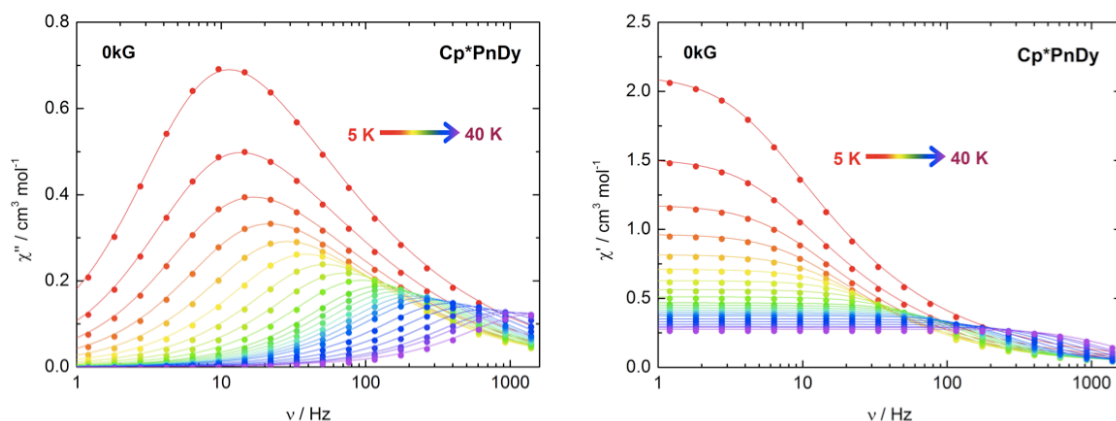


Figure 2.12 Frequency dependence of the out-of-phase (χ'' , left) and in-phase (χ' , right) component of the ac susceptibility for **2.6** in zero applied dc field.¹⁰²

The related Ln(III) mixed-sandwich complex, $(\eta^8\text{-COT})\text{ErCp}^*$,¹⁰⁶ studied by Wang and Gao *et al.*⁶ also shows two magnetic relaxation processes, which these researchers linked to the presence of two static conformations of the COT ring in its crystal structure.³³ This Er^{3+} complex also showed QTM at zero dc field and low temperature which was attributed to the deviation from ideal axial symmetry induced by an 8° tilting of the planar COT/Cp* rings. Compound **2.6** shows crystallographic disorder in the Cp* ligand although it is more likely that this arises from dynamic positional disorder rather than the coexistence of two static conformers. The ratio of the Cp* positions was determined to be 57:43 by refinement of the X-ray data at 173 K.

QTM can be effectively suppressed by performing the ac magnetic measurements in the presence of an external dc field, resulting in significant improvement of the ac response of the complex. In the presence of a 1000 Oe applied dc field, the χ'' vs ν plots for **2.6** show clear maxima which are frequency and temperature dependent (Figure 2.13, left).

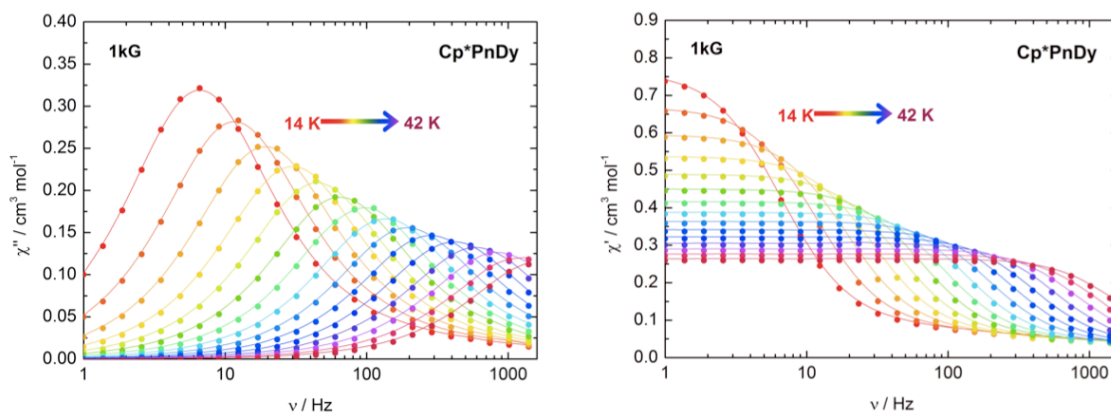


Figure 2.13 Frequency dependence of the out-of-phase (χ'' , left) and in-phase (χ' , right) component of the ac susceptibility for **2.6** in 1000 Oe applied dc field.¹⁰²

A quantitative analysis method of SMM behavior is the construction of an out-of-phase (χ'') vs in-phase (χ') ac susceptibility plot, known as a Cole-Cole plot.^{84,87} This type of plot is particularly useful for describing the distribution of relaxation times with an empirical parameter, α .⁸³ The χ'' vs χ' data for **2.6** were fitted to a modified Debye model (Figure 2.14, left),^{107,108} giving an α -parameter which is close to zero ($0.073 \geq \alpha$), indicating a narrow distribution of relaxation times. This is consistent with one dominant relaxation process, suggesting that the 1000 Oe applied dc field leads to suppression of the QTM in **2.6**.

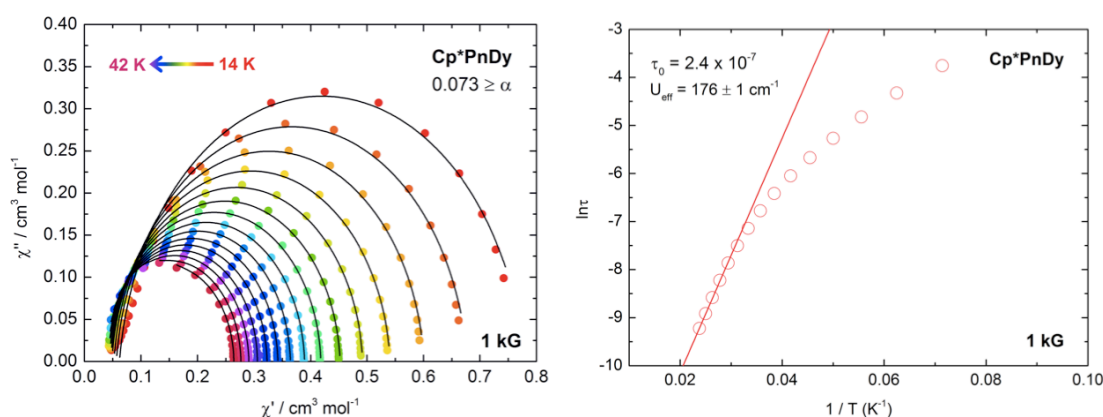


Figure 2.14 Cole-Cole (left) and Arrhenius (right) plots for **2.6** in 1000 Oe applied dc field. Black lines represent a best fit of the data at each temperature between 14 - 42 K. The red line is the best fit of the data in the thermally activated regime ($T > 42 \text{ K}$).¹⁰²

The χ'' data were plotted as a function of frequency for each temperature, which allows the relaxation time constant (τ) to be calculated using $\tau = 1/(2\pi\nu)$ where ν is the frequency corresponding to the χ'' maxima. A plot of τ vs T allows the experimental data to be fitted to an Arrhenius law:

$$\tau = \tau_0 \exp \left[\frac{U_{\text{eff}}}{k_B T} \right] \quad \text{Equation 2.4}$$

where τ_0 (in units of s) is a pre-exponential factor that depends on the environment of the individual molecules and U_{eff} (in units of cm^{-1}) is the effective barrier to magnetisation reversal (or the anisotropy barrier). The magnitude of U_{eff} is one way of

comparing the success of different SMMs, especially lanthanide based SMMs due to the prevalence of QTM. The greater the barrier, the more prominent the SMM properties at higher temperatures.⁸⁸ The Arrhenius plot of $\ln(\tau)$ against $1/T$ is linear in the high temperature region (Figure 2.14, right). Fitting the data above this temperature to the Arrhenius law produced a U_{eff} of $176 \pm 1 \text{ cm}^{-1}$ and $\tau_0 = 2.4 \times 10^{-7} \text{ s}$. This value is of the order of magnitude of lanthanide single ion SMMs with COT ligands found in the literature (Table 2.8).

Table 2.8 Effective barriers recorded for single ion Ln^{3+} SMMs with COT ligands.

Compound	$U_{\text{eff}} / \text{cm}^{-1}$	τ_0 / s	dc field / Oe	ref
(COT)ErCp*	(i) 137 (ii) 224	(i) 8.17×10^{-11} (ii) 3.13×10^{-7}	0	6
(COT)HoCp*	(i) 23.5 (ii) 17.0	(i) 2.4×10^{-5} (ii) 7.0×10^{-6}	6000	98
(COT)DyCp*	25.2	1×10^{-6}	100	98
$[(\text{COT})_2\text{Er}][\text{K}(18\text{-C-}6)]$	147	8.3×10^{-8}	0	100
$[(\text{COT})_2\text{Dy}][\text{K}(18\text{-C-}6)]$	9	2.7×10^{-8}	0	4
$[(\text{COT}')_2\text{Er}][\text{Li}(\text{DME})_3]$	130	4×10^{-8}	0	99
$[(\text{COT}')_2\text{Dy}][\text{Li}(\text{DME})_3]$	17.4	6.1×10^{-6}	0	4

In the hysteresis measurement the change in magnetisation of the sample is monitored as the field is swept from $+H$ to $-H$ and back to $+H$ at a range of temperatures.¹⁰⁹ Hysteresis loops are observed when the magnetisation of the sample depends on its history, which is the basis of the use of magnets for storing information.⁸⁴ Variable field measurements of **2.6** within $\pm 2 \text{ T}$ (Figure 2.15) revealed a waist-restricted hysteresis loop at 1.8 and 2 K at a sweep rate of 7.6 mT s^{-1} , which is indicative of SMM behaviour. The sharp change in magnetisation at zero field is attributed to efficient quantum tunneling of magnetisation (QTM), which is a common occurrence in organolanthanide SMMs.^{88,98}

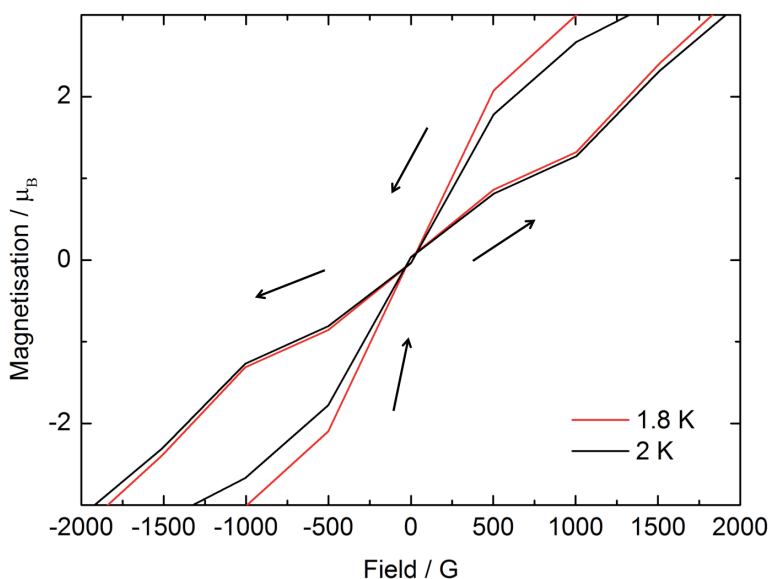


Figure 2.15 Variable field magnetisation for **2.6** near zero field, revealing hysteresis.¹⁰²

Magnetic dilution studies are required to confirm whether it is indeed a single ion feature rather than a long-range interaction that is responsible for the observed hysteresis.^{43,98,100} However in literature examples such as (COT)DyCp*,⁶ magnetic site dilution leads to enhanced SMM properties. Diluted samples with approximate composition $[(\eta^8\text{-Pn}^\dagger)\text{Dy}_{0.05}\text{Y}_{0.95}\text{Cp}^*]$ were readily prepared by co-crystallisation of **2.6** with the Y^{3+} complex **2.8**, as the structures are isomorphous. Unfortunately, magnetic studies on the diluted samples were not possible due to time constraints.

2.4 Conclusions

The synthesis of anti-bimetallic complexes of the divalent lanthanides was first investigated, with the half-sandwich $\text{Cp}^*\text{Ln}(\text{BPh})_4$ precursor allowing for the preparation of base-free complexes $[\text{Cp}^*\text{Ln}]_2(\mu\text{-Pn}^\dagger)$ for $\text{Ln} = \text{Yb}$ (**2.1**), Eu (**2.2**) and Sm (**2.3**). Isolation of latter compound is a particular achievement, given that it could not be prepared by a similar method using the $[\text{Cp}^*\text{Sm}(\mu\text{-I})(\text{THF})_2]_2$ half-sandwich precursor, due to THF activation. The attempted synthesis of a pentalene bridged U(III) bimetallic by a parallel synthetic route was unsuccessful, but did provide a reliable new route for the preparation of mononuclear complex $(\eta^8\text{-Pn}^\dagger)\text{UCp}^*$, which is of interest for small molecule activation.

The $\text{Ln}(\text{II})$ anti-bimetallic complexes were characterised by XRD analysis, which revealed similarities between the symmetrical structures **2.1** and **2.3**, and those of THF

solvates $[\text{Cp}^*\text{Ln}\{\text{THF}\}_2]_2(\mu\text{-Pn}^\dagger)$ ($\text{Ln} = \text{Yb}$ and Eu) previously reported by Cloke *et al.* Unexpectedly, **2.3** showed a solid state molecular structure in which one Eu centre interacts with all 8 carbons of the Pn^\dagger ring, which was attributed to crystal packing forces. Paramagnetic complexes **2.2** and **2.3** were studied by variable temperature and field SQUID magnetometry, which revealed very similar magnetic behaviour to their respective mononuclear $\text{Cp}^*_2\text{Ln}(\text{II})$ complexes. The lack of magnetic interaction between the metal centres may be explained by the large $\text{Ln}\cdots\text{Ln}$ distance ($> 5 \text{ \AA}$) and the ‘core-like’ radial distribution of f-orbitals.

Electrochemical studies of $[\text{Cp}^*\text{Ln}]_2(\mu\text{-Pn}^\dagger)$ were complicated by their reactivity with polar solvents. The $\text{Sm}(\text{II})$ complex **2.3** showed sufficient stability in $\text{THF}/[^n\text{Bu}_4\text{N}][\text{PF}_6]$ over 1 h, and its CV was qualitatively comparable to that for the $\text{Yb}(\text{II})$ complex studied in this solvent. In each case the first oxidation processes had some reversibility, with $E_{1/2}$ values that are consistent with the thermodynamic trend for the $\text{Ln}^{3+/2+}$ couple. However the second process was irreversible, suggesting that the product of this second oxidation is not stable under the conditions and timescale of the experiment.

Attempted synthesis of a mixed-valence $[\text{Ln}^{\text{III}}\text{-Ln}^{\text{II}}]$ complex by chemical oxidation of **2.1** with $[\text{FeCp}^*_2][\text{B}(\text{C}_6\text{F}_5)_4]$ lead to dissociation and a mononuclear half-sandwich cation **2.4**, was isolated and structurally characterised. Reaction of $\text{Sm}(\text{II})$ complex **2.3** with carbon monoxide also yielded a mononuclear complex $(\eta^8\text{-Pn}^\dagger)\text{SmCp}^*$, which further illustrates the preference of Pn^\dagger for η^8 -hapticity in f-block metal complexes.

The synthesis of the mononuclear mixed-sandwich complexes, $(\eta^8\text{-Pn}^\dagger)\text{LnCp}^*$ ($\text{Ln} = \text{Dy}$ (**2.6**), Tb (**2.7**) and Y (**2.9**)) was achieved *via* a rational salt metathesis route, however attempts to prepare the Yb analogue by this method instead yielded the bis(pentalene) ‘ate’ complex **2.5**. The magnetic properties of the Dy complex **2.6** were studied by SQUID magnetometry, including variable-frequency ac susceptibility measurements. These studies identified **2.6** as the first known example of a pentalene based SMM, with a closed-waist hysteresis loop observed up to 2 K. Further work is warranted to fully investigate the effects the axial $\text{Pn}^\dagger/\text{Cp}^*$ ligand environment have on the magnetic properties of Dy^{3+} (**2.6**) and other highly anisotropic ions Tb^{3+} (**2.7**), Ho^{3+} and Er^{3+} . It would also be of interest to incorporate these Ln^{3+} ions into pentalene bridged anti-bimetallics as models for multi-decker single chain magnets,^{84,110} which have potential applications in quantum information processing and spintronics.¹¹¹

2.5 Experimental Details for Chapter Two

General experimental details are given in appendix A1.

2.5.1 Synthesis of $[\text{Cp}^*\text{Yb}]_2(\mu\text{:}\eta^5, \eta^5\text{-Pn}^\dagger)$ (**2.1**)

$[\text{K}]_2\text{Pn}^\dagger$ (580 mg, 1.18 mmol) in benzene (20 mL) was added portionwise to a green solution of $\text{Cp}^*\text{Yb}(\text{BPh}_4)$ (1.479 g, 2.357 mmol) in benzene (50 mL) at room temperature and allowed to stir overnight. The resulting brown suspension was filtered through Celite on a frit and evaporated to dryness *in vacuo*, to afford a brown residue. Recrystallisation from SiMe_4 at -35°C afforded X-ray quality crystals of **2.1**.(SiMe_4).

Total yield: 744 mg (61% with respect to $[\text{K}]_2\text{Pn}^\dagger$).

^1H NMR (C_6D_6 , 499.9 MHz, 303 K): δ_{H} 6.69 (2H, d, $^3J_{\text{HH}} = 2.5$ Hz, Pn CH), 5.58 (2H, d, $^3J_{\text{HH}} = 2.5$ Hz, Pn CH), 2.01 (30H, s, Cp^* CH_3), 1.28 (6H, septet, $^3J_{\text{HH}} = 7.3$ Hz, ^iPr CH), 1.13 (36H, d, $^3J_{\text{HH}} = 7.3$ Hz, ^iPr CH_3).

$^{13}\text{C}\{^1\text{H}\}$ NMR (C_6D_6 , 125.7 MHz, 303 K): δ_{C} 138.3 (Pn bridgehead C), 114.7 (Cp^* -C CH_3), 94.92 (Pn CH), 89.77 (Pn C-Si), 19.91 (^iPr CH_3), 13.32 (^iPr CH), 11.49 (Cp^* -C CH_3).

$^{29}\text{Si}\{^1\text{H}\}$ NMR (C_6D_6 , 79.4 MHz, 303 K): δ_{Si} -2.02.

$^{171}\text{Yb}\{^1\text{H}\}$ NMR (C_6D_6 , 69.9 MHz, 303 K): δ_{Yb} 59.9.

EI-MS: $m/z = 1004$ (65%), $[\text{M} - \text{CCH}_3]^+$; 723 (15%), $[\text{M} - \text{YbCp}^*]^+$.

Anal. found (calcd. for $\text{C}_{46}\text{H}_{76}\text{Yb}_2\text{Si}_2$): C, 53.69 (53.57); H, 7.36 (7.43) %.

Crystal data for **2.1**. SiMe_4 : $2(\text{C}_{27}\text{H}_{50}\text{Si}_2\text{Yb})$, $M_r = 603.89$, monoclinic, space group $P 2_1/c$, brown block, $a = 13.133(3)$ Å, $b = 17.767(4)$ Å, $c = 13.725(3)$ Å, $\alpha = \gamma = 90^\circ$, $\beta = 114.10(3)^\circ$, $V = 2923.2(10)$ Å³, $T = 173$ K, $Z = 4$, $R_{\text{int}} = 0.0821$, $\lambda_{\text{Mo}}(\text{K}\alpha) = 0.71073$ Å, $\theta_{\text{max}} = 27.48^\circ$, $R_1 [I > 2\sigma(I)] = 0.0457$, wR_2 (all data) = 0.0946, $\text{Goof} = 1.008$.

Addition of 5 drops of THF to a C_6D_6 solution of **2.1** resulted in a brown solution, with a characteristic IR band at ν 1582 cm^{-1} and an ^1H NMR spectrum consistent with the known complex $[\text{Cp}^*\text{Yb}\{\text{THF}\}]_2(\mu\text{:}\eta^5, \eta^5\text{-Pn}^\dagger)$.¹²

2.5.2 Synthesis of $[Cp^*Eu]_2(\mu-Pn^\dagger)$ (**2.2**)

A solution of $[K]_2Pn^\dagger$ (313 mg, 0.635 mmol) in toluene (30 mL) was added dropwise to a solution of $Cp^*Eu(BPh_4)$ (750 mg, 1.237 mmol) in a mixture of toluene-benzene (1:1 ratio, 60 mL) and allowed to stir overnight. The resulting orange suspension was filtered through Celite and the filtrate evaporated to dryness *in vacuo* to give an orange residue. Recrystallisation by slow evaporation of a toluene-pentane solution (1:3 ratio, 6 mL) at -35 °C afforded orange X-ray quality crystals of **2.2**·(C₇H₈). Duplicate microanalysis measurements on samples of powdered crystalline **2.2**·(C₇H₈)_x from two independent facilities best fit to a value of $x = 1.6$.

Total yield: 484 mg (68% with respect to $[K]_2Pn^\dagger$).

EI-MS: $m/z = 988$ (45%), $[M]^+$; 853 (50%), $[M - Cp^*]^+$.

Anal. found (calcd. for C₄₆H₇₆Eu₂Si₂·(C₇H₈)_{1.6}): C, 60.59 (60.44); H, 8.02 (7.87) %.

Mag. suscep. (Evans method, C₆D₆, 303 K): $\mu_{\text{eff}} = 7.64 \mu_B$ per M; (SQUID, 300 K): $\mu_{\text{eff}} = 7.68 \mu_B$ per M.

Crystal data for **2.2**·(C₇H₈): C₅₃H₈₄Eu₂Si₂, $M_r = 1081.30$, monoclinic, space group $P 2_1/n$, orange block, $a = 16.8151(6) \text{ \AA}$, $b = 15.4458(7) \text{ \AA}$, $c = 20.1800(7) \text{ \AA}$, $\alpha = \gamma = 90^\circ$, $\beta = 99.859(3)^\circ$, $V = 5163.8(4) \text{ \AA}^3$, $T = 173 \text{ K}$, $Z = 4$, $R_{\text{int}} = 0.0715$, $\lambda_{\text{Cu}}(\text{K}\alpha) = 1.54184 \text{ \AA}$, $\theta_{\text{max}} = 71.507^\circ$, $R_1 [I > 2\sigma(I)] = 0.0470$, wR_2 (all data) = 0.1229, $\text{Goof} = 1.057$.

Addition of 5 drops of THF to **2.2** resulted in an orange solution, with a characteristic IR band at $\nu 1145 \text{ cm}^{-1}$ and a IR fingerprint matching that of an authentic sample of the known complex $[Cp^*Eu\{\text{THF}\}]_2(\mu:\eta^5, \eta^5-Pn^\dagger)$.¹²

2.5.3 Synthesis of $[Cp^*Sm]_2(\mu:\eta^5, \eta^5-Pn^\dagger)$ (**2.3**)

A solution $[K]_2Pn^\dagger$ (471 mg, 0.957 mmol) in benzene (60 mL) was added dropwise to a solution of $Cp^*Sm(BPh_4)$ (1.159 g, 1.916 mmol) in benzene (30 mL) and allowed to stir for 8 h. The resulting brown-green suspension was filtered through Celite and the filtrate evaporated to dryness *in vacuo* to give a brown-green residue. Recrystallisation from pentane at -35 °C afforded X-ray quality crystals of **2.3**. In the solid state and solution, **2.3** slowly decomposes at room temperature to give a green compound, presumably $(\eta^8-Pn^\dagger)SmCp^*$, and therefore requires storage at -35 °C or below.

Total yield: 437 mg (46% with respect to $[\text{K}]_2\text{Pn}^\dagger$).

^1H NMR (C_6D_6 , 499.9 MHz, 303 K, selected data): δ_{H} 20.09 (6H, br, ^iPr CH), 15.53 (36H, br, ^iPr CH_3), 10.15 (2H, br, Pn H), 7.50 (2H, br, Pn H), -2.71 (30H, s, Cp^*CH_3).

$^{13}\text{C}\{^1\text{H}\}$ NMR (C_6D_6 , 125.7 MHz, 303 K): δ_{C} 24.50, 17.22, 6.45, -6.73, -24.04, -35.04, -45.84, -93.11.

$^{29}\text{Si}\{^1\text{H}\}$ NMR (C_6D_6 , 79.4 MHz, 303 K): δ_{Si} 117.7.

EI-MS: m/z = 976-992 (principal peak 985, 25%), $[\text{M}]^+$; 696-705 (principal peak 701, 100%), $[\text{M} - \text{SmCp}^*]^+$; 558-571 (principal peak 567, 35%), $[\text{M} - \text{SmCp}^*_2]^+$.

Anal. found (calcd. for $\text{C}_{46}\text{H}_{76}\text{Sm}_2\text{Si}_2$): C, 55.87 (56.03); H, 7.56 (7.77) %.

Mag. suscep. (Evans method, toluene- d_8 , 213 K): $\mu_{\text{eff}} = 3.15 \mu_{\text{B}}$ per M; (SQUID, 200 K): $\mu_{\text{eff}} = 3.04 \mu_{\text{B}}$ per M.

Crystal data for **2.3**: $\text{C}_{46}\text{H}_{76}\text{Sm}_2\text{Si}_2$, $M_r = 985.95$, triclinic, space group $P-1$, brown needle, $a = 8.3909(10) \text{ \AA}$, $b = 11.4240(15) \text{ \AA}$, $c = 24.064(3) \text{ \AA}$, $\alpha = 94.072(7)^\circ$, $\beta = 94.267(7)^\circ$, $\gamma = 92.703(7)^\circ$, $V = 2291.3(5) \text{ \AA}^3$, $T = 100 \text{ K}$, $Z = 2$, $R_{\text{int}} = 0.1189$, $\lambda_{\text{Mo}}(\text{K}\alpha) = 0.71073 \text{ \AA}$, $\theta_{\text{max}} = 25.03^\circ$, $R_1 [I > 2\sigma(I)] = 0.0698$, wR_2 (all data) = 0.1508, $\text{Goof} = 1.044$.

Removal of the solvent from the supernatant solution followed by recrystallisation from SiMe_4 at -35°C afforded green crystals, which were identified by ^1H NMR spectroscopy as the known complex, $(\eta^8\text{-Pn}^\dagger)\text{SmCp}^*$,²¹ in 22% yield with respect to $[\text{K}]_2\text{Pn}^\dagger$.

2.5.4 Synthesis of $[\text{Cp}^*\text{Yb}(\text{OEt})_3][\text{B}(\text{C}_6\text{F}_5)_4]$ (**2.4**)

To a stirred suspension of **2.1** (79 mg, 0.077 mmol) in Et_2O (10 mL) at -40°C was added $[\text{FeCp}^*_2][\text{B}(\text{C}_6\text{F}_5)_4]$ (77 mg, 0.077 mmol), and the resultant orange mixture was allowed to warm to room temperature. After 30 min the solvent was removed under reduced pressure to afford an orange-brown residue that was washed thoroughly with pentane (1 x 50, 2 x 5 mL) to remove FeCp^*_2 until the washings were colourless. The residue was then extracted with Et_2O (4 mL), concentrated to ca. 3 mL and 5 drops of $(\text{Me}_3\text{Si})_2\text{O}$ were added. Cooling this solution to -35°C produced yellow crystals that were isolated by decantation and dried *in vacuo*.

Total yield: 63 mg (68% with respect to **2.1**).

^1H NMR (THF- d_8 , 399.5 MHz, 303 K): δ_{H} 3.38 (12H, q, $^3J_{\text{HH}} = 7.0$ Hz, $\text{OEt}_2 \text{CH}_2$), 1.97 (15H, s, $\text{Cp}^* \text{CH}_3$), 1.11 (18H, t, $^3J_{\text{HH}} = 7.0$ Hz, $\text{OEt}_2 \text{CH}_3$).

$^{13}\text{C}\{^1\text{H}\}$ NMR (THF- d_8 , 100.5 MHz, 303 K): δ_{C} 113.6 (Cp^* ring C), 66.46 ($\text{OEt}_2 \text{CH}_2$), 15.82 ($\text{OEt}_2 \text{CH}_3$), 11.37 ($\text{Cp}^* \text{CH}_3$).

^{19}F NMR (THF- d_8 , 375.9 MHz, 303 K): δ_{F} -130.9 (br, *o-F*), -163.3 (t, $^3J_{\text{FF}} = 20.2$ Hz, *p-F*), -166.8 (br t, $^3J_{\text{FF}} = 17.5$ Hz, *m-F*).

$^{11}\text{B}\{^1\text{H}\}$ NMR (THF- d_8 , 128.2 MHz, 303 K): δ_{B} -14.74.

$^{171}\text{Yb}\{^1\text{H}\}$ NMR (THF- d_8 , 69.9 MHz, 303 K): δ_{Yb} 89.04.

EI-MS: No volatility.

Anal. found (calcd. for $\text{C}_{46}\text{H}_{45}\text{BF}_{20}\text{O}_3\text{Yb}$): C, 45.55 (45.67); H, 3.87 (3.75) %.

Crystal data for **2.4**: $\text{C}_{46}\text{H}_{45}\text{BF}_{20}\text{O}_3\text{Yb}$, $M_r = 1209.67$, monoclinic, space group $P2_1/c$, yellow block, $a = 12.660(3)$ Å, $b = 28.204(6)$ Å, $c = 13.915(3)$ Å, $\alpha = \gamma = 90^\circ$, $\beta = 103.12(3)^\circ$, $V = 4838.8(17)$ Å³, $T = 173$ K, $Z = 4$, $R_{\text{int}} = 0.0966$, $\lambda_{\text{Mo(K}\alpha)} = 0.71075$ Å, $\theta_{\text{max}} = 27.47^\circ$, $R_1 [I > 2\sigma(I)] = 0.0475$, wR_2 (all data) = 0.1043, $\text{Goof} = 1.009$.

2.5.5 Synthesis of $[(\eta^8\text{-Pn}^\dagger)\text{Yb}][\text{K}]$ (**2.5**)

THF (20 mL) was added to a solid mixture of YbI_3 (312 mg, 0.563 mmol) and $[\text{K}]_2\text{Pn}^\dagger$ (276 mg, 0.563 mmol) and the resultant green suspension was stirred at room temperature for 4 h. Solid NaCp^* (89 mg, 0.563 mmol) was added slowly, stirred at room temperature for 2 d and refluxed at 70°C for 5 h. The mixture was stripped to dryness and the residues were extracted with pentane (3 x 4 mL) and filtered through Celite on a frit. The bright green filtrate was concentrated to *ca.* 2 mL and following storage at -35°C produced green crystals, which were isolated by decantation and dried *in vacuo*.

Total yield: 88 mg (15% with respect to $[\text{K}]_2\text{Pn}^\dagger$).

^1H NMR (THF- d_8 , 399.5 MHz, 303 K): δ_{H} 4.90 (6H br, $\Delta\nu_{1/2} = 80$ Hz, $^i\text{Pr CH}$), 1.77 (36H br, $\Delta\nu_{1/2} = 58$ Hz, $^i\text{Pr CH}_3$), 1.10 (12H br, $\Delta\nu_{1/2} = 62$ Hz, $^i\text{Pr CH}$), -47.66 (4H br, $\Delta\nu_{1/2} = 550$ Hz, Pn H).

^{13}C , ^{29}Si and ^{171}Yb NMR resonances were not observed due to the paramagnetic nature of **2.5**.

EI-MS: $m/z = 1042$ (100%), $[M]^+$.

Anal. found (calcd. for $C_{52}H_{92}KSi_4Yb$): C, 60.05 (59.95); H, 9.32 (8.90) %.

Partially refined crystal data for **2.5**: $C_{52}H_{92}KSi_4Yb$, $M_r = 1041.78$, monoclinic, space group $P2_1/n$, green plate, $a = 14.0303(10)$ Å, $b = 35.391(3)$ Å, $c = 23.0682(16)$ Å, $\alpha = \gamma = 90^\circ$, $\beta = 93.8875(16)^\circ$, $V = 11428(12)$ Å³, $T = 100$ K, $Z = 4$, $\lambda_{Mo}(K\alpha) = 0.71075$ Å, $\theta_{max} = 27.5^\circ$, $R_1 [I > 2\sigma(I)] = 0.1271$, wR_2 (all data) = 0.4027, $Goof = 1.096$.

2.5.6 Synthesis of $(\eta^8\text{-Pn}^\dagger)\text{UCp}^*$

A solution of $[K]_2\text{Pn}^\dagger$ (159 mg, 0.324 mmol) in benzene (15 mL) was added dropwise to a solution of $\text{Cp}^*_2\text{U}(\text{BPh}_4)$ (268 mg, 0.324 mmol) in benzene (20 mL) and allowed to stir for 12 h. The resulting brown suspension was filtered through Celite and the filtrate evaporated to dryness *in vacuo* to give a brown residue. Recrystallisation from pentane at -35°C afforded brown crystals of the known compound, $(\eta^8\text{-Pn}^\dagger)\text{UCp}^*$,⁵⁷ in 40% yield with respect to $[K]_2\text{Pn}^\dagger$.

2.5.7 Synthesis of $(\eta^8\text{-Pn}^\dagger)\text{DyCp}^*$ (**2.6**)

A solution of $[K]_2\text{Pn}^\dagger$ (590 mg, 1.20 mmol) in THF (20 mL) was added dropwise to a suspension of DyCl_3 (322 mg, 1.20 mmol) in THF (40 mL) and allowed to stir for 3 h. Solid NaCp^* (189 mg, 1.19 mmol) was added slowly and the resultant orange mixture was stirred at room temperature for 12 h, then at 75°C for 3 h. The solvent was removed *in vacuo* and the residues were extracted with hexane (3 x 10 mL) and filtered through Celite on a frit. The filtrate was stripped to dryness and the crude orange solids were recrystallised from pentane at -35°C .

Total yield: 290 mg (34% with respect to $[K]_2\text{Pn}^\dagger$).

EI-MS: $m/z = 712$ (100%), $[M]^+$; 669 (25%), $[M - ^i\text{Pr}]^+$; 577 (20%), $[M - \text{Cp}^*]^+$.

Anal. found (calcd. for $C_{36}H_{61}\text{DySi}_2$): C, 60.52 (60.68); H, 8.72 (9.62) %.

Mag. suscep. (SQUID, 200 K): $\mu_{eff} = 9.85 \mu_B$.

Crystal data for **2.6**: $C_{36}H_{61}\text{DySi}_2$, $M_r = 712.52$, triclinic, space group $P-1$, yellow block, $a = 9.6968(5)$ Å, $b = 12.7898(6)$ Å, $c = 16.0392(7)$ Å, $\alpha = 71.948(4)^\circ$, $\beta = 75.157(4)^\circ$, $\gamma = 80.771(4)^\circ$, $V = 1821.05(16)$ Å³, $T = 173$ K, $Z = 2$, $R_{int} = 0.0519$, $\lambda_{Cu}(K\alpha) = 1.54184$ Å, $\theta_{max} = 71.520^\circ$, $R_1 [I > 2\sigma(I)] = 0.0474$, wR_2 (all data) = 0.1130, $Goof = 0.937$.

The magnetic site 20-fold diluted complex was synthesised by combination of the crude solids **2.8** and **2.6** in a 20:1 mole ratio, followed by recrystallisation from pentane at -35 °C. The presence of **2.8** and **2.6** in the resulting orange crystals was confirmed by EI-MS.

2.5.8 Synthesis of $(\eta^8\text{-Pn}^\dagger)\text{TbCp}^*$ (**2.7**)

Following a procedure analogous to the preparation of **2.6** starting from TbI_3 (479 mg, 0.888 mmol) afforded crystals of **2.7** in 36% yield.

EI-MS: $m/z = 706\text{--}710$ (principal peak 708, 100%), $[\text{M}]^+$; 665 (15%), $[\text{M} - \text{}^i\text{Pr}]^+$.

Anal. found (calcd. for $\text{C}_{36}\text{H}_{61}\text{Si}_2\text{Tb}$): C, 60.83 (60.99); H, 8.76 (8.67) %.

Crystal data for **2.7**: $\text{C}_{36}\text{H}_{61}\text{Si}_2\text{Tb}$, $M_r = 708.94$, the unit cell parameters are isomorphous with **2.6**, $T = 173\text{ K}$, $Z = 2$, $R_{\text{int}} = 0.0322$, $\lambda_{\text{Mo}}(\text{K}\alpha) = 0.71073\text{ \AA}$, $\theta_{\text{max}} = 29.210^\circ$, $R_1 [I > 2\sigma(I)] = 0.0394$, wR_2 (all data) = 0.0943, $\text{Goof} = 1.056$.

2.5.9 Synthesis of $(\eta^8\text{-Pn}^\dagger)\text{YCp}^*$ (**2.8**)

Following a procedure analogous to the preparation of **2.6** starting from YCl_3 (153 mg, 0.784 mmol) afforded **2.8** in 30% yield. X-ray quality crystals were grown from a saturated pentane-toluene solution (10:1 v/v) at -35 °C.

^1H NMR (C_6D_6 , 399.5 MHz, 303 K): δ_{H} 6.74 (2H, dd, $J_{\text{YH}} = 1.1$, $^3J_{\text{HH}} = 3.0\text{ Hz}$, Pn H), 5.40 (2H, d, $^3J_{\text{HH}} = 3.1\text{ Hz}$, Pn H), 1.96 (15H, s, Cp^*CH_3), 1.26 (6H, m, $^i\text{Pr CH}$), 1.15 (18H, d, $^3J_{\text{HH}} = 7.2\text{ Hz}$, $^i\text{Pr CH}_3$), 1.03 (18H, d, $^3J_{\text{HH}} = 7.3\text{ Hz}$, $^i\text{Pr CH}_3$).

$^{13}\text{C}\{^1\text{H}\}$ NMR (C_6D_6 , 125.7 MHz, 303 K): δ_{C} 147.1 (d, $J_{\text{YC}} = 3.2\text{ Hz}$, Pn bridgehead C), 131.8 (d, $J_{\text{YC}} = 1.4\text{ Hz}$, Pn CH), 119.5 (d, $J_{\text{YC}} = 1.8\text{ Hz}$, Pn CH), 103.1 (s, Cp^*CCH_3), 98.48 (d, $J_{\text{YC}} = 1.7\text{ Hz}$, Pn C-Si), 19.68 (s, $^i\text{Pr CH}_3$), 19.47 (s, $^i\text{Pr CH}_3$), 12.76 (s, $^i\text{Pr CH}$), 11.50 (s, $\text{Cp}^*\text{-CCH}_3$).

$^{29}\text{Si}\{^1\text{H}\}$ NMR (C_6D_6 , 79.4 MHz, 303 K): δ_{Si} 1.98.

EI-MS: $m/z = 639$ (100%), $[\text{M}]^+$.

Anal. found (calcd. for $\text{C}_{36}\text{H}_{61}\text{Si}_2\text{Y}$): C, 67.51 (67.67); H, 9.58 (9.62) %.

Crystal data for **2.8**: $\text{C}_{36}\text{H}_{61}\text{Si}_2\text{Y}$, $M_r = 638.93$, the unit cell parameters are isomorphous with **2.6** and **2.7**, $T = 173\text{ K}$, $Z = 2$, $R_{\text{int}} = 0.0399$, $\lambda_{\text{Mo}}(\text{K}\alpha) = 0.71073\text{ \AA}$, $\theta_{\text{max}} = 26.37^\circ$, $R_1 [I > 2\sigma(I)] = 0.0415$, wR_2 (all data) = 0.0972, $\text{Goof} = 1.039$.

2.6 References for Chapter Two

1. T. Tsuji, N. Hosoya, S. Fukazawa, R. Sugiyama, T. Iwasa, H. Tsunoyama, H. Hamaki, N. Tokitoh, and A. Nakajima, *J. Phys. Chem. C*, 2014, **118**, 5896–5907.
2. N. Hosoya, K. Yada, T. Masuda, E. Nakajo, S. Yabushita, and A. Nakajima, *J. Phys. Chem. A*, 2014, **118**, 3051–3060.
3. N. Ishikawa, T. Iino, and Y. Kaizu, *J. Am. Chem. Soc.*, 2002, **124**, 11440–11447.
4. J. J. Le Roy, M. Jeletic, S. I. Gorelsky, I. Korobkov, L. Ungur, L. F. Chibotaru, and M. Murugesu, *J. Am. Chem. Soc.*, 2013, **135**, 3502–3510.
5. N. Magnani, C. Apostolidis, A. Morgenstern, E. Colineau, J.-C. Griveau, H. Bolvin, O. Walter, and R. Caciuffo, *Angew. Chem. Int. Ed. Engl.*, 2011, **50**, 1696–1698.
6. S.-D. Jiang, B.-W. Wang, H.-L. Sun, Z.-M. Wang, and S. Gao, *J. Am. Chem. Soc.*, 2011, **133**, 4730–4733.
7. W. Geiger, *Organometallics*, 2007, **26**, 5739.
8. L. R. Morss, *Chem. Rev.*, 1976, **76**, 827–841.
9. C. J. Kuehl, R. E. Da Re, B. L. Scott, D. E. Morris, and K. D. John, *Chem. Commun.*, 2003, 2336–2337.
10. J. M. Veauthier, E. J. Schelter, C. N. Carlson, B. L. Scott, R. E. D. Re, J. D. Thompson, J. L. Kiplinger, D. E. Morris, and K. D. John, *Inorg. Chem.*, 2008, **47**, 5841–5849.
11. P. Watson and T. Tulip, *Organometallics*, 1990, **9**, 1999–2009.
12. O. T. Summerscales, S. C. Jones, F. G. N. Cloke, and P. B. Hitchcock, *Organometallics*, 2009, **28**, 5896–5908.
13. H. Schumann, M. Glanz, H. Hemling, and F. H. Görlitz, *J. Organomet. Chem.*, 1993, **462**, 155–161.
14. W. J. Evans, T. A. Ulibarri, L. R. Chamberlain, J. W. Ziller, and D. Alvarez, *Organometallics*, 1990, **9**, 2124–2130.
15. W. J. Evans, K. J. Forrestal, and J. W. Ziller, *J. Am. Chem. Soc.*, 1998, **120**, 9273–9282.
16. W. J. Evans, T. M. Champagne, and J. W. Ziller, *Organometallics*, 2007, **26**, 1204–1211.
17. W. J. Evans, J. R. Walensky, F. Furche, A. G. DiPasquale, and A. L. Rheingold, *Organometallics*, 2009, **28**, 6073–6078.
18. W. J. Evans, J. Walensky, and T. Champagne, *J. Organomet. Chem.*, 2009, **694**, 1238.
19. M. Schultz, C. J. Burns, D. J. Schwartz, and R. A. Andersen, *Organometallics*, 2000, **19**, 781–789.
20. D. J. Berg, C. J. Burns, R. A. Andersen, and A. Zalkin, *Organometallics*, 1989, **8**, 1865–1870.
21. O. T. Summerscales, D. R. Johnston, F. G. N. Cloke, and P. B. Hitchcock, *Organometallics*, 2008, **27**, 5612–5618.
22. A. G. Avent, M. A. Edelman, M. F. Lappert, and G. A. Lawless, *J. Am. Chem. Soc.*, 1989, **111**, 3423–3425.
23. J. M. Keates and G. A. Lawless, *Organometallics*, 1997, **16**, 2842–2846.
24. K. Izod, P. O'Shaughnessy, J. M. Sheffield, W. Clegg, and S. T. Liddle, *Inorg. Chem.*, 2000, **39**, 4741–4748.
25. M. Niemeyer, *Inorg. Chem.*, 2006, **45**, 9085–9095.

26. G. B. Deacon and C. M. Forsyth, *Chem.–Eur. J.*, 2004, **10**, 1798–1804.
27. P. B. Hitchcock, M. F. Lappert, and S. Tian, *Organometallics*, 2000, **19**, 3420–3428.
28. A. Edelmann, S. Blaurock, V. Lorenz, L. Hilfert, and F. T. Edelmann, *Angew. Chem. Int. Ed.*, 2007, **46**, 6732–6734.
29. D. J. Schwartz and R. A. Andersen, *Organometallics*, 1995, **14**, 4308–4318.
30. J. Mason, *Chem. Rev.*, 1987, **87**, 1299–1312.
31. J. M. Keates, G. A. Lawless, and M. P. Waugh, *Chem. Commun.*, 1996, 1627–1628.
32. W. J. Evans, M. A. Johnston, M. A. Greci, and J. W. Ziller, *Organometallics*, 1999, **18**, 1460–1464.
33. W. J. Evans, M. A. Johnston, R. D. Clark, and J. W. Ziller, *J. Chem. Soc., Dalton Trans.*, 2000, 1609–1612.
34. W. J. Evans, M. Johnston, R. Clark, R. Anwender, and J. Ziller, *Polyhedron*, 2001, **20**, 2483–2490.
35. N. G. Connelly and W. E. Geiger, *Chem. Rev.*, 1996, **96**, 877–910.
36. J. Evans, *J. Chem. Soc.*, 1959, 2003–2005.
37. E. M. Schubert, *J. Chem. Educ.*, 1992, **69**, 62.
38. T. Fukuda, W. Kuroda, and N. Ishikawa, *Chem. Commun.*, 2011, **47**, 11686–11688.
39. J. H. Van Vleck, *The Theory of Electric and Magnetic Susceptibilities*, Clarendon Press, 1932.
40. A. F. Orchard, *Magnetochemistry*, Oxford University Press, 2003.
41. N. M. Edelstein, T. J. Marks, and R. D. Fischer, *Organometallics of the f Elements*, D. Reidel Publishing Company: Dordrecht, Holland, 1979.
42. N. Edelstein, T. J. Marks, I. L. Fraga, and D. Reidel, *Fundamental and Technological Aspects of Organo-f-Element Chemistry*, D. Reidel, Dordrecht, 1985.
43. J. J. Le Roy, L. Ungur, I. Korobkov, L. F. Chibotaru, and M. Murugesu, *J. Am. Chem. Soc.*, 2014, **136**, 8003–8010.
44. W. J. Evans, L. A. Hughes, and T. P. Hanusa, *Organometallics*, 1986, **5**, 1285–1291.
45. C. J. Burns and R. A. Andersen, *J. Organomet. Chem.*, 1987, **325**, 31–37.
46. T. P. Hanusa, *Chem. Rev.*, 1993, **93**, 1023–1036.
47. R. D. Shannon, *Acta. Crystallogr. Sect. A.*, 1976, **32**, 751–767.
48. T. D. Tilley, R. A. Andersen, B. Spencer, H. Ruben, A. Zalkin, and D. H. Templeton, *Inorg. Chem.*, 1980, **19**, 2999–3003.
49. W. J. Evans, J. W. Grate, H. W. Choi, I. Bloom, W. E. Hunter, and J. L. Atwood, *J. Am. Chem. Soc.*, 1985, **107**, 941–946.
50. W. J. Evans, R. D. Clark, M. A. Ansari, and J. W. Ziller, *J. Am. Chem. Soc.*, 1998, **120**, 9555–9563.
51. W. J. Evans, L. A. Hughes, and T. P. Hanusa, *J. Am. Chem. Soc.*, 1984, **106**, 4270–4272.
52. T. D. Tilley, R. A. Andersen, and A. Zalkin, *J. Am. Chem. Soc.*, 1982, **104**, 3725–3727.
53. T. D. Tilley, R. A. Andersen, and A. Zalkin, *Inorg. Chem.*, 1984, **23**, 2271–2276.
54. J. M. Boncella and R. A. Andersen, *Organometallics*, 1985, **4**, 205–206.
55. W. J. Evans, D. K. Drummond, H. Zhang, and J. L. Atwood, *Inorg. Chem.*, 1988, **27**, 2904–2904.

56. P. B. Hitchcock, S. A. Holmes, and M. F. Lappert, *J. Chem. Soc., Chem. Commun.*, 1994, 2691–2692.
57. F. G. N. Cloke and P. B. Hitchcock, *J. Am. Chem. Soc.*, 2002, **124**, 9352–9353.
58. J. C. Green, M. L. H. Green, and G. Parkin, *Chem. Commun.*, 2012, **48**, 11481–11503.
59. O. T. Summerscales and F. G. N. Cloke, *Coord. Chem. Rev.*, 2006, **250**, 1122–1140.
60. R. G. Compton and C. E. Banks, *Understanding Voltammetry*, Imperial College Press, 2nd edn. 2011.
61. W. E. Geiger and F. Barrière, *Acc. Chem. Res.*, 2010, **43**, 1030–1039.
62. G. B. Deacon and C. M. Forsyth, *Chem. Commun.*, 2002, 2522–2523.
63. G. B. Deacon, C. M. Forsyth, and P. C. Junk, *Eur. J. Inorg. Chem.*, 2005, **2005**, 817–821.
64. G. Balazs, F. G. N. Cloke, J. Green, R. Harker, A. Harrison, P. Hitchcock, C. Jardine, and R. A. Walton, *Organometallics*, 2007, **26**, 3111–3119.
65. D. R. Johnston, *MPhil studies, University of Sussex*.
66. A. Ashley, G. Balazs, A. Cowley, J. Green, C. H. Booth, and D. O'Hare, *Chem. Commun.*, 2007, 1515–1517.
67. W. J. Evans, J. W. Grate, L. A. Hughes, H. Zhang, and J. L. Atwood, *J. Am. Chem. Soc.*, 1985, **107**, 3728–3730.
68. W. J. Evans, R. A. Keyer, and J. W. Ziller, *J. Organomet. Chem.*, 1990.
69. W. J. Evans, S. L. Gonzales, and J. W. Ziller, *J. Am. Chem. Soc.*, 1991, **113**, 7423–7424.
70. O. T. Summerscales, F. G. N. Cloke, P. B. Hitchcock, J. C. Green, and N. Hazari, *J. Am. Chem. Soc.*, 2006, **128**, 9602–9603.
71. O. Summerscales, F. G. N. Cloke, P. Hitchcock, J. Green, and N. Hazari, *Science*, 2006, **311**, 829–831.
72. A. S. P. Frey, F. G. N. Cloke, M. P. Coles, L. Maron, and T. Davin, *Angew. Chem. Int. Ed. Engl.*, 2011, **50**, 6881–6883.
73. N. Tsoureas, O. T. Summerscales, F. G. N. Cloke, and S. M. Roe, *Organometallics*, 2012, 1353–1362.
74. N. Tsoureas, L. Castro, A. F. R. Kilpatrick, L. Maron, and F. G. N. Cloke, *Chem. Sci.*, 2014, **5**, 3777–3788.
75. W. J. Evans, G. W. Nyce, K. J. Forrestal, and J. W. Ziller, *Organometallics*, 2002, **21**, 1050–1055.
76. P. J. Fagan, J. M. Manriquez, E. A. Maatta, A. M. Seyam, and T. J. Marks, *J. Am. Chem. Soc.*, 1981, **103**, 6650–6667.
77. W. J. Evans, J. Perotti, and J. Ziller, *J. Am. Chem. Soc.*, 2005, **127**, 3894–3909.
78. C. P. Larch, F. G. N. Cloke, and P. B. Hitchcock, *Chem. Commun.*, 2007, 82.
79. N. Tsoureas, A. F. R. Kilpatrick, O. T. Summerscales, J. F. Nixon, F. G. N. Cloke, and P. B. Hitchcock, *Eur. J. Inorg. Chem.*, 2013, 4085–4089.
80. R. Sessoli, D. Gatteschi, D. N. Hendrickson, and G. Christou, *MRS Bull*, 2000, **25**, 66.
81. R. Giraud, W. Wernsdorfer, A. M. Tkachuk, D. Mailly, and B. Barbara, *Phys. Rev. Lett.*, 2001, **87**, 057203.
82. L. Sorace, C. Benelli, and D. Gatteschi, *Chem. Soc. Rev.*, 2011, **40**, 3092–3104.
83. R. Sessoli and A. K. Powell, *Coord. Chem. Rev.*, 2009, **253**, 2328–2341.
84. D. Gatteschi, R. Sessoli, and J. Villain, *Molecular Nanomagnets*, Oxford University Press, 2006.
85. J. D. Rinehart and J. R. Long, *Chem. Sci.*, 2011, **2**, 2078.

86. F. Habib and M. Murugesu, *Chem. Soc. Rev.*, 2013, **42**, 3278–3288.
87. H. L. C. Feltham and S. Brooker, *Coord. Chem. Rev.*, 2014, **276**, 1–33.
88. R. A. Layfield, *Organometallics*, 2014, **33**, 1084–1099.
89. R. A. Layfield, J. J. W. McDouall, S. A. Sulway, F. Tuna, D. Collison, and R. E. P. Winpenny, *Chem.–Eur. J.*, 2010, **16**, 4442–4446.
90. S. A. Sulway, R. A. Layfield, F. Tuna, W. Wernsdorfer, and R. E. P. Winpenny, *Chem. Commun.*, 2012, **48**, 1508–1510.
91. N. Ishikawa, T. Iino, and Y. Kaizu, *J. Phys. Chem. A*, 2002, **106**, 9543–9550.
92. N. Ishikawa, M. Sugita, T. Okubo, N. Tanaka, T. Iino, and Y. Kaizu, *Inorg. Chem.*, 2003, **42**, 2440–2446.
93. N. Ishikawa, M. Sugita, T. Ishikawa, S.-Y. Koshihara, and Y. Kaizu, *J. Am. Chem. Soc.*, 2003, **125**, 8694–8695.
94. N. Ishikawa, *J. Phys. Chem. A*, 2003, **107**, 5831–5835.
95. N. Ishikawa, M. Sugita, T. Ishikawa, S.-Y. Koshihara, and Y. Kaizu, *J. Phys. Chem. B*, 2004, **108**, 11265–11271.
96. N. Ishikawa, *Struct. Bond.*, 2010, **135**, 211–228.
97. M. Jeletic, P.-H. Lin, J. J. Le Roy, I. Korobkov, S. I. Gorelsky, and M. Murugesu, *J. Am. Chem. Soc.*, 2011, **133**, 19286–19289.
98. S.-D. Jiang, S.-S. Liu, L.-N. Zhou, B.-W. Wang, Z.-M. Wang, and S. Gao, *Inorg. Chem.*, 2012, **51**, 3079–3087.
99. J. J. Le Roy, I. Korobkov, and M. Murugesu, *Chem. Commun.*, 2013, **50**, 1602–1604.
100. K. R. Meihaus and J. R. Long, *J. Am. Chem. Soc.*, 2013, **135**, 17952–17957.
101. J. J. Le Roy, I. Korobkov, J. E. Kim, E. J. Schelter, and M. Murugesu, *Dalton Trans.*, 2014, **43**, 2737–2740.
102. N. F. Chilton, F. G. N. Cloke, A. F. R. Kilpatrick, R. A. Layfield, T. Pugh, and F. Tuna, *Manuscript in progress*.
103. J. D. Rinehart, M. Fang, W. J. Evans, and J. R. Long, *Nat. Chem.*, 2011, **3**, 538–542.
104. S.-D. Jiang, B.-W. Wang, G. Su, Z.-M. Wang, and S. Gao, *Angew. Chem. Int. Ed.*, 2010, **49**, 7448–7451.
105. R. J. Blagg, L. Ungur, F. Tuna, J. Speak, P. Comar, D. Collison, W. Wernsdorfer, E. J. L. McInnes, L. F. Chibotaru, and R. E. P. Winpenny, *Nat. Chem.*, 2013, **5**, 673–678.
106. H. Schumann, R. D. Koehn, F. W. Reier, A. Dietrich, and J. Pickardt, *Organometallics*, 1989, **8**, 1388–1392.
107. K. S. Cole and R. H. Cole, *J. Chem. Phys.*, 1941, **9**, 341.
108. C. Böttcher, *Theory of Electric Polarisation*, Elsevier, 1952.
109. W. J. Evans, M. A. Johnston, R. D. Clark, and J. W. Ziller, *J. Chem. Soc., Dalton Trans.*, 2000, **276**, 1609–1612.
110. L. Bogani, A. Vindigni, R. Sessoli, and D. Gatteschi, *J. Mater. Chem.*, 2008, **18**, 4750.
111. L. Bogani and W. Wernsdorfer, *Nat. Mater.*, 2008, **7**, 179–186.

3 CHAPTER THREE: Towards Oligomeric and Heteronuclear Pentalene-Bridged Iron Complexes

3.1 Introduction

The discovery of ferrocene,¹⁻³ and the elucidation of its then unprecedented sandwich structure⁴ spurred a frenzy of research interest in the chemistry of the transition metals with cyclopentadienyl (= Cp) ligands that has lasted for over 60 years.^{5,6} This landmark discovery was further extended to prepare trivalent lanthanide (Ln) complexes, of the general formula $\text{Ln}(\text{Cp})_3$.⁷ Lanthanide elements (Yb, Eu and Sm) with an easily accessible +2 oxidation state also form bis(cyclopentadienyl) complexes,^{8,9} but these are polymeric in the solid state, and suffer from low solubility in organic solvents.¹⁰ Increasing steric bulk on the $[\text{C}_5\text{R}_5]^-$ ligand, most commonly with $\text{R} = \text{Me}$ (Cp^*), significantly enhanced the steric and electronic stability of these complexes and allowed the isolation of soluble $\text{Cp}^*_2\text{Ln}(\text{L})_x$ complexes (where L is a donor solvent) for $\text{Ln}(\text{II}) = \text{Yb}, \text{Eu}, \text{Sm}$.¹¹⁻¹³ The use of sterically hindered Cp^{R} ligands was beneficial for the isolation of the first metallocene complex of $\text{Tm}(\text{II})$,¹⁴ and the ‘ate’-complexes of $\text{Dy}(\text{II})$,¹⁵ $\text{Nd}(\text{II})$,¹⁶ and recently for all of the other remaining Ln^{2+} ions,¹⁷⁻²⁰ except the radioactive promethium.

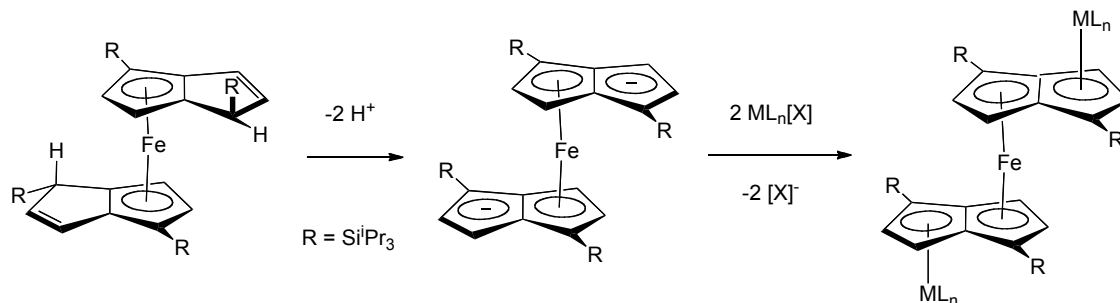
The bonding in ferrocene and its first row transition metal analogues is well described by molecular orbital methods, involving a symmetry adapted linear combination of π -orbitals from the two aromatic rings and the metal 3d-orbitals.^{21,22} In contrast, the ligand-metal bonding in $\text{Ln}(\text{III})$ sandwich complexes is thought to be more electrostatic than covalent.^{23,24} The picture is less clear for the $\text{Ln}(\text{II})$ metallocenes, since the electronic properties of the ligand do have a significant influence on their reduction potentials and observed reactivity,^{25,26} and a contribution from the metal 5d orbitals has been invoked in the bonding description.²⁷

As described in chapter one, the pentalene ligand $[\text{C}_8\text{H}_6]^{2-}$ (= Pn) has shown ability to delocalise electron density between metal centres in anti-bimetallic transition metal compounds. The parallels between mononuclear Cp chemistry and bimetallic Pn complexes provides a model for investigating the extent of delocalisation of electron density in homonuclear anti-bimetallic complexes of the divalent lanthanides.²⁸ As an extension of this study, the introduction of a transition metal into a heteronuclear anti-

bimetallic complex was suggested as a method of probing the d-orbital influence. Furthermore because there is a tendency for the Pn^{\dagger} ligand favour an η^8 - coordination mode over η^5 - with f-block metals (particularly upon oxidation of Ln^{2+} to Ln^{3+} , as described in chapter two), it was necessary to exploit a strongly η^5 -coordinating metal for heteronuclear complexes, for which iron seemed the rational choice.

3.2 Iron Bis(Pentalene) Complexes

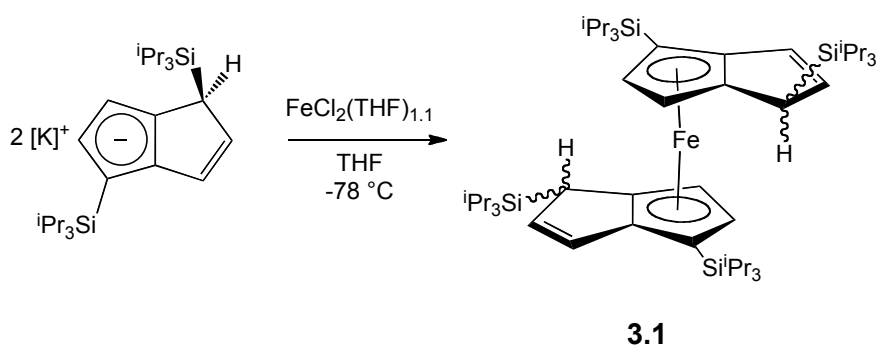
The X-ray structure of the homoleptic iron(II) complex $Fe(\eta^5-Pn^{\dagger}H)_2$ (**3.1**) was previously determined by Cloke *et al.*²⁹ and provided a convenient entry point for these synthetic studies. With a view to extending the metal-pentalene chain of **3.1**, a strategy analogous to that employed by Manriquez *et al.* was envisaged (Scheme 3.1),³⁰ in which deprotonation of the uncoordinated ring of a bound hydropentalenyl ligand would provide an opportunity for coordination of the resultant anion to other organometallic fragments (ML_n). The doubly deprotonated Fe(II) bis(pentalenyl) dianion was targeted, with the aim of incorporating two additional ML_n units into the metal-pentalene chain in one synthetic step.



Scheme 3.1 Proposed route to polymetallic Fe/M-pentalene complexes.

3.2.1 Synthesis and characterisation of $Fe(\eta^5-Pn^{\dagger}H)_2$ (**3.1**)

Compound **3.1** was prepared by reaction of the hydropentalenyl mono-potassium salt $[K]Pn^{\dagger}H$ with $FeCl_2(THF)_{1.1}$ in THF at $-78\text{ }^{\circ}C$ which gave a red suspension upon warming to room temperature. After pentane work-up a crude red solid was isolated which was recrystallised from Et_2O at $-50\text{ }^{\circ}C$ to afford **3.1** in 65% yield (Scheme 3.2).



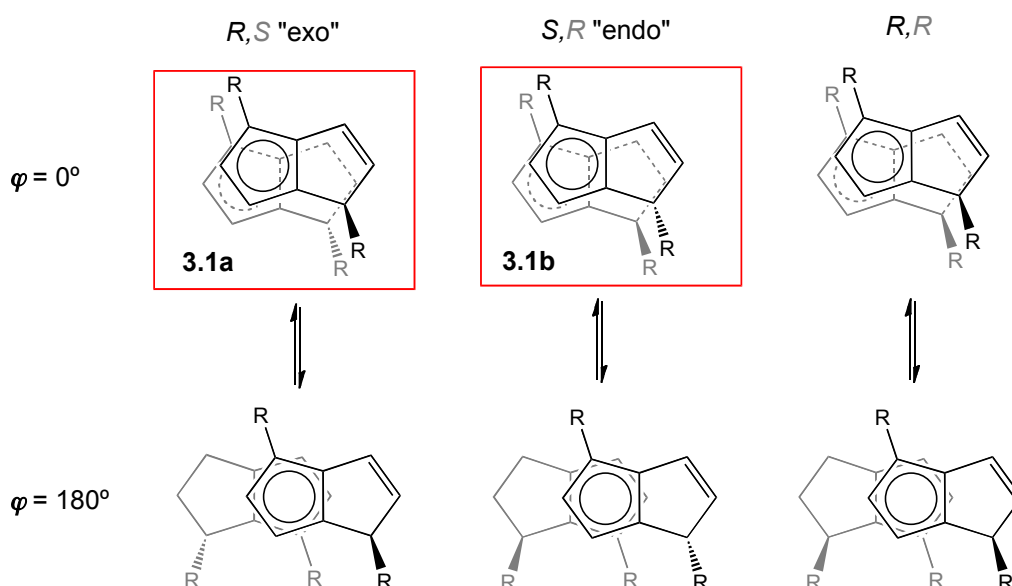
Scheme 3.2 Synthesis of **3.1**.

The ^1H NMR spectrum of **3.1** in C_6D_6 shows two sets of five peaks in ratio *ca.* 2:1, suggesting **3.1** crystallises as a mixture of two products. A similar phenomenon has been reported for Katz's $\text{Fe}(\eta^5\text{-PnH})_2$ complex which crystallises as two double-bond isomers.³¹ Analytical methods agreed with the molecular formula of two Pn^+H ligands and one Fe atom, thus confirming purity and corroborating NMR spectroscopy over the existence of two isomers. Variable temperature NMR studies showed that the two isomers do not interconvert in toluene- d_8 solution at 110 °C. NMR spectral assignments (Table 3.1) were verified by recourse to 2D correlation experiments (^1H - ^1H , ^{13}C - ^1H and ^{29}Si - ^1H).

Table 3.1 ^1H and $^{29}\text{Si}\{^1\text{H}\}$ NMR chemical shifts (ppm) in C_6D_6 for isomers of **3.1**.

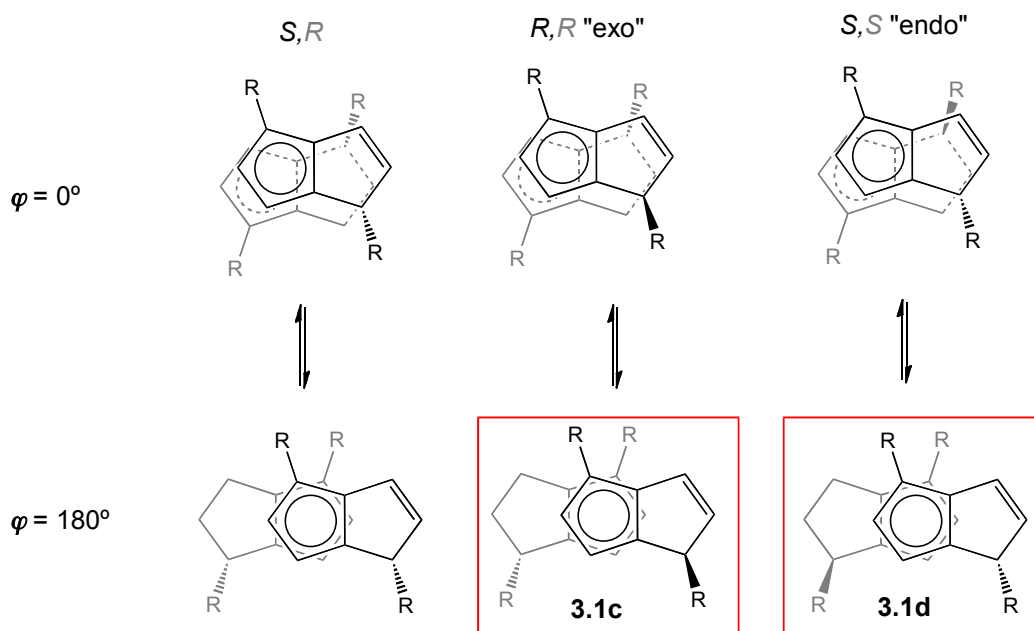
Nucleus	Assignment	Isomer I	Isomer II
δ_{H}	Pn^+ vinylic H	6.63, 6.51	6.59, 6.22
	Pn^+ aromatic H	4.01, 3.93	4.20, 4.14
	Pn^+ allylic H	3.58	2.29
	$i\text{Pr}$ CH (overlapping)	1.36	1.36
	$i\text{Pr}$ CH_3	1.29, 1.27, 1.14, 1.04	1.31, 1.26, 1.10, 1.03
δ_{Si}	allylic $Si^i\text{Pr}_3$	5.50	5.67
	aromatic $Si^i\text{Pr}_3$	5.22	4.58

The Pn^+H ligand is facially enantiotopic; hence its sandwich complexes would be expected to exist, in principle, as different diastereomers. In an idealised conformation with the frameworks of the carbocyclic rings eclipsing, there are two possible arrangements of the 1,4- Si^iPr_3 substituents on each ligand; eclipsed and staggered. With eclipsed Si^iPr_3 groups on each ligand three diastereomers are possible (Scheme 3.3), two with the Si^iPr_3 groups on the sp^3 carbon of the uncoordinated ring mutually *exo* and *endo* (*S,R* and *R,S*) and one diastereomer that exists as a pair of enantiomers (*R,R* and *S,S*). A 180° rotation about one Fe–centroid bond would relieve the relative strain energy due to the bulky Si^iPr_3 groups.



Scheme 3.3 Possible isomers of **3.1** with eclipsed 1,4- R ($= \text{Si}^i\text{Pr}_3$) substituents. The *S,S* stereoisomer has been omitted for clarity.

A further three diastereomers are possible with Si^iPr_3 groups staggered (in a conformation with the two pentalene frameworks eclipsed); again one *exo*, one *endo* and one chiral (Scheme 3.4). A 180° rotation about one Fe–centroid bond this time introduces symmetry to the *R,R* and *S,S* diastereomers.

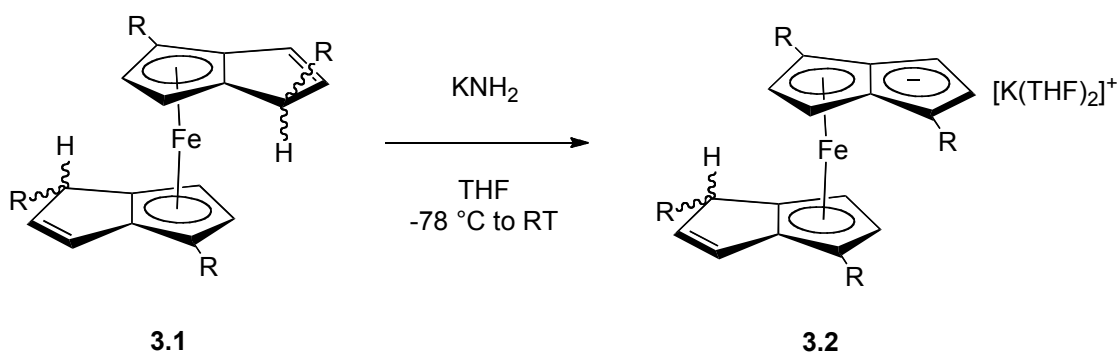


Scheme 3.4 Possible isomers of **3.1** with staggered 1,4-R (= SiⁱPr₃) substituents. The *R,S* stereoisomer has been omitted for clarity.

Given that the room temperature ¹H NMR spectrum of **3.1** shows five Pn[†]H ring signals per isomer, the two ligands must be related by symmetry over the timescale of the experiment, which implies **a**, **b**, **c**, and **d** as possible structures (highlighted in red in Scheme 3.3 and 3.4). It is postulated that the extra strain of the SiⁱPr₃ groups pointing in towards the rest of the molecule in an *endo* conformation would make these isomers less favourable energetically. Therefore **a** and **c** are proposed as the two isomers formed. The stereochemistry of the crystallographically characterised molecule (see Section 3.2.3, Figure 3.1) corresponds to that of diastereomer **3.1a**, adopting a conformation in the solid state with a dihedral angle (φ , defined by the angle between the mean planes of the Fe atom and the wing-tip C atoms of the two Pn[†]H ligands, see Section 3.2.3, Figure 3.3) of 113.88(7)° that lies between the two idealised conformations depicted in Scheme 3.3. Assuming in solution the energy barrier to rotation about the metal-centroid bonds is small in comparison with $k_B T$, the two Pn[†]H rings within each isomer are chemically equivalent on the NMR timescale.

3.2.2 Synthesis and characterisation of $(\eta^5\text{-Pn}^{\dagger}\text{H})\text{Fe}[\eta^5\text{-Pn}^{\dagger}(\eta^5\text{-K}\{\text{THF}\}_2)]$ (**3.2**)

Facile mono and double deprotonation of Katz's $\text{Fe}(\eta^5\text{-PnH})_2$ complex was achieved using *n*- and *t*-butyllithium,³¹ showing that the allylic proton on the uncoordinated ring of the hydropentalenyl ligand is relatively acidic. The ligand fragment produced, effectively a pentalenyl dianion, would have stability as a fully delocalised 10π electron aromatic system. It was proposed the trialkylsilyl-substituted hydropentalenyl ligands in **3.1** may be relatively more acidic than their unsubstituted equivalents in $\text{Fe}(\eta^5\text{-PnH})_2$, given that the allylic proton is α - to silicon.^{32,33} However, **3.1** proved to be surprisingly unreactive towards many strong bases, and no reaction was observed with *n*- or *t*-BuLi/TMEDA, KH, $\text{K}(\text{N}\{\text{SiMe}_3\}_2)$, Bu_2Mg , or $\text{Ca}(\text{N}\{\text{SiMe}_3\}_2)_2$. Reaction of **3.1** with two equivalents of potassium amide in THF at -78°C , produced a red-green colour upon warming to room temperature. Work-up and recrystallisation from pentane at -50°C afforded dark red crystals which were identified by XRD analysis as the mono-deprotonated species, **3.2** (Scheme 3.5). The molecular structure of **3.2** is discussed in Section 3.2.3.



Scheme 3.5 Mono-deprotonation of **3.1**. $\text{R} = \text{Si}^i\text{Pr}_3$.

Complex **3.2** was found to be extremely air and moisture sensitive and satisfactory elemental analysis could not be obtained. Furthermore, the ^1H NMR spectrum in $\text{THF-}d_8$ was complex and could not be assigned unambiguously.

Subsequent attempts to doubly deprotonate **3.1** using an excess of KNH_2 (6 mol equivalents) and 18-crown-6 were unsuccessful, yielding complex **3.2** exclusively. Hence, it was decided to use **3.2** without prior isolation in attempts to incorporate additional organometallic moieties into the chain.

3.2.3 X-ray crystallographic studies of **3.1** and **3.2**

The molecular structures of **3.1** (Figure 3.1)²⁹ and **3.2** (Figure 3.2) were determined by X-ray crystallography allowing for comparison of their metric parameters (Table 3.2). These sandwich structures have very similar geometries around the Fe centre, with metal-centroid distances and near linear centroid–metal–centroid angles which are consistent with ferrocene and its pentalene analogues that have been previously determined by X-ray diffraction studies.^{34–38}

Removal of an allylic proton from **3.1** to form **3.2** results in a formal negative charge on the five membered ring of the coordinated pentalene ligand, to which potassium coordinates in an η^5 - mode. The K–C_{ring} bond lengths for **3.2** lie in the range 2.943(4) - 3.046(4) Å, which are comparable with potassium cyclopentadienyl derivatives such as [K–Cp']_n (2.988(8) - 3.074(10) Å).³⁹

Key structural differences are found in the carbocyclic ligands when comparing compounds bearing a Pn[†]H ligand with one C₅-ring that is not coordinated to a metal, such as **3.1**, with bimetallic complexes bearing a dianionic Pn[†] ligand, such as **3.2**. In particular the C6–C7 bond for **3.1** (1.339(3) Å) is significantly shorter than the other C–C distances in the pentalene skeleton (1.421(3) - 1.517(3) Å). This is consistent with a localised double bond, and similar values are found in previously reported hydropentalenyl compounds Fe(η^5 -PnH)₂,³⁴ [Re(CO)₃](η^5 -PnH),⁴⁰ and (η^8 -Pn[†])Sm(η^5 -Pn[†]H),⁴¹ (*d*_{C=C} = 1.329(8), 1.377(9) and 1.354(7) Å respectively).

The C2–C1–Si1 bond angles for **3.1** and **3.2** (126.85(18)° and 125.0(2)° respectively) are consistent with a near planar C1 in the η^5 -coordinated ring of both Pn[†]H and Pn[†] ligands. This contrasts with the C7–C8–Si2 angles (115.08(17)° and 125.3(3)° respectively), which are significantly smaller for **3.1** illustrating the near tetrahedral geometry of the allylic C8 in the uncoordinated ring of these complex. The allylic protons H8 and H27 in **3.1** are arranged *endo* to the Fe centre and are sterically shielded by the *exo* SiⁱPr₃ groups, which is a possible reason for the difficulty of deprotonation at these positions with strong bases such as ^tBuLi. Both Pn[†] and Pn[†]H ligands serve as 5 electron donors (L₂X) to each metal centre in η^5 -mode, but in the Pn[†]H case the π -electron density is only delocalised around one half of the pentalene skeleton.^{31,42} This is reflected in shorter Fe–Ct1 distances and smaller \angle values for **3.1** compared with **3.2**.

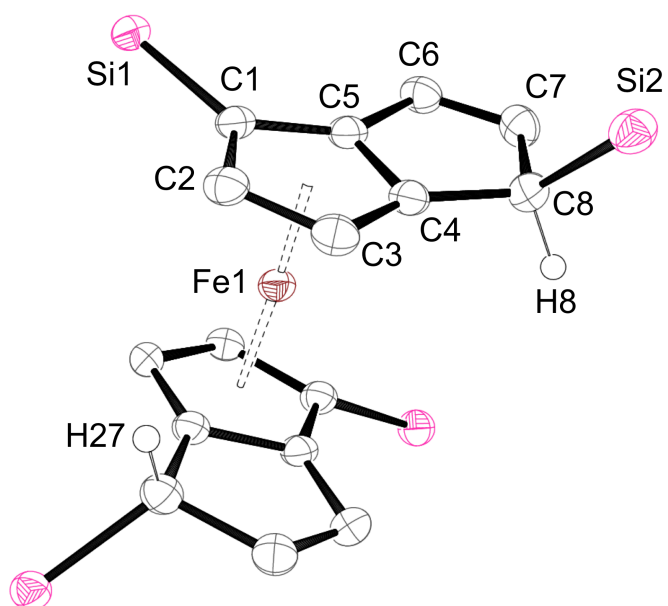


Figure 3.1 Displacement ellipsoid plot (50% probability) of **3.1**.²⁹
H atoms (except H8 and H27) and ⁱPr groups omitted for clarity.

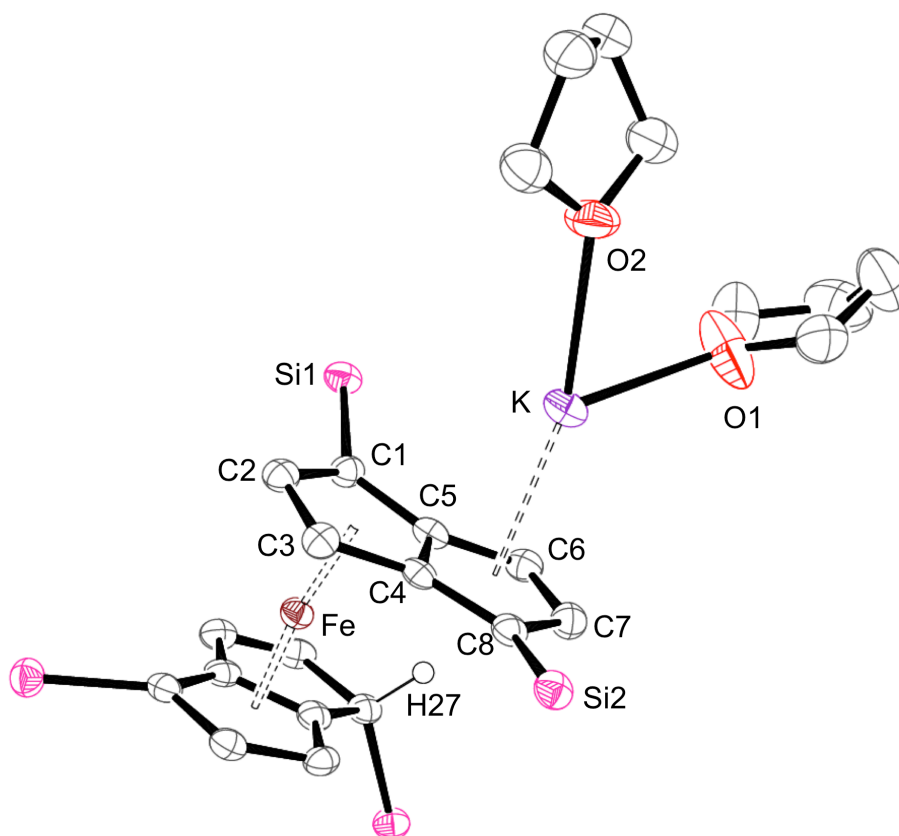


Figure 3.2 Displacement ellipsoid plot (50% probability) of **3.2**.
H atoms (except H27) and ⁱPr groups omitted for clarity.

Table 3.2 Selected distances (Å), angles (°) and parameters (defined in Figure 3.3) for **3.1** and **3.2**. Ct1 and Ct3 correspond to the η^5 -centroids of the Pn1 and Pn2 rings respectively.

Parameter	3.1	3.2
Fe–C1	2.086(2)	2.085(3)
Fe–C2	2.022(2)	2.024(4)
Fe–C3	2.051(2)	2.065(5)
Fe–C4	2.098(2)	2.173(4)
Fe–C5	2.094(2)	2.120(3)
φ	113.9	95.7
$\Delta_{\text{Fe-Ct1}}$	0.043	0.089
Fe–Ct1	1.6731(11)	1.6936(5)
Fe–Ct3	1.6719(10)	1.6756(5)
Ct1–Fe–Ct3	173.48(5)	170.83(8)
C1–C2	1.451(3)	1.454(5)
C2–C3	1.429(3)	1.429(5)
C6–C7	1.339(3)	1.384(6)
C7–C8	1.517(3)	1.423(5)
av. C–C _{ring}	1.444(3)	1.436(5)
C2–C1–Si1	126.85(18)	125.0(2)
C7–C8–Si2	115.08(17)	125.3(3)
Fe...K	-	4.773

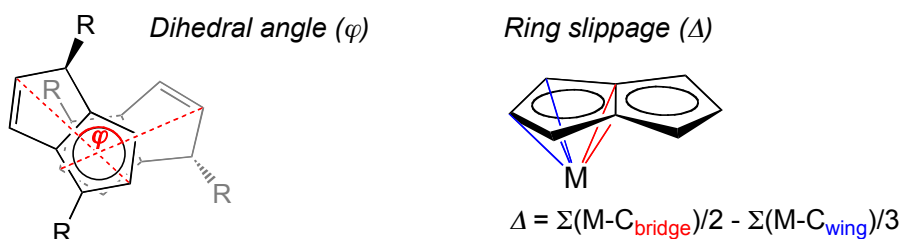
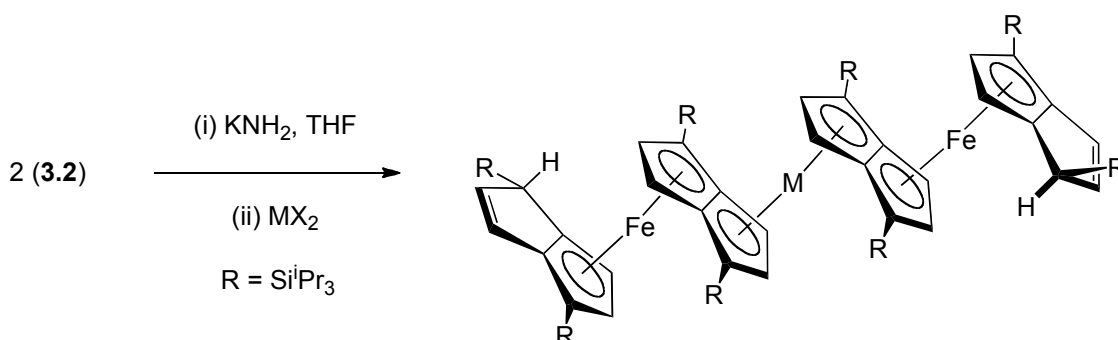


Figure 3.3

3.2.4 Reactions of **3.2**

Taking inspiration from the quadruple-decker iron-pentalene complexes of Manriquez *et al.*, two equivalents of the monoanionic **3.2** were reacted with one equivalent of a divalent metal salt, MX_2 , in an attempt to link two bis(pentalenyl)iron fragments *via* a divalent metal (Scheme 3.6). Possible candidates for M^{2+} included Fe and Yb, since they would give diamagnetic products.



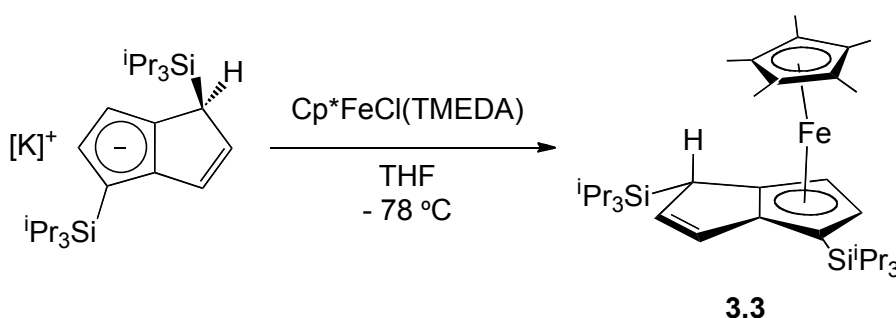
Scheme 3.6 Proposed route to trimetallic complexes.

A solution of **3.2** in THF, generated *in situ*, was added dropwise to a suspension of $\text{FeCl}_2(\text{THF})_{1.1}$ in THF at -78°C . The reaction mixture was allowed to warm to room temperature and stir for five days, resulting in a red solution and the precipitation of a dark solid. Unfortunately after work-up the only constituent of the resultant crude solution was **3.1** (present as a mixture of isomers, **3.1a** and **3.1c** *inter alia*). Further work was carried out in an attempt to use **3.2** to incorporate further organometallic fragments, by reaction with divalent metal salts ($\text{MX}_2 = \text{Fe}(\text{acac})_2$ and YbI_2) and mono- Cp^* complexes ($\text{Cp}^*\text{MX} = \text{Cp}^*\text{Fe}(\text{acac})$, $\text{Cp}^*\text{FeCl}(\text{TMEDA})$). In all cases the products isolated after work-up were identified by EI-MS and NMR as $\text{Fe}(\eta^5\text{-Pn}^\dagger\text{H})_2$, present as mixture of three diastereomers. Clearly the decomposition of **3.2** to **3.1** in these reactions involves protonation of a bound Pn^\dagger ligand. The fact that **3.1** is produced as a mixture of diastereomers suggests protonation of the planar pentalene ring occurs in a stereochemically undefined process, and therefore likely to arise from an intermolecular decomposition reaction or by solvent activation.

3.3 Mixed-Sandwich Iron Complexes

3.3.1 Synthesis and characterisation of $\text{Cp}^*\text{Fe}(\eta^5\text{-Pn}^\dagger\text{H})$ (**3.3**)

An alternative route to heterobimetallics was explored *via* mixed-sandwich complexes, with $\text{Pn}^\dagger\text{H}$ and Cp^* ligands, which possess higher symmetry allowing for more straightforward interpretation of NMR spectra and potentially avoid the formation of isomers complicating the situation. Synthesis of **3.3** was achieved by reaction of $[\text{K}]\text{Pn}^\dagger\text{H}$ with $\text{Cp}^*\text{FeCl}(\text{TMEDA})$ in THF, which following work-up, was isolated as orange crystals in 81% yield (Scheme 3.7).



Scheme 3.7 Synthesis of **3.3**.

Mass spectrometry and elemental analysis confirmed the identity and purity of the product. ^1H , $^{13}\text{C}\{^1\text{H}\}$ and $^{29}\text{Si}\{^1\text{H}\}$ NMR spectroscopy showed the existence of a single species and the spectra consisted of signals corresponding to the proposed formula. The latter was ultimately confirmed by single crystal XRD study which agrees with solution NMR spectroscopy. The molecular structure and metric parameters are discussed in Section 3.3.3.

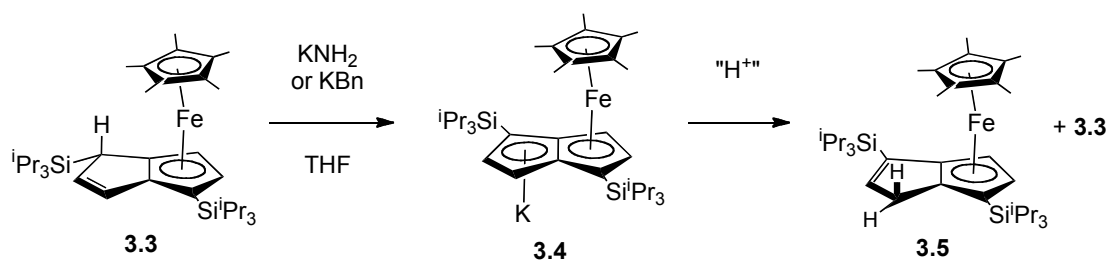
3.3.2 Synthesis and characterisation of $[\text{FeCp}^*(\mu\text{-}\eta^5\text{:}\eta^5\text{-Pn}^\dagger)] [\text{K}]$ (**3.4**)

With a view to extending the metal-pentalene chain of **3.3**, the ‘building block’ synthetic approach of Manriquez *et al.* was again pursued, in which deprotonation of the uncoordinated ring of a bound $\text{Pn}^\dagger\text{H}$ ligand would provide an opportunity for coordination of the resultant anion to other metal units. However, as found with the homoleptic analogue **3.1**, complex **3.3** was unreactive with many strong bases, including $t\text{BuLi}$, MeLi , NaNH_2 , MeK and KH . Given that Manriquez *et al.* reported that deprotonation of the unsubstituted complex $\text{Cp}^*\text{Fe}(\eta^5\text{-PnH})$ is facile with $n\text{BuLi}$, it is

postulated that the bulky *exo* SiⁱPr₃ group hinders deprotonation of H8 (H8 in Section 3.3.3, Figure 3.4).

Reaction of **3.3** with an excess of KNH₂ in THF-*d*₈ resulted in a colour change from orange to dark red over 4 days. ¹H NMR spectroscopy of the red solution after filtration revealed complete disappearance of the five pentalene ring signals for **3.3** and the appearance of a new set of peaks, including four doublets in equal ratio which were assigned to an aromatic pentalenyl ligand. ²⁹Si{¹H} NMR showed two peaks indicating an asymmetric Pn[†] ring and the formulation of a deprotonated species [Cp*Fe(μ-η⁵:η⁵-Pn[†])] [K] (**3.4**) was proposed. ¹H, ¹³C and ²⁹Si NMR assignments were corroborated through the use of two dimensional ¹H-¹H, ¹³C-¹H and ²⁹Si-¹H correlation experiments. Single crystals of **3.4** suitable for X-ray studies were grown from Et₂O and the molecular structure is discussed in Section 3.3.3. Elemental analysis of crystalline samples of **3.4** gave unsatisfactory carbon values (*ca.* 0.5% higher than calculated), presumably due to partial decomposition.

The anion-cation pair **3.4** is extremely sensitive to air and moisture, readily decomposing to afford, *inter alia*, complex **3.3** unless the most stringent precautions are taken with all glassware (flame-dried under vacuum before use) and solvents (THF and benzene pre-dried and distilled from Na/K alloy before use). Furthermore, solutions of **3.4** in THF are unstable upon solvent removal *in vacuo*; a J. Young NMR tube containing a spectroscopically pure sample of **3.4** in THF-*d*₈ was carefully exposed to dynamic vacuum, taken to dryness, and then redissolved in C₆D₆. The ¹H NMR spectrum of the resulting solution showed the presence of **3.3** with the appearance of five new ring H signals, corresponding to a previously unidentified decomposition product, **3.5**, in *ca.* 25% conversion. Compound **3.5** was separated from the reaction mixture by toluene extraction and recrystallisation from Et₂O. X-ray diffraction analysis identified these green crystals as Cp*Fe(η⁵-C₈H₅{SiⁱPr₃-1,4}2) (**3.5**), the double bond isomer of **3.3** (Section 3.3.3, Figure 3.6). The ¹H NMR spectrum of **3.5** showed two allylic H signals at 2.93 and 2.67 ppm, with a geminal coupling (²*J*_{HH} = 21.5 Hz) corroborating the migration of the C=C double bond. Complex **3.5** was further characterised by ¹³C{¹H} and ²⁹Si{¹H} NMR spectroscopy, mass spectrometry and elemental analysis. The deprotonation of mixed-sandwich iron complex **3.3** to form **3.4**, and the subsequent decomposition pathway of the latter are summarised in Scheme 3.8.



Scheme 3.8 Synthesis and decomposition of **3.4**.

3.3.3 X-ray crystallographic studies of **3.3**, **3.4** and **3.5**

As found for **3.1** and **3.2**, there are variations in ligand bond lengths and angles of the complexes with $\text{Pn}^{\dagger}\text{H}$ ligands (**3.3** and **3.5**) compared with Pn^{\dagger} (**3.4**). Comparing **3.5** and **3.3**, which can be considered as isomers of $\text{Cp}^*\text{Fe}(\eta^5\text{-Pn}^{\dagger}\text{H})$, reveals a decrease in distance C7–C8 of 0.091 Å and an elongation along C6–C7 of 0.059 Å, which is consistent with the migration of the double bond. Inspection of the metal-centroid distances shows that the mono-metallated $\text{Pn}^{\dagger}\text{H}$ ligand in **3.3** and **3.5** allows for closer coordination of the Fe centre compared with the di-metallated Pn^{\dagger} ligand in **3.4**. This situation is also observed between the two ligands in **3.2** and other bimetallic iron complexes, $[\text{Cp}^*\text{M}](\mu\text{-}\eta^5\text{:}\eta^5\text{-Pn})[\text{Fe}(\text{PnH})]$ where $\text{M} = \text{Fe}$ or Co .^{37,36}

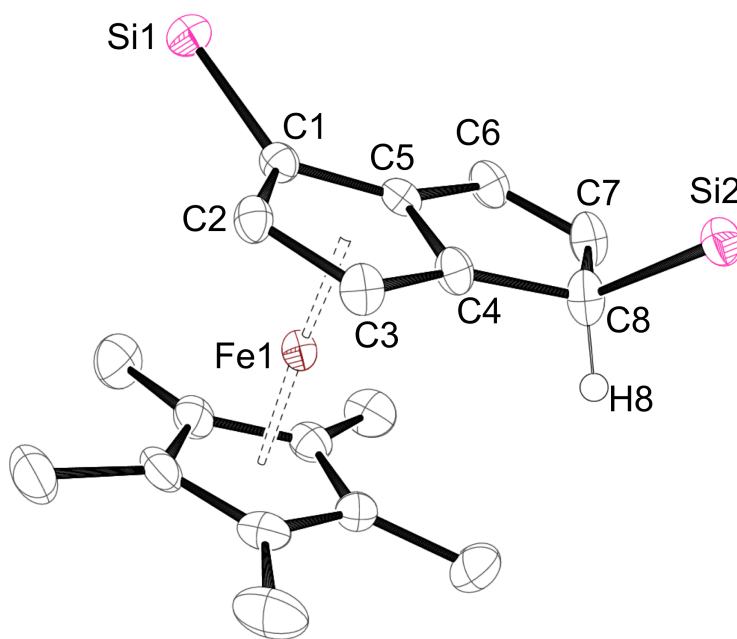


Figure 3.4 Displacement ellipsoid plot (50% probability) of **3.3**.

H atoms (except H8) and ^iPr groups omitted for clarity.

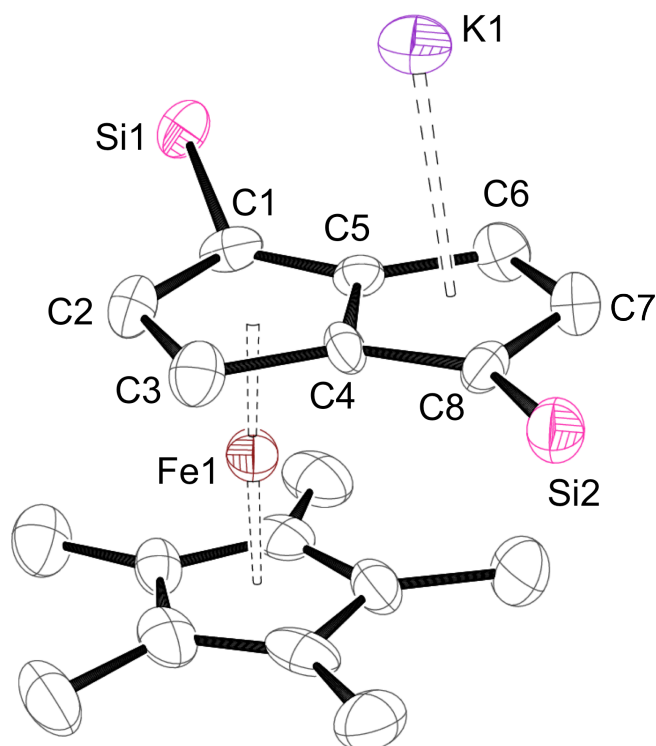


Figure 3.5 Displacement ellipsoid plot (50% probability) of **3.4**.
H atoms and ⁱPr groups omitted for clarity.

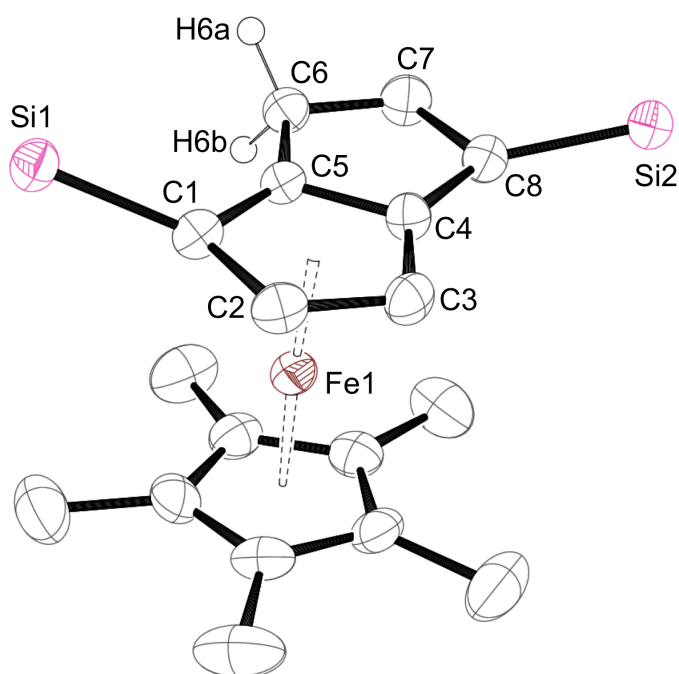


Figure 3.6 Displacement ellipsoid plot (50% probability) of **3.5**.
H atoms (except H6a and H6b) and ⁱPr groups omitted for clarity.

Table 3.3 Selected distances (Å), angles (°) and parameters (Figure 3.3) for **3.3**, **3.4** and **3.5**. Ct1 and Ct3 correspond to the η^5 -centroids of Pn and Cp* rings respectively.

Parameter	3.3	3.4	3.5
Fe–C1	2.101(3)	2.088(4)	2.079(3)
Fe–C2	2.043(3)	2.014(4)	2.029(3)
Fe–C3	2.050(3)	2.052(4)	2.057(3)
Fe–C4	2.079(3)	2.183(4)	2.136(3)
Fe–C5	2.069(3)	2.135(4)	2.091(3)
$\Delta_{\text{Fe-Ct1}}$	0.009	0.108	0.059
Fe–Ct1	1.6700(16)	1.6937(18)	1.6799(18)
Fe–Ct3	1.6667(17)	1.6468(18)	1.701(2)
Ct1–Fe–Ct3	175.53(6)	173.91(11)	176.56(8)
C1–C2	1.446(4)	1.457(6)	1.455(4)
C2–C3	1.426(4)	1.436(6)	1.419(5)
C6–C7	1.350(4)	1.393(6)	1.420(4)
C7–C8	1.504(4)	1.432(6)	1.409(4)
av. C–C _{ring}	1.443(4)	1.440(6)	1.436(5)
C2–C1–Si1	122.2(2)	121.2(3)	125.0(2)
C7–C8–Si2	113.3(3)	122.4(3)	123.1(3)
Fe...K	-	4.834	-

The K atom is closer to the Pn^{\dagger} ring in **3.4** than in **3.2**, such that it should not be considered as a discrete $[\text{LFePn}^{\dagger}][\text{K}]^+$ ion pair. Interestingly, the K atom also has close interactions with the Cp* ring of another molecule in the lattice, with K–C distances in the range 3.077(4) - 3.285(4) Å. An extended ellipsoid plot (Figure 3.7) shows that **3.4** is an organometallic polymer in the solid state.

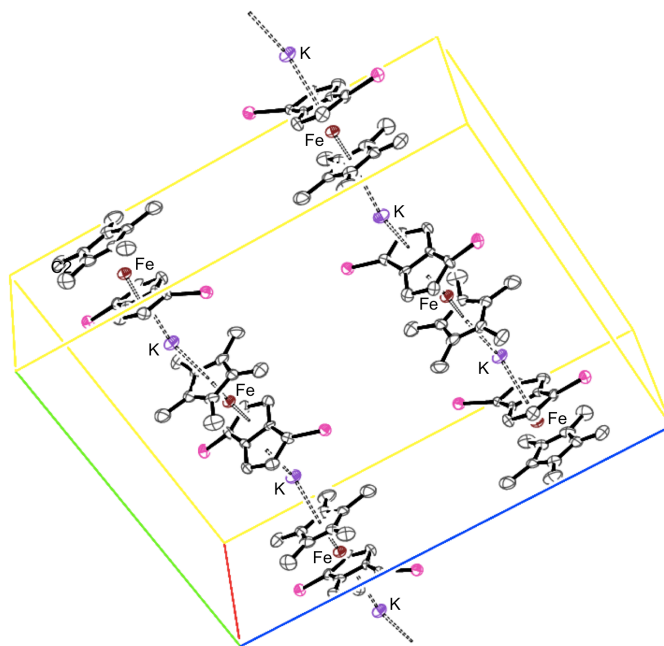


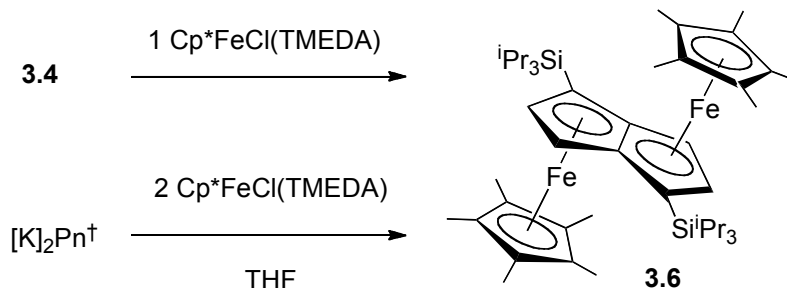
Figure 3.7 ORTEP view of the unit cell of **3.4** (50% ellipsoids).
H atoms and ⁱPr groups removed for clarity.

3.3.4 Synthesis and characterisation of $[\text{FeCp}^*]_2(\mu\text{:}\eta^5, \eta^5\text{-Pn}^\dagger)$ (**3.6**)

Despite its extreme sensitivity, Fe/K complex **3.4** presents a potentially useful precursor for other Fe/M' anti-bimetallics or for introducing additional substituents to the Pn^\dagger ligand. As an initial proof of concept, the synthesis of a homonuclear bimetallic from **3.4** was attempted.

To a solution of **3.4** in $\text{THF-}d_8$, generated from an equimolar mixture of **3.3** and benzylpotassium, was added one equivalent of $\text{Cp}^*\text{FeCl}(\text{TMEDA})$. The tube was shaken and a colour change to brown was observed after 4 h with the appearance of a brown solid, which was removed by filtration. ^1H NMR spectroscopy of the filtrate showed complete disappearance of the four aromatic signals of **3.4**, and appearance of two new doublets at 4.67 and 3.69 ppm, assigned to $[\text{Cp}^*\text{Fe}]_2(\mu\text{:}\eta^5, \eta^5\text{-Pn}^\dagger)$ (**3.6**) in *ca.* 40% conversion by integration. Additional products identified by ^1H NMR were $\text{Cp}^*\text{Fe}(\eta^5\text{-Pn}^\dagger\text{H})$ isomers **3.3** and **3.5** resulting from adventitious protonation of **3.4**. Despite the presence of additional decomposition products, the stepwise synthesis of homonuclear bimetallic **3.6** (Scheme 3.9, top) from the deprotonated species **3.4** presents a proof of concept, which was then expanded as a potential route towards trimetallic and heteronuclear organoiron complexes.

The homonuclear bimetallic complex **3.6** was independently synthesised in a single step by reaction of two equivalents of $\text{Cp}^*\text{FeCl}(\text{TMEDA})$ with $[\text{K}]_2\text{Pn}^\dagger$ in THF (Scheme 3.9, bottom), and isolated after work-up as dark green crystals in 34% yield.



Scheme 3.9 Synthetic routes to **3.6**.

Analytical and spectroscopic measurements were consistent with the proposed formulation of **3.6**, and the molecular structure of **3.6** was confirmed by a single crystal XRD study (Figure 3.8). **3.6** was poorly soluble in aliphatic and aromatic hydrocarbons and polar solvents (MeCN, $t\text{BuOMe}$, and Et_2O) at room temperature, despite the precedent for improved solubility of complexes with Si^iPr_3 substituted pentalene ligands.⁴³ However, **3.6** was sufficiently soluble in $\text{THF-}d_8$ for its ^1H NMR to be identified and allowed for its electrochemistry to be studied in this solvent (see Section 3.4). Multinuclear (^1H , ^{13}C , ^{29}Si) NMR spectra of **3.6** were consistent with a centrosymmetric structure on the NMR timescale (see chapter two, Table 2.3). The Pn^\dagger ligand exhibits metallocene-like $\mu\text{-}\eta^5\text{:}\eta^5$ coordination of the two metal centres in **3.6**, but with the Fe atoms more distant from the bridgehead carbon atoms (C4 and C4') than the three wingtip carbons (C1, C2 and C3), as quantified by the large ring-slippage (Δ) value of 0.128 Å for this complex. A similar slipping distortion has been reported in several indenyl-⁴⁴ and pentalenyl-^{37,45} metal complexes. This has been attributed in the latter to a maximisation of interaction of the metal with the π -electron density of the fused ring system, which is delocalised around its perimeter. Homo-bimetallic **3.6** shows the longest average C–C ring distances (1.454(4) Å) of the complexes in this work, and in general a smaller range of ring C–C distances are found in those complexes bearing the aromatic Pn^\dagger ligand. For comparison the ring C–C distances in Fe/K hetero-bimetallic complexes **3.2** and **3.4** are intermediate between these extremes of ‘aromatic’ and ‘localised’ character.

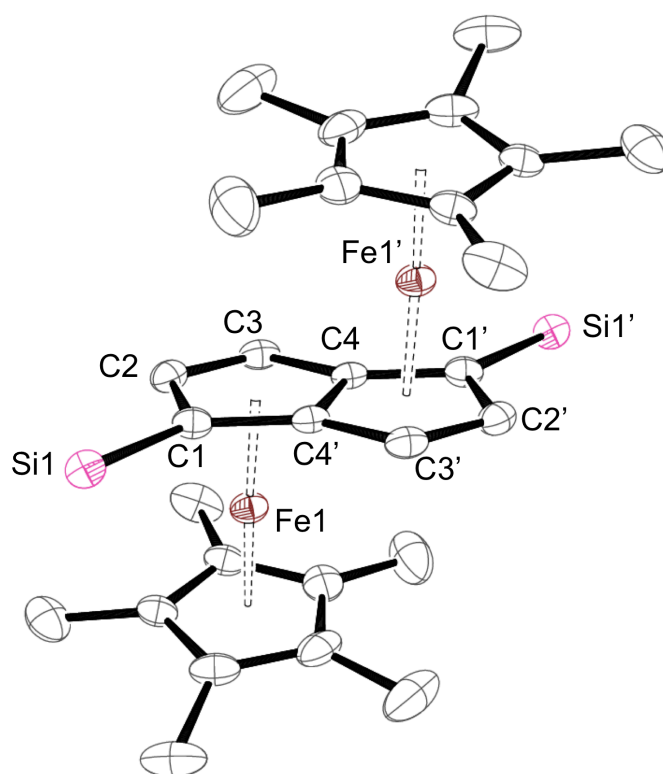


Figure 3.8 Displacement ellipsoid plot (50% probability) of **3.6**. H atoms and ⁱPr groups omitted for clarity. Primed atoms are generated by symmetry.

Table 3.4 Selected distances (Å), angles (°) and parameters (Figure 3.3) for **3.6**. Ct1 and Ct3 are the η^5 -centroids of the Pn and Cp* rings respectively.

Parameter	3.6	Parameter	3.6
Fe–C1	2.123(3)	Fe–Ct1	1.7193(13)
Fe–C2	2.033(3)	Fe–Ct3	1.7064(13)
Fe–C3	2.045(3)	Ct1–Fe–Ct3	173.36(7)
Fe–C4	2.195(3)	C1–C2	1.456(4)
$\angle_{\text{Fe-Ct1}}$	0.128	C2–C3	1.425(4)
Fe...Fe	4.132	C2–C1–Si1	125.4(2)

3.3.5 Towards oligomeric and heteronuclear pentalene-bridged complexes

Following the successful synthesis of **3.6**, the same methodology was employed in the attempted synthesis of heteronuclear Fe/Ln pentalene complexes, $\text{Cp}^*\text{Fe}(\mu\text{-Pn}^\dagger)\text{LnCp}^*$ ($\text{Ln} = \text{Yb}, \text{Sm}$). As a general procedure, a THF solution of **3.4** was prepared *in situ* and treated with one equivalent (per Ln) of half-sandwich complexes $[\text{Cp}^*\text{Ln}(\mu\text{-I})\{\text{THF}\}]_2$ or $\text{Cp}^*\text{Ln}(\text{BPh}_4)$. The reaction mixture was then filtered and analysed by ^1H NMR spectroscopy and mass spectrometry. In each case, monometallic $\text{Cp}^*\text{Fe}(\eta^5\text{-Pn}^\dagger\text{H})$ isomers **3.3** and **3.5** were the sole products identified in the ^1H NMR spectra, and EI-MS showed a parent ion at $m/z = 607$ (100%) with no higher peaks assignable to bimetallic complexes.

The deprotonated complex **3.4** is clearly unsuitable for the synthesis of heterobimetallic Fe/Ln pentalene complexes *via* salt metathesis reactions with $\text{Cp}^*\text{Ln}(\text{II})$ reagents. This may be rationalised by inspecting the DFT structure of unsubstituted analogue $[\text{CpFe}(\eta^5\text{-Pn})]^-$, reported by Saillard *et al.*⁴⁶ The net charges on the uncomplexed part of the pentalene ring in this model complex do not show any significant carbanionic character (Figure 3.9), which is consistent with it being less nucleophilic at these positions. However calculated charges are method dependent (it is assumed Saillard *et al.* employed Mulliken charges, although details are not specified in their report)⁴⁶ and other computational methods give C6 and C8 as the most negatively charged of the Pn ligand.⁴⁷ The MOs of $[\text{CpFe}(\eta^5\text{-Pn})]^-$ calculated by Green (see appendix A1.3.9 for computational methods) show a HOMO which has approximately equal ligand:metal character (Figure 3.10, left).

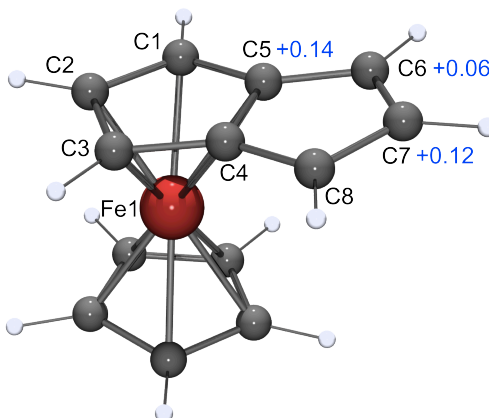


Figure 3.9 Ball and stick diagram of calculated structure of $[\text{CpFe}(\eta^5\text{-Pn})]^-$ constructed from coordinates published by Saillard *et al.*⁴⁶ Net charges on C atoms shown in blue.

The uncoordinated ring resembles the 'allyl' functionality of Pn and has an out-of-phase interaction with the d_{xy} orbital of Fe. This suggests a repulsive interaction between Fe and the uncoordinated allyl fragment, which is consistent with the larger ring slippage in the molecular structure of **3.4** relative to **3.3** ($\Delta = 0.108$ and 0.009 respectively).

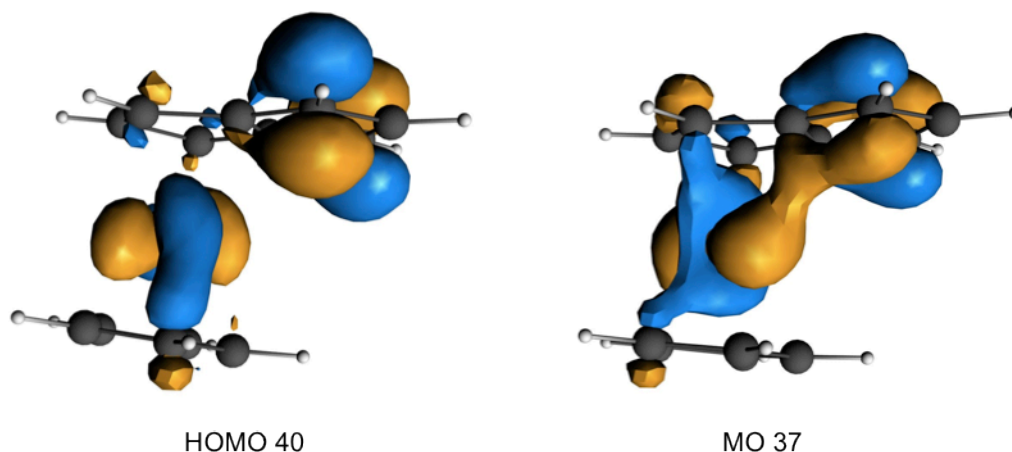


Figure 3.10 Isosurfaces for selected orbitals of $[\text{CpFe}(\eta^5\text{-Pn})]^-$.⁴⁷

It must be emphasized that these DFT modelled structures do not take into account the Si^iPr_3 substituent on the uncoordinated ring in **3.4**, which is likely to obstruct the approach of a large $\text{Cp}^*\text{Ln(II)}$ electrophile. Furthermore **3.4** exists as an oligomer in the solid state and if this structure persists to some extent in solution, it may provide an additional kinetic barrier to substitution reactions with Cp^*LnX .

3.4 Electrochemical Studies

The electrochemistry of the Fe(II) complexes in THF was studied by cyclic voltammetry (CV) to gain insight into the electron donating properties of silylated pentalene ligands, and their ability to delocalise charge over two metal centres in anti-bimetallic complexes. The use of $[\text{Bu}_4\text{N}][\text{B}(\text{C}_6\text{F}_5)_4]$ as the supporting electrolyte resulted in better resolution CV data compared with $[\text{Bu}_4\text{N}][\text{PF}_6]$, due to its lower ion-pairing capabilities (spherical diameter $[\text{B}(\text{C}_6\text{F}_5)_4]^- = 10 \text{ \AA}$; $[\text{PF}_6]^- = 3.3 \text{ \AA}$)⁴⁸ which is beneficial for the study of multi-electron processes with positively charged analytes.⁴⁹

Complexes **3.1** and **3.3** (Figure 3.11) each show a single diffusion controlled redox process assigned to the Fe(III)/Fe(II) couple. Repetitive potential cycling over electrochemical events revealed that the voltammetric responses for the oxidative and reductive waves are stable, while varying the scan rate again revealed that the voltammetry was under diffusion control and that no fouling or adsorption onto the electrode surface was occurring. In each case the ratio of oxidative and reductive peak currents (i_{pa}/i_{pc}) is close to unity, signifying a quasi-reversible process. The peak-to-peak separation (ΔE_{pp}) is comparable to that for ferrocene under the same conditions (*ca.* 100 mV), showing that only one electron is being transferred. The ideal ΔE_{pp} for a fully reversible single electron transfer at 298 K is 59 mV,⁵⁰ however this discrepancy is attributed to Ohmic losses (iR drop) in THF rather than sluggish electron transfer kinetics.

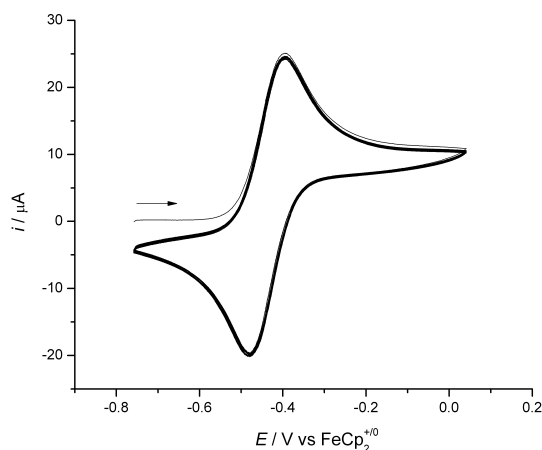
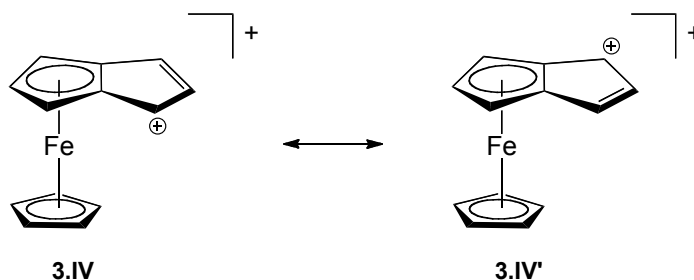


Figure 3.11 Overlaid CV scans (20 cycles) for **3.3** in THF / 50 mM [n Bu₄N][B(C₆F₅)₄], scan rate 100 mV s⁻¹.

The mid-peak potential ($E_{1/2} = \{E_{pa} + E_{pc}\}/2$) of substituted ferrocene complexes shift to more negative values as the electron donor properties of the ligand increases.^{51,52} For example the $E_{1/2}$ of decamethylferrocene under these conditions is -0.52 V (vs FeCp₂⁺⁰, a convention which is assumed for all potentials quoted henceforth),⁴⁸ due to the electron donating (+I effect) of the methyl substituents on the Cp* ring. The $E_{1/2}$ for **3.1** and **3.3** are -0.21 and -0.42 V respectively, implying that the electron donating properties of the η^5 - ligands to the Fe(II) centre increases in the sequence Cp < Pn[†]H < Cp* (Table 3.5). In this context the η^5 -Pn[†]H ligand can be viewed as one cyclopentadienyl ring with one silyl and two alkyl substituents, leading to an increased +I effect with respect to Cp.

The electrochemistry of **3.4** was of interest in terms of the bonding in the anionic $[\text{Cp}^*\text{Fe}(\eta^5\text{-Pn}^\dagger)]^-$ fragment, for comparison with the DFT calculations on model systems reported by Saillard *et al.*⁴⁶ These researchers predicted $[\text{CpFe}(\eta^5\text{-Pn})]^-$ to be stable due to its large HOMO-LUMO gap (1.68 eV), isoelectronic structure with ferrocene (18 VE on Fe) and lack of strong carbanionic character on the uncomplexed part of the pentalene ring (Section 3.3.5, Figure 3.9). In contrast, the $[\text{CpFe}(\eta^5\text{-Pn})]^+$ cation, was predicted to be highly reactive (HOMO-LUMO gap = 0.68 eV). Inspection of the LUMO revealed that the electron deficiency is shared between the Fe centre and the two 'wing-side' carbon atoms of the pentalene ligand (C4 and C6 in the labeling convention outlined in chapter one), making it susceptible to hydride attack at these positions to give hydropentalenyl complexes, which have been experimentally observed.^{31,34} Therefore a Lewis structure with an 18-electron count on Fe was preferred (**3.IV** and **3.IV'** in Scheme 3.10), resulting in a formally neutral pentalene ligand made of an anionic aromatic C_5 -ring linked to an allylic cation.



Scheme 3.10 The canonical Lewis formulae for $[\text{CpFe}(\eta^5\text{-Pn})]^+$.⁴⁶

The CV of **3.4** (Figure 3.12) shows two quasi-reversible one electron processes at -1.88 and -0.35 V. In the context of the DFT bonding interpretation in the aforementioned model systems,⁴⁶ these two successive oxidation processes to $[\text{Cp}^*\text{Fe}(\eta^5\text{-Pn}^\dagger)]^0$ and $[\text{Cp}^*\text{Fe}(\eta^5\text{-Pn}^\dagger)]^+$ may be considered as originating from orbitals that have both metal and ligand character, rather than purely metal based processes corresponding to Fe(II)/Fe(III) and Fe(III)/Fe(IV) oxidations respectively. DFT analysis by Green revealed that removal of two electrons from the $[\text{CpFe}(\eta^5\text{-Pn})]^-$ HOMO (Section 3.3.5, Figure 3.10) resulted in the 'allyl' portion of the uncoordinated ring becoming weakly bonding with the Fe orbitals.⁴⁷ This was accompanied by a 0.17 Å shift in Fe position towards the 'wing-side' carbon atoms (C6 and C8) in the calculated structure of the

$[\text{CpFe}(\eta^5\text{-Pn})]^+$ cation (see appendix A2 for MOs). Further experiments such as *in situ* UV-Vis spectroelectrochemistry would be required to determine the extent to which the two oxidations of **3.4** are metal or ligand based. The reversibility of the two processes suggests that the $[\text{Cp}^*\text{Fe}(\eta^5\text{-Pn}^\dagger)]^+$ cation is stable on the experimental timescale, however due to time constraints the synthesis of this complex on a preparative scale was not pursued in this study.

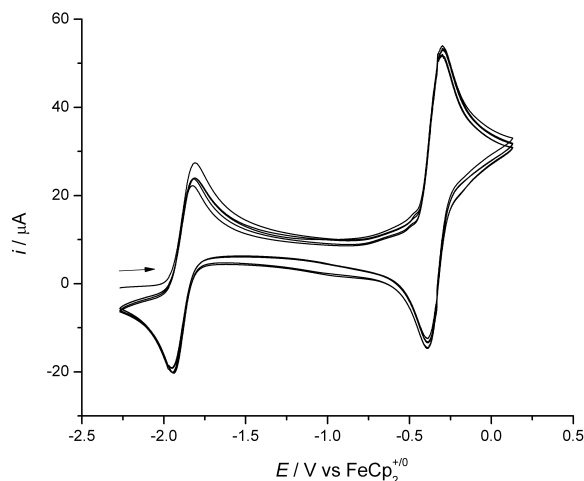


Figure 3.12 Overlaid CV scans (10 cycles) for **3.4** in THF / 50 mM $[\text{}^n\text{Bu}_4\text{N}][\text{B}(\text{C}_6\text{F}_5)_4]$, scan rate 100 mV s^{-1} .

Table 3.5 Electrode potentials ($E_{1/2}$) vs $\text{FeCp}_2^{+/0}$ in THF/ $[\text{}^n\text{Bu}_4\text{N}][\text{A}]$.

Compound	$E_{1/2} / \text{V}$	electrolyte $[\text{A}]^-$	ref
FeCp_2	0.00	$[\text{B}(\text{C}_6\text{F}_5)_4]$	by definition
$\text{Fe}(\eta^5\text{-Pn}^\dagger\text{H})_2$ (3.1)	-0.28	$[\text{B}(\text{C}_6\text{F}_5)_4]$	this work
$\text{Cp}^*\text{Fe}(\eta^5\text{-Pn}^\dagger\text{H})$ (3.3)	-0.41	$[\text{B}(\text{C}_6\text{F}_5)_4]$	this work
FeCp^*_2	-0.52	$[\text{B}(\text{C}_6\text{F}_5)_4]$	⁴⁸
$[\text{Cp}^*\text{Fe}(\eta^5\text{-Pn}^\dagger)][\text{K}]$ (3.4)	(I) -1.88 (II) -0.35	$[\text{B}(\text{C}_6\text{F}_5)_4]$	this work
$[\text{Cp}^*\text{Fe}]_2(\mu\text{-Pn}^\dagger)$ (3.6)	(I) -0.41 (II) +0.45 ^a	$[\text{B}(\text{C}_6\text{F}_5)_4]$	this work
$[\text{Cp}^*\text{Fe}]_2(\mu\text{-Pn})$	(I) -0.84 ^b (II) +0.01 ^b	$[\text{ClO}_4]$	⁵³

^a Irreversible anodic process.

^b Converted using $E_{1/2}(\text{FeCp}_2^{+/0}) = 0.53 \text{ V vs SCE in THF}/[\text{}^n\text{Bu}_4\text{N}][\text{ClO}_4]$.⁵⁴

As outlined in chapter one, CV allows an initial investigation into the stability of the mixed-valence states in bimetallic complexes e.g. $[\text{Fe}^{\text{II}}-\text{Fe}^{\text{III}}]^+$, and enables the appropriate chemical redox agent to be chosen for their large-scale preparation. The CV of **3.6** (Figure 3.13) shows two successive one-electron transfers: the first redox process centred at $E_{1/2}^{(1)} = -0.41$ V was stable over 20 cycles, and is assigned to a quasi-reversible oxidation of **3.6** the mixed valence $\text{Fe}^{\text{II}}-\text{Fe}^{\text{III}}$ mono-cation. The second process was an irreversible oxidation peak at $E_{\text{pa}}^{(2)} = +0.45$ V indicating that the $\text{Fe}^{\text{III}}-\text{Fe}^{\text{III}}$ di-cation is not stable under the conditions and timescale of the experiment. The CV was recorded at a potential scan rate of 100 mV s^{-1} , and using faster scan rates up to 1 V s^{-1} did not improve the irreversibility of this second electrochemical event.

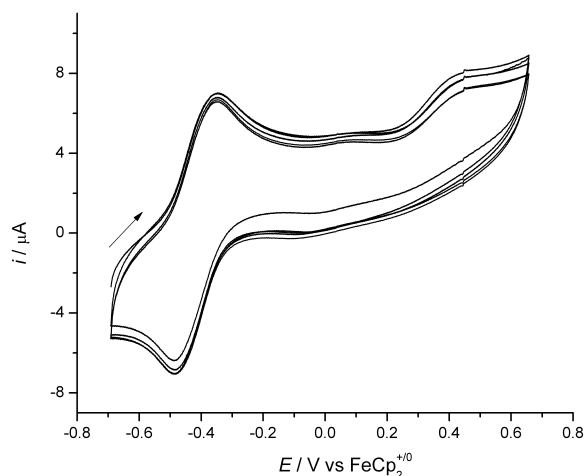


Figure 3.13 Overlaid CV scans (5 cycles) for **3.6** in THF / 50 mM $[\text{nBu}_4\text{N}][\text{B}(\text{C}_6\text{F}_5)_4]$, scan rate 100 mV s^{-1} .

The potential separation between the two electrochemical events, $\Delta E^{(2)-(1)} = 0.86 \text{ V}$, is consistent with the strong electronic interaction between the Fe centres and extensive delocalisation in the mixed-valence state, of the same magnitude as that recorded for the unsubstituted pentalene analogue $[\text{Cp}^*\text{Fe}]_2(\mu\text{-Pn})$ in THF ($\Delta E_{1/2} = 0.85 \text{ V}$).⁵³ However the $E_{1/2}$ values are notably different for $[\text{Cp}^*\text{Fe}]_2(\mu\text{-Pn})$ and **3.6** (Table 3.5), which is presumably due to the different supporting electrolytes used ($[\text{nBu}_4\text{N}][\text{ClO}_4]$ in the former case), as the electron density at the Fe(II) centres are expected to be similar for these complexes. Preliminary redox experiments on a preparative scale suggested that **3.6**, like $[\text{Cp}^*\text{Fe}]_2(\mu\text{-Pn})$, is oxidised by a stoichiometric amount of $[\text{FeCp}_2][\text{BF}_4]$ in

THF to form the mixed-valence species **[3.6][BF₄]**. However in the interest of time, and the wealth of homo-bimetallic iron complexes already present in the literature, these experiments were not pursued.

3.5 Conclusions

In these studies towards oligomeric and heteronuclear organometallic complexes, a total of six new Fe(II) compounds incorporating silylated pentalene ligands have been synthesised and characterised. A combination of NMR spectroscopic and single crystal XRD methods were used to elucidate the different isomers that form in the case of the homoleptic $\text{Pn}^{\dagger}\text{H}$ complex **3.1**. Subsequent synthetic studies showed that **3.1** could be singly deprotonated to form the mono-potassium salt **3.2**, however the latter was unsuitable as a synthon for incorporating further metal fragments into the chain, and instead underwent decomposition reactions to a mixture of isomers. The mixed-sandwich $\text{Pn}^{\dagger}\text{H}/\text{Cp}^*$ complex **3.3**, formed as a single isomer, was synthesised as a more symmetrical precursor to trimetallic and heteronuclear complexes. Complex **3.3** could also be deprotonated to form potassium salt **3.4**, which shows an intriguing polymeric structure in the solid state. Compound **3.4** was utilised in the stepwise synthesis of homonuclear bimetallic **3.6**, albeit in poor yield, but ultimately **3.4** also proved unsuitable for the synthesis of trimetallic or heterobimetallic Fe-Ln(II) complexes.

Electrochemical studies were used to quantify the relative electron donating ability of the η^5 - ligands to the Fe(II) centre, and $\text{Pn}^{\dagger}\text{H}$ was found to be more electron donating than Cp but less than Cp^* ligands. CV of the anion **3.6** revealed two oxidation processes, suggesting the $[\text{Cp}^*\text{Fe}(\text{Pn}^{\dagger}\text{H})]^+$ cation has some stability on the experimental timescale but further work is required to isolate this species. The difference in redox potentials between centres bridged by the Pn^{\dagger} ligand in **3.6**, was of a similar order to that of found by Manriquez *et al.* using Pn, however the second oxidation process for **3.6** was irreversible. The conclusion of this work is that the Pn^{\dagger} ligand is not as suitable for the synthesis of extended Fe 'nanowires' as was envisaged.

3.6 Experimental Details for Chapter Three

3.6.1 Synthesis of $Fe(\eta^5-Pn^{\dagger}H)_2$ (3.1)

[K]Pn[†]H (1.60 g, 3.37 mmol) in THF (20 mL) was added dropwise to a suspension of FeCl₂(THF)_{1.1} (0.45 g, 2.18 mmol) in THF (20 mL) while stirring at -78 °C; the resulting mixture was then allowed to warm to room temperature and stirred overnight. The volatiles were removed under reduced pressure, and the products extracted into pentane (3 x 20 mL) and filtered through Celite. The filtrate was stripped to dryness to afford a crude red solid. **3.1** was recrystallised from a saturated Et₂O (20 mL) solution at -50 °C as dark red crystals which were washed with pentane at -78 °C and dried *in vacuo*.

Yield: 1.26 g (65% with respect to FeCl₂(THF)_{1.1}).

Major isomer ¹H NMR (C₆D₆, 399.5 MHz, 303 K): δ_H 6.63 (2H, dd, ³J_{HH} = 5.3, 2.2 Hz, Pn vinylic *H*), 6.51 (2H, dd, ³J_{HH} = 5.3, ⁴J_{HH} = 1.6 Hz, Pn vinylic *H*), 4.01 (2H, d, ³J_{HH} = 1.8 Hz, Pn aromatic *H*), 3.93 (2H, d, ³J_{HH} = 1.8 Hz, Pn aromatic *H*), 3.58 (2H, apparent t, ³J_{HH} = 2.2 Hz, Pn allylic *H*), 1.36 (12H, m, ¹Pr CH), 1.29 (18H, br, ¹Pr CH₃), 1.27 (18H, d, ³J_{HH} = 7.1 Hz, ¹Pr CH₃), 1.14 (18H, br, ¹Pr CH₃), 1.04 (18H, br, ¹Pr CH₃).

¹³C{¹H} NMR (C₆D₆, 100.5 MHz, 303 K): δ_C 138.48 (Pn vinylic C), 129.80 (Pn vinylic C), 102.76 (Pn bridgehead C), 99.42 (Pn bridgehead C), 78.46 (Pn aromatic C), 68.99 (Pn aromatic C), 59.99 (Pn aromatic C-Si), 36.20 (Pn allylic C), 19.78 (¹Pr CH), 19.73 (¹Pr CH), 19.54 (¹Pr CH), 19.29 (¹Pr CH), 12.68 (¹Pr CH₃), 12.04 (¹Pr CH₃).

²⁹Si{¹H} NMR (C₆D₆, 79.4 MHz, 303 K): δ_{Si} 5.50 (allylic Si), 5.22 (aromatic Si).

Minor isomer ¹H NMR (C₆D₆, 399.5 MHz, 303 K): δ_H 6.59 (2H, dd, ³J_{HH} = 5.2, ⁴J_{HH} = 1.1 Hz, Pn vinylic *H*) 6.22 (2H, dd, ³J_{HH} = 5.2, 2.3 Hz, Pn vinylic *H*), 4.20 (2H, d, ³J_{HH} = 1.7 Hz, Pn aromatic *H*), 4.14 (2H, d, ³J_{HH} = 1.7 Hz, Pn aromatic *H*), 2.29 (2H, apparent t, ³J_{HH} = 2.2 Hz, Pn allylic *H*), 1.36 (12H, m, ¹Pr CH), 1.31 (18H, br, ¹Pr CH₃), 1.26 (18H, d, ³J_{HH} = 7.1 Hz, ¹Pr CH₃), 1.10 (18H, br, ¹Pr CH₃), 1.03 (18H, br, ¹Pr CH₃).

¹³C{¹H} NMR (C₆D₆, 100.5 MHz, 303 K): δ_C 137.36 (Pn vinylic C), 125.88 (Pn vinylic C), 102.03 (Pn bridgehead C), 98.26 (Pn bridgehead C), 78.13 (Pn aromatic C), 64.68 (Pn aromatic C), 59.53 (Pn aromatic C-Si), 26.51 (Pn allylic C), 19.62 (¹Pr CH), 19.45 (¹Pr CH), 19.20 (¹Pr CH), 12.75 (¹Pr CH₃), 12.27 (¹Pr CH₃).

$^{29}\text{Si}\{^1\text{H}\}$ NMR (C_6D_6 , 79.4 MHz, 303 K): δ_{Si} 5.67 (allylic Si), 4.58 (aromatic Si).

EI-MS: $m/z = 887$ (100%), $[\text{M}]^+$.

Anal. found (calcd. for $\text{C}_{52}\text{H}_{94}\text{FeSi}_4$): C, 70.48 (70.37); H, 10.60 (10.68) %.

Crystal data for **3.1**: $\text{C}_{52}\text{H}_{94}\text{FeSi}_4$, $M_r = 887.48$, triclinic, space group $P-1$, red prism, $a = 13.7619(4)$ Å, $b = 14.2017(4)$ Å, $c = 14.2557(3)$ Å, $\alpha = 89.584(2)^\circ$, $\beta = 87.110(2)^\circ$, $\gamma = 71.362(1)^\circ$, $V = 2636.58(12)$ Å³, $T = 173$ K, $Z = 2$, $R_{\text{int}} = 0.060$, $\lambda_{\text{Mo}}(\text{K}\alpha) = 0.71073$ Å, $\theta_{\text{max}} = 27.09^\circ$, $R_1 [I > 2\sigma(I)] = 0.051$, wR_2 (all data) = 0.126, $\text{Goof} = 1.017$.

3.6.2 Synthesis of $(\eta^5\text{-Pn}^t\text{H})\text{Fe}[\eta^5\text{-Pn}^t(\eta^5\text{-K}\{\text{THF}\}_2)]$ (**3.2**)

Pre-cooled THF (-78°C , 20 mL) was added to an ampoule containing a solid mixture of **3.1** (48 mg, 0.07 mmol) and KNH_2 (8 mg, 0.14 mmol) at -78°C . The resulting suspension was stirred at -78°C for 30 min, then allowed to warm to room temperature and stir for 12 h yielding a red-green solution. The volatiles were removed under reduced pressure and the resulting solids extracted into pentane (20 mL) and filtered. Concentration of the filtrate and subsequent cooling to -50°C yielded dark red crystals of **3.2** suitable for XRD analysis.

Yield: 39 mg (52% with respect to **3.1**).

^1H NMR ($\text{THF-}d_8$, 399.5 K, 303 K, selected data): δ_{H} 6.92 (1H, br s, Pn H), 6.81 (1H, d, $^3J_{\text{HH}} = 3.4$ Hz, Pn H), 6.58 (1H, d, $^3J_{\text{HH}} = 3.7$ Hz, Pn H), 5.48 (1H, d, $^3J_{\text{HH}} = 3.7$ Hz, Pn H), 5.39 (1H, br d, $^3J_{\text{HH}} = 3.6$ Hz, Pn H), 5.22 (1H, d, $^3J_{\text{HH}} = 3.4$ Hz, Pn H), 4.74 (1H, br s, Pn H), 4.39 (1H, br d, $^3J_{\text{HH}} = 1.6$ Hz, Pn H), 3.41 (1H, br d, $^3J_{\text{HH}} = 2.0$ Hz, Pn H), 1.37 (12H, m, $^i\text{Pr CH}$), 1.23 (18H, d, $^3J_{\text{HH}} = 7.4$ Hz, $^i\text{Pr CH}_3$), 1.00 (18H, d, $^3J_{\text{HH}} = 7.4$ Hz, $^i\text{Pr CH}_3$), 0.97 (18H, d, $^3J_{\text{HH}} = 7.5$ Hz, $^i\text{Pr CH}_3$), 0.93 (9H, d, $^3J_{\text{HH}} = 7.3$ Hz, $^i\text{Pr CH}_3$).

$^{13}\text{C}\{^1\text{H}\}$ NMR ($\text{THF-}d_8$, 100.5 MHz, 303 K, selected data): δ_{C} 138.2 (Pn C), 132.8 (Pn C), 122.1 (Pn C), 100.5 (Pn C), 98.79 (Pn C), 78.18 (Pn C), 75.51 (Pn C), 73.86 (Pn C), 71.27 (Pn C), 54.24 (Pn C), 43.20 (Pn C), 19.74 ($^i\text{Pr CH}_3$), 19.72 ($^i\text{Pr CH}_3$), 19.69 ($^i\text{Pr CH}_3$), 19.64 ($^i\text{Pr CH}_3$), 19.57 ($^i\text{Pr CH}_3$), 19.55 ($^i\text{Pr CH}_3$), 19.49 ($^i\text{Pr CH}_3$), 19.44 ($^i\text{Pr CH}_3$), 13.04 ($^i\text{Pr CH}$), 13.01 ($^i\text{Pr CH}$), 12.98 ($^i\text{Pr CH}$), 12.83 ($^i\text{Pr CH}$).

$^{29}\text{Si}\{^1\text{H}\}$ NMR ($\text{THF-}d_8$, 79.4 MHz, 303 K, selected data): δ_{Si} 8.53, -2.74.

EI-MS: No volatility.

Anal. found (calcd. for $C_{60}H_{107}FeKO_2Si_4$): C, 70.48 (67.49); H, 10.60 (10.10) %.

Crystal data for **3.2**: $C_{60}H_{107}FeKO_2Si_4$, $M_r = 1069.78$, triclinic, space group $P-1$, purple block, $a = 17.2509(3)$ Å, $b = 18.7591(4)$ Å, $c = 21.6908(4)$ Å, $\alpha = 66.853(1)^\circ$, $\beta = 73.831(1)^\circ$, $\gamma = 82.968(1)^\circ$, $V = 6198.4(2)$ Å³, $T = 120$ K, $Z = 4$, $R_{int} = 0.068$, $\lambda_{Mo}(K\alpha) = 0.71073$ Å, $\theta_{max} = 27.48^\circ$, $R_1 [I > 2\sigma(I)] = 0.081$, wR_2 (all data) = 0.170, $Goof = 1.082$.

3.6.3 Synthesis of $Cp^*Fe(\eta^5-Pn^\dagger H)$ (**3.3**)

[K]Pn[†]H (4.35 mmol) in THF (30 mL) was added dropwise to a green solution of $FeCp^*Cl(TMEDA)$ (1.492 g, 342.7 mmol) in THF (20 mL) at $-78^\circ C$, and allowed to warm to room temperature overnight. The resulting red suspension was stripped of solvent, and the products extracted into hexane (100 mL) and filtered through Celite on a frit. The solvent was removed under reduced pressure to afford a crude orange solid. **3.6** was recrystallised from a saturated Et_2O (40 mL) solution at $-20^\circ C$ as orange-red blocks which were washed with pentane at $-78^\circ C$ and dried *in vacuo*. A second crop of crystals was obtained from slow cooling the combined supernatant and washings to $-50^\circ C$.

Total yield: 1.58 g (81% with respect to [K]Pn[†]H).

1H NMR (C_6D_6 , 499.9 MHz, 303 K): δ_H 6.49 (1H, dd, $^3J_{HH} = 5.4, 2.1$ Hz, Pn vinylic *H*), 6.43 (1H, dd, $^3J_{HH} = 5.4, ^4J_{HH} = 1.7$ Hz, Pn vinylic *H*), 3.79 (1H, d, $^3J_{HH} = 2.1$ Hz, Pn aromatic *H*), 3.67 (1H, d, $^3J_{HH} = 1.9$ Hz, Pn aromatic *H*), 3.26 (1H, apparent t, $^3J_{HH} = 2.1$ Hz, Pn allylic *H*), 1.74 (15H, s, Cp^*CH_3), 1.39 (3H, m, iPr CH), 1.27 (9H, d, $^3J_{HH} = 7.4$ Hz, iPr CH_3), 1.25 (9H, d, $^3J_{HH} = 7.4$ Hz, iPr CH_3), 1.20 (3H, m, iPr CH), 1.14 (9H, br, iPr CH_3), 1.08 (9H, br, iPr CH_3).

$^{13}C\{^1H\}$ NMR (C_6D_6 , 125.7 MHz, 303 K): δ_C 135.85 (Pn vinylic *C*), 129.05 (Pn vinylic *C*), 102.34 (Pn bridgehead *C*), 98.50 (Pn bridgehead *C*), 80.77 (Pn aromatic *C*), 78.27 (Cp^*-CCH_3), 68.75 (Pn aromatic *C*), 61.20 (Pn aromatic *C-Si*), 32.68 (Pn allylic *C*), 19.78 (iPr CH), 19.68 (iPr CH), 19.57 (iPr CH), 19.39 (iPr CH), 12.42 (iPr CH_3), 12.09 (iPr CH_3), 10.69 (Cp^*CH_3).

$^{29}Si\{^1H\}$ NMR (C_6D_6 , 79.4 MHz, 303 K): δ_{Si} 5.62 (allylic *Si*), 5.57 (aromatic *Si*).

EI-MS: $m/z = 607$ (100%), $[M]^+$.

Anal. found (calcd. for $C_{36}H_{62}FeSi_2$): C, 71.15 (71.25); H, 10.25 (10.30) %.

Crystal data for **3.3**: $C_{36}H_{62}FeSi_2$, $M_r = 606.89$, triclinic, space group $P-1$, orange block, $a = 10.905(2)$ Å, $b = 11.529(2)$ Å, $c = 16.367(3)$ Å, $\alpha = 69.87(3)^\circ$, $\beta = 80.46(3)^\circ$, $\gamma = 66.41(3)^\circ$, $V = 1769.7(6)$ Å³, $T = 173$ K, $Z = 2$, $R_{int} = 0.0800$, $\lambda_{Mo}(K\alpha) = 0.71073$ Å, $\theta_{max} = 27.12^\circ$, $R_1 [I > 2\sigma(I)] = 0.0555$, wR_2 (all data) = 0.1347, $Goof = 1.031$.

3.6.4 Synthesis of $[Cp^*Fe(\eta^5-Pn^+)] [K]$ (**3.4**)

An ampoule was charged with **3.3** (107 mg, 0.18 mmol) and KNH_2 (19 mg, 0.80 mmol) to which was added THF (20 mL). The mixture was stirred for 4 days yielding a dark red suspension. Filtration on a frit through dry Celite yields a red solution containing **3.4** in approx. quantitative yield by NMR spectroscopy. The volatiles were removed under reduced pressure and the resulting residue extracted into Et_2O (10 mL). Storage of this solution at $-35^\circ C$ yielded dark red crystals of **3.4** suitable for X-Ray diffraction.

Yield: 85 mg (75% with respect to **3.3**).

1H NMR (C_6D_6 / THF- d_8 , 499.9 MHz, 303 K): δ_H 7.33 (1H, d, $^3J_{HH} = 3.7$ Hz, Fe-Pn CH), 5.65 (1H, d, $^3J_{HH} = 3.7$ Hz, Fe-Pn wingtip CH), 4.14 (1H, d, $^3J_{HH} = 2.0$ Hz, K-Pn CH), 3.35 (1H, d, $^3J_{HH} = 2.0$ Hz, K-Pn wingtip CH), 1.84 (15H, s, $Cp^* CH_3$), 1.54 (3H, overlapping m, iPr CH), 1.46 (3H, overlapping m, iPr CH), 1.41 (9H, d, $^3J_{HH} = 7.4$ Hz, iPr CH_3), 1.36 (9H, d, $^3J_{HH} = 7.4$ Hz, iPr CH_3), 1.35 (9H, br, iPr CH_3), 1.33 (9H, br, iPr CH_3).

$^{13}C\{^1H\}$ NMR (C_6D_6 / THF- d_8 , 125.7 MHz, 303 K): δ_C 138.28 (Fe-Pn CH), 110.53 (Pn bridgehead C), 98.91 (Pn bridgehead C), 93.66 (Fe-Pn wingtip CH), 76.88 (Fe-Pn C-Si), 76.53 (K-Pn CH), 76.10 (Cp^*-CCH_3), 61.25 (K-Pn wingtip CH), 48.18 (K-Pn C-Si), 20.60 (iPr CH_3), 20.54 (iPr CH_3), 20.36 (iPr CH_3), 20.33 (iPr CH_3), 14.67 57 (iPr CH), 13.86 57 (iPr CH), 11.22 ($Cp^* CH_3$).

$^{29}Si\{^1H\}$ NMR (C_6D_6 , 79.4 MHz, 303 K): δ_{Si} 5.60 (Fe-Pn Si), -5.98 (K-Pn Si).

EI-MS: $m/z = 607$ (100%), $[M - K + H]^+$.

Anal. found (calcd. for $C_{36}H_{61}FeKSi_2$): C, 67.51 (67.04); H, 9.97 (9.53) %.

Crystal data for **3.4**: $C_{36}H_{61}FeKSi_2$, $M_r = 644.98$, monoclinic, space group $P2_1/c$, red plate, $a = 8.5189(17)$ Å, $b = 18.474(4)$ Å, $c = 22.809(5)$ Å, $\alpha = \gamma = 90^\circ$, $\beta = 94.48(3)^\circ$,

$V = 3578.7(12) \text{ \AA}^3$, $T = 173 \text{ K}$, $Z = 4$, $R_{\text{int}} = 0.0553$, $\lambda_{\text{Mo}}(\text{K}\alpha) = 0.71073 \text{ \AA}$, $\theta_{\text{max}} = 27.43^\circ$, $R_1 [I > 2\sigma(I)] = 0.0632$, $wR_2 (\text{all data}) = 0.2077$, $\text{Goof} = 0.824$.

3.6.5 Characterisation of double bond isomer $\text{Cp}^*\text{Fe}(\eta^5\text{-Pn}^\dagger\text{H})$ (**3.5**)

^1H NMR (toluene- d_8 , 399.5 MHz, 303 K, selected data): δ_{H} 6.57 (1H, s, Pn vinylic CH), 3.75 (1H, d, $^3J_{\text{HH}} = 2.3 \text{ Hz}$, Pn vinylic CH), 3.64 (1H, d, $^3J_{\text{HH}} = 2.6 \text{ Hz}$, Pn vinylic CH), 2.93 (1H, dd, $^2J_{\text{HH}} = 22.3$, $^3J_{\text{HH}} = 1.7 \text{ Hz}$, Pn allylic CH), 2.67 (1H, dd, $^2J_{\text{HH}} = 22.3$, $^3J_{\text{HH}} = 2.5 \text{ Hz}$, Pn allylic CH), 1.76 (15H, s, $\text{Cp}^* \text{CH}_3$), 1.31 (6H, overlapping m, ^iPr CH), 1.21 (9H, d, $^3J_{\text{HH}} = 6.9 \text{ Hz}$, ^iPr CH_3), 1.17 (18H, br, ^iPr CH_3), 1.05 (6H, d, $J = 7.1 \text{ Hz}$, ^iPr CH).

$^{13}\text{C}\{^1\text{H}\}$ NMR (C_6D_6 , 125.7 MHz, 303 K, selected data): δ_{C} 135.85 (Pn vinylic C), 148.91 (Pn vinylic CH), 148.77 (Pn vinylic C-Si), 106.49 (Pn bridgehead C), 97.44 (Pn bridgehead C), 80.78 (Pn aromatic C), 79.30 ($\text{Cp}^* \text{CCH}_3$), 68.52 (Pn aromatic C), 64.22 (Pn aromatic C-Si), 37.02 (Pn allylic C), 20.09 (^iPr CH), 19.87 (^iPr CH), 19.72 (^iPr CH), 19.61 (^iPr CH), 12.60 (^iPr CH_3), 12.43 (^iPr CH_3), 11.59 ($\text{Cp}^* \text{CCH}_3$).

$^{29}\text{Si}\{^1\text{H}\}$ NMR (C_6D_6 , 79.4 MHz, 303 K, selected data): δ_{Si} 6.20, -0.66.

EI-MS: $m/z = 607$ (100%), $[\text{M}]^+$.

Anal. found (calcd. for $\text{C}_{36}\text{H}_{62}\text{FeSi}_2$): C, 71.13 (71.25); H, 10.20 (10.30) %.

Crystal data for **3.5**: $\text{C}_{36}\text{H}_{62}\text{FeSi}_2$, $M_r = 606.89$, triclinic, space group $P-1$, green plate, $a = 10.245(2) \text{ \AA}$, $b = 13.108(2) \text{ \AA}$, $c = 15.104(3) \text{ \AA}$, $\alpha = 67.52(3)^\circ$, $\beta = 73.87(3)^\circ$, $\gamma = 76.97(3)^\circ$, $V = 1784.1(6) \text{ \AA}^3$, $T = 173 \text{ K}$, $Z = 2$, $R_{\text{int}} = 0.0709$, $\lambda_{\text{Mo}}(\text{K}\alpha) = 0.71073 \text{ \AA}$, $\theta_{\text{max}} = 27.60^\circ$, $R_1 [I > 2\sigma(I)] = 0.0588$, $wR_2 (\text{all data}) = 0.1752$, $\text{Goof} = 1.032$.

3.6.6 Synthesis of $[\text{Cp}^*\text{Fe}]_2(\mu\text{:}\eta^5, \eta^5\text{-Pn}^\dagger)$ (**3.6**)

$[\text{K}]_2\text{Pn}^\dagger$ (119 mg, 0.241 mmol) in THF (15 mL) was added dropwise to a green solution of $\text{FeCp}^*\text{Cl}(\text{TMEDA})$ (166 mg, 0.482 mmol) in THF (10 mL) at -78°C ; the reaction flask was then sealed and allowed to warm to room temperature overnight. The resulting brown suspension was stripped of solvent, and the products extracted with hot (*ca.* 80°C) toluene (2 x 40 mL), followed by brief sonication and filtration on a frit through dry Celite. The solution was concentrated to 15 mL and the precipitated solid

was warmed to *ca.* 80 °C and brought back into solution. Green crystals of **3.6** were formed by slowly cooling this solution to ambient temperature. A second crop of crystals was obtained by removal of the solvent from the supernatant and recrystallisation of the resulting brown residues from Et₂O (3 mL) at -35 °C.

Total Yield: 66 mg (34% with respect to [K]₂Pn[†]).

¹H NMR (toluene-*d*₈, 499.9 MHz, 303 K): δ_H 4.67 (2H, d, ³J_{HH} = 2.1 Hz, Pn CH), 3.69 (2H, d, ³J_{HH} = 2.1 Hz, Pn CH), 2.15 (6H, septet, ³J_{HH} = 7.5 Hz, ⁱPr CH), 1.67 (18H, d, ³J_{HH} = 7.6 Hz, ⁱPr CH₃), 1.54 (18H, d, ³J_{HH} = 7.6 Hz, ⁱPr CH₃), 1.51 (30H, s, Cp* CH₃).

¹³C{¹H} NMR (toluene-*d*₈, 125.7 MHz, 303 K): δ_C 102.34 (Pn bridgehead C), 98.50 (Pn bridgehead C), 87.65 (Pn CH), 78.06 (Cp* CCH₃), 65.32 (Pn CH), 61.20 (Pn C-Si), 22.10 (ⁱPr CH₃), 21.65 (ⁱPr CH₃), 17.20 (ⁱPr CH), 11.84 (Cp* CCH₃).

²⁹Si{¹H} NMR (toluene-*d*₈, 79.4 MHz, 303 K): δ_{Si} 6.89.

EI-MS: *m/z* = 797 (15%), [M]⁺; 605 (100%), [M - FeCp*]⁺; 562 (40%), [M - FeCp* - ⁱPr]⁺; 448 (20%), [M - FeCp* - SiⁱPr₃]⁺.

Anal. found (calcd. for C₄₆H₇₆Fe₂Si₂): C, 69.25 (69.33); H, 9.69 (9.61) %.

Crystal data for **3.6**: C₄₆H₇₆Fe₂Si₂, *M*_r = 796.94, monoclinic, space group *P* 2₁/*n*, green plate, *a* = 8.8330(18) Å, *b* = 13.215(3) Å, *c* = 18.360(4) Å, α = γ = 90°, β = 91.30(3)°, *V* = 2142.5(7) Å³, *T* = 173 K, *Z* = 4, *R*_{int} = 0.0580, λ_{Mo}(Kα) = 0.71073 Å, θ_{max} = 27.47°, *R*₁ [*I* > 2σ(*I*)] = 0.0492, *wR*₂ (all data) = 0.1195, *Goof* = 1.019.

3.7 References for Chapter Three

1. T. J. Kealy and P. L. Pauson, *Nature*, 1951, **168**, 1039–1040.
2. S. A. Miller, J. A. Tebboth, and J. F. Tremaine, *J. Chem. Soc.*, 1952, 632–635.
3. E. O. Fischer and W. Pfab, *Z. Naturforsch. B*, 1952, **7**, 377–379.
4. G. Wilkinson, M. Rosenblum, M. C. Whiting, and R. B. Woodward, *J. Am. Chem. Soc.*, 1952, **74**, 2125–2126.
5. N. J. Long, *Metallocenes: an Introduction to Sandwich Complexes*, Blackwell Science Oxford, UK, 1998.
6. P. Štěpnička, *Ferrocenes: Ligands, Materials and Biomolecules*, Wiley, 2008.
7. G. Wilkinson and J. M. Birmingham, *J. Am. Chem. Soc.*, 1954, **76**, 6210–6210.
8. E. O. Fischer and H. Fischer, *Angew. Chem.*, 1964, **76**, 52.
9. E. O. Fischer and H. Fischer, *J. Organomet. Chem.*, 1966, **6**, 141–148.
10. G. W. Watt and E. W. Gillow, *J. Am. Chem. Soc.*, 1969, **91**, 775–776.
11. W. J. Evans, I. Bloom, W. E. Hunter, and J. L. Atwood, *Organometallics*, 1985, **4**, 112–119.
12. W. J. Evans, L. A. Hughes, and T. P. Hanusa, *J. Am. Chem. Soc.*, 1984, **106**, 4270–4272.
13. W. J. Evans, J. W. Grate, H. W. Choi, I. Bloom, W. E. Hunter, and J. L. Atwood, *J. Am. Chem. Soc.*, 1985, **107**, 941–946.
14. W. J. Evans, N. T. Allen, and J. W. Ziller, *Angew. Chem. Int. Ed. Engl.*, 2002, **41**, 359–361.
15. F. Jaroschik, F. Nief, X.-F. Le Goff, and L. Ricard, *Organometallics*, 2007, **26**, 1123–1125.
16. F. Jaroschik, A. Momin, F. Nief, X.-F. Le Goff, G. B. Deacon, and P. C. Junk, *Angew. Chem. Int. Ed. Engl.*, 2009, **48**, 1117–1121.
17. M. N. Bochkarev, *Coord. Chem. Rev.*, 2004, **248**, 835–851.
18. F. Nief, *Dalton Trans.*, 2010, **39**, 6589–6598.
19. M. R. MacDonald, J. E. Bates, M. E. Fieser, J. W. Ziller, F. Furche, and W. J. Evans, *J. Am. Chem. Soc.*, 2012, **134**, 8420–8423.
20. M. R. MacDonald, J. E. Bates, J. W. Ziller, F. Furche, and W. J. Evans, *J. Am. Chem. Soc.*, 2013, **135**, 9857–9868.
21. J. C. Green, *Chem. Soc. Rev.*, 1998, **27**, 263.
22. T. A. Albright, J. K. Burdett, and M. H. Whangbo, *Orbital Interactions in Chemistry*, Wiley, 2nd edn. 2013.
23. W. J. Evans, *Polyhedron*, 1987, **6**, 803–835.
24. S. Cotton, *Lanthanide and Actinide Chemistry*, Wiley, 2007, vol. 27.
25. J. M. Veauthier, E. J. Schelter, C. N. Carlson, B. L. Scott, R. E. D. Re, J. D. Thompson, J. L. Kiplinger, D. E. Morris, and K. D. John, *Inorg. Chem.*, 2008, **47**, 5841–5849.
26. S. Labouille, F. Nief, X.-F. Le Goff, L. Maron, D. R. Kindra, H. L. Houghton, J. W. Ziller, and W. J. Evans, *Organometallics*, 2012, **31**, 5196–5203.
27. S. Labouille, C. Clavaguéra, and F. Nief, *Organometallics*, 2013, **32**, 1265–1271.
28. O. T. Summerscales, S. C. Jones, F. G. N. Cloke, and P. B. Hitchcock, *Organometallics*, 2009, **28**, 5896–5908.
29. D. R. Johnston, M. P. Coles, and F. G. N. Cloke, *Unpublished results*.
30. B. Oelckers, I. Chávez, J. M. Manriquez, and E. Roman, *Organometallics*, 1993, **12**, 3396–3397.
31. T. J. Katz and M. Rosenberger, *J. Am. Chem. Soc.*, 1963, **85**, 2030–2031.

32. D. J. Peterson, *J. Org. Chem.*, 1968, **33**, 780–784.
33. M. B. Gillies, J. E. Tønder, D. Tanner, and P.-O. Norrby, *J. Org. Chem.*, 2002, **67**, 7378–7388.
34. E. Molins, W. Maniukiewicz, C. Miravittles, M. Mas, J. M. Manriquez, I. Chavez, B. Oelckers, J. Farran, and J. L. Brianso, *Acta Crystallogr., Sect. C: Cryst. Struct. Commun.*, 1996, **52**, 2414–2416.
35. P. Seiler and J. D. Dunitz, *Acta Crystallogr. Sect. B*, 1979, **35**, 1068–1074.
36. C. Miravittles, E. Molins, W. Maniukiewicz, M. Mas, J. M. Manriquez, I. Chavez, B. Oelckers, A. Alvarez-Larena, and J. L. Brianso, *Acta Crystallogr., Sect. C: Cryst. Struct. Commun.*, 1996, **52**, 3047–3049.
37. A. Alvarez-Larena, J. L. Brianso, J. F. Piniella, J. Farran, J. M. Manriquez, I. Chavez, B. Oelckers, E. Molins, and C. Miravittles, *Acta Crystallogr., Sect. C: Cryst. Struct. Commun.*, 1996, **52**, 2754–2757.
38. M. R. Churchill and K. K. G. Lin, *Inorg. Chem.*, 1973, **12**, 2274–2279.
39. J. D. Smith, in *Advances in Organometallic Chemistry*, Elsevier, 1998, vol. 43, pp. 267–348.
40. S. Jones, P. Roussel, T. Hascall, and D. O'Hare, *Organometallics*, 2006, **25**, 221–229.
41. O. T. Summerscales, D. R. Johnston, F. G. N. Cloke, and P. B. Hitchcock, *Organometallics*, 2008, **27**, 5612–5618.
42. T. J. Katz, M. Rosenberger, and R. K. O'Hara, *J. Am. Chem. Soc.*, 1964, **86**, 249–252.
43. F. G. N. Cloke, *Pure Appl. Chem.*, 2001, **73**, 233–238.
44. J. M. O'Connor and C. P. Casey, *Chem. Rev.*, 1987, **87**, 307–318.
45. E. E. Bunel, L. Valle, N. L. Jones, P. J. Carroll, C. Barra, M. Gonzalez, N. Munoz, G. Visconti, A. Aizman, and J. M. Manriquez, *J. Am. Chem. Soc.*, 1988, **110**, 6596–6598.
46. S. Bendjaballah, S. Kahlal, K. Costuas, E. Bévilion, and J.-Y. Saillard, *Chem.–Eur. J.*, 2006, **12**, 2048–2065.
47. J. C. Green, Personal Communication.
48. H. J. Gericke, N. I. Barnard, E. Erasmus, J. C. Swarts, M. J. Cook, and M. A. S. Aquino, *Inorg. Chim. Acta*, 2010, **363**, 2222–2232.
49. W. E. Geiger and F. Barrière, *Acc. Chem. Res.*, 2010, **43**, 1030–1039.
50. R. G. Compton and C. E. Banks, *Understanding Voltammetry*, Imperial College Press, 2nd edn. 2011.
51. R. Materikova, V. Babin, I. Lyatifov, T. K. Kurbanov, E. Fedin, P. Petrovskii, and A. Lutsenko, *J. Organomet. Chem.*, 1977, **142**, 81–87.
52. I. Noviandri, K. N. Brown, D. S. Fleming, P. T. Gulyas, P. A. Lay, A. F. Masters, and L. Phillips, *J. Phys. Chem. B*, 2011, **103**, 6713–6722.
53. J. M. Manriquez, M. D. Ward, W. M. Reiff, J. C. Calabrese, N. L. Jones, P. J. Carroll, E. E. Bunel, and J. S. Miller, *J. Am. Chem. Soc.*, 1995, **117**, 6182–6193.
54. D. Chang, T. Malinski, A. Ulman, and K. M. Kadish, *Inorg. Chem.*, 1984, **23**, 817–824.

4 CHAPTER FOUR: Double-Sandwich Complexes of the d-Block Elements

4.1 Introduction

Bimetallic complexes of the type $(L)_2M_2$ (L = aromatic ligand), so-called ‘double-sandwiches’, have attracted increasing attention due to their propensity to facilitate metal–metal bonding and display unusual electronic and magnetic properties.¹⁻³ Considerable theoretical interest has also been paid to organometallic sandwich nanowires, $[M_x(L)]_n$, as models for molecular ferromagnets and spintronic devices.⁴⁻⁷

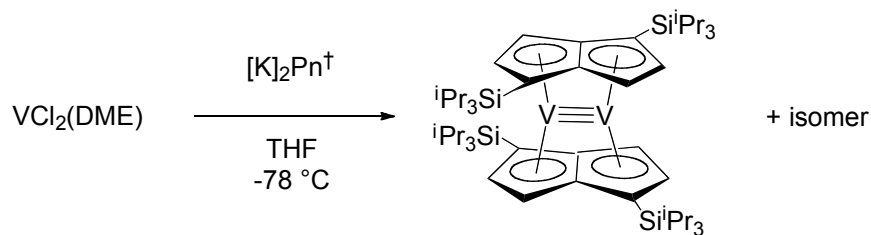
As outlined in chapter one, the aromatic pentalene dianion, $[C_8H_6]^{2-} = Pn$, displays a unique variety of coordination modes in its organometallic complexes.⁸ In particular its ability to coordinate two metals in a syn-facial manner has proved ideal for the synthesis of such double-sandwich complexes. Katz *et al.* reported the first $(Pn)_2M_2$ complexes, for $M = Co, Ni$, in which the double-metallocene structure was proposed.^{9,10} These dimers are diamagnetic, in contrast to the paramagnetic behaviour shown by their monometallic cyclopentadienyl (Cp) counterparts. Cloke and co-workers established η^5, η^5 -ligation of the silylated pentalene ligand, $[C_8H_4\{Si^iPr_3-1,4\}_2]^{2-} = Pn^\dagger$, with a metal–metal bonded core in $(Pn^\dagger)_2Mo_2$, confirmed by X-ray crystallography.¹¹ These researchers have since reported bis(pentalene) dimers for $M = Cr, Mn, Rh$ and Pd .¹²⁻¹⁴ A comprehensive study of double-sandwiches of the first-row d-block elements was also reported by O’Hare *et al.*, using the permethylated pentalene ligand, $[C_8Me_6]^{2-} = Pn^*$, in the successful synthesis of $(Pn^*)_2M_2$ complexes $M = V, Cr, Mn, Co, Ni$.¹⁵

This chapter details synthetic studies towards expanding the range of syn-bimetallic complexes of d-block metals with pentalene ligands. The synthesis of early transition metal $M = V, Ti$ and Sc double-sandwich complexes was targeted, which were of particular interest in potentially providing a very rare example of $M-M$ multiple bonding for these atoms. Furthermore, the rich and varied chemistry shown by these electron-deficient metals makes the target compounds potentially reactive with small molecule substrates.

4.2 Vanadium

4.2.1 Synthesis and characterisation of $(\mu:\eta^5,\eta^5\text{-Pn}^\dagger)_2\text{V}_2$

The conventional synthetic route to $(\text{Pn})_2\text{M}_2$ complexes involves a salt metathesis reaction of the pentalene dianion with a divalent metal salt in which there is a degree of metal-metal interaction already in place. For example, the synthesis and characterisation of syn-bimetallic complex $(\mu:\eta^5,\eta^5\text{-Pn}^\dagger)_2\text{V}_2$ was reported during the course of these studies,¹⁶ as part of work in collaboration with the author. The preparation of this complex parallels that of the permethylpentalene analogue $(\mu:\eta^5,\eta^5\text{-Pn}^*)_2\text{V}_2$ reported by O'Hare *et al.*,¹⁵ in which the choice of V(II) precursor $\text{VCl}_2(\text{DME})$, with all-bridging chloride ligands, proved critical to the isolation of the metal-metal bonded bimetallic (Scheme 4.1).



Scheme 4.1 Synthesis of $(\mu:\eta^5,\eta^5\text{-Pn}^\dagger)_2\text{V}_2$.

Complex $(\mu:\eta^5,\eta^5\text{-Pn}^\dagger)_2\text{V}_2$ was isolated as a red crystalline solid in 35% yield. Multinuclear (^1H , ^{13}C , ^{29}Si , ^{51}V) NMR of the crystalline product revealed two products in *ca.* 2:3 ratio, which both show D_2 symmetry in solution on the NMR timescale. Mass spectrometry and elemental analysis were fully consistent with the formula proposed, suggesting that co-crystallised compounds were isomeric. Single-crystal XRD analysis revealed a molecular structure with the pentalene rings in a near parallel configuration, and the bulky 1,4- $\text{Si}^\text{t}\text{Pr}_3$ groups of each ligand adopting a mutually staggered conformation (Figure 4.1).

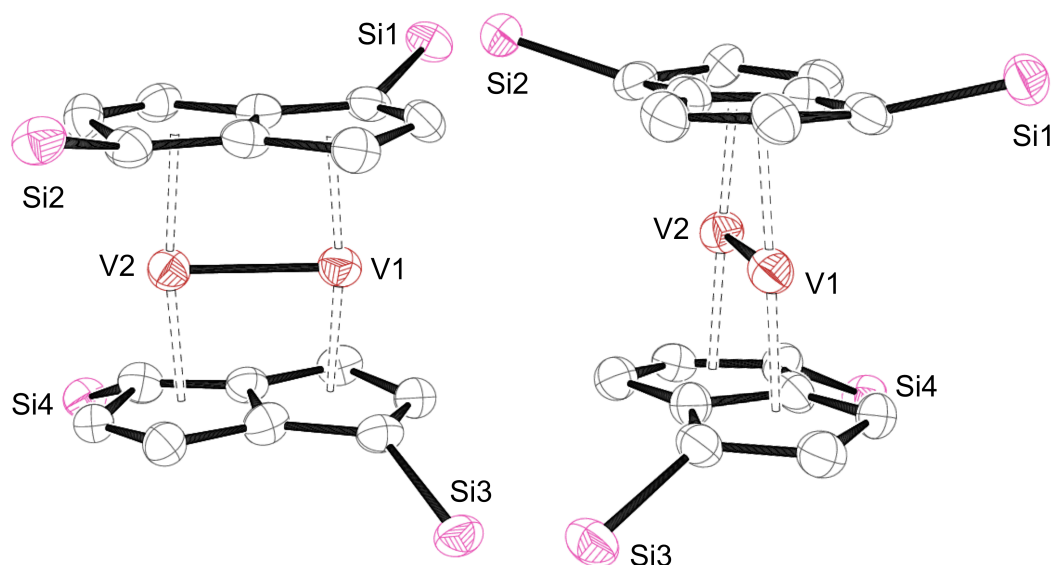


Figure 4.1 ORTEP (50% probability) views of $(\mu:\eta^5,\eta^5\text{-Pn}^\dagger)_2\text{V}_2$.¹⁶
H atoms and ^iPr groups omitted for clarity.

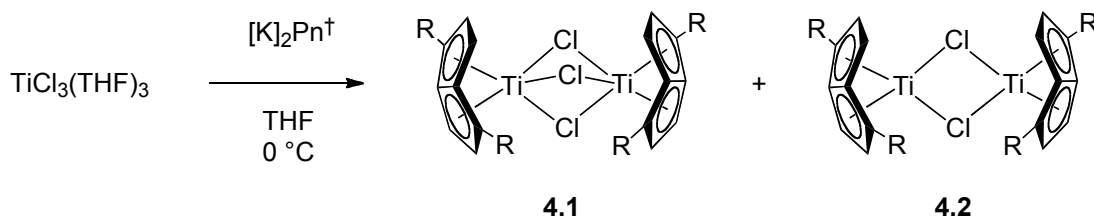
It was postulated that the minor component of the $(\mu:\eta^5,\eta^5\text{-Pn}^\dagger)_2\text{V}_2$ mixture featured 1,4- Si^iPr_3 groups of each ligand in the more sterically demanding eclipsed conformation. The intermetallic distance in the crystallographically characterised complex was 2.204(2) Å, which lies within the expected range of a V–V triple bond (1.978(2) – 2.462(2) Å).^{17,18} By analogy with the MO scheme in the related permethylpentalene complex,¹⁵ the V–V bonding was best described by σ , π and δ components. Furthermore, variable temperature NMR spectra for $(\mu:\eta^5,\eta^5\text{-Pn}^\dagger)_2\text{V}_2$ showed that the chemical shifts of the aromatic ring protons do not obey the Curie law between 180–375 K. This was attributed to a diamagnetic ground state with a low-lying paramagnetic excited state, as observed in the related $\text{V}\equiv\text{V}$ bonded complex $[\text{CpV}]_2\text{Pn}$.¹⁹ Reactivity studies of $(\mu:\eta^5,\eta^5\text{-Pn}^\dagger)_2\text{V}_2$ in C_6D_6 with small molecules H_2 , CO , and CO_2 showed no reaction by ^1H NMR spectroscopy, and it was assumed that the steric demands of the bulky 1,4- Si^iPr_3 groups prevented approach of these small molecules to the potentially redox active $[\text{V}_2]^{4+}$ core.

4.3 Titanium

4.3.1 Synthesis and characterisation of $[(\eta^8\text{-Pn}^\dagger)\text{Ti}]_2(\mu\text{-Cl})_3$ (**4.1**)

Given the rich and varied chemistry of low-valent group IV sandwich complexes,²⁰ and the prospect of a very rare example of a Ti–Ti multiple bond, the aim henceforth was to synthesise an analogous di-titanium bis(pentalene) complex. Previous studies toward this end by Cloke *et al.* established that the reaction of $[\text{K}]_2\text{Pn}^\dagger$ with TiCl_2 in THF resulted in disproportionation, producing an insoluble metallic solid, assumed to be $\text{Ti}(0)$, and the Ti(IV) complex $\text{Ti}(\text{Pn}^\dagger)_2$.²¹ An alternative route to double-sandwich complexes that has proved successful in the synthesis of a variety of M–M bonded species involves reduction of a metal halide precursor with an excess of a strong reducing agent.^{22–26}

The stoichiometric reaction of $[\text{K}]_2\text{Pn}^\dagger$ with $\text{TiCl}_3(\text{THF})_3$ was carried out, involving a very slow dropwise addition of a THF solution of $[\text{K}]_2\text{Pn}^\dagger$ to a stirred suspension of $\text{TiCl}_3(\text{THF})_3$ in THF at 0 °C. These conditions were optimised as to best keep the sparingly soluble Ti(III) salt in constant excess with respect to Pn^\dagger , in order to promote the desired salt metathesis reaction and minimise the competing disproportionation pathway to Ti metal and $\text{Ti}(\text{Pn}^\dagger)_2$. The resultant dark green solution was stirred overnight at 0 °C, and following work-up from toluene, afforded a dark green solid. Elemental analysis of this solid formulated as $\text{Pn}^\dagger_2\text{Ti}_2\text{Cl}_x$ best fit to a value of $x = 2.6$ suggesting a mixture of products **4.1** and **4.2** was formed (Scheme 4.2).



Scheme 4.2 Synthesis of **4.1** and **4.2**. $\text{R} = \text{Si}^i\text{Pr}_3$.

Complex $[(\eta^8\text{-Pn}^\dagger)\text{Ti}]_2(\mu\text{-Cl})_3$ (**4.1**) was isolated from the crude mixture by extraction with THF and cooling to -35 °C, as a red-green dichroic solid in 80% yield. EI-MS and elemental analysis confirmed the identity and purity of the microcrystalline product.

Compound **4.1** was found to be temperature sensitive in the solid state and solution, decomposing over *ca.* 12 h at room temperature to give an unidentified orange compound. Red crystals of **4.1** were studied by X-ray diffraction and while disorder in the Pn^\dagger and Cl ligands meant the final refinement parameters did not converge to a satisfactory level ($R_1 = 11.7\%$), basic connectivity could be established (Figure 4.2).

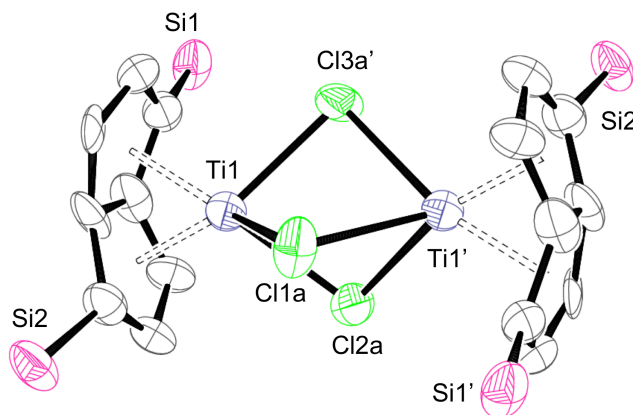


Figure 4.2 Partially refined model of **4.1** with thermal ellipsoids at 50% probability. Hydrogen atoms and $i\text{Pr}$ groups have been omitted for clarity. The Pn^\dagger and Cl ligands are both disordered over two positions, with only part 1 shown.

The pentalene ligand binds in an η^8 -fashion to each Ti centre, as is commonly encountered in its complexes with early transition metals,²⁷⁻³¹ with bridging chloride ligands. The analogous permethylpentalene complex $[(\eta^8\text{-Pn}^*)\text{Ti}]_2(\mu\text{-Cl})_3$, synthesised by reduction of $[(\eta^8\text{-Pn}^*)\text{TiCl}(\mu\text{-Cl})]_2$ with KC_8 , has been structurally characterised by O'Hare *et al.*³² The molecular structure of $[(\eta^8\text{-Pn}^*)\text{Ti}]_2(\mu\text{-Cl})_3$ shows a near parallel arrangement of Pn^* ligands, and a tripodal disposition of bridging Cl ligands between the Ti centres. Despite a relatively short Ti...Ti distance (3.219 Å), $[(\eta^8\text{-Pn}^*)\text{Ti}]_2(\mu\text{-Cl})_3$ did not produce a Ti(II) complex with excess reducing agent.³³

The proposed formulation implies **4.1** is a formally mixed-valence Ti(III)/Ti(IV) species, however since the molecular structure could not be solved unambiguously by X-ray crystallography, the electronic and magnetic properties were investigated in detail.

4.3.2 Electronic and magnetic studies of **4.1**

Electron paramagnetic resonance (EPR) spectroscopy is a powerful technique for elucidating the environment of the unpaired electron in paramagnetic compounds. The g -value in EPR can provide information about the orbital in which the unpaired electron resides. The g -value for the free electron ($g_e = 2.002319$ to 6 d.p.) is a fundamental constant, related to the magnetic moment of the electron due to its spin angular momentum. In real materials the measured g -value is not equal to g_e because of an orbital angular momentum contribution to the magnetic moment. This can be mediated by the electronic ground state with a large orbital moment, or mixing with excited states *via* spin-orbit coupling (SOC). The latter has a small orbital moment that is related to the energy gap between the excited state and the ground state (ΔE), as expressed in Equation 4.1.

$$g = g_e - \frac{a^2 n \lambda}{\Delta E} \quad \text{Equation 4.1}$$

where,

$$\lambda = \text{SOC constant}$$

$$a^2 (\leq 1) = \text{covalency parameter}$$

$$n = \text{quantum mechanical coefficient}$$

Transition metal ions typically have a relatively small ΔE due to crystal field splittings, but a large λ value, so g varies significantly from g_e and is often discussed according to a ‘ g -shift’ (Δg) as expressed in Equation 4.2.

$$\Delta g = g - g_e \quad \text{Equation 4.2}$$

Polycrystalline EPR spectra are broadened by dipolar coupling between molecules and EPR spectroscopy of fluid solutions also give isotropic spectra due to the free tumbling of molecules. When immobilised in a frozen solution, the different excited states of a molecule contribute to the magnetic moment in different orientations, and hence g -values are anisotropic and dependent on molecular symmetry.

EPR spectra of polycrystalline **4.1** at 293 and 10 K exhibit a single broad resonance (Figure 4.3), so while this signal could be attributed to a single paramagnetic species, the large linewidth may obscure other paramagnetic impurities. For a d^1 system such as

the Ti^{3+} ion, the unpaired electron is coupling with an empty orbital, which results in a negative contribution to Δg . This is consistent with the isotropic g -value of 1.985 for polycrystalline **4.1** at 293 K.

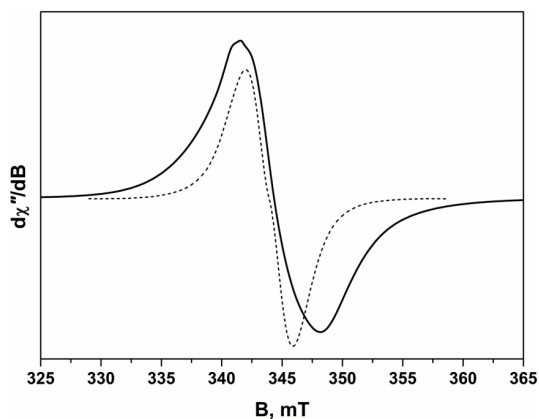


Figure 4.3 X-band EPR spectra of solid **4.1** at 293 K (solid line) and 10 K (dashed).

The X-band EPR spectrum of **4.1** in toluene solution at 293 K (see appendix A2) shows a principal signal at $g = 1.985$ assigned to $[(\eta^8\text{-Pn}^\dagger)\text{Ti}]_2(\mu\text{-Cl})_3$, and two additional features ($g = 1.996$ and 1.993) assigned to a trace Ti-based impurity. The X-band spectrum of a frozen toluene solution at 150 K (Figure 4.4) shows a rhombic signal with three principal g -values simulated, giving an average g -value ($g_{\text{iso}} = \{g_1 + g_2 + g_3\}/3$) of 1.986. An additional feature is observed on the low-field side of g_2 , which is assigned to a Ti-based decomposition product. The Q-band EPR spectrum of **4.1** in frozen toluene solution (see appendix A2) similarly shows a rhombic signal with $g_{\text{iso}} = 1.983$.

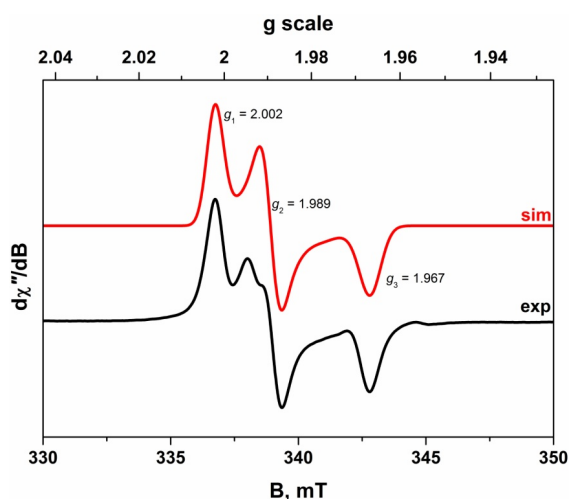


Figure 4.4 X-band EPR spectrum of **4.1** in toluene solution at 150 K (black) and corresponding simulation (red).

These data are consistent with a formally mixed-valence Ti(III)/Ti(IV) species with an $S = 1/2$ ground state. EPR studies by Mach *et al.* of a related complex with 1,4-bis(trimethylsilyl)cyclooctatetraenyl $[\text{COT}']^{2-}$ ligands, $[(\eta^8\text{-COT}')\text{Ti}]_2(\mu\text{-Cl})_3$ ($\text{COT}' = \text{C}_8\text{H}_6\{\text{SiMe}_3\text{-1,4}\}_2$),³⁴ show a comparable $g_{\text{iso}} = 1.988$. The latter compound was prepared by an analogous synthetic route to **4.1**, also involving disproportionation to give the mixed-valence Ti(III)/Ti(IV) species.

In the ^1H NMR spectrum of **4.1** only broad signals were observed, and the solution magnetic moment determined by the Evans method was $1.70 \mu_{\text{B}}$ per dimer at 303 K.^{35,36} Comparable data were observed in the solid state by SQUID magnetometry, $\mu_{\text{eff}}(250 \text{ K}) = 1.72 \mu_{\text{B}}$, a value consistent with 1 unpaired electron per dimer. Figure 4.5 shows the linear dependence of χ_{m}^{-1} vs T between 2 - 250 K, which is typical of a Curie-Weiss paramagnet with $C = 0.370 \text{ K}^{-1} \text{ mol}^{-1}$ and $\Theta = -3.5 \text{ K}$, suggesting there are no magnetic exchange interactions between the two Ti centres in **4.1** at these temperatures.

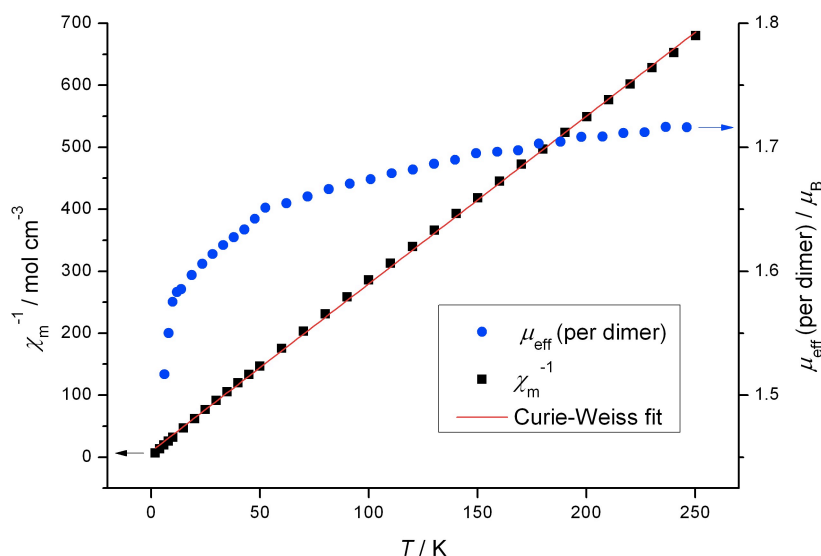


Figure 4.5 Temperature dependence of the solid state μ_{eff} and χ_{m}^{-1} for **4.1** at 1 Tesla.

The redox properties of **4.1** in THF were investigated by cyclic voltammetry. Using $[\text{nBu}_4\text{N}][\text{PF}_6]$ electrolyte two processes were observed inside the electrochemical window, a quasi-reversible process at $E_{1/2} = -1.53 \text{ V}$ vs $\text{FeCp}_2^{+/0}$ assigned to a one-electron reduction, and an irreversible oxidative process at $E_{\text{pa}} = -0.88 \text{ V}$. Chemical reduction of **4.1**, to a formally Ti(II)-Ti(II) double-sandwich complex would require a 3

electron gain per dimer. Based on the reduction potential of **4.1** a strong reducing agent such as Na or K ($E^\circ = -2.25$ and -2.38 V vs $\text{FeCp}_2^{+/0}$ respectively)^{37,38} would be required.

4.3.3 Synthesis and characterisation of $[(\eta^8\text{-Pn}^\dagger)\text{Ti}(\text{py})(\mu\text{-Cl})]_2$ (**4.2(py)**)₂

A second component was isolated from the reaction of $\text{TiCl}_3(\text{THF})_3$ and $[\text{K}]_2\text{Pn}^\dagger$ by fractional crystallisation. The crude green residue from the reaction was treated with hexane and 5 drops of pyridine, resulting in a colour change to brown. The mixture was filtered and cooled to -35°C , which provided red crystals of suitable quality for XRD analysis. The molecular structure (Figure 4.6) revealed a centrosymmetric dimer, with a coordinated pyridine and two bridging chloride ligands resulting in a formal electron count of 17 VE per Ti.

The pyridine ligand in **4.2(py)**₂ is coordinated to the Ti(III) centres with a Ti–N bond length of $2.275(3)$ Å, comparable with the titanocene(II) dimethylaminopyridine (DMAP) adduct $(\text{Cp}^{\text{Me}_4\text{iPr}})_2\text{Ti}(\text{DMAP})$, (Ti–N = $2.2437(11)$ Å).³⁹ The the average Ti–centroid and the average Ti–($\mu\text{-Cl}$) distances are slightly longer than those in the related Ti(IV) complex, $[(\eta^8\text{-Pn}^*)\text{TiCl}(\mu\text{-Cl})]_2$ ($1.955(2)$ and $2.485(1)$ Å respectively),³⁰ as would be expected for the larger Ti(III) centre in **4.2** ($r_{\text{Ti}^{3+}} = 0.670$ Å, $r_{\text{Ti}^{4+}} = 0.605$ Å).⁴⁰ The fold angle of 31.3° is typical for that of an η^8 -pentalene ligand bound to group IV metal.⁸ The $\eta^8\text{-Pn}^\dagger$ ligands are in a perfect eclipsed arrangement (twist angle = 0°) and interestingly the Si^iPr_3 substituents also adopt an eclipsed confirmation. The Ti··Ti distance in **4.2** ($3.8834(12)$ Å) reflects the large separation between the Pn^\dagger ligands within the dimer, and hence the strain associated with the more congested disposition of these bulky substituents is not the dominant factor in the solid-state structure of the molecule as a whole. The only previous structurally authenticated example of eclipsed Si^iPr_3 groups in $\eta^8\text{-Pn}^\dagger$ chemistry is the tantalum(V) methylene-bridged dimer, $[(\eta^8\text{-Pn}^\dagger)\text{TaCl}(\mu\text{-CH}_2)]_2$.⁴¹ Furthermore a di-molybdenum double-sandwich complex $(\mu:\eta^5, \eta^5\text{-Pn}^\dagger)_2\text{Mo}_2$ with eclipsed Si^iPr_3 groups, has recently been identified by an X-ray diffraction study.¹⁶ The latter finding settles some debate in the original report of $(\mu:\eta^5, \eta^5\text{-Pn}^\dagger)_2\text{Mo}_2$, concerning the structure of the minor isomer which was identified by NMR spectroscopy.¹¹

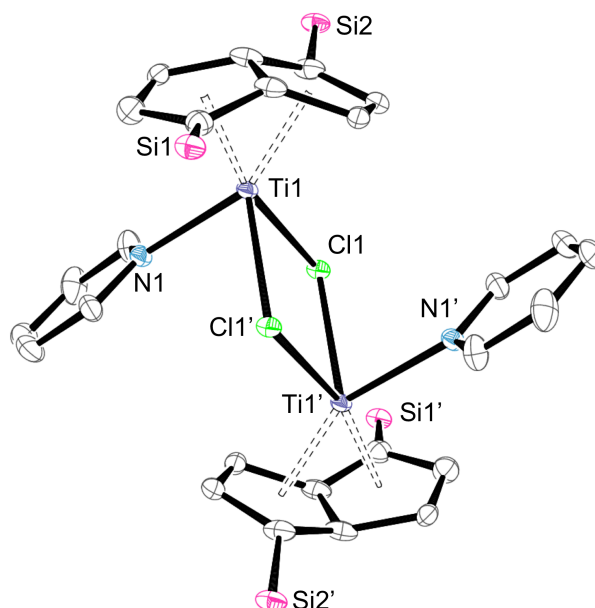


Figure 4.6 ORTEP (30% probability) diagram of **4.2(py)₂**. H atoms and ⁱPr groups omitted for clarity. Primed atoms are generated by symmetry.

Table 4.1 Selected distances (Å), angles (°) and parameters (defined in Figure 4.7) for **4.2(py)₂**. Ct denotes the η⁵-centroid of the Pn ring.

Parameter	4.2(py)₂	Parameter	4.2(py)₂
Ti1···Ti1'	3.8834(12)	Ti1–Cl1–Ti1'	100.33(4)
Ti1–Cl1	2.5207(10)	Cl1–Ti1–Cl1'	79.67(4)
Ti1–Cl1'	2.5366(13)	Ct1–Ti–Ct1'	56.38(8)
Ti1–N1	2.275(3)	Twist angle	0
Ti–Ct ^a	1.989(2)	Hinge Angle	2.9(5)
Ti–C _{ring} ^a	2.370(2)	Fold angle	31.343(5)

^a Average values

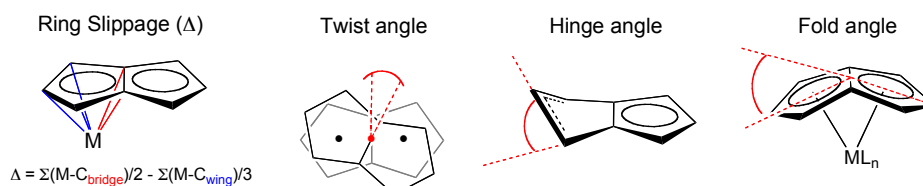


Figure 4.7

The solution magnetic moment of **4.2(py)₂** determined by the Evans method was 2.13 μ_B per dimer (1.50 μ_B per M) at 303 K.^{35,36} Solid-state SQUID magnetometry data show a μ_{eff} of 2.14 μ_B per dimer (1.51 μ_B per M) at 250 K, which is larger than the corresponding value for **4.1**, and is comparable with [Cp₂Ti(μ -Cl)]₂ (μ_{eff} (260 K) = 2.08 μ_B per dimer).^{42,43} The structural and magnetic properties of the latter compound, and the analogous dimers [Cp^{Me}₂Ti(μ -Cl)]₂ and [Cp^{Me}₂Ti(μ -Br)]₂, have been studied in depth by Stucky *et al.*⁴⁴ These researchers described antiferromagnetic interactions which increase as metal-metal distance decreases: a magnetic exchange pathway mediated by direct overlap of metal orbitals rather than superexchange through the halide bridges. In contrast, the solid-state magnetic susceptibility data for complex **4.1** (Figure 4.8) do not show signs of antiferromagnetic behaviour, despite a shorter distance between the two Ti centres in the molecular structure. The inverse magnetic susceptibility was fitted to the Curie-Weiss law between 60-250 K to give $C = 0.600 \text{ K}^{-1} \text{ mol}^{-1}$ and $\Theta = -14.3 \text{ K}$.

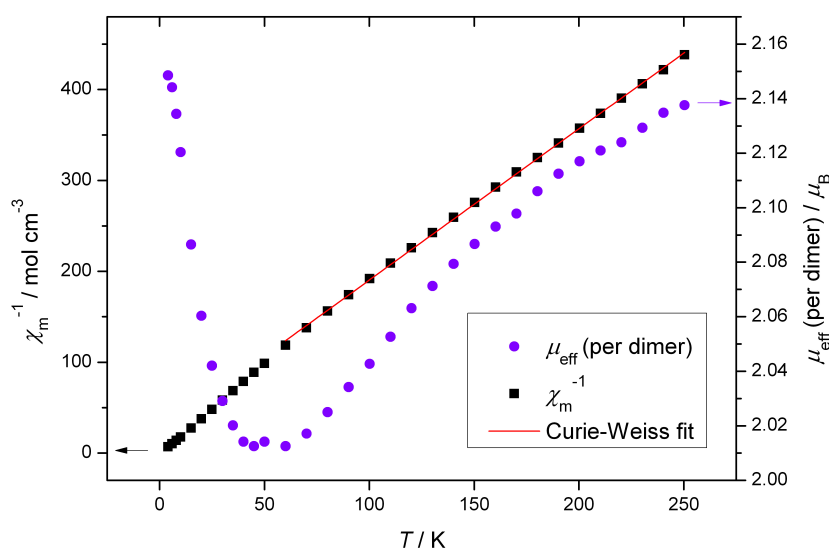
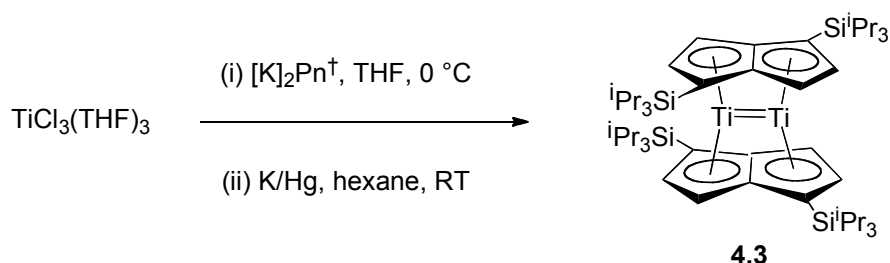


Figure 4.8 Temperature dependence of the solid state μ_{eff} and χ_m^{-1} for **4.2(py)₂** at 1 Tesla.

EPR spectroscopy of **4.2** in a frozen toluene solution revealed series of very broad features were observed which could not be adequately simulated (see appendix A2). It is possible that some dissociation of the pyridine occurs upon dissolution in toluene, which could explain the broad and convoluted EPR spectra.

4.3.4 Synthesis and characterisation of $(\mu:\eta^5, \eta^5\text{-Pn}^\dagger)_2\text{Ti}_2$ (**4.3**)

4.1 and **4.2** may be exploited as starting materials for the synthesis of a di-titanium double-sandwich complex. In preliminary experiments both complexes reacted with an excess of KC_8 in toluene- d_8 , each giving a red complex with a diamagnetic ^1H NMR spectrum (*vide infra*). Multi-gram scale reactions were carried out without isolation of the individual components of the $\text{TiCl}_3(\text{THF})_3$ / $[\text{K}]_2\text{Pn}^\dagger$ reaction mixture in order to optimise yields, with potassium amalgam chosen as the most convenient reducing agent on these scales. The optimised procedure is outlined in Scheme 4.3 which, following pentane work-up, afforded deep red $(\mu:\eta^5, \eta^5\text{-Pn}^\dagger)_2\text{Ti}_2$ (**4.3**) in 60% yield, as identified by NMR spectroscopy, elemental analysis and X-ray crystallography.



Scheme 4.3 Synthetic route to **4.3**.

Single crystals of **4.3** suitable for X-ray diffraction studies were obtained from a concentrated pentane solution at $-50\text{ }^\circ\text{C}$ (Figure 4.9 and Table 4.2).

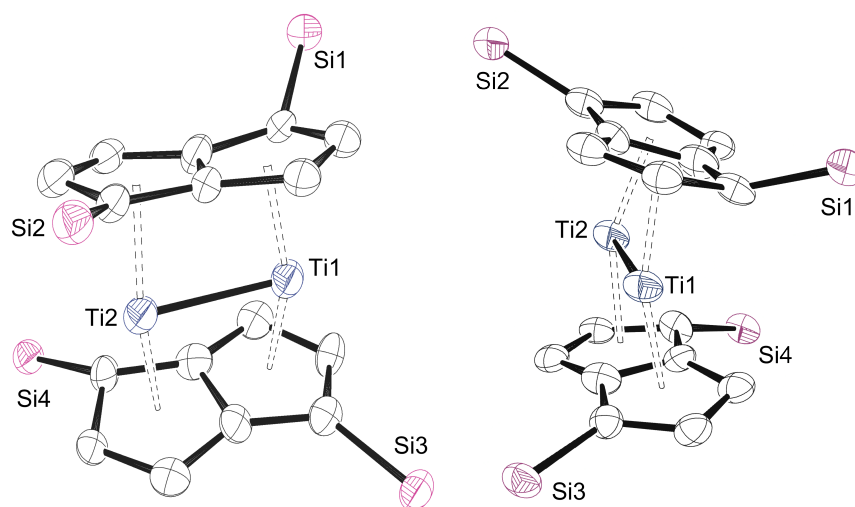


Figure 4.9 ORTEP views of **4.3**. H atoms and ^iPr groups omitted for clarity. Ellipsoids at 50% probability.

Table 4.2 Selected distances (Å), angles (°) and parameters (defined in Figure 4.7) for **4.3**. Ct denotes the η^5 -centroid of the Pn ring.

Parameter	4.3	Parameter	4.3
Ti1–Ti2	2.399(2)	\angle^a	0.005(7)
Ti–Ct ^a	2.036(4)	Twist angle	20.1(8)
Ti–C _{ring} ^a	2.378(7)	Hinge angle	3.8(8)
C–C _{ring} ^a	1.449(10)	Fold angle	8.7(4)
Ct–Ti–Ct ^a	155.2(2)		

^aAverage values.

The most noteworthy structural feature in **4.3** is the bent arrangement of the pentalene ligands around the Ti₂ core; the centroid–metal–centroid angles around Ti1 and Ti2 are 153.84(17)° and 156.6(2)° respectively. This bending is unprecedented amongst (Pn)₂M₂ complexes reported to date, all of which exhibit near-parallel pentalene rings in an idealised *D*_{2h} structure. The short Ti–Ti distance of 2.399(2) Å indicates significant bonding between the Ti atoms. This distance in **4.3** considerably shorter than that found in the metal (2.951 Å for Ti(α) at 25 °C),⁴⁵ and the only shorter titanium–titanium bond in the literature is 2.326(2) Å for (COT')₂Ti₂.²³ The latter complex makes an excellent comparison with **4.3**, since the bridging COT' ligands in the centrosymmetric dimer are concave-bent to allow $\mu\text{:}\eta^5, \eta^5$ -coordination, thus resembling a pentalene ligand but lacking a C–C bond at its bridgehead (Figure 4.10, left). The metal– η^5 -centroid distances in **4.3** (2.023(4) and 2.061(4) Å for Ti1, 2.042(4) and 2.016(4) Å for Ti2) are considerably longer than those in (COT')₂Ti₂ (1.808(4) and 1.810(4) Å) but are comparable to those found in monomeric titanocenes which have been structurally characterised [Ti(η^5 -C₅Me₄{Si^tBuMe₂})₂],⁴⁶ $d(\text{Ti}–\text{Ct}(\text{Cp})) = 2.018(4)$ Å; Ti(η^5 -C₅Me₄{SiMe₃})₂,⁴⁷ $d(\text{Ti}–\text{Ct}(\text{Cp})) = 2.020(2)$ Å, where Ct(Cp) denotes the η^5 -centroid of the corresponding Cp ring].

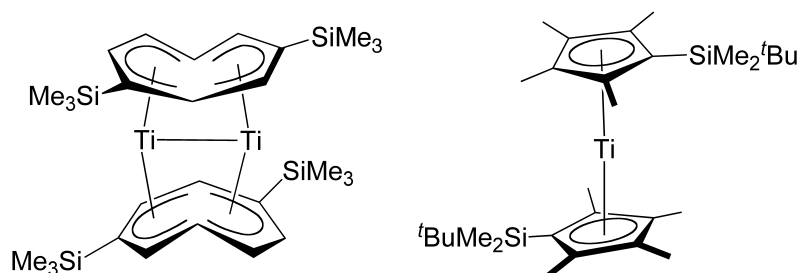


Figure 4.10 Examples of structurally characterised Ti(II) sandwich complexes.^{23,46}

The identity of **4.3** was also confirmed by spectroscopic and analytical methods. The ^1H NMR spectrum consists of two doublets at 6.83 and 6.34 ppm in the aromatic region, indicative of chemical equivalence of the Pn^\dagger rings on the NMR timescale. This can be attributed to a fluxional process involving ring slippage across the Ti_2 core, resulting in an averaged structure of D_2 symmetry. Variable temperature studies show the two Pn^\dagger rings remain chemically equivalent on the NMR timescale down to $-80\text{ }^\circ\text{C}$. The sharp signals observed and negligible temperature dependence of their chemical shift are consistent with a diamagnetic complex. This is in direct contrast to the mononuclear titanocenes $\text{Ti}(\eta^5\text{-C}_5\text{Me}_4\text{R})_2$, ($\text{R} = \text{Me},^{48} \text{Et},^{49} \text{iPr}, \text{tBu},^{50} \text{Ph}, 3,5\text{-Me}_2\text{-C}_6\text{H}_3,^{49} \text{Si}^i\text{BuMe}_2,^{46} \text{SiMe}_3,^{47} \text{SiMe}_2\text{CH}_2\text{CH}_2\text{Ph}, \text{SiMe}_2\text{Ph}, \text{and SiMePh}_2^{51}$), and $\text{Ti}(\eta^5\text{-C}_5\text{H}_3\text{-1,3-tBu}_2)_2$,⁵² which are all paramagnetic. The parent ion for **4.3** in the mass spectrum (EI) has a complex mass envelope in the region $m/z = 910\text{--}928$ amu and an isotopic pattern consistent with two Ti atoms.

DFT calculations were carried out by Green using the model ligand $[\text{C}_8\text{H}_6]^{2-}$ (Pn) using two codes (ADF and Gaussian, see appendix A1 for details).⁵³ The dimer Pn_2Ti_2 was optimised with no symmetry restrictions and subsequently with both D_{2h} (**4.IIIa**) and C_{2v} (**4.IIIb**) symmetry. Important structural parameters are listed in Table 4.3, in which ADF values are in normal font and Gaussian values are given in *italics*.

Table 4.3 Selected structural parameters (\AA , $^\circ$) for calculated structures of Pn_2Ti_2 .

Structure	Symmetry	Ti-Ti	Ti-Ct	Ct-Ti-Ct
4.IIIa	D_{2h}	2.33, 2.34	2.01, 2.01	180, 180
4.IIIb	C_{2v}	2.37, 2.31	2.00, 2.03	153, 158

The energy difference between the two structures was within computational error ($E(\mathbf{4.IIIb}) - E(\mathbf{4.IIIa}) / \text{kcal mol}^{-1} = -2; +1$), which supports the idea of rapid interconversion between geometries in solution. The D_{2h} structure (**4.IIIa**) had one imaginary frequency of b_{2u} symmetry and wavenumber $-80i \text{ cm}^{-1}$. The C_{2v} structure (**4.IIIb**) had all positive frequencies indicating a local minimum. The calculated Ti–Ti distances for **4.IIIb** (2.37, 2.31 Å) are in good agreement with the experimental value for **4.3** (2.399(2) Å), as are the centroid-metal-centroid angles (calc.: 153° , 158° ; exp.: $155.2(2)^\circ$ av.). The metal based frontier orbitals for **4.IIIa** and **4.IIIb** (Figure 4.11) are occupied by four electrons resulting in a double bond between the Ti atoms. When the symmetry is lowered from D_{2h} to C_{2v} the HOMO and HOMO-1 become 'a' symmetry and mix to give two bonds, equivalent to a σ and a π component. The Pn_2Ti_2 LUMO is only weakly metal-metal bonding due to poor overlap, in contrast to the vanadium analogue in which it is doubly occupied.¹⁵

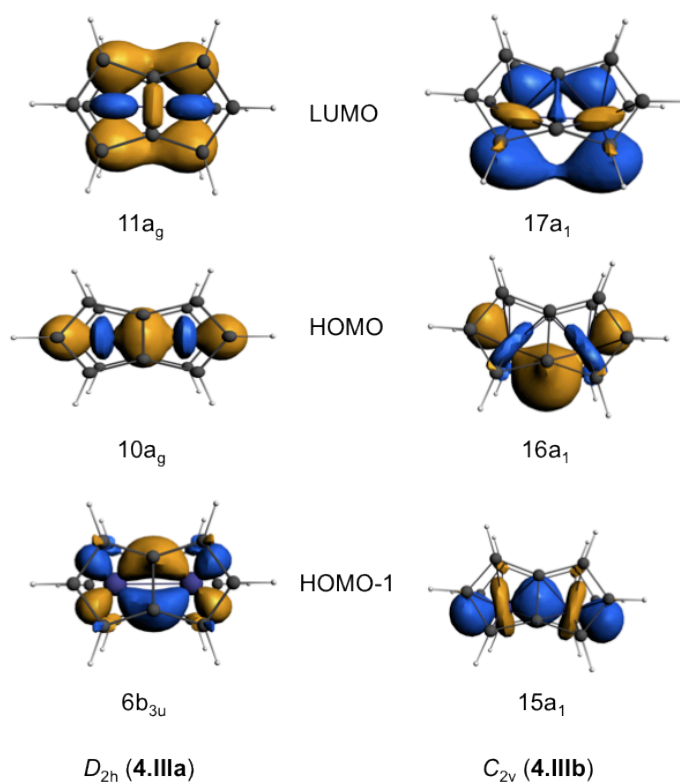


Figure 4.11 Isosurfaces of the frontier orbitals for Pn_2Ti_2 .⁵³

Pentalene can be considered a 5-electron (L_2X) donor to each metal centre in a neutral counting scheme,⁵⁴ meaning a M–M bond order of 2 (with σ and π components, Figure 4.11) results in 16 electrons (ML_4X_4) per Ti for **4.3**.

4.3.5 Electrochemical studies; synthesis and characterisation of $[(\mu:\eta^5, \eta^5\text{-Pn}^\dagger)_2\text{Ti}_2][B(C_6F_5)_4]$ (**4.4**).

As outlined in the previous chapters, cyclic voltammetry (CV) allows an initial investigation into the stability of the mixed-valence state in bimetallic complexes and enables the appropriate chemical redox agent to be chosen for their large-scale preparation.

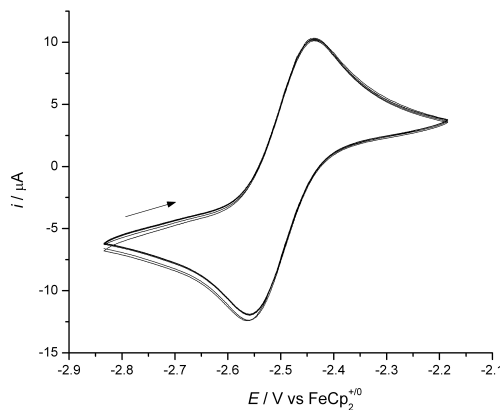


Figure 4.12 Overlaid CV scans (3 cycles) for **4.3** in THF / 0.1 M $[n\text{Bu}_4\text{N}][\text{PF}_6]$, scan rate 100 mV s^{-1} .

Complex **4.3** exhibits two successive one-electron transfers; the first process centered at $E_{1/2} = -2.50 \text{ V}$ is assigned to a one electron oxidation (Figure 4.12), and the second process an irreversible oxidation at $E_{\text{pa}} = -0.95 \text{ V}$, is tentatively assigned to a two-step process involving oxidative cleavage of the M–M bond after oxidation (*vide infra*). The first electrochemical event did not display the ideal ΔE_{pp} of 59 mV for a fully reversible single-electron transfer at 298 K, indicating that this process is quasi-reversible on the timescale of the experiment.⁵⁵ However, the quasi-reversibility of this oxidation does indicate that the $[\mathbf{4.3}]^+$ cation is stable on the timescale of the CV experiment, and therefore its synthesis by chemical methods was attempted, using a relatively mild oxidising agent, $[\text{FeCp}^*_2][B(C_6F_5)_4]$ ($E_{1/2} = -0.52 \text{ V}$ in THF).

Reaction of **4.3** with $[\text{FeCp}^*_2][B(C_6F_5)_4]$ at -35°C resulted in a brown suspension. Following evaporation of the solvent and removal of FeCp^*_2 by washing with hexane,

the residues were recrystallised from a concentrated Et₂O/hexane solution at -35 °C yielding [4.3][B(C₆F₅)₄] (= 4.4) as green crystals in 15% (non-optimised) yield. Ion-pair 4.4 was characterised by NMR spectroscopy, elemental analysis and X-ray crystallography. The molecular structure (Figure 4.13) reveals a ‘naked’ double-sandwich cation with no interactions between the anion and the metal-metal bonded core.

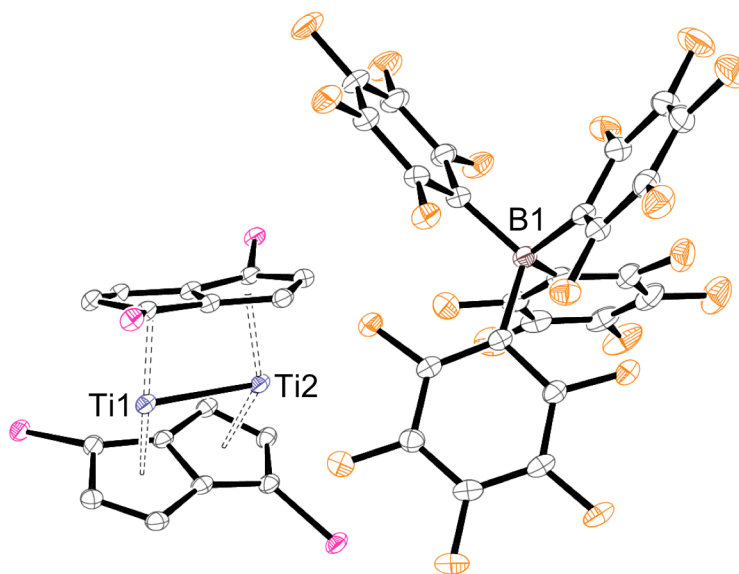


Figure 4.13 Displacement ellipsoid plot (30% probability) of 4.4. H atoms and ⁱPr groups omitted for clarity. F and Si atoms are shown in orange and pink respectively.

Table 4.4 Selected distances (Å), angles (°) and parameters (defined in Figure 4.7) for 4.4. Ct denotes the η⁵-centroid of the Pn ring.

Parameter	4.4	Parameter	4.4
Ti1–Ti2	2.5091(9)	Ct–Ti–Ct ^a	142.38(6)
Ti–Ct ^a	2.0233(14)	Δ ^a	0.105(3)
Ti–C _{ring} ^a	2.384(3)	Twist angle	14.44(9)
C–C _{ring} ^a	1.437(4)	Hinge angle	5.5(3)
Ti1–B1	7.134(4)	Fold angle	8.38(13)

^a Average values.

The important structural parameters are shown in Table 4.4, the most noteworthy being the significantly longer Ti-Ti bond distance in **4.4** (2.5091(9) Å) compared with **4.3** (2.399(2) Å). This elongation is consistent with the removal of an electron from the M–M bonding HOMO (16a₁) in the molecular orbital scheme for Pn₂Ti₂ (Figure 4.11). There is no significant difference in Ti–C and Pn C–C bond lengths between **4.3** and **4.4**, however the pentalene ligands bend around the Ti₂ core to a greater extent in the cationic complex; the centroid–metal–centroid angles around Ti1 and Ti2 are 142.28(6)° and 142.48(6)° respectively, compared with the respective angles 153.84(17)° and 156.6(2)° in the neutral complex. The decamethyltitanocene cation in [Cp*₂Ti][BPh₄]⁵⁶ also adopts a more bent structure than in neutral titanocenes.^{46,47} Ab initio calculations on the [Cp₂M]⁺ system (M = Sc and La) by Schleyer *et al.* indicated these metallocene cations prefer a bent structure due to covalent σ-bonding contributions to the metal d-orbitals.⁵⁷

The cation in **4.4** is, to the best of the authors knowledge, the first example of a formally a Ti(II)-Ti(III) mixed-valence species. As expected **4.4** is paramagnetic; the ¹H, ¹³C, and ²⁹Si NMR spectra in THF-*d*₈ are broad and uninformative, however the ¹⁹F and ¹¹B{¹H} NMR spectra showed well-resolved signals at δ_F -132.7, -165.2 and -168.7 and δ_B -14.75 respectively, attributable to the outer-sphere tetrakis(perfluorophenyl)borate anion. The solution phase magnetic moment of **4.4** determined by the Evans method was 1.96 μ_B per dimer which is slightly greater than the spin-only moment for one unpaired electron (1.73 μ_B). The SOMO is assumed to be 16a₁ in Figure 4.11, which may show hyperfine coupling to the two Ti centres (⁴⁷Ti, *I* = 5/2, 7.4%; ⁴⁹Ti, *I* = 7/2, 5.4%). Time constraints precluded characterisation of **4.4** by EPR spectroscopy. The poor crystalline yield obtained from the reaction mixture meant there was insufficient material for SQUID magnetometry. The CV of **4.4** in 0.1 M [ⁿBu₄N][B(C₆F₅)₄] / THF showed a single irreversible process, which is tentatively assigned to a chemical change after oxidation (a so-called EC process),⁵⁵ possibly involving metal-metal bond cleavage. However the peak potential (*E*_{pa}) for this oxidation, +0.43 V vs FeCp₂⁺⁰, is in poor agreement with the second oxidation in the CV of **4.3** (-0.59 V) and should be treated with caution, since **4.4** was found to polymerise THF over the course of 12 h.

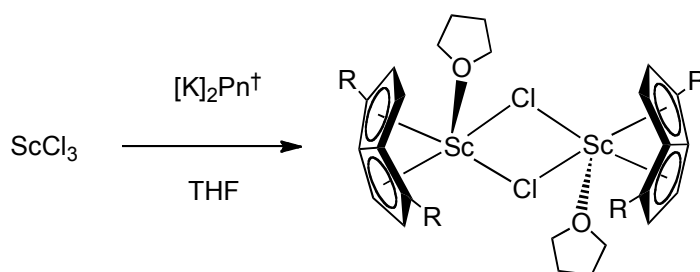
In summary, four new bimetallic Ti pentalene complexes have been synthesised and characterised. The double-sandwich species **4.3** is particularly noteworthy, as it adopts an unprecedented bent structure in the solid state with a very short intermetallic distance

consistent with a Ti–Ti double bond. DFT calculations indicate very little difference in energy between structures with bent and parallel pentalene rings, and **4.3** is consequently fluxional in solution. Given the rich and varied chemistry of low-valent Ti sandwich complexes,²⁰ the reactivity of complex **4.3** towards small molecules, in particular CO and CO₂, was investigated and the results are discussed in chapter five and chapter six.

4.4 Scandium

4.4.1 Synthesis and characterisation of $[(\eta^8\text{-Pn}^\dagger)\text{Sc}(\text{THF})(\mu\text{-Cl})]_2$ (**4.5**)

Following on from the successful synthesis of titanium double-sandwich compound **4.3**, *via* bridging chloride complex **4.2**, the synthesis of a scandium congener was attempted using a parallel synthetic pathway. Reaction of ScCl₃ with [K]₂Pn[†] in THF at room temperature afforded, after pentane work up, orange crystals of $[(\eta^8\text{-Pn}^\dagger)\text{Sc}(\text{THF})(\mu\text{-Cl})]_2$ (**4.5**) in 86% yield (Scheme 4.4).



Scheme 4.4 Synthesis of **4.5**. R = SiⁱPr₃.

The ¹H NMR spectrum of **4.5** in C₆D₆ contains two aromatic resonances at 6.77 and 6.34 ppm corresponding to the Pn[†] ring protons in a D₂ structure on the NMR timescale, and resonances at 1.38, 1.27 and 1.23 ppm are assigned to the ⁱPr groups, with the anticipated multiplicity. ¹H NMR signals at 3.66 and 1.40 are assigned to a THF molecule coordinated to the highly Lewis acidic scandium centre, with an integration ratio consistent with one THF molecule per Pn[†] ligand. Multinuclear (¹³C and ²⁹Si) NMR spectra were consistent with this interpretation.

Mass spectrometry (EI) showed a parent ion at $m/z = 875$, suggesting redistribution to the homoleptic species $[\text{Pn}^\dagger_2\text{Sc}]^+$ occurs in the gas phase, which has also been observed for Ln(III) pentalene complexes in chapter three.

Orange crystals of **4.5** were analysed by X-ray diffraction, however, due to disorder in the THF ligands, the final refinement indices are somewhat high ($R_1 = 12.6\%$) and only tentative conclusions may be drawn. Nonetheless, the molecular structure (Figure 4.14) provides an unambiguous confirmation of connectivity. The asymmetric unit contains one and a half-molecules, which both have very similar geometries. In a similar fashion to the Ti(III) bridged chloride complex **4.2.(py)**₂ the $\eta^8\text{-Pn}^\dagger$ ligands in **4.5** are in a near parallel arrangement and the Si^iPr_3 groups adopt an eclipsed conformation.

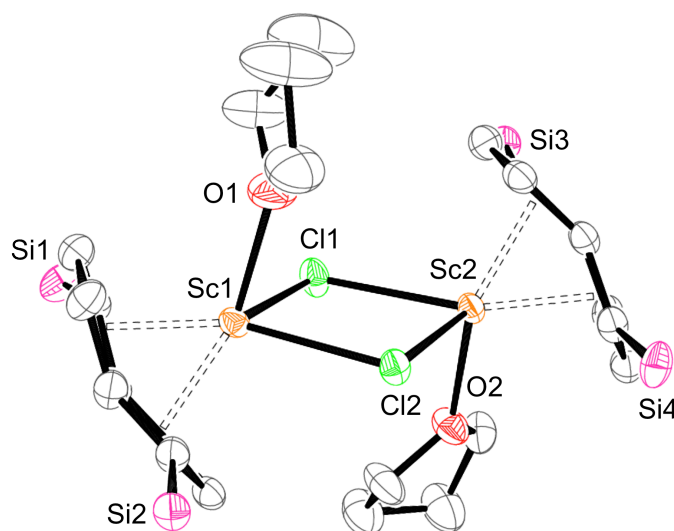


Figure 4.14 Partially refined molecular structure of **4.5**, with thermal ellipsoids at 50% probability. Hydrogen atoms and ^iPr groups omitted for clarity.

Complex **4.5** exists as a THF solvated dimer to alleviate the co-ordinatively unsaturated and electron deficient scandium centre, in a similar manner to the bis(cyclopentadienyl) complex $[\text{Cp}_2\text{ScCl}(\text{THF})]_2$,⁵⁸ and the related yttrium iodide-bridged dimer $[(\eta^8\text{-Pn}^\dagger)\text{Y}(\text{THF})(\mu\text{-I})]_2$.⁵⁹ Attempts to desolvate **4.5** *in vacuo* at temperatures up to 150 °C/ 10^{-6} mbar were unsuccessful; no sublimation occurred and ^1H NMR spectroscopy of the orange residue showed decomposition. $[\text{Cp}_2\text{ScCl}(\text{THF})]_2$, although volatile does not lose coordinated THF upon sublimation,⁵⁸ whereas the 16 VE monomers $(\text{Cp}^{\text{Me}4\text{R}})_2\text{ScCl}(\text{THF})$ ($\text{R} = \text{H}$ or Me) sublime to afford base-free complexes,

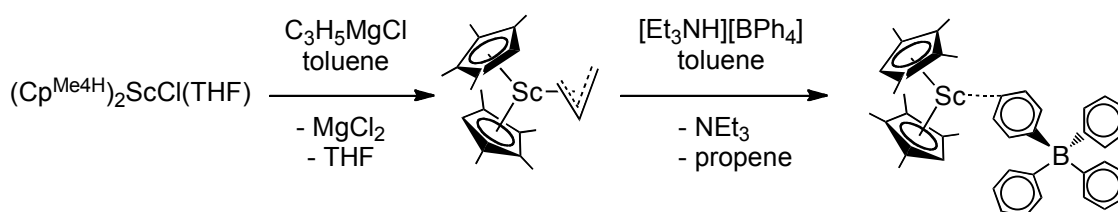
$(\text{Cp}^{\text{Me4R}})_2\text{ScCl}$.^{60,61} This difference has been attributed to the degree of steric saturation provided by two bulky Cp^{Me4R} ligands,⁶⁰ which is not provided in this case with a single Pn^\dagger ligand.

4.4.2 Reactivity studies of 4.5.

Compound **4.5** is the first well-defined scandium Pn^\dagger complex, one which should be a useful precursor to a wide range of derivatives of this class. Reactions of **4.5** with various strong reducing agents (Na amalgam, K metal, NaK_3 alloy, KC_8 , etc.) under a range of conditions were explored. In all cases no reaction was observed by ^1H NMR spectroscopy, reflecting the stability of the Sc(III) oxidation state.

An alternative synthetic route to low-valent scandium was pursued, taking inspiration from the recent report of a scandium dinitrogen complex, $[(\text{Cp}^{\text{Me4H}})_2\text{Sc}]_2(\mu\text{-}\eta^2\text{:}\eta^2\text{-N}_2)$, by Evans *et al.*⁶¹ The latter complex was formed by KC_8 reduction of $[(\text{Cp}^{\text{Me4H}})_2\text{Sc}][\text{BPh}_4]$ under an N_2 atmosphere, and tetraphenylborate salts of metallocene cations have proven to be excellent starting materials for the general synthesis of reduced dinitrogen complexes for yttrium and the lanthanides.^{62,63} It was postulated by Evans *et al.* that these reactions proceed *via* a putative divalent metallocene intermediate, an idea which if extended to a hypothetical ' $\text{Pn}^\dagger\text{Sc(II)}$ ' species in the present case, may undergo dimerisation in the absence of N_2 to give a double-sandwich complex.

The synthetic sequence to $[(\text{Cp}^{\text{Me4H}})_2\text{Sc}][\text{BPh}_4]$ is outlined in Scheme 4.5, in which the scandium allyl complex $(\text{Cp}^{\text{Me4H}})_2\text{Sc}(\eta^3\text{-C}_3\text{H}_5)$ was isolated free from coordinating THF. Base free alkyl precursors appear to be a prerequisite for the synthesis of cationic tetraphenylborate complexes *via* protonolysis routes such as this, since Evans *et al.* have suggested that tightly-bound THF ligands can lead to problems in reactions with the Brønsted acid $[\text{Et}_3\text{NH}][\text{BPh}_4]$.⁶⁴



Scheme 4.5 Synthetic route to a scandium tetraphenylborate complex by Evans *et al.*⁶¹

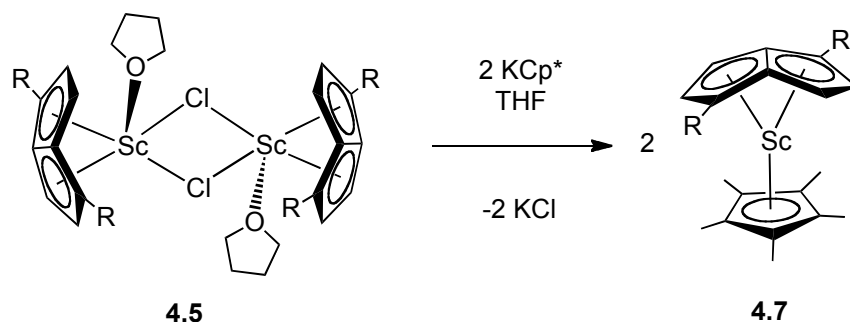
Following this logic, an unsolvated complex of the type $[\text{Pn}^{\dagger}\text{ScR}]$ was targeted, and preliminary reactivity studies of **4.5** were carried out. Reaction of allylmagnesium chloride with **4.5** in toluene at $-78\text{ }^{\circ}\text{C}$ produced an orange solution after warming to room temperature. Work-up and recrystallisation from pentane afforded a yellow crystalline solid which is given the tentative formulation $[(\eta^8\text{-Pn}^{\dagger})\text{Sc}(\text{C}_3\text{H}_5)(\text{THF})]_x$ (**4.6**) on the basis of NMR spectroscopy in C_6D_6 . The Pn^{\dagger} ligand was identified by aromatic signals at 6.71 and 5.50 ppm and ^1Pr signals at 1.30, 1.23 and 1.14 ppm with the expected multiplicity. Signals at 6.35 and 3.29 ppm in 1:4 ratio by integration, were assigned to the CH and CH_2 groups of the allyl ligand respectively, with broad linewidths ($\Delta\nu_{1/2} = 1.3\text{ Hz}$) possibly indicative of fluxionality between η^1 - and η^3 -binding modes as has been observed for allyl derivatives of *ansa*-scandocenes.⁶⁵ Coordinated THF was identified by signals at 3.24 and 0.97 ppm in the ^1H NMR spectrum and signals at 67.2 and 25.3 ppm in the $^{13}\text{C}\{^1\text{H}\}$ spectrum. Relative integration of the ^1H signals indicated the presence of 1 mole of THF per allyl ligand. Elemental analysis of **4.6** show consistently low carbon values over repeat measurements, even when combusted with added V_2O_5 oxidant. This problem has been reported previously for organoscandium complexes with a high carbon-content,⁶⁵⁻⁶⁹ and has been attributed to the formation of inert carbide species.⁵⁶ The reactivity of **4.6** with $[\text{Et}_3\text{NH}][\text{BPh}_4]$ in toluene- d_8 was tested on an NMR scale, however only intractable mixtures of different products were observed by NMR spectroscopy. Evidently the presence of coordinated THF in the isolated product means it is not a suitable candidate for the synthesis of an unsolvated $[(\eta^8\text{-Pn}^{\dagger})\text{Sc}]^+$ cation *via* protonolysis with $[\text{Et}_3\text{NH}][\text{BPh}_4]$, and further efforts to purify and fully characterise complex **4.6** were abandoned.

4.4.3 Synthesis and characterisation of $(\eta^8\text{-Pn}^{\dagger})\text{ScCp}^*$ (**4.7**)

Pentalene can be considered as an 8 electron donor (L_3X_2 in a neutral counting scheme)⁵⁴ when coordinated in an η^8 - fashion to a single metal centre, which means the formal electron count of the $(\eta^8\text{-Pn}^{\dagger})\text{Sc}$ moiety is 2 less than that of $(\text{Cp}^{\text{Me}4\text{H}})_2\text{Sc}$. Therefore an R ligand with an electron count 2 greater than for $\text{R} = \eta^3\text{-C}_3\text{H}_5$ (L_2X) would give the desired base-free $(\eta^8\text{-Pn}^{\dagger})\text{ScR}$ complex the same electron count as $(\text{Cp}^{\text{Me}4\text{H}})_2\text{Sc}(\eta^3\text{-C}_3\text{H}_5)$. A suitable candidate was $\text{R} = \text{Cp}^*$ which is a 5 electron donor

(L₂X) and the permethylated ring was chosen specifically to provide steric stabilisation and potentially give a monomeric complex.

Reaction of **4.5** with KCp* in THF produced a red mixture which after work-up and recrystallisation from pentane furnished (η^8 -Pn[†])ScCp* (**4.7**) as orange crystals in 43% yield (Scheme 4.6).



Scheme 4.6 Synthesis of **4.7**. R = SiⁱPr₃.

Multinuclear (¹H, ¹³C, ²⁹Si) NMR spectra in C₆D₆ show the expected resonances due to the Pn[†] and Cp* ligands, and confirmed the absence of coordinating THF. Mass spectrometry (EI) and elemental analysis were consistent with the proposed formulation.

X-ray diffraction analysis of **4.7** reveals a molecular structure (Figure 4.15) comparable with those of **2.6**, **2.7** and **2.8** in this work, and the f-element mixed sandwich complexes (η^8 -Pn[†])SmCp* and (η^8 -Pn[†])UCp* reported by Cloke *et al.*^{70,71} Structural data for this complex listed in Table 4.5, show that the smaller radius of the Sc³⁺ ion ($r_{\text{Sc}^{3+}} = 0.745$ Å) allows for closer approach of the carbocyclic ligands and, in turn, the pentalene ring folds about its bridgehead bond to a greater extent (30.1°) to accommodate the smaller metal.

4.7 is the first example of a scandium complex bearing a trialkylsilyl-substituted pentalene ligand to be characterised by X-ray diffraction and to the best of the authors knowledge the only other scandium pentalene complexes outside this work are (η^8 -Pn)ScR{THF} R = Cp, Cp*, indenyl, reported in a patent by Jonas *et al.*⁷² However no crystallographic data have been reported for any of the latter, which precludes any structural comparison with **4.7**.

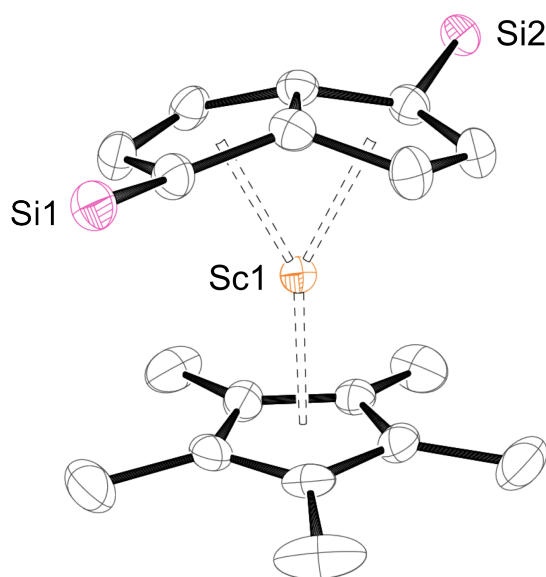


Figure 4.15 Displacement ellipsoid plot (50% probability) of **4.7**. H atoms and ⁱPr groups omitted for clarity. The Cp*-CH₃ groups were disordered over two positions with only part 1 shown.

Table 4.5 Selected distances (Å), angles (°) and parameters for **4.7**. Ct1 and Ct2 are the η^5, η^5 -centroids and Ct4 is the midpoint of the bridgehead bond of the Pn ring. Ct3 is the η^5 -centroid of the Cp* ring.

Parameter	4.7	Parameter	4.7
Sc1–Ct1	2.0631(11)	C–C _{ring} (Pn) ^a	1.433(3)
Sc1–Ct2	2.0617(11)	Ct1–Sc1–Ct2	152.18(7)
Sc1–Ct3	2.147(2)	Ct2–Sc1–Ct3	54.77(7)
Sc1–Ct4	2.094(18)	Ct4–Sc1–Ct3	179.22(7)
Sc–C _{ring} (Pn) ^a	2.435(2)	Fold angle	30.06(12)

^aAverage values.

An orange solution of **4.7** in toluene-*d*₈ was treated with [Et₃NH][BPh₄] and heated to 100 °C for 3 days, however no reaction was observed by ¹H NMR spectroscopy. Despite examples from Evans *et al.* of facile protonolysis of Cp* ligands bound to

Ln(II) centres (as discussed in chapter two), this ligand interacts more strongly with the highly ionic Sc(III) centre, as exemplified by the shorter metal–Cp* centroid distance in **4.7** (2.147(2) Å) compared with those in [Cp*Ln]₂(μ-Pn[†]) (range 2.397(3) - 2.540(2) Å). Therefore protonolysis with [Et₃NH][BPh₄] to give Cp*H (pK_a = 26.1),⁷³ Et₃N and the desired (η⁸-Pn[†])Sc(BPh₄) complex is not viable. Other candidates for R ligands which may be more labile when attached to the Sc(III) centre include pentadienyl, mesityl, CH(SiMe₃)₂, CH₂Ph, and CHPh₂. However due to time constraints further reactivity studies of **4.5** were not undertaken.

4.5 Experimental Details for Chapter Four

4.5.1 Synthesis of [(η⁸-Pn[†])Ti]₂(μ-Cl)₃ (**4.1**)

A THF (50 mL) solution of [K]₂Pn[†] (1.376 g, 2.79 mmol) was added dropwise to a stirred suspension of TiCl₃(THF)₃ (1.089 g, 2.96 mmol) in THF (100 mL) at 0 °C. The resultant olive green reaction mixture was allowed to warm to room temperature whilst stirring overnight, after which time the solvent was removed *in vacuo* and the solid residues were extracted with toluene (100 mL) and filtered through Celite on a frit. The resultant solution was stripped to dryness to afford a green microcrystalline solid.

Total yield: 1.220 g (80% with respect to TiCl₃(THF)₃).

An analytically pure sample of **4.1**, and crystals suitable for X-ray diffraction were obtained by slow cooling of a saturated THF solution to -35 °C. In the solid state and solution, **4.1** slowly decomposes at room temperature to give an uncharacterised orange coloured compound and requires storage at -35 °C or below.

¹H NMR (C₆D₆, 399.5 MHz, 303 K): δ_H 1.09 (br, Δν_{1/2} = 80 Hz, ⁱPr CH), 1.46, (br, Δν_{1/2} = 98 Hz, ⁱPr CH₃).

EPR (solid state, 293 K, X-band): g_{iso} = 1.985; (toluene, 150 K, X-band) g₁ = 2.002, g₂ = 1.989, g₃ = 1.967, g_{iso} = 1.986; (toluene, 150 K, Q-band): g₁ = 2.001, g₂ = 1.987, g₃ = 1.961, g_{iso} = 1.983.

IR (NaCl): 2963, 2944, 2890, 2866, 1671, 1463, 1415, 1382, 1261 cm⁻¹.

EI-MS: $m/z = 1031$ (25%), $[M]^+$; 996 (15%), $[M - Cl]^+$; 913 (90%), $[M - TiCl_2]^+$; 877 (85%), $[M - TiCl_3]^+$.

Anal. found (calcd for $C_{52}H_{92}Cl_3Si_4Ti_2$): C, 60.25 (60.54); H, 8.82 (8.99)%.

Mag. suscep. (toluene- d_8 , 303 K): $\mu_{\text{eff}} = 1.70 \mu_B$ per dimer; (solid state, 250 K): $\mu_{\text{eff}} = 1.72 \mu_B$ per dimer; (calcd. from solid state EPR spectrum using $g_{\text{iso}} = 1.985$, 293 K): $\mu_{\text{eff}} = 1.72 \mu_B$ per dimer.

Partially refined crystal data for **4.1**: $C_{52}H_{92}Cl_3Si_4Ti_2$, $M_r = 1396.1$, red blade, triclinic, space group $P-1$, $a = 8.511(4) \text{ \AA}$, $b = 13.784(6) \text{ \AA}$, $c = 14.767(5) \text{ \AA}$, $\alpha = 59.36(2)^\circ$, $\beta = 69.98(3)^\circ$, $\gamma = 83.67(4)^\circ$, $V = 1396(12) \text{ \AA}^3$, $T = 100 \text{ K}$, $Z = 1$, $\lambda_{\text{Mo}}(K\alpha) = 0.71073 \text{ \AA}$, $\theta_{\text{max}} = 27.6^\circ$, $R_1 [I > 2\sigma(I)] = 0.1168$, wR_2 (all data) = 0.3674, $\text{Goof} = 1.432$.

4.5.2 Synthesis of $[(\eta^8\text{-Pn}^\dagger)\text{Ti}\{\text{py}\}]_2(\mu\text{-Cl})_2$ (**4.2**)(py)₂

The reaction of $[K]_2\text{Pn}^\dagger$ and $TiCl_3(\text{THF})_3$ was carried out as above and a 100 mg sample of the crude green solid was treated with hexane (3 mL) and pyridine (1 mL) resulting in a colour change to brown. The volatiles were removed under reduced pressure and the solid residues were extracted with toluene (2 mL) and filtered. The filtrate was cooled to -35°C , affording (**4.2**)(py)₂ as red crystals which were isolated by decantation, washed with pentane (1 mL) at -35°C , and dried *in vacuo*.

^1H NMR (toluene- d_8 , 399.5 MHz, 303 K): δ_H 2.90 (br, $\Delta\nu_{1/2} = 80 \text{ Hz}$, $^i\text{Pr CH}$), 1.46, (br, $\Delta\nu_{1/2} = 98 \text{ Hz}$, $^i\text{Pr CH}_3$).

IR (NaCl): 2943, 2866, 1603, 1462, 1442, 1386, 1260, 1172, 1070, 1018, cm^{-1} .

EI-MS: $m/z = 526\text{-}535$ (principal peak 532, 25%), $[M - \text{TiPn}^\dagger - 2\text{py}]^+$; 489 (100%), $[M - \text{TiPn}^\dagger - ^i\text{Pr} - 2\text{py}]^+$.

Anal. found (calcd. for $C_{62}H_{102}Cl_2N_2Si_4Ti_2$): C, 64.05 (64.50); H, 8.92 (8.91); N, 2.50 (2.43) %.

Mag. suscep. (toluene- d_8 , 303 K): $\mu_{\text{eff}} = 2.13 \mu_B$ per dimer; (solid state, 250 K): $\mu_{\text{eff}} = 2.14 \mu_B$ per dimer.

Crystal data for **4.2**(py)₂: $C_{62}H_{102}Cl_2N_2Si_4Ti_2$, $M_r = 1154.51$, triclinic, space group $P-1$, dark red plate, $a = 10.6847(8) \text{ \AA}$, $b = 11.5207(8) \text{ \AA}$, $c = 14.2783(10) \text{ \AA}$, $\alpha = 78.884(8)^\circ$, $\beta = 70.774(7)^\circ$, $\gamma = 89.374(9)^\circ$, $V = 1625.8(2) \text{ \AA}^3$, $T = 100 \text{ K}$, $Z = 1$, $R_{\text{int}} = 0.0681$,

$\lambda_{\text{Mo}}(\text{K}\alpha) = 0.71073 \text{ \AA}$, $\theta_{\text{max}} = 25.242^\circ$, $R_1 [I > 2\sigma(I)] = 0.0726$, $wR_2 (\text{all data}) = 0.1946$, $\text{Goof} = 1.05$.

4.5.3 Synthesis of $(\mu:\eta^5, \eta^5\text{-Pn}^\dagger)_2\text{Ti}_2$ (**4.3**)

To a solution of **4.1** (355 mg, 0.344 mmol) in hexane (40 mL) was added potassium amalgam, freshly prepared from mercury (4 mL) and potassium (109 mg, 2.79 mmol). The reaction mixture was stirred vigorously for 24 h at room temperature, to afford a red suspension that was filtered through Celite and the solvent removed *in vacuo*. Complex **2** was recrystallised from a saturated pentane (5 mL) solution at -50°C as deep red blocks, which were isolated by decantation and dried *in vacuo*.

Total yield: 79 mg (25% with respect to **4.1**). Improved crystalline yields of **4.3** (60% with respect to $[\text{K}]_2\text{Pn}^\dagger$ on a 3.3 mmol scale) were obtained in a one-pot synthesis *via* K/Hg reduction of **4.1** the without latter being isolated.

^1H NMR (C_6D_6 , 399.5 MHz, 303 K): δ_{H} 6.83 (4H, d, $^3J_{\text{HH}} = 3.1 \text{ Hz}$, Pn *H*), 6.34 (4H, d, $^3J_{\text{HH}} = 3.2 \text{ Hz}$, Pn *H*), 1.16 (12H, m, ^iPr CH), 0.91 (36H, d, $^3J_{\text{HH}} = 7.4 \text{ Hz}$, ^iPr CH_3), 0.77 (36H, d, $^3J_{\text{HH}} = 7.4 \text{ Hz}$, ^iPr CH_3).

$^{13}\text{C}\{^1\text{H}\}$ NMR (C_6D_6 , 100.5 MHz, 303 K): δ_{C} 133.44 (Pn bridgehead C), 132.63 (Pn aromatic C), 111.28 (Pn aromatic C), 102.28 (Pn aromatic C-Si), 19.24 (^iPr CH_3), 19.03 (^iPr CH_3), 13.44 (^iPr CH).

$^{29}\text{Si}\{^1\text{H}\}$ NMR (C_6D_6 , 79.4 MHz, 303 K): δ_{Si} 4.32.

EI-MS: $m/z = 916\text{-}927$ (principal peak 922, 100%), $[\text{M}]^+$; 877 (50%), $[\text{M} - \text{Ti}]^+$.

Anal. found (calcd. for $\text{C}_{52}\text{H}_{92}\text{Si}_4\text{Ti}_2$): C, 67.38 (67.49); H, 9.91 (10.02) %.

IR (NaCl): 2941, 2889, 2863, 1463, 1410, 1382, 1261 cm^{-1} .

Crystal data for **4.2**: $\text{C}_{52}\text{H}_{92}\text{Si}_4\text{Ti}_2$, $M_r = 925.42$, triclinic, space group *P*-1, orange plate, $a = 13.055(7) \text{ \AA}$, $b = 13.064(5) \text{ \AA}$, $c = 19.698(10) \text{ \AA}$, $\alpha = 95.75(6)^\circ$, $\beta = 103.67(7)^\circ$, $\gamma = 119.44(3)^\circ$, $V = 2749(2) \text{ \AA}^3$, $T = 100 \text{ K}$, $Z = 2$, $R_{\text{int}} = 0.1059$, $\lambda_{\text{Mo}}(\text{K}\alpha) = 0.71073 \text{ \AA}$, $\theta_{\text{max}} = 24.71^\circ$, $R_1 [I > 2\sigma(I)] = 0.0927$, $wR_2 (\text{all data}) = 0.2008$, $\text{Goof} = 1.079$.

4.5.4 Synthesis of $[(\mu\text{-}\eta^5, \eta^5\text{-Pn}^\dagger)_2\text{Ti}_2][\text{B}(\text{C}_6\text{F}_5)_4]$ (**4.4**).

To a stirred, solid mixture of **4.3** (81.5 mg, 0.088 mmol) and $[\text{FeCp}^*_2][\text{B}(\text{C}_6\text{F}_5)_4]$ (127 mg, 0.126 mmol) at $-35\text{ }^\circ\text{C}$ was added Et_2O (3 mL), pre-cooled to $-35\text{ }^\circ\text{C}$, and the resultant brown mixture was allowed to warm to room temperature. After 20 mins the solvent was removed under reduced pressure to afford a brown residue that was washed thoroughly with hexane ($4 \times 15\text{ mL}$) to remove FeCp^*_2 until the washings ran colourless. The residue was then extracted with Et_2O ($2 \times 2\text{ mL}$), filtered and the brown filtrate concentrated to *ca.* 1 mL by slow evaporation at ambient pressure. Cooling this solution to $-35\text{ }^\circ\text{C}$ produced green crystals that were isolated by decantation and dried *in vacuo*.

Total yield: 21 mg (15% with respect to **4.3**).

^1H NMR ($\text{THF-}d_8$, 399.5 MHz, 303 K): δ_{H} 2.97 (br, $\Delta\nu_{1/2} = 79\text{ Hz}$, $^i\text{Pr H}$). ^{13}C and ^{29}Si NMR resonances were not observed due to the paramagnetic nature of **4.4**.

^{19}F NMR ($\text{THF-}d_8$, 375.9 MHz, 303 K): δ_{F} -132.7 (br, *o-F*), -165.2 (t, $^3J_{\text{FF}} = 20.2\text{ Hz}$, *p-F*), -168.7 (br t, $^3J_{\text{FF}} = 19.3\text{ Hz}$, *m-F*).

$^{11}\text{B}\{^1\text{H}\}$ NMR ($\text{THF-}d_8$, 128.2 MHz, 303 K): δ_{B} -14.75.

EI-MS: No volatility.

Anal. found (calcd. for $\text{C}_{76}\text{H}_{92}\text{BF}_{20}\text{Si}_4\text{Ti}_2$): C, 56.72 (56.89); H, 5.83 (5.78) %.

Mag. suscep. ($\text{THF-}d_8$, 303 K): $\mu_{\text{eff}} = 1.96\text{ }\mu_{\text{B}}$ per dimer.

Crystal data for **4.4**. $\frac{1}{2}(\text{C}_6\text{H}_{14})$: $\text{C}_{79}\text{H}_{99}\text{BF}_{20}\text{Si}_4\text{Ti}_2$, $M_r = 1647.55$, triclinic, space group *P-1*, green plate, $a = 14.217(3)\text{ \AA}$, $b = 15.491(3)\text{ \AA}$, $c = 19.366(4)\text{ \AA}$, $\alpha = 89.30(3)^\circ$, $\beta = 88.71(3)^\circ$, $\gamma = 67.67(3)^\circ$, $V = 3944.1(16)\text{ \AA}^3$, $T = 100\text{ K}$, $Z = 2$, $R_{\text{int}} = 0.079$, $\lambda_{\text{Mo}}(\text{K}\alpha) = 0.71075\text{ \AA}$, $\theta_{\text{max}} = 26.372^\circ$, $R_1 [I > 2\sigma(I)] = 0.0562$, wR_2 (all data) = 0.1656, $\text{Goof} = 1.025$.

4.5.5 Synthesis of $[(\eta^8\text{-Pn}^\dagger)\text{Sc}(\text{THF})(\mu\text{-Cl})]_2$ (**4.5**)

A solution of $[\text{K}]_2\text{Pn}^\dagger$ (650 mg, 1.32 mmol) in THF (20 mL) was added dropwise to a suspension of ScCl_3 (200 mg, 1.32 mmol) in THF (100 mL) and stirred overnight at room temperature. The resultant red mixture was stripped to dryness and the solid

residues were extracted with pentane (3×10 mL) and filtered through Celite on a frit. The orange filtrate was concentrated to *ca.* 5 mL and filtered. Cooling this solution to -50 °C produced orange crystals that were isolated by decantation and dried *in vacuo*.

Total yield: 643 mg (86% with respect to $[\text{K}]_2\text{Pn}^\dagger$).

^1H NMR (C_6D_6 , 399.5 MHz, 303 K): δ_{H} 6.77 (4H, d, $^3J_{\text{HH}} = 2.8$ Hz, Pn *H*), 6.34 (4H, br s, $\Delta\nu_{1/2} = 16.5$ Hz, Pn *H*), 3.66 (8H, br s, $\Delta\nu_{1/2} = 14.3$ Hz, THF OCH_2), 1.40 (s, THF CH_2), 1.38 (m, ^iPr *CH*), 1.27 (36H, d, $^3J_{\text{HH}} = 7.3$ Hz, ^iPr CH_3), 1.23 (36H, d, $^3J_{\text{HH}} = 7.3$ Hz, ^iPr CH_3).

$^{13}\text{C}\{^1\text{H}\}$ NMR (C_6D_6 , 125.7 MHz, 303 K): δ_{C} 149.1 (Pn aromatic C), 68.45 (THF OCH_2), 25.76 (THF CH_2), 20.88 - 18.41 (overlapping signals, ^iPr CH_3), 13.67 - 11.25 (overlapping signals, ^iPr *CH*).

$^{29}\text{Si}\{^1\text{H}\}$ NMR (C_6D_6 , 79.4 MHz, 303 K): δ_{Si} -25.00.

$^{45}\text{Sc}\{^1\text{H}\}$ NMR (C_6D_6 , 97.04 MHz, 303 K): δ_{Sc} -7.14.

EI-MS: $m/z = 874$ (100%), $[\text{Pn}^\dagger_2\text{Sc}]^+$; 831 (15%), $[\text{Pn}^\dagger_2\text{Sc} - ^i\text{Pr}]^+$.

Anal. found (calcd. for $\text{C}_{60}\text{H}_{106}\text{Cl}_2\text{O}_2\text{Sc}_2\text{Si}_4$): C, 63.45 (63.62); H, 9.38 (9.43)%.

Partially refined crystal data for **4.5**: $\text{C}_{60}\text{H}_{108}\text{Cl}_2\text{O}_2\text{Sc}_2\text{Si}_4$, $M_r = 1134.6$, triclinic, space group *P*-1, orange block, $a = 15.211(4)$ Å, $b = 17.520(6)$ Å, $c = 19.602(7)$ Å, $\alpha = 82.38(3)^\circ$, $\beta = 71.63(2)^\circ$, $\gamma = 77.84(3)^\circ$, $V = 4834(3)$ Å³, $T = 100$ K, $Z = 3$, $\lambda_{\text{Mo}}(\text{K}\alpha) = 0.71073$ Å, $\theta_{\text{max}} = 24.5^\circ$, $R_1 [I > 2\sigma(I)] = 0.1256$, wR_2 (all data) = 0.3096, $\text{Goof} = 1.156$.

4.5.6 Synthesis of $[(\eta^8\text{-Pn}^\dagger)\text{Sc}(\text{C}_3\text{H}_5)\{\text{THF}\}]_x$ (**4.6**)

A solution of allylmagnesium chloride (32 mL, 0.649 mmol, 2.0 M in THF) was added to a solution of **4.5** (350 mg, 0.309 mmol) in toluene (10 mL) at -78 °C. The orange reaction mixture was stirred for 40 min at -78 °C and then allowed to warm to room temperature. After 5 h the solvent was removed under reduced pressure, yielding an orange residue which was treated with hexane (20 mL) and dried *in vacuo*. Extraction with 1,4 dioxane (1 mL) in hexane (50 mL), followed by standing for 3 h allowed the separation of a white precipitate. The yellow-orange supernatant was decanted and filtered through Celite on a frit. Removal of the solvent yielded **4.6** as a bubbly yellow solid, which was recrystallised from pentane at -35 °C.

Total yield: 89 mg (24% with respect to $\text{C}_3\text{H}_5\text{MgCl}$).

^1H NMR (C_6D_6 , 499.9 MHz, 303 K): δ_{H} 6.72 (2H, d, $^3J_{\text{HH}} = 2.5$ Hz, Pn *H*), 6.35 (1H, m, $J = 11.1$ Hz, allyl *CH*), 5.51 (2H, d, $^3J_{\text{HH}} = 2.9$ Hz, Pn *H*), 3.29 (4H, br s, $\Delta\nu_{1/2} = 1.28$ Hz, allyl CH_2), 3.24 (4H, br t, $^3J_{\text{HH}} = 6.4$ Hz, THF OCH_2), 1.30 (m, ^iPr *CH*), 1.23 (18H, d, $^3J_{\text{HH}} = 7.0$ Hz, ^iPr CH_3), 1.14 (18H, d, $^3J_{\text{HH}} = 7.2$ Hz, ^iPr CH_3), 0.97 (4H, br t, $^3J_{\text{HH}} = 6.5$ Hz, THF CH_2).

$^{13}\text{C}\{^1\text{H}\}$ NMR (C_6D_6 , 125.7 MHz, 303 K): δ_{C} 145.20 (Pn bridgehead C), 142.60 (allyl *CH*), 131.50 (Pn C), 104.29 (Pn C), 95.45 (Pn C-Si), 71.00 (allyl CH_2), 67.24 (THF OCH_2), 25.17 (THF CH_2), 19.66 (^iPr CH_3), 13.00 (^iPr *CH*).

$^{29}\text{Si}\{^1\text{H}\}$ NMR (C_6D_6 , 79.4 MHz, 303 K): δ_{Si} 0.69.

EI-MS: $m/z = 873$ (100%), $[\text{Pn}^{\dagger}_2\text{Sc}]^+$; 716 (30%), $[\text{Pn}^{\dagger}_2\text{Sc} - \text{Si}^i\text{Pr}_3]^+$.

Anal. found (calcd. for $\text{C}_{33}\text{H}_{58}\text{OScSi}_2$): C, 53.31, 58.92 (69.30); H, 8.22, 8.21 (10.22)%.

4.5.7 Synthesis of $(\eta^8\text{-Pn}^{\dagger})\text{ScCp}^*$ (**4.7**)

To a stirred mixture of **4.5** (301 mg, 0.266 mmol) and KCp^* (94 mg, 0.540 mmol) was added THF (50 mL) at room temperature. After 12 h the solvent was removed under reduced pressure, yielding an orange residue which was treated with pentane (20 mL) and dried *in vacuo*. Extraction with pentane (2×50 mL) followed by filtration and removal of the solvent yielded **4.7** as a bubbly orange solid, which was recrystallised from pentane at -35 °C.

Total yield: 138 mg (43% with respect to KCp^*).

^1H NMR (C_6D_6 , 399.5 MHz, 303 K): δ_{H} 6.74 (2H, d, $^3J_{\text{HH}} = 3.0$ Hz, Pn *H*), 5.29 (2H, d, $^3J_{\text{HH}} = 3.0$ Hz, Pn *H*), 1.98 (15H, s, Cp^* CH_3), 1.25 (6H, m, ^iPr *CH*), 1.14 (18H, d, $^3J_{\text{HH}} = 7.4$ Hz, ^iPr CH_3), 1.11 (18H, d, $^3J_{\text{HH}} = 7.4$ Hz, ^iPr CH_3).

$^{13}\text{C}\{^1\text{H}\}$ NMR (C_6D_6 , 125.7 MHz, 303 K): δ_{C} 151.65 (Pn bridgehead C), 135.09 (Pn aromatic *CH*), 120.36 (Cp^* CCH_3), 105.86 (Pn aromatic *CH*), 102.20 (Pn aromatic C-Si), 19.75 (^iPr CH_3), 19.50 (^iPr CH_3), 12.65 (^iPr *CH*), 12.12 (Cp^* CH_3).

$^{29}\text{Si}\{^1\text{H}\}$ NMR (C_6D_6 , 79.4 MHz, 303 K): δ_{Si} 1.56.

EI-MS: $m/z = 594$ (90%), $[\text{M}]^+$; 551 (75%), $[\text{M} - ^i\text{Pr}]^+$; 437 (10%), $[\text{M} - \text{Si}^i\text{Pr}_3]^+$.

Anal. found (calcd. for $C_{36}H_{61}Sc_2Si_2$): C, 72.59 (72.67); H, 10.42 (10.33)%.

Crystal data for **4.6**: $C_{36}H_{61}Sc_2Si_2$, $M_r = 594.98$, triclinic, space group $P-1$, orange block, $a = 9.3802(19)$ Å, $b = 12.717(3)$ Å, $c = 15.862(3)$ Å, $\alpha = 78.23(3)^\circ$, $\beta = 77.28(3)^\circ$, $\gamma = 77.98(3)^\circ$, $V = 1780.2(7)$ Å³, $T = 100$ K, $Z = 2$, $R_{\text{int}} = 0.0549$, $\lambda_{\text{Mo}}(\text{K}\alpha) = 0.71073$ Å, $\theta_{\text{max}} = 27.482^\circ$, $R_1 [I > 2\sigma(I)] = 0.0512$, wR_2 (all data) = 0.1385, $\text{Goof} = 1.018$.

4.6 References for Chapter Four

1. S. Barlow and D. O'Hare, *Chem. Rev.*, 1997, **97**, 637–667.
2. P. Aguirre-Etcheverry and D. O'Hare, *Chem. Rev.*, 2010, **110**, 4839–4864.
3. I. Resa, E. Carmona, E. Gutierrez-Puebla, and A. Monge, *Science*, 2004, **305**, 1136–1138.
4. H. Xiang, J. Yang, J. G. Hou, and Q. Zhu, *J. Am. Chem. Soc.*, 2006, **128**, 2310–2314.
5. L. Shen, S.-W. Yang, M.-F. Ng, V. Ligatchev, L. Zhou, and Y. Feng, *J. Am. Chem. Soc.*, 2008, **130**, 13956–13960.
6. X. Wu and X. C. Zeng, *J. Am. Chem. Soc.*, 2009, **131**, 14246–14248.
7. T. Zhang, L. Zhu, Q. Wu, S.-W. Yang, and J. Wang, *J. Chem. Phys.*, 2012, **137**, 164309.
8. O. T. Summerscales and F. G. N. Cloke, *Coord. Chem. Rev.*, 2006, **250**, 1122–1140.
9. T. J. Katz, N. Acton, and J. McGinnis, *J. Am. Chem. Soc.*, 1972, **94**, 6205–6206.
10. T. J. Katz and N. Acton, *J. Am. Chem. Soc.*, 1972, **94**, 3281–3283.
11. M. Kuchta and F. G. N. Cloke, *Organometallics*, 1998, **17**, 1934–1936.
12. G. Balazs, F. G. N. Cloke, A. Harrison, P. B. Hitchcock, J. Green, and O. T. Summerscales, *Chem. Commun.*, 2007, 873–875.
13. G. Balazs, F. G. N. Cloke, L. Gagliardi, J. C. Green, A. Harrison, P. B. Hitchcock, A. R. M. Shahi, and O. T. Summerscales, *Organometallics*, 2008, **27**, 2013–2020.
14. O. T. Summerscales, C. J. Rivers, M. J. Taylor, P. B. Hitchcock, J. C. Green, and F. G. N. Cloke, *Organometallics*, 2012, **31**, 8613–8617.
15. A. E. Ashley, R. T. Cooper, G. G. Wildgoose, J. C. Green, and D. O'Hare, *J. Am. Chem. Soc.*, 2008, **130**, 15662–15677.
16. A. D. Smith, M.Chem. Dissertation, University of Sussex, 2012.
17. F. Cotton and L. Daniels, *Angew. Chem. Int. Ed. Engl.*, 1992, **31**, 737–738.
18. F. A. Cotton, B. A. Frenz, and L. Kruczynski, *J. Am. Chem. Soc.*, 1973, **95**, 951–952.
19. S. C. Jones and D. O'Hare, *Chem. Commun.*, 2003, 2208–2209.
20. P. J. Chirik, *Organometallics*, 2010, **29**, 1500–1517.
21. O. T. Summerscales, D.Phil Thesis, University of Sussex, 2007.
22. F. A. Cotton, C. A. Murillo, and R. A. Walton, *Multiple Bonds Between Metal Atoms*, Clarendon Press, 3rd edn. 2005.
23. M. Horáček, V. Kupfer, U. Thewalt, P. Štěpnička, M. Polášek, and K. Mach, *J. Organomet. Chem.*, 1999, **584**, 286–292.
24. T. Nguyen, A. Sutton, M. Brynda, J. Fettinger, G. Long, and P. Power, *Science*,

- 2005, **310**, 844–847.
25. K. A. Kreisel, G. P. A. Yap, O. Dmitrenko, C. R. Landis, and K. H. Theopold, *J. Am. Chem. Soc.*, 2007, **129**, 14162–14163.
 26. A. Noor, F. R. Wagner, and R. Kempe, *Angew. Chem. Int. Ed.*, 2008, **47**, 7246–7249.
 27. Q. A. Abbasali, F. G. N. Cloke, P. B. Hitchcock, and S. C. P. Joseph, *Chem. Commun.*, 1997, 1541–1542.
 28. K. Jonas, P. Kolb, G. Kollbach, and B. Gabor, *Angew. Chem. Int. Ed. Engl.*, 1997, **36**, 1714.
 29. F. G. N. Cloke, P. B. Hitchcock, M. C. Kuchta, and N. A. Morley-Smith, *Polyhedron*, 2004, **23**, 2625–2630.
 30. R. T. Cooper, F. M. Chadwick, A. E. Ashley, and D. O'Hare, *Organometallics*, 2013, **32**, 2228–2233.
 31. F. M. Chadwick, R. T. Cooper, A. E. Ashley, J. C. Buffet, and D. M. O'Hare, *Organometallics*, 2014, **33**, 3775–3785.
 32. R. J. West, Part II Thesis, University of Oxford, 2008.
 33. R. T. Cooper, Personal Communication.
 34. M. Horáček, V. Kupfer, U. Thewalt, M. Polášek, and K. Mach, *J. Organomet. Chem.*, 1998, **579**, 126–132.
 35. J. Evans, *J. Chem. Soc.*, 1959, 2003–2005.
 36. E. M. Schubert, *J. Chem. Educ.*, 1992, **69**, 62.
 37. H. Strehlow, in *The Chemistry of Non-Aqueous Solvents*, ed. J. J. Lagowski, Academic Press, New York, 1966, vol. 1, p. 129.
 38. N. G. Connelly and W. E. Geiger, *Chem. Rev.*, 1996, **96**, 877–910.
 39. T. E. Hanna, E. Lobkovsky, and P. J. Chirik, *Eur. J. Inorg. Chem.*, 2007, **2007**, 2677–2685.
 40. R. D. Shannon, *Acta. Crystallogr. Sect. A.*, 1976, **32**, 751–767.
 41. F. G. N. Cloke, *Pure Appl. Chem.*, 2001, **73**, 233–238.
 42. R. S. P. Coutts, P. C. Wailes, and R. L. Martin, *J. Organomet. Chem.*, 1973, **47**, 375–382.
 43. R. Coutts, R. L. Martin, and P. C. Wailes, *Aust. J. Chem.*, 1973, **26**, 2101–2104.
 44. R. Jungst, D. Sekutowski, J. Davis, M. Luly, and G. Stucky, *Inorg. Chem.*, 1977, **16**, 1645–1655.
 45. R. M. Wood, *Proc. Phys. Soc.*, 1962, **80**, 783.
 46. P. B. Hitchcock, F. M. Kerton, and G. A. Lawless, *J. Am. Chem. Soc.*, 1998, **120**, 10264–10265.
 47. M. Horáček, V. Kupfer, U. Thewalt, P. Štěpnička, M. Polášek, and K. Mach, *Organometallics*, 1999, **18**, 3572–3578.
 48. H. Brintzinger and J. E. Bercaw, *J. Am. Chem. Soc.*, 1971, **93**, 2045–2046.
 49. T. E. Hanna, E. Lobkovsky, and P. J. Chirik, *Organometallics*, 2009, **28**, 4079–4088.
 50. T. E. Hanna, E. Lobkovsky, and P. J. Chirik, *J. Am. Chem. Soc.*, 2004, **126**, 14688–14689.
 51. L. Lukešová, M. Horáček, P. Štěpnička, K. Fejfarová, R. Gyepes, I. Císařová, J. Kubišta, and K. Mach, *J. Organomet. Chem.*, 2002, **663**, 134–144.
 52. M. D. Walter, C. D. Sofield, and R. A. Andersen, *Organometallics*, 2008, **27**, 2959–2970.
 53. J. C. Green, A. F. R. Kilpatrick, and F. G. N. Cloke, *Manuscript in progress*.
 54. J. C. Green, M. L. H. Green, and G. Parkin, *Chem. Commun.*, 2012, **48**, 11481–11503.

55. R. G. Compton and C. E. Banks, *Understanding Voltammetry*, Imperial College Press, 2nd edn. 2011.
56. M. W. Bouwkamp, J. de Wolf, I. Del Hierro Morales, J. Gercama, A. Meetsma, S. I. Troyanov, B. Hessen, and J. H. Teuben, *J. Am. Chem. Soc.*, 2002, **124**, 12956–12957.
57. M. Kaupp, O. P. Charkin, and P. V. R. Schleyer, *Organometallics*, 1992, **11**, 2765–2767.
58. L. E. Manzer, *J. Organomet. Chem.*, 1976, **110**, 291–294.
59. F. G. N. Cloke, J. C. Green, R. Harker, and P. B. Hitchcock, *Unpublished results*.
60. M. E. Thompson, S. M. Baxter, A. R. Bulls, B. J. Burger, M. C. Nolan, B. D. Santarsiero, W. P. Schaefer, and J. E. Bercaw, *J. Am. Chem. Soc.*, 1987, **109**, 203–219.
61. S. Demir, S. E. Lorenz, M. Fang, F. Furche, G. Meyer, J. W. Ziller, and W. J. Evans, *J. Am. Chem. Soc.*, 2010, **132**, 11151–11158.
62. W. J. Evans and D. S. Lee, *Can. J. Chem.*, 2005, **83**, 375–384.
63. S. E. Lorenz, B. M. Schmiede, D. S. Lee, J. W. Ziller, and W. J. Evans, *Inorg. Chem.*, 2010, **49**, 6655–6663.
64. W. J. Evans, C. A. Seibel, and J. W. Ziller, *J. Am. Chem. Soc.*, 1998, **120**, 6745–6752.
65. M. B. Abrams, J. C. Yoder, C. Loeber, M. W. Day, and J. E. Bercaw, *Organometallics*, 1999, **18**, 1389–1401.
66. J. C. Yoder, M. W. Day, and J. E. Bercaw, *Organometallics*, 1998, **17**, 4946–4958.
67. M. W. Bouwkamp, P. H. M. Budzelaar, J. Gercama, I. Del Hierro Morales, J. de Wolf, A. Meetsma, S. I. Troyanov, J. H. Teuben, and B. Hessen, *J. Am. Chem. Soc.*, 2005, **127**, 14310–14319.
68. S. Standfuss, E. Abinet, T. P. Spaniol, and J. Okuda, *Chem. Commun.*, 2011, **47**, 11441–11443.
69. B. F. Wicker, H. Fan, A. K. Hickey, M. G. Crestani, J. Scott, M. Pink, and D. J. Mindiola, *J. Am. Chem. Soc.*, 2012, **134**, 20081–20096.
70. O. T. Summerscales, D. R. Johnston, F. G. N. Cloke, and P. B. Hitchcock, *Organometallics*, 2008, **27**, 5612–5618.
71. F. G. N. Cloke and P. B. Hitchcock, *J. Am. Chem. Soc.*, 2002, **124**, 9352–9353.
72. K. Jonas, P. Kolb, and G. Kollbach, *US Pat. 5959132 A*, 1999.
73. F. G. Bordwell and M. J. Bausch, *J. Am. Chem. Soc.*, 1983, **105**, 6188–6189.

5 CHAPTER FIVE: Reactivity of $(\mu:\eta^5, \eta^5\text{-Pn}^\dagger)_2\text{Ti}_2$ with Carbon Monoxide and Carbon Dioxide

5.1 Introduction

Despite the considerable number of di-metal bis(pentalene) ‘double-sandwich’ complexes known prior to this study,¹⁻³ no subsequent reaction chemistry had been reported. The first of these complexes to be structurally authenticated $(\text{Pn}^\dagger)_2\text{Mo}_2$, ($\text{Pn}^\dagger = [\text{C}_8\text{H}_4\{\text{Si}^i\text{Pr}_{3-1,4}\}_2]^{2-}$) shows a near-parallel arrangement of pentalene ligands with the Si^iPr_3 groups staggered.⁴ DFT calculations describe a Mo–Mo bond order of two and a formal electron count of 28 per dimer, indicating an electronically deficient system.⁵ However the implicit effect on reactivity was not observed and $(\text{Pn}^\dagger)_2\text{Mo}_2$ shows resistance to coordination of Lewis bases such as CO or PMe_3 , attributed to the sterically crowded environment around the metal centres.⁴ Recent work by Cloke *et al.* has shown that $(\text{Pn}^\dagger)_2\text{V}_2$, containing a reduced $[\text{V}_2]^{4+}$ core with a V–V triple bond, also showed no reaction with H_2 , CO or CO_2 .⁶ The previous chapter describes the synthesis and characterisation of the di-titanium bis(pentalene) complex, $(\mu:\eta^5, \eta^5\text{-Pn}^\dagger)_2\text{Ti}_2$ (**4.3**), which features a rare example of a Ti–Ti multiple bond. **4.3** has a solid state structure unique amongst the Pn_2M_2 complexes, in which the pentalene ligands are non-parallel and tilted around the Ti_2 core. DFT studies on model system Pn_2Ti_2 calculated a M–M bond order of 2 (with σ and π components), and an optimised C_{2v} molecular symmetry, providing a relatively open structure in which the frontier orbitals are sterically accessible.⁷

The prospect of a low valent group 4 metal with the unusual characteristics of a metal-metal bond prompted a reactivity study of **4.3** with small molecules, in particular CO and CO_2 . Previous reports of CO and CO_2 activation at low valent titanium centres and comparable M–M bonded complexes will be briefly summarised.

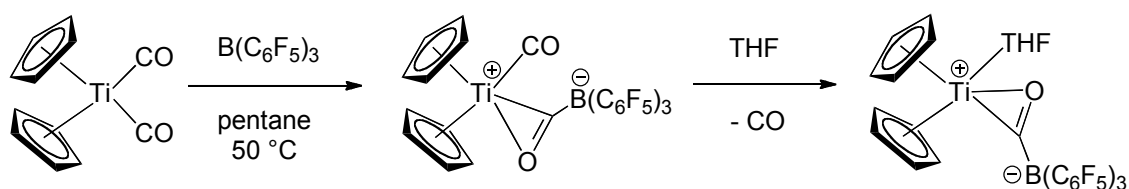
5.1.1 Carbon monoxide

Carbon monoxide, CO, is the most extensively studied ligand in transition metal chemistry,^{8,9} and carbonyl complexes are known for each one of the transition metals.¹⁰⁻¹² Bonding in transition metal carbonyls is a synergic process involving

electron donation from the filled σ -orbital on carbon into an empty metal orbital of the same symmetry and similar energy, and back donation from filled metal π -orbitals into the empty π^* -antibonding orbital of the CO ligand. Therefore carbonyl complexes are stabilised by low oxidation state metals, which have electrons available for back donation. This feature was exploited for Ti(II) by Murray in 1959 with the first preparation of a titanium carbonyl complex, $\text{Cp}_2\text{Ti}(\text{CO})_2$, by reduction of Cp_2TiCl_2 in the presence of CO.¹³ In this reaction, the coordination of two neutral (L) ligands is a prerequisite for trapping the highly reactive ‘titanocene’ (Cp_2Ti) intermediate, which was later established to be unstable with respect to the fulvalene-bridged Ti(III) hydride dimer, $(\mu\text{-C}_{10}\text{H}_8)[(\eta^5\text{-Cp})\text{Ti}(\mu\text{-H})]_2$.^{14,15} Higher yielding synthetic routes to $\text{Cp}_2\text{Ti}(\text{CO})_2$ were subsequently developed,¹⁶⁻¹⁹ leading to its structural characterisation by X-ray crystallography,²⁰ which confirmed that the carbonyl groups bond to titanium in a strictly linear fashion. Given that a simple titanocene precluded isolation and spectroscopic characterisation, $\text{Cp}_2\text{Ti}(\text{CO})_2$ is a relatively stable diamagnetic complex, and provided a convenient entry point for reactivity studies of the Ti(II) oxidation state.

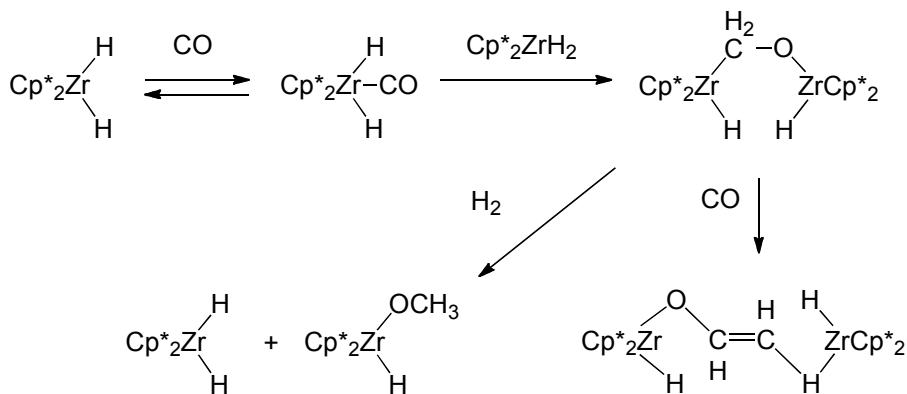
Pioneering work by Floriani *et al.* using $\text{Cp}_2\text{Ti}(\text{CO})_2$ with electrophilic substrates (including azobenzene, alkynes, organic disulfides, and acyl halides) showed primarily metal-based reactivity with liberation of carbon monoxide, and helped establish the carbenoid-like behavior of the Cp_2Ti moiety.²¹⁻²⁶ Substituted titanocene di-carbonyl complexes, $(\text{Cp}^{\text{R}})_2\text{Ti}(\text{CO})_2$ ($\text{Cp}^{\text{R}} = [\eta^5\text{-C}_5\text{R}_5]^-$, $\text{R} = \text{H}, \text{Me}$), have also proved useful as a source of the respective $(\text{Cp}^{\text{R}})_2\text{Ti}$ fragment in coupling reactions of organic carbonyl-containing compounds (including aldehydes, ketones, and diethyl ketomalonate) to give pinacols and olefins.^{27,28}

Examples from titanium chemistry in which a bound CO undergoes further reactivity are limited, largely due to the thermodynamic barrier from the extremely high CO bond enthalpy ($1076.5 \pm 0.4 \text{ kJ mol}^{-1}$).²⁹ However, Choukroun *et al.* have reported that the reaction of $\text{Cp}_2\text{Ti}(\text{CO})_2$ with $\text{B}(\text{C}_6\text{F}_5)_3$ leads to the acylborane complex $\text{Cp}_2\text{Ti}(\text{CO})(\eta^2\text{-OC-B}\{\text{C}_6\text{F}_5\}_3)$ in which the electrophilic borane attaches to the carbon of the carbonyl moiety rather than the oxygen atom (Scheme 5.1).³⁰



Scheme 5.1 Carbonyl based reactivity of $\text{Cp}_2\text{Ti}(\text{CO})_2$ with $\text{B}(\text{C}_6\text{F}_5)_3$.³⁰

The action of syngas ($\text{CO} + \text{H}_2$) on $\text{Cp}_2\text{Ti}(\text{CO})_2$ has also been reported, resulting in the hydrogenation of carbon monoxide to methane, and a hexanuclear cluster with stoichiometry $[\text{Ti}_6\text{O}_8\text{Cp}_6]$ as a by-product.³¹ Although making methane from syngas is not in itself a desirable transformation,³² the production of higher C_n products in the Fischer-Tropsch process is of high industrial importance for use as liquid fuels and bulk chemicals.³³⁻³⁶ Group 4 metal complexes, primarily with zirconium, have attracted considerable interest as well-defined models for homogeneous Fischer-Tropsch chemistry, as reactive Zr(IV) hydrides are able to reduce CO ,³⁷⁻⁴¹ and in some cases give C–C coupled products (Scheme 5.2).^{42,43}

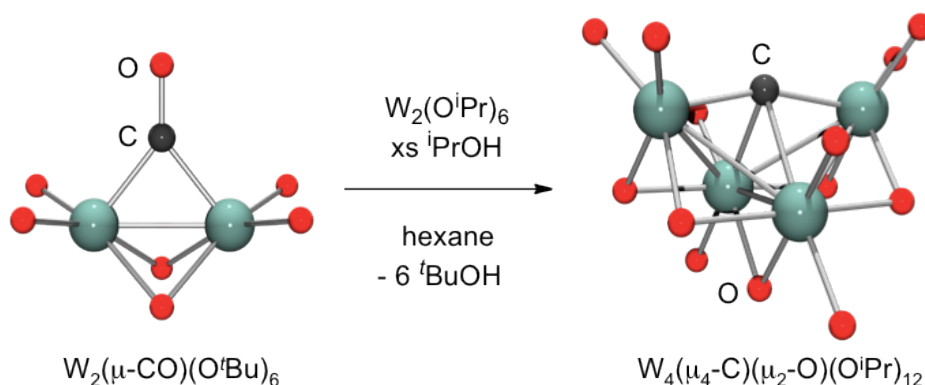


Scheme 5.2 Nucleophilic Zr(IV) hydrides for the coupling of CO .⁴²

Multiple metal-metal bonded complexes provide an interesting scaffold for CO binding and activation, due to the close proximity of the metals in the M_2 core and the unusual oxidation states that can be supported in these complexes. Given the paucity of homonuclear bonds between group 4 metals in the literature,^{44,45} examples pertinent to the current study may be found in the group 6 complexes of the type $\text{M}_2(\text{OR})_6$ reported by Cotton and Chisholm *et al.*⁴⁶ These complexes contain an electron rich $[\text{M}_2]^{6+}$ centre

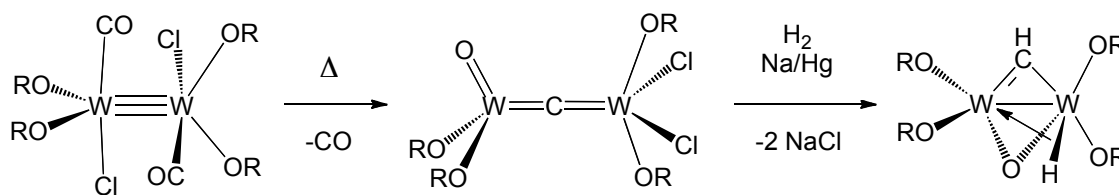
with supporting ligands in which the R group can be modified to change the steric and electronic properties, as exemplified by their extensive redox chemistry with π -acceptor organic molecules.

The first example of a carbonyl ligand bridging a metal-metal double bond was synthesised by treatment of $\text{Mo}_2(\text{O}^t\text{Bu})_6$ with CO in a reversible reaction to form $\text{Mo}_2(\mu\text{-CO})(\text{O}^t\text{Bu})_6$.⁴⁷ The analogous di-tungsten carbonyl complex, $\text{W}_2(\mu\text{-CO})(\text{O}^t\text{Bu})_6$, is kinetically stable to CO loss.⁴⁸ The X-ray structures of these Mo_2 and W_2 complexes both show symmetrical binding of the CO ligand between the two metal atoms (Scheme 5.3, left), with low $\nu(\text{CO})$ IR bands at 1625 and 1575 cm^{-1} respectively. Reaction of the di-tungsten carbonyl complex with $\text{W}_2(\text{O}^i\text{Pr})_6$ in the presence of an excess of $^i\text{PrOH}$ results in the reductive cleavage of CO to carbide and oxo ligands in tetranuclear clusters (Scheme 5.3, right).⁴⁹



Scheme 5.3 Reductive cleavage of CO by W(III) alkoxide clusters. Alkyl groups omitted and W atoms in green. CO/carbide/oxo ligands labelled for clarity.⁴⁹

Further studies on triply bonded di-tungsten complexes with $[\text{Bu}_3\text{SiO}]^-$ (= silox) ligands by Wolczanski *et al.* showed that treatment of $[(\text{silox})_4\text{W}_2\text{Cl}_2]$ with CO afforded the dicarbonyl complex, $[(\text{silox})_4\text{W}_2\text{Cl}_2(\text{CO})_2]$.⁵⁰ Upon thermolysis this dimer loses one CO and cleaves the remaining one to give a bridging carbide-oxo-dichloride (Scheme 5.4). Reduction of this complex was possible upon exposure to H_2 with Na/Hg, resulting in partial hydrogenation of the carbide bridge to generate a bridging methylidyne-oxo-hydride complex.



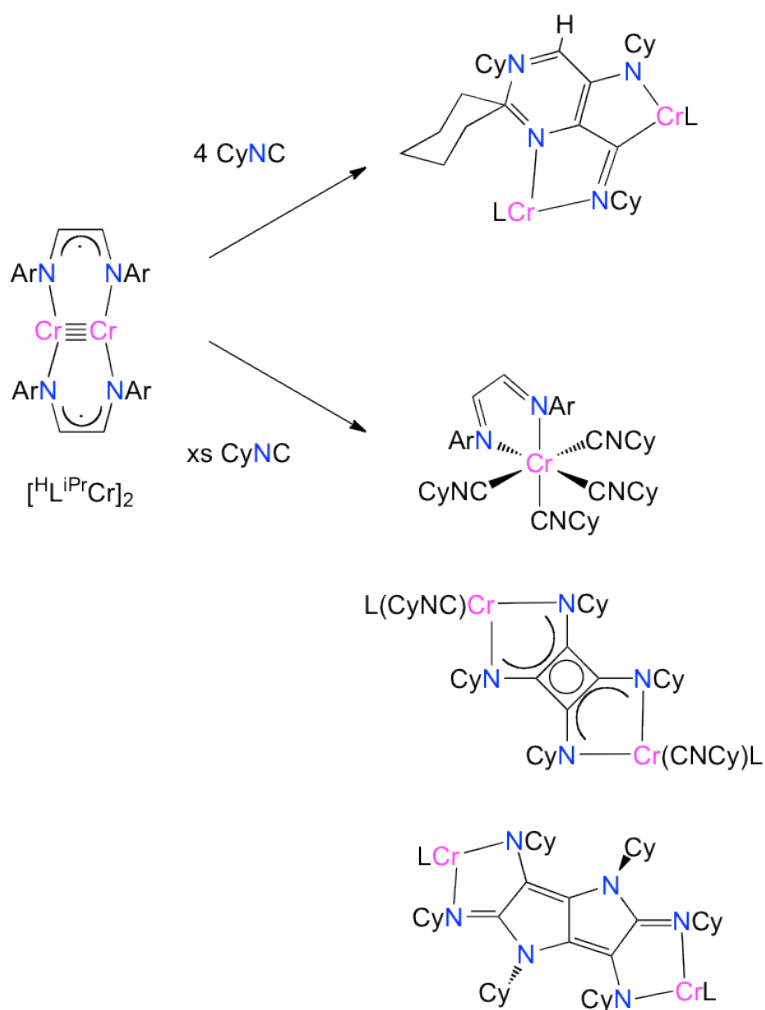
Scheme 5.4 Carbide formation *via* CO dissociation across a W≡W bond. R = Si^{*t*}Bu₃.⁵⁰

5.1.2 Isocyanides

Organic isocyanides (RNC) are considered to be isolobal with carbon monoxide, and have shown interesting reactivity with low-valent transition metals and M–M bonded complexes to complement that of CO.⁵¹ Titanocene(II) complexes are known to form di-isocyanide adducts of the type Cp₂Ti(L)₂, in a similar manner to their CO and PR₃ adducts.⁵² The first crystallographically characterised Ti(II) example being the *ansa*-bridged complex Me₂SiCp₂Ti(CNXyl)₂ which shows linear bonding of the isocyanide groups.⁵³ Isocyanides have also proved useful as model molecules for CO to study the mechanism for reduction by zirconocene hydrides.^{54,55}

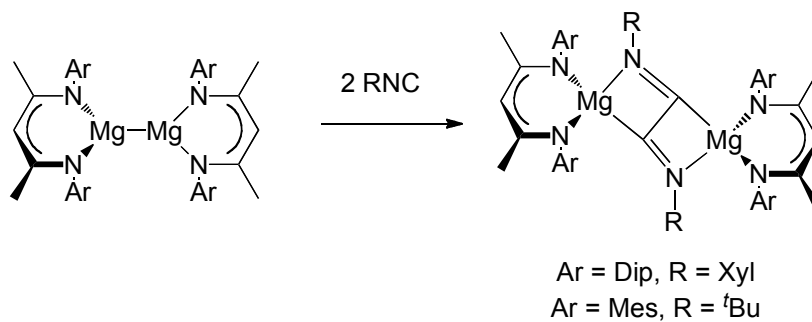
It has been well established that reaction of isocyanides with di-metal complexes with [Cr₂]⁴⁺, [Mo₂]⁴⁺, [W₂]⁴⁺ or [Re₂]⁶⁺ cores, which are not supported by bridging ligands, leads to cleavage of the metal-metal bond and formation of mononuclear products.^{56–60} However, di-tungsten hexaalkoxides W₂(O^{*i*}Bu)₆ and W₂(O^{*i*}Pr)₆(py)₂ form stable 1:1 adducts with isocyanides, RNC (R = Xyl and ^{*t*}Bu).⁶¹ The XylNC complexes were structurally characterised by XRD, which revealed the isocyanide ligand adopting a bridging binding mode, similar to that found in their mono-CO counterparts.⁴⁸ The bridging isocyanide is asymmetrically bound between the W₂ core in these complexes, with a significant bending about the nitrogen atom (C–N–C *ca.* 130°).

There is growing interest in the coupling of isocyanides to alkynes,⁶² and longer chain organic molecules,^{63,64} and metal-metal bonded compounds have provided some breakthrough examples. Theopold *et al.* have recently reported the reductive coupling of CyNC by the quintuply bonded α -diimine chromium dimer [H^{*i*}PrCr]₂ to produce several nitrogen heterocycles (Scheme 5.5).⁶⁵



Scheme 5.5 Reductive coupling of isocyanides by Cr(I) dimer.⁶⁵

Another notable example is the reactivity of β -diketiminate coordinated Mg(I) dimers $(\text{L})_2\text{Mg}_2$ ($\text{L} = [(\text{ArNCMe})_2\text{CH}_2]^-$, Ar = Mes or Dip = $\text{C}_6\text{H}_3^{\text{iPr}}\text{Pr}_2\text{-2,6}$) with $^t\text{BuNC}$ and XylNC, which give the C–C coupled 1,4-diazadiene-2,3-diyl fragments (Scheme 5.6).⁶⁶



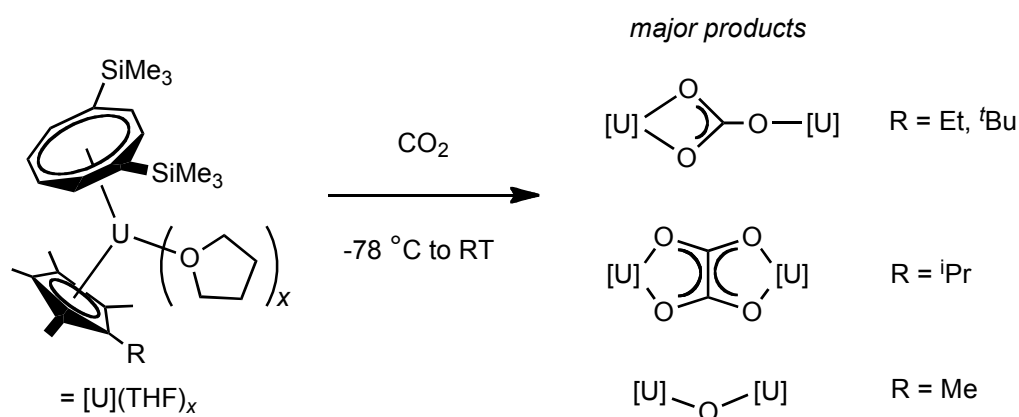
Scheme 5.6 Reductive coupling of isocyanides by Mg(I) dimers.

5.1.3 Carbon dioxide

In light of increasing global energy demands and environmental concerns over anthropogenic climate change,⁶⁷ there is considerable interest in the utilisation of CO₂ as a renewable C1 feedstock for industrially important chemicals.⁶⁸⁻⁷⁰ One of the most promising methods is the use of transition metal catalysts to bring about selective and energy-efficient CO₂ incorporation into organic compounds or reduction to CO, which can then be converted into liquid fuels *via* Fisher-Tropsch chemistry.³²

The difficulty in achieving CO₂ reduction lies in the thermodynamic stability of the CO₂ molecule and the kinetic barrier to its activation. As a result highly reducing oxophilic metal complexes are typically employed. Stoichiometric CO₂ activation has been achieved using well-defined complexes of the main group and transition metals,⁷¹⁻⁷⁴ as well as metal free systems based on frustrated Lewis pairs (FLPs).⁷⁵⁻⁷⁷ Nonetheless better understanding of the mechanisms for these reductive transformations is required, with a view to tuning the structure of the active complex or the reaction conditions to give more useful product outcomes, and assess the potential for catalytic turnover.

Evans *et al.* have shown that samarium(II) metallocenes facilitate the reductive coupling of CO₂ to oxalate [O₂CCO₂]²⁻,^{78,79} and the reductive disproportionation of COS to [S₂CO]²⁻ and CO.⁷⁹ More recently, organouranium(III) complexes have gained significant interest due to their high ability for CO₂ activation.⁸⁰⁻⁸² For example, trivalent uranium metallocenes U(Cp^R)₃ reductively activate CO₂ (for Cp^R = [η⁵-C₅H₄{SiMe₃}]⁻) and COS (for Cp^R = [η⁵-C₅H₄Me]⁻) to generate μ-oxo/μ-sulfido products, with concomitant release of CO.^{83,84} DFT studies by Maron *et al.* have provided insight into the mechanism of reductive CO₂ and COS activation at Sm(II)⁸⁵ and U(III)^{86,87} centres, and in each case a reaction pathway involving a bimetallic μ-CO₂ complex was implicated, in which carbon dioxide was doubly reduced. The possibility of a concerted pathway involving an monometallic CO₂ intermediate with a radical anionic [CO₂]⁻ ligand was ruled out on the basis of the observed product outcomes. Recent studies by Cloke *et al.* with mixed-sandwich U(III) complexes (COT')UCp^{Me4R}{THF}_x (COT' = [η⁸-C₈H₆{SiMe₃-1,4₂}]²⁻, R = Me, Et, ⁱPr, ^tBu) have shown that the steric environment around the metal centre plays a key role in guiding the possible reductive transformation pathways of CO₂, i.e. reductive coupling, disproportionation, or deoxygenation (Scheme 5.7).⁸⁸

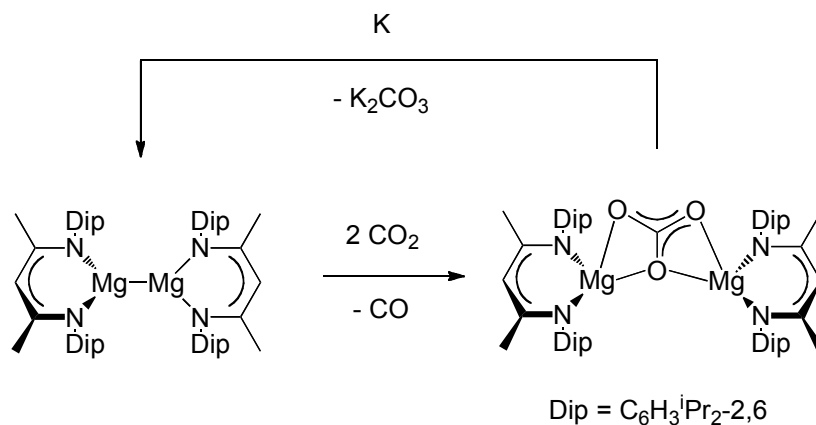


Scheme 5.7 Selectivity control in CO_2 reduction by U(III) complexes.⁸⁸

Divalent titanium sandwich complexes have shown rich and varied chemistry with a variety of small molecules,^{89,90} however there are very few examples of Ti(II)-promoted CO_2 activation. Alt *et al.* reported the synthesis of a titanium CO_2 adduct $\text{Cp}_2\text{Ti}(\text{CO}_2)(\text{PMe}_3)$,⁹¹ via simple ligand substitution of $\text{Cp}_2\text{Ti}(\text{PMe}_3)_2$. Although $\text{Cp}_2\text{Ti}(\text{CO}_2)(\text{PMe}_3)$ precluded characterisation by X-ray diffraction, an isotope labelling study by Mascetti *et al.* enabled detailed assignment of its IR spectrum, revealing a C-coordinated CO_2 ligand.⁹²

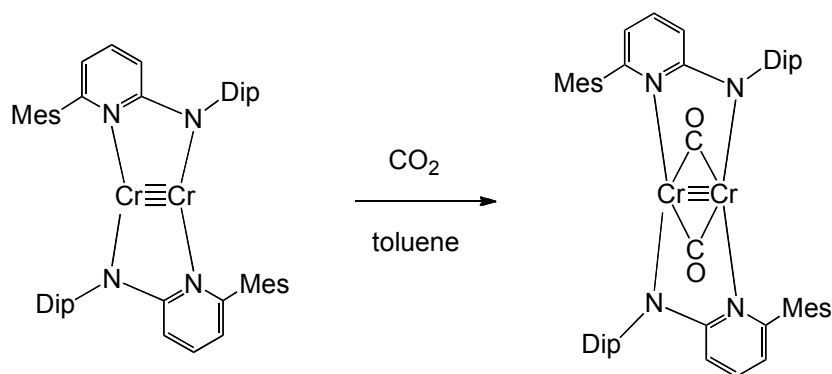
A number of acetylene complexes of Cp_2Ti exhibit CO_2 insertion into the Ti–C bond of the titanacyclopentadiene ring.^{93–96} Reductive disproportionation of CO_2 has been achieved by $\text{Cp}_2\text{Ti}(\text{CO})_2$ to generate CO and the carbonate-bridged tetranuclear structure $[(\text{Cp}_2\text{Ti})_2(\text{CO}_3)]_2$.⁹⁷ Titanium(III) complexes have also shown efficacy for the reductive transformations of CO_2 to yield oxo-,⁹⁷ carbonate-,^{97–100} and oxalate-¹⁰¹ products, and the relative inexpensive and low toxicity of this metal makes it attractive for potential use in a catalytic system.

Homonuclear M–M bonded complexes have also shown ability to facilitate the reductive activation of CO_2 . For example, Jones *et al.* have shown that the β -diketiminate coordinated Mg(I) dimer, $(\text{L})_2\text{Mg}_2$ ($\text{L} = [(\text{DipN}(\text{CMe})_2\text{CH}_2)]^-$, Dip = $\text{C}_6\text{H}_3^i\text{Pr}_{2-2,6}$), can facilitate the reductive disproportionation of CO_2 to yield free CO and a carbonate bridged Mg(II) complex in high yield (Scheme 5.8).¹⁰²



Scheme 5.8 Reductive disproportionation of CO_2 by a Mg(I) dimer.¹⁰²

More recently, Kempe *et al.* have described a quintuply bonded di-chromium complex stabilised by aminopyridinato ligands which activates CO_2 , yielding to a doubly CO bridged chromium complex in which the metal-metal bond order is formally reduced (Scheme 5.9).¹⁰³ The suggested by-product was a paramagnetic $[\text{CrO}]_4$ cluster, as a result of oxygen abstraction from CO_2 .



Scheme 5.9 Reductive activation CO_2 by a Cr_2 dimer.¹⁰³

5.2 Reactivity of **4.3** with CO and Related Molecules

5.2.1 Synthesis and characterisation of $(\mu:\eta^5, \eta^5\text{-Pn}^\dagger)_2\text{Ti}_2(\text{CO})$ (**5.1**).

Following the varied reactivity of Ti(II) and reduced M–M bonded complexes reported in the literature, and the aforementioned electronic and steric attributes of **4.3**, its reactivity with carbon monoxide was investigated.

Depending on the stoichiometry of CO gas employed in the reaction with **4.3**, different adducts form. The mono-carbonyl complex **5.1** was synthesised by the slow addition of one equivalent of CO to solutions of **4.3** at -78°C *via* Toepler line. ^1H NMR spectroscopy showed the reaction is quantitative, and red crystals of **5.1** were isolated from pentane at -35°C in 62% yield. The ^1H NMR spectrum of **5.1** consists of eight doublet signals in the aromatic region (Figure 5.1), consistent with an unsymmetrical structure in which all of the ring protons in the two Pn^\dagger ligands are chemically inequivalent. The ^1H NMR spectrum of the isotopically labelled product ^{13}C -**5.1** (Figure 5.1, inset) differs from ^{12}C -**5.1** in that the Pn^\dagger ring signal at 7.69 ppm appears as a triplet ($J = 3.2\text{ Hz}$) with a ^1H - ^{13}C (HMBC) correlation to the isotopically enriched $\mu\text{-}^{13}\text{CO}$. Inspection of the $^{29}\text{Si}\{^1\text{H}\}$ NMR spectra, which consists of four singlets for ^{12}C -**5.1**, reveals one signal splitting into a doublet ($J = 1.5\text{ Hz}$) for ^{13}C -**5.1** (Figure 5.2).

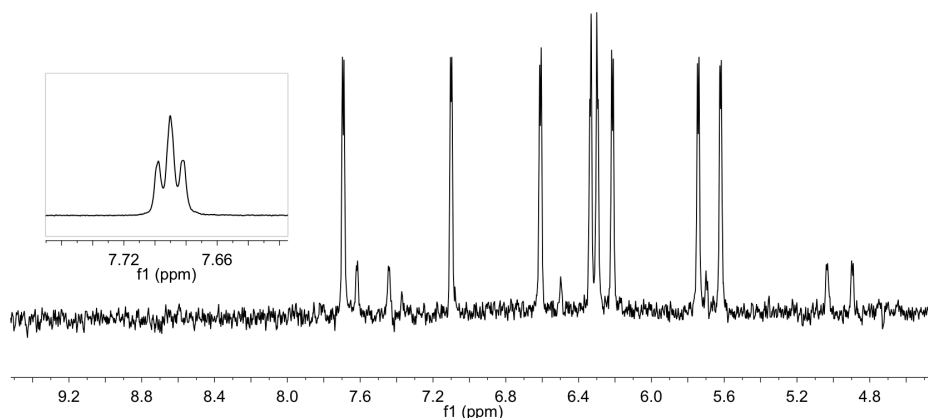


Figure 5.1 Selected regions of the ^1H NMR spectra of **5.1** and ^{13}C -**5.1** (inset).

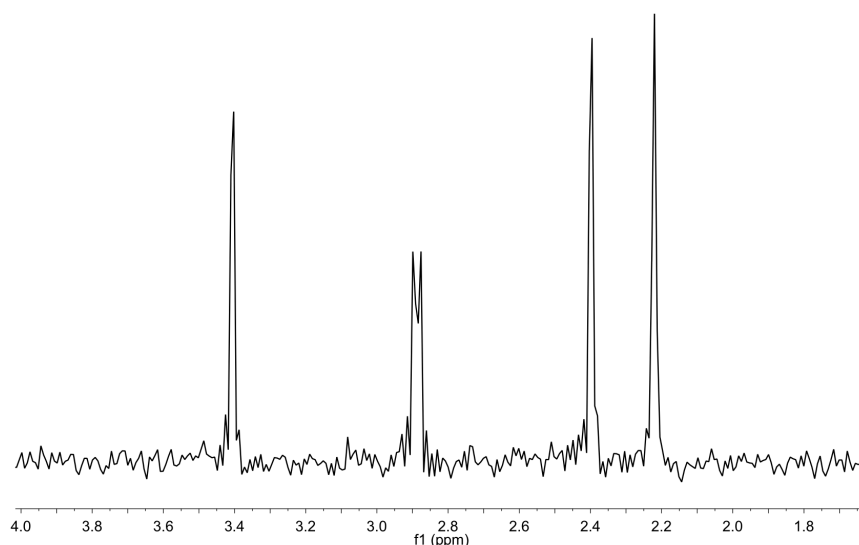


Figure 5.2 $^{29}\text{Si}\{^1\text{H}\}$ NMR spectrum of ^{13}C -**5.1** in methylcyclohexane- d_{14} .

These features are attributed to through-space J couplings between the carbonyl carbon and the hydrogen and silicon in the proximal ‘wing-side’ position of the Pn^\dagger ligands above and below (Figure 5.3). The average distance between the C_{CO} and these H and Si atoms in the solid state structure (Section 5.2.5) are 2.807(8) and 3.846(11) Å respectively.

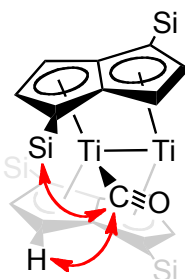


Figure 5.3 Through-space coupling between CO and Pn^\dagger wing-side substituents.

The solid-state IR spectrum of **5.1** exhibits a broad CO stretching band at 1655 cm^{-1} , which shifts to 1616 cm^{-1} upon ^{13}C isotopic substitution. Abnormally low $\nu(\text{CO})$ frequencies are characteristic of bridging carbonyl ligands which can act as $4e^-$ donors, bonding to the metal through one of the CO π bonds as well as the carbon atom.

Compound **5.1** is, to the best of the author’s knowledge, the first example of a semibridging carbonyl ligand between two titanium centres, and heterometallic examples involving titanium carbonyls are very rare. A weak semibridging carbonyl-

gold interaction was inferred in the anionic gold-titanium complex $[\text{K}(15\text{-crown-5})_2][\text{Ti}(\text{CO})_6(\text{AuPEt}_3)]$ on the basis of X-ray structural parameters and a difference between the solid-state and solution IR $\nu(\text{CO})$ stretching frequencies.¹⁰⁴ Semibridging carbonyls have also been observed in Ti/M heterobimetallics $\text{Cp}_2\text{Ti}(\mu\text{-PEt}_3)(\mu\text{-}\eta^1\text{:}\eta^2\text{-OC})\text{M}(\text{CO})\text{Cp}$ ($\text{M} = \text{Mo}, \text{W}$),¹⁰⁵ $\text{Cp}_2\text{Ti}(\mu\text{-C}\{\text{R}\}\text{CH}_2\text{-})(\mu\text{-}\eta^1\text{:}\eta^2\text{-OC})\text{W}(\text{CO})\text{Cp}$,^{106,107} and $\text{Cp}_2\text{Ti}(\mu\text{-CR})(\mu\text{-}\eta^1\text{:}\eta^2\text{-OC})\text{W}(\text{CO})\text{Cp}$ ($\text{R} = p\text{-Tol}$),¹⁰⁸ which show substantial reduction in the C–O bond order compared to typical terminal carbonyl moieties, as evidenced by the C–O bond distance and $\nu(\text{CO})$.

5.2.2 Synthesis and characterisation of $(\mu\text{:}\eta^5, \eta^5\text{-Pn}^\dagger)_2[\text{Ti}(\text{CO})]_2$ (**5.2**).

Reaction of **4.3** with two equivalents of CO, produced a green-brown solution, found to be the di-carbonyl complex $(\mu\text{:}\eta^5, \eta^5\text{-Pn}^\dagger)_2[\text{Ti}(\text{CO})]_2$ (**5.2**). ^1H NMR spectroscopy shows the reaction is quantitative, however due to the extreme solubility of the complex in hydrocarbon solvents, brown crystals of **5.2** were isolated from pentane at -35°C in a modest 39% yield. The molecular structure determined by single crystal XRD is discussed in Section 5.2.5.

Complex **5.2** shows four ^1H NMR signals in the aromatic region of the spectrum, consistent with a C_2 structure on the NMR timescale, in contrast to the ^1H NMR spectrum of **4.3**, which shows only two aromatic signals due to fluxionality in solution. The $^{13}\text{C}\{^1\text{H}\}$ spectrum of **5.2** shows a sharp resonance at 232 ppm assigned to the two chemically equivalent carbonyl ligands. The IR stretching frequencies of the CO ligands are observed at 1991 and 1910 cm^{-1} , and a frequency shift is observed when using ^{13}C labelled gas ($\nu_{\text{CO}} = 1947$ and 1867 cm^{-1}) each with a $^{13}\text{C}/^{12}\text{C}$ isotopic ratio R (0.9779 and 0.9774), consistent with the value calculated using the reduced mass ratio, $\mu(^{13}\text{CO})/\mu(^{12}\text{CO}) = 0.9777$.^{109,110} These stretching frequencies are considerably higher than those of titanocene mono-carbonyls characterised by IR,¹¹¹ indicating the metal centres in the double-sandwich complex are more electron deficient.

Carbonyl complexes **5.1** and **5.2** are stable with respect to CO loss following exposure to a turbo pump operating at *ca.* 10^{-6} mbar for 1 h at room temperature, as confirmed by ^1H NMR spectroscopy and elemental analysis. However loss of carbonyl ligands from **5.1** and **5.2** is facile under the conditions of the mass spectrometer in EI mode.

5.2.3 Synthesis and characterisation of $(\mu:\eta^5, \eta^5\text{-Pn}^\dagger)_2[\text{Ti}(\text{CO})]_2(\mu\text{-CO})$ (**5.3**).

Exposure of a pentane solution of **4.3** to an excess of CO at $-78\text{ }^\circ\text{C}$ led to a rapid colour change from deep red to orange-brown. Removal of CO gas from the reaction headspace followed by warming to room temperature resulted in a colour change to a green-brown solution, characteristic of the di-carbonyl complex **5.2**. These observations hinted that an additional product is formed in the presence of excess CO at low temperatures, which was investigated by NMR spectroscopy.

Addition of an excess of ^{13}CO (0.86 bar) to a solution of isotopically labelled ^{13}C -**5.2** in methylcyclohexane- d_{14} , resulted in a colour change to the darker orange-brown of **5.3**. The J. Young NMR tube was sealed under a ^{13}CO atmosphere and variable temperature NMR studies were carried out in $5\text{ }^\circ\text{C}$ increments between -70 and $30\text{ }^\circ\text{C}$. The $^{13}\text{C}\{^1\text{H}\}$ NMR spectrum at $30\text{ }^\circ\text{C}$ (Figure 5.4, top) showed a very broad resonance centred at 232 ppm ($\Delta\nu_{1/2} = 190\text{ Hz}$). The spectrum is resolved by cooling to $-70\text{ }^\circ\text{C}$ (Figure 5.4, bottom) showing two labelled ^{13}C peaks in *ca.* 2:1 ratio at 268 and 257 ppm, and a peak at 186 ppm corresponding to free ^{13}CO in solution. These three ^{13}C peaks broaden upon warming and coalesce at $5\text{ }^\circ\text{C}$ (Figure 5.4, middle), consistent with a dynamic intermolecular exchange process between ^{13}C -**5.2** and free ^{13}CO .

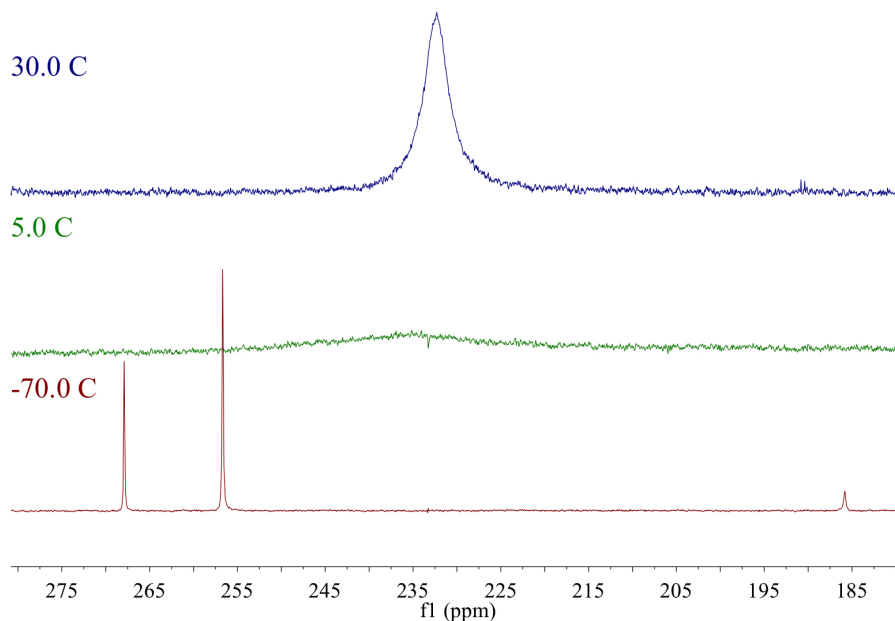
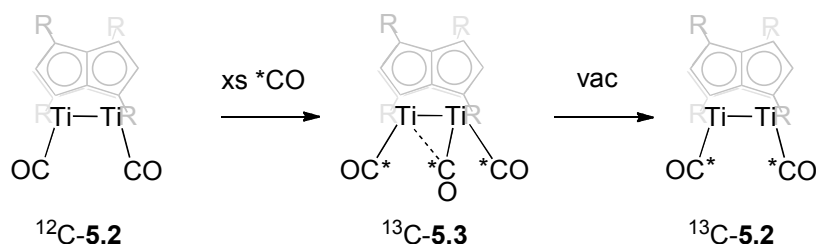


Figure 5.4 Selected VT $^{13}\text{C}\{^1\text{H}\}$ NMR spectra of ^{13}C -**5.3** in MeCy- d_{14} solution.

The ^1H NMR spectrum at $-70\text{ }^\circ\text{C}$ consists of four sharp peaks in the aromatic region, the peak at 6.35 ppm shifts downfield to 7.01 ppm upon warming to $5\text{ }^\circ\text{C}$ and broadens significantly ($\Delta\nu_{1/2} = 57\text{ Hz}$). This ^1H resonance continues to shift downfield upon warming to $30\text{ }^\circ\text{C}$ and the peak sharpens ($\delta_{\text{H}} 7.80$, $\Delta\nu_{1/2} = 8\text{ Hz}$). Removal of the ^{13}CO headspace from the NMR tube resulted in quantitative conversion of ^{13}C -**5.3** to ^{13}C -**5.2**. The proposed formulation of **5.3** based on spectroscopic evidence is $(\mu:\eta^5, \eta^5\text{-Pn}^+)_2[\text{Ti}(\text{CO})]_2(\mu\text{-CO})$, with a bridging carbonyl ligand that is chemically inequivalent to the two terminal carbonyls at $-70\text{ }^\circ\text{C}$.

The dynamic behavior of terminal and bridging CO ligands of **5.3** in methylcyclohexane- d_{14} was further investigated by an isotopic labelling experiment. The $^{13}\text{C}\{^1\text{H}\}$ NMR ($30\text{ }^\circ\text{C}$) spectrum of **5.2**, was collected over 1000 scans, which was not sufficiently large an acquisition to observe the natural abundance carbonyl ^{13}C signal. To this was added an excess of ^{13}CO (0.86 bar) at $-78\text{ }^\circ\text{C}$ producing an orange-brown solution of ^{13}C -**5.3** which was identified by a very broad resonance centred at 235 ppm ($\Delta\nu_{1/2} = 837\text{ Hz}$) in its $^{13}\text{C}\{^1\text{H}\}$ NMR ($30\text{ }^\circ\text{C}$, 1000 scans) spectrum. Removal of the headspace from the NMR tube by exposure to an argon atmosphere resulted in a colour change back to green-brown and the $^{13}\text{C}\{^1\text{H}\}$ NMR ($30\text{ }^\circ\text{C}$, 1000 scans) spectrum displayed a sharp peak at 231 ppm. Incorporation of labelled ^{13}CO into the dicarbonyl complex **5.2** implies there is dynamic intramolecular exchange of bridging and terminal carbonyl ligands in **5.3** (Scheme 5.10), in addition to the intermolecular exchange with free CO. This was confirmed by a ^{13}C - ^{13}C EXSY experiment ($-40\text{ }^\circ\text{C}$, mixing time = 500 ms) following the addition of excess ^{13}CO (4 mol eq.) to a solution of **4.3** in methylcyclohexane- d_{14} . Cross peaks were observed between the bridging and terminal carbonyl ligands of **5.3** which both, in turn, showed cross peaks with the carbonyl ligands of **5.2**, also present in the reaction mixture.



Scheme 5.10 Summary of NMR experiments with isotopically labelled CO.

The carbonylation of **4.3** was studied by *in situ* IR spectroscopy. An excess of CO (0.86 bar) was added *via* Toepler line to **4.3** in methylcyclohexane solution at -55 °C and IR spectra were collected every 5 s. In the initial 4 min following the first gas addition cycle an IR band in the $\nu(\text{CO})$ region at 1992 cm^{-1} is formed, which then decreases in intensity and levels off as a $\nu(\text{CO})$ stretch at 1910 cm^{-1} grows in. This lower energy $\nu(\text{CO})$ stretch became the major IR band at -55 °C once gas addition was complete (Figure 5.5).

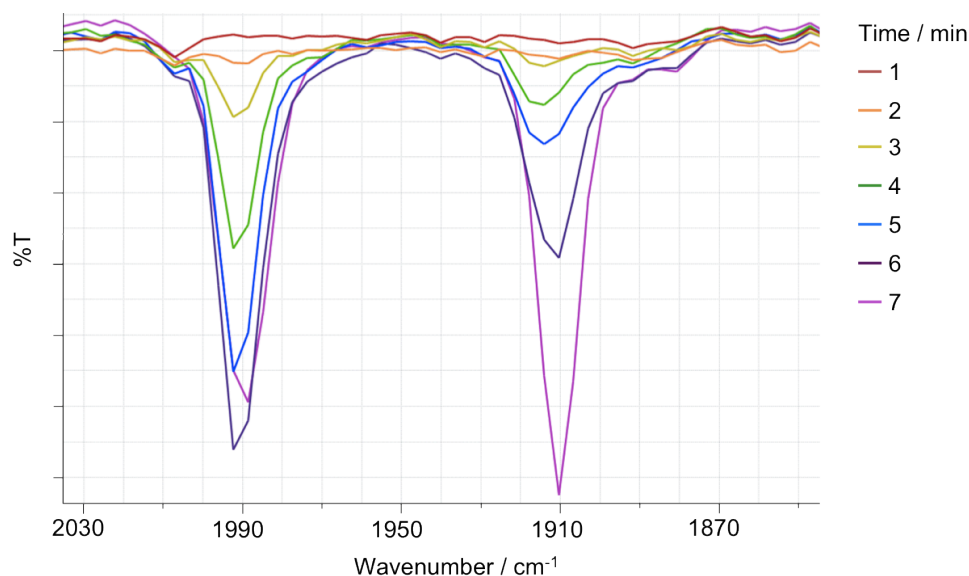
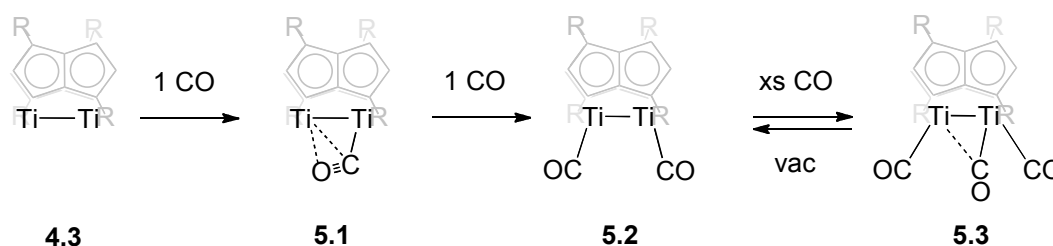


Figure 5.5 $\nu(\text{CO})$ region of the React IR spectrum of **4.3** with CO at -55 °C.

The solution was warmed to 26 °C under CO, and the intensities of the two bands reversed, with 1992 cm^{-1} as the major $\nu(\text{CO})$ stretching band. Removal of the CO headspace *in vacuo* led to near complete removal in the lower energy $\nu(\text{CO})$ stretch at 1910 cm^{-1} . These results suggest that the band centred at 1992 cm^{-1} is the di-carbonyl complex **5.2**, which is the major product in the initial stages of reaction and upon warming to 26 °C when CO becomes less soluble. The IR band at 1910 cm^{-1} is assigned to the terminal $\nu(\text{CO})$ stretch in complex **5.3**, which is the major product in solution under excess CO at -55 °C, but diminishes following removal of the reaction headspace and warming to room temperature. An analogous experiment was performed using ^{13}CO , and gave similar qualitative results with IR bands at 1948 cm^{-1} and 1867 cm^{-1} assigned to the terminal $\nu(\text{CO})$ in ^{13}C -**5.2** and ^{13}C -**5.3** respectively. IR bands for the

bridging CO ligands, expected in the region $1850\text{--}1600\text{ cm}^{-1}$,¹¹² were not observed in the solution spectra for **5.1** and **5.3**, presumably due to extensive broadening.

Orange crystals of **5.3** were grown under an atmosphere of CO from a saturated toluene solution stored at $-80\text{ }^{\circ}\text{C}$. Unfortunately analysis of the orange plates by XRD was hampered by their deterioration when placed in vacuum oil, with effervescence of gas accompanying crystalline decomposition. However, elemental analysis of the orange crystals was consistent with the proposed formulation for **5.3**.



Scheme 5.11 Summary of reactions of **4.3** with carbon monoxide ($\text{R} = \text{Si}^i\text{Pr}_3$).

5.2.4 Reactivity of **4.3** with isocyanides

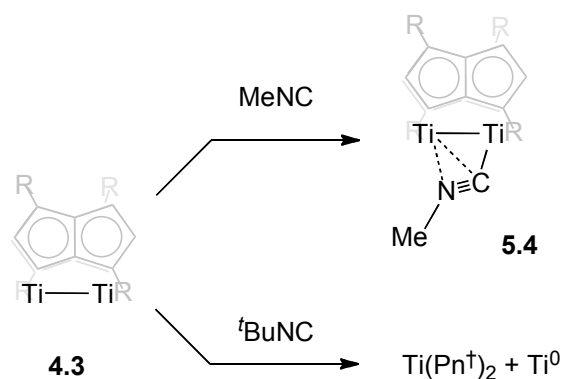
Treatment of a solution of **4.3** in toluene- d_8 with two equivalents of MeNC resulted in a purple mixture, the ^1H NMR spectrum of which showed eight doublet signals in the aromatic region, similar to that of mono-carbonyl adduct **5.1**. A ^1H signal at 3.25 ppm was assigned to the methyl group of coordinated MeNC, with a signal at 1.18 ppm for the free isocyanide in approximately equal ratio by integration. These observations are consistent with a 1:1 adduct **5.4** as the sole product (Scheme 5.12, top). Excess MeNC was identified by a singlet signal at 1.18 ppm in the ^1H NMR spectrum. Apparently, the steric congestion due to the Si^iPr_3 groups prevents ligation of a second molecule of MeNC, in contrast to the multiple adducts formed with **4.3** and CO. The quaternary MeNC carbon in **5.4** was identified in the ^{13}C NMR spectrum at 289 ppm, and the Pn^+ ring ^{13}C signals were consistent with an unsymmetrical structure in which the two ligands are chemically inequivalent.

The solution structure was confirmed in the solid state by a single crystal XRD study, revealing a $\mu\text{-CNMe}$ ligand asymmetrically bridging the Ti_2 core (Section 5.2.5, Figure 5.6). The IR spectrum of **5.4** shows a $\nu(\text{CN})$ stretch at 1642 cm^{-1} , which is unusually

low for bridging isocyanide ligands in bimetallic complexes, which typically range from 1700 to 1870 cm^{-1} .¹¹³ However the aforementioned di-tungsten mono(μ -CNR) adducts reported by Chisholm *et al.* also showed very low $\nu(\text{CN})$ IR bands (*ca.* 1530 cm^{-1}),⁶¹ which these researchers attributed to a high degree of back bonding from the metal d-orbitals to the vacant high-energy π^* -orbitals of the isocyanide ligand.

The reaction of **4.3** with $t\text{BuNC}$ was carried out to investigate the effect of increasing steric bulk on the isocyanide ligand. Addition of an excess of $t\text{BuNC}$ to **4.3** in C_6D_6 resulted in a metallic precipitate and a brown solution, the ^1H NMR spectrum of which showed a complex mixture of products. A prominent ion at $m/z = 878$ (90%) corresponding to the homoleptic Ti(IV) species, $[\text{Ti}(\text{Pn}^+)_2]^+$, was observed in the mass spectrum of the crude residue, suggesting possible cleavage of the M–M bond had occurred. A possible by-product of the proposed disproportionation reaction would be the 18-electron complex $\text{Ti}(\text{CN}^t\text{Bu})_7$ and a corresponding peak at $m/z = 631$ was identified in the mass spectrum, albeit with low intensity (10%). However, zero-valent $\text{Ti}(\text{CN}^t\text{Bu})_7$ is expected to be unstable with respect to Ti metal, which is the likely identity of the precipitate formed in this reaction. The analogous zero-valent carbonyl complex $\text{Ti}(\text{CO})_7$ is unknown, however thermodynamically stable derivatives, $\text{Ti}(\text{CO})_3(\text{R}_2\text{PC}_2\text{H}_2\text{PR}_2)_2$ ($\text{R} = \text{Me}, \text{Et}$), have been synthesised by Wreford and co-workers.¹¹⁴ Attempts to isolate and purify the soluble products by recrystallisation failed.

The reactions of **4.3** with MeNC and $t\text{BuNC}$ are summarised in Scheme 5.12. The reason for the observed difference in reactivity of **4.3** with these alkyl isocyanides is unclear, however one may speculate that the increased σ -donating character of the $t\text{BuNC}$ ligand leads to M–M bond cleavage over adduct formation.



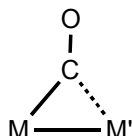
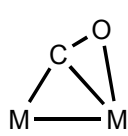
Scheme 5.12 Reactivity of **4.3** with alkyl isocyanides.

5.2.5 X-ray crystallographic studies of **5.1**, **5.2** and **5.4**

The solid-state structure of **5.1** determined by X-ray crystallography (Figure 5.6, top) shows the CO ligand bound side-on, asymmetrically bridging the two Ti centres. The carbonyl group was disordered and the disorder was adequately modeled over two crystallographic positions (by restraining the C–O bond lengths to be equal within ESDs). Hence, a degree of caution must be taken when interpreting bond lengths for the carbonyl moiety from these X-ray data (Table 5.2). The proximal Ti atom lies closer to the CO ligand in **5.1** than in the di-carbonyl complex **5.2**, and additional interaction between the CO and the distal Ti atom is clearly in effect in the former complex ($\text{Ti1-C53a} = 2.245(10) \text{ \AA}$, $\text{Ti1-O1a} = 2.294(5) \text{ \AA}$), causing the O–C53–Ti_{proximal} angle to bend considerably from linearity.

The geometric function $\Omega = \exp[d(\text{M}_{\text{distal}}\text{-C})/d(\text{M}_{\text{distal}}\text{-O})]$ measures the extent of interaction of the distal metal with the C and O ends of the CO ligand.¹¹⁵ This function can be used to differentiate between C- and O- bonded metal carbonyls in ‘end on’ ($\Sigma\text{-CO}$) and ‘side-on’ ($\Pi\text{-CO}$) disposition (Table 5.1), although there is no obvious break in values for conventional C-bridging and $\Pi\text{-CO}$. The average value for **5.1** ($\Omega = 2.69$) lies comfortably in the range for a $\Pi\text{-CO}$, and comparable values are found for the aforementioned Ti/M heterobimetallics with semibridging CO ligands, $\text{Cp}_2\text{Ti}(\mu\text{-C}\{p\text{-Tol}\}\text{CH}_2)(\mu\text{-}\eta^1\text{:}\eta^2\text{-OC})\text{W}(\text{CO})\text{Cp}$ ($\Omega = 2.65$),^{106,107} and $\text{Cp}_2\text{Ti}(\mu\text{-C}\{p\text{-Tol}\})(\mu\text{-}\eta^1\text{:}\eta^2\text{-OC})\text{W}(\text{CO})\text{Cp}$ ($\Omega = 2.63$).¹⁰⁸

Table 5.1 The disposition of CO in bimetallic systems.

CO disposition	C-bridging	$\Pi\text{-CO}$	$\Sigma\text{-CO}$
Diagram			$\text{M} - \text{CO} - \text{M}'$
Typical Ω range	1.7 - 2.3	2.2 - 3.3	3.9 - 5.0

The C–O bond distance in **5.1** (av. 1.211(11) Å) is lengthened with respect to free CO (1.128 Å),¹¹⁶ to an extent that is comparable to Σ -CO complexes $\text{Cp}_2\text{Ti}(\text{THF})(\text{OC})\text{Mo}(\text{CO})_2\text{Cp}$ (1.201(8) Å)¹¹⁷ and $\text{Cp}^*_2\text{Ti}(\text{Me})(\text{OC})\text{Mo}(\text{CO})_2\text{Cp}$ (1.212(5) Å)¹¹⁸ in which the titanocene moiety behaves as a Lewis acid, coordinating to an oxygen atom of the Lewis basic $[\text{CpMo}(\text{CO})_3]^-$ fragment.

Comparison of the solid-state structures of side-on mono-CO (**5.1**) and mono-MeNC (**5.4**) adducts reveals slightly longer Ti–Ti and Ti–C53 distances in the latter complex. However **5.4** shows a closer approach of the MeNC-nitrogen atom to the distal Ti atom compared with that of the CO-oxygen atom in **5.1**, consistent with the relative availability of the N lone pair in valence bond structure for isocyanides,¹¹⁹ compared with the predominantly zwitterionic valence bond character of CO.¹²⁰ This is reflected in a more acute angle Ti2–C53–E about the semibridging carbon atom in **5.4** (133.3(6)°, E=N1) compared with **5.1** (143.8(13)°, E=O1a). However, the relatively poor quality of the structure of **5.4** due to low resolution X-ray data at high diffraction angle, warrants a degree of caution with regard to this interpretation.

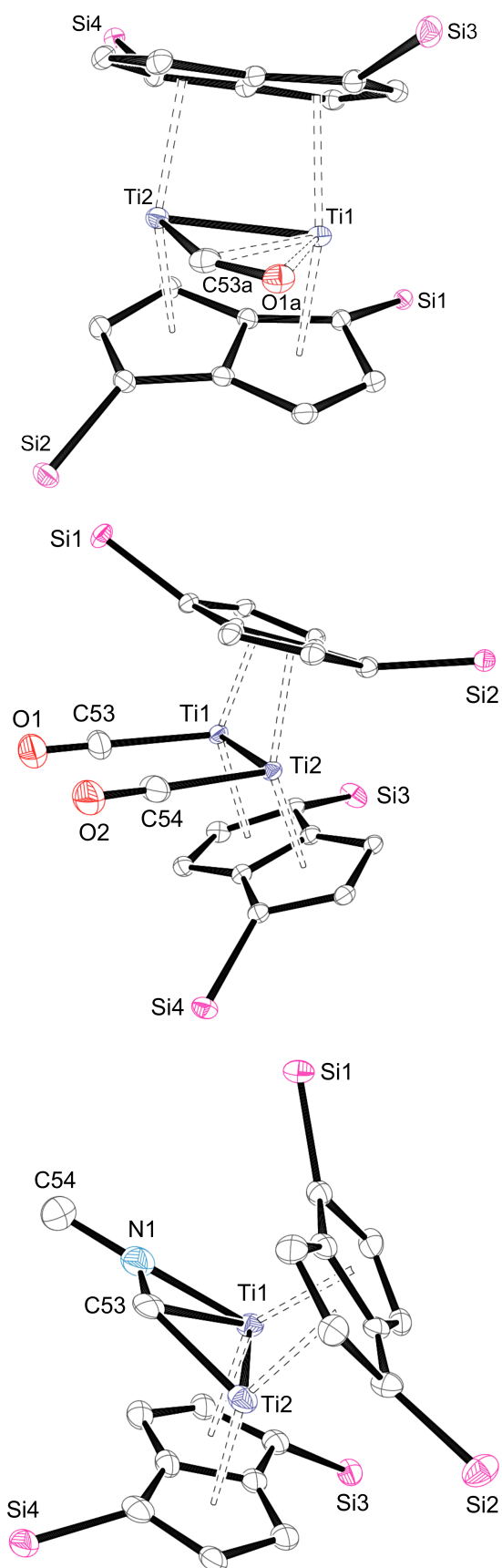


Figure 5.6 ORTEP plots of (top-bottom) **5.1** part 1, **5.2** and **5.4**.

H atoms and ⁱPr groups omitted for clarity. 30% ellipsoids.

Table 5.2 Selected distances (Å), angles (°) and parameters (defined in Figure 5.7) for **4.3**, **5.1**, **5.2**, and **5.4**. Ct denotes the η^5 -centroid of a Pn ring.

Parameter	4.3	5.1	5.2	5.4
Ti–Ti	2.399(2)	2.4047(5)	2.425(10)	2.4120(15)
C53–Ti _{proximal}	-	1.975(9) ^a	2.100(5) ^a	2.016(6)
C53–Ti _{distal}	-	2.322(15) ^a	-	2.326(7)
O1/N1–Ti _{distal}	-	2.352(6) ^a	-	2.147(6)
C53–O1/N1	-	1.211(11) ^a	1.141(6) ^a	1.219(10)
Ti–Ct ^a	2.036(4)	2.058(9)	2.0453(15)	2.080(2)
Ti–C _{ring} ^a	2.378(7)	2.395(2)	2.382(2)	2.412(2)
Ct–Ti–Ct ^a	155.22(19)	146.41(5)	144.53(8)	142.94(11)
Ti–C53–O1/N1	-	143.8(13) ^a	178.05(4) ^a	133.3(6)
Δ ^a	0.005(7)	0.093(2)	0.083(2)	0.103
Twist angle	20.1(8)	17.02(15)	15.3(3)	17.5(4)
Hinge angle ^a	3.8(8)	5.0(2)	5.0(2)	4.6(2)
Fold angle ^a	8.7(4)	5.85(2)	7.5(2)	5.1

^a Average values.

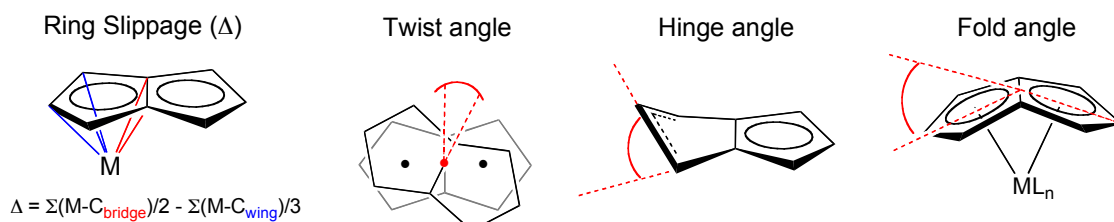


Figure 5.7

5.2.6 DFT studies of **5.1**, **5.2** and **5.3**

Theoretical calculations by Green on the carbonyl adducts employed a model system with the pentalene substituents replaced by H atoms.¹²¹ Key structural parameters are given in Table 5.3. Data for the two different computational methods, ADF and Gaussian, are given in normal font and *italics* respectively.

Geometry optimisation of $\text{Pn}_2\text{Ti}_2(\text{CO})$ had C_s symmetry with the carbonyl ligand bound sideways-on to the Ti dimer (**5.I**). A double bond is retained between the two Ti atoms in **5.I** (Figure 5.8, 55a) and the calculated Ti–Ti distances (2.38, 2.36 Å) are in reasonable agreement with the X-ray interpretation (2.4047(5) Å). The wavenumber for the CO stretch was calculated as 1644 cm^{-1} in **5.I**, which is lower than the range for symmetric bridging carbonyls ($1850\text{--}1600\text{ cm}^{-1}$),¹¹² but in good agreement with the experimental value of 1655 cm^{-1} in **5.1**.

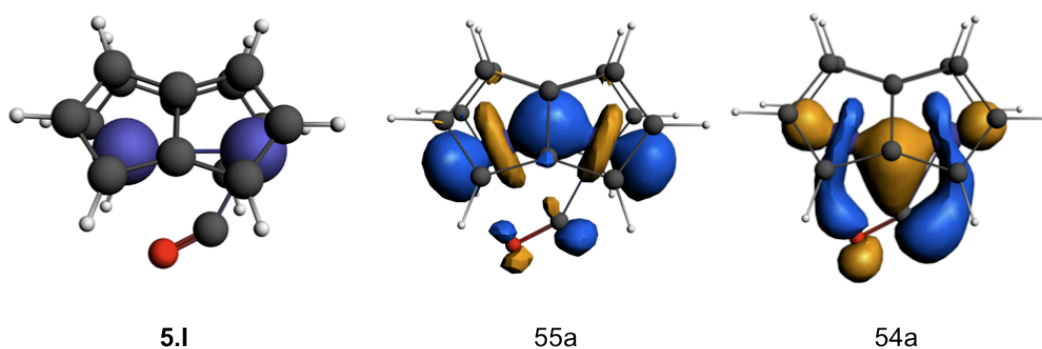


Figure 5.8 Calculated structure for **5.I** and its HOMO 55a and HOMO-1 54a.¹²¹

Geometry optimisation of $\text{Pn}_2\text{Ti}_2(\text{CO})_2$ (**5.II**) by both computational methods gave a structure of C_s symmetry only slightly displaced from C_{2v} symmetry, which agrees well with that found experimentally. The Ti–Ti bonding orbital, 36a (Figure 5.9), remains intact but is straighter than found for the other derivatives, consistent with the slightly elongated Ti–Ti distance in **5.2** (2.425(10) Å) with no reduction in bond order. Back-bonding to both carbonyl ligands occurs in orbital 35a, which has clear origins in the HOMO-1 of Pn_2Ti_2 ($6b_{3u}$ of **4.IIIa**, see Section 4.3.4, Figure 4.11). The calculated vibrations for the antisymmetric and symmetric CO stretches in **5.II** are 1947, 1899, and 1878, 1810 cm^{-1} respectively, which are higher than the $\nu(\text{CO})$ values found experimentally in **5.2** (1910 and 1987 cm^{-1}), but reasons for this discrepancy are unclear.

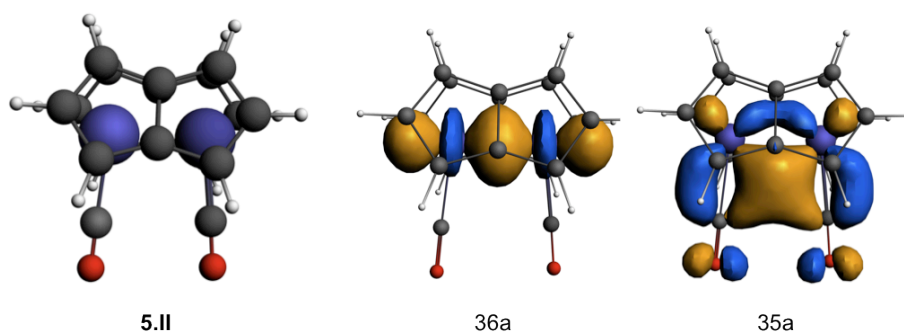


Figure 5.9 Calculated structure for **5.II** and its MOs.¹²¹

Geometry optimisation of $\text{Pn}_2\text{Ti}_2(\text{CO})_3$ resulted in structure **5.III** (Figure 5.10), which is particularly insightful given that the labile nature of the tricarbonyl species **5.3**. The Ti–Ti distance is significantly longer than found in **4.III**, **5.I** and **5.II**. The structure is asymmetric with two terminal carbonyls and one semibridging. The two highest occupied orbitals, 65a and 64a (Figure 5.10), are principally involved in back-donation to the CO ligands. The HOMO 65a is focused on the titanium atom with just one CO bound. The HOMO-1 64a binds two CO ligands but retains a small amount of Ti–Ti bonding character. Three IR active CO stretches were predicted for **5.III** (1941, 1894, 1873, 1918, 1868, 1835 cm^{-1}), however the lowest frequency vibration has a relatively low calculated intensity, which may explain why only two CO stretches are observed in the IR spectrum of **5.3** (1991, 1910 cm^{-1}).

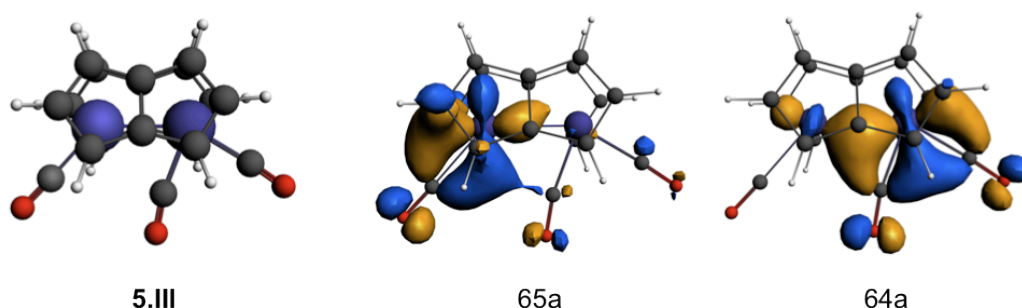


Figure 5.10 Calculated structure for **5.III** and its HOMO 65a and HOMO-1 64a.

The structural parameters for $\text{Pn}_2\text{Ti}_2(\text{CNMe})$ (**5.IV**) calculated using DFT (Table 5.3) are in reasonable agreement with the experimental values for **5.4**, and are in keeping with the comparison with the mono-CO complex, showing slightly longer Ti–Ti, C–Ti_{proximal} and C–O/N distances and a stronger interaction between the MeNC–nitrogen atom to the distal Ti atom in **5.IV** compared with that of the CO–oxygen atom in **5.I**.

Table 5.3 Selected structural parameters (Å, °) for calculated structures.¹²¹ Ct denotes the η^5 -centroid of a Pn ring. ADF values are in normal font, Gaussian values in *italics*.

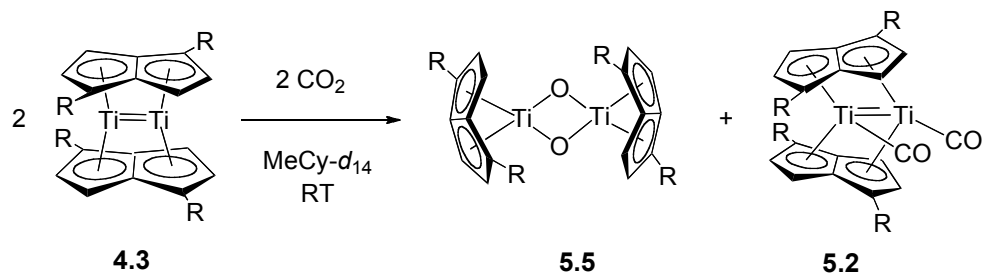
Parameter	5.I	5.II	5.III	5.IV
Ti–Ti	2.38, 2.36	2.42, 2.42	2.63, 2.64	2.40
C53–Ti _{proximal}	2.04, 2.02	2.08, 2.08	2.02, 1.99 2.06, 2.05 2.07, 2.03	2.05
O/N–Ti _{distal}	2.35, 2.26	-	-	2.15
C53–O/N	1.21, 1.25	1.17, 1.17	1.17, 1.19 1.17, 1.19 1.16, 1.18	1.26
Ti–Ct	2.06, 2.08	2.05, 2.05	2.04, 2.07 2.09, 2.11	2.09, 2.07
Ct–Ti–Ct	143, 143	144, 144 142, 144	143, 142 137, 137	140, 144

The facile coordination of carbon monoxide and isocyanides to complex **4.3** marks the first reported example of reactivity of di-metal bis(pentalene) double-sandwich complexes. The ability of **4.3** to form multiple adducts illustrates the sterically accessible nature of the frontier orbitals of this complex, which were well described using DFT calculations using a model ligand system. The propensity for these unsaturated substrates to bridge across the two metals may be exploited in further chemistry. The mono-carbonyl complex **5.1** is of particular interest because semibridging CO is implicated as a precursor to the cleavage of CO on metal surfaces, such as those employed in Fischer-Tropsch catalysis.^{115,122} Further studies are required to investigate **5.1** for potential CO cleavage and reduction, however due to time constraints these are not pursued in the current study.

5.3 Reactivity of **4.3** with CO₂

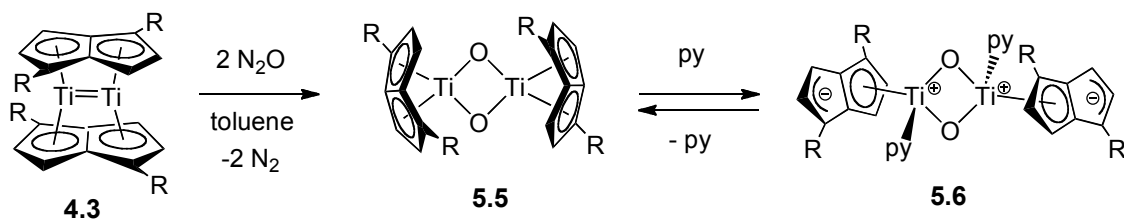
5.3.1 Reaction of **4.3** with CO₂ at room temperature

Exposure of a deep red solution of **4.3** to a stoichiometric amount of CO₂ gas at room temperature resulted in an instantaneous colour change to red brown, and subsequent analysis of the ¹H NMR spectrum showed complete conversion to two compounds, **5.5** and **5.2** (Scheme 5.13) in approximately equal ratio.



Scheme 5.13 Room temperature reaction of **4.3** with CO₂. R = SiⁱPr₃.

The reaction mixture was left to stand at room temperature overnight and deposited orange crystals, which were isolated (77% yield) and identified as component **5.5** by ¹H NMR, mass spectrometry and elemental analysis. The crystals were analysed by XRD and though a fully refined model could not be achieved, the data were of adequate quality to verify connectivity (see appendix A2). Compound **5.5** is a bis(μ-oxo) dimer which lacks a Ti–Ti bond and the pentalene ligands bind in an η⁸- fashion to each formally Ti(IV) centre. **5.5** was independently prepared in high yields (90%) by treatment of **4.3** with two molar equivalents of N₂O, a reagent commonly used as a source of oxygen atoms for the synthesis of oxometallocenes (Scheme 5.14).^{98,123} **5.5** is sparingly soluble in hydrocarbon and ethereal solvents, but can be fully dissolved by treatment with pyridine to form [(η⁵-Pn⁺)Ti(μ-O)(py)]₂ (**5.6**). Cooling a hexane solution of **5.6** afforded X-ray quality red crystals (48% yield), which were prone to solvent loss and reformed **5.5** in the absence of excess pyridine, as confirmed by spectroscopic and analytical data.



Scheme 5.14 Synthesis of **5.5** and **5.6**. R = SiⁱPr₃.

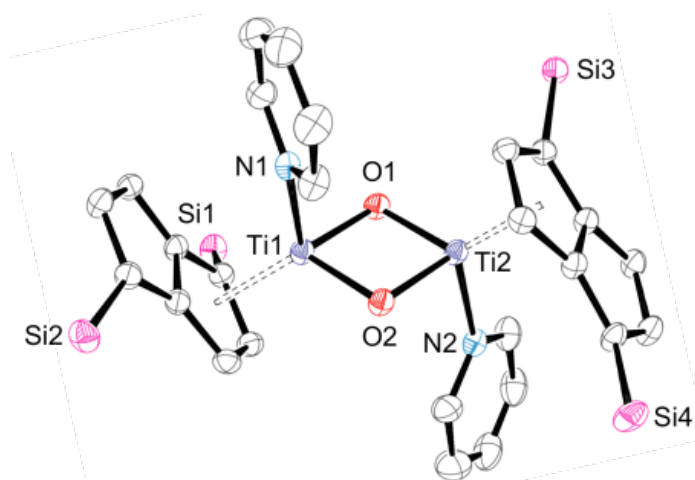


Figure 5.11 Displacement ellipsoid plot (30% probability) of **5.6**. Hydrogen atoms and ⁱPr groups omitted for clarity.

Table 5.4 Selected interatomic distances (Å), angles (°) and parameters (defined in Figures 5.9 and 5.14) for **5.6**. Ct denotes the η⁵-centroid of the Pn[†] ligand.

Parameter	5.6	Parameter	5.6
Ti1···Ti2	2.7376(6)	Ti1–O1–Ti2	95.35(8)
Ti1–O1	1.8531(17)	Ti1–O1–Ti2	95.33(8)
Ti1–O2	1.8416(17)	Ti1–N1	2.174(2)
Ti2–O1	1.8495(17)	Ti2–N2	2.165(2)
Ti2–O2	1.8615(17)	Ti–C _{ring} ^a	2.338(2)
Ti–Ct ^a	1.9949(9)	φ	162.12(7)
Δ ^a	0.046(2)	Fold angle ^a	0.62(15)

^aAverage values.

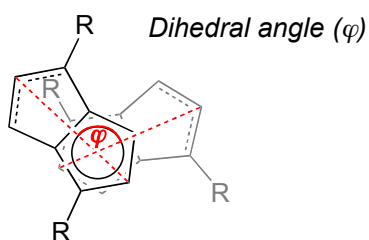


Figure 5.12

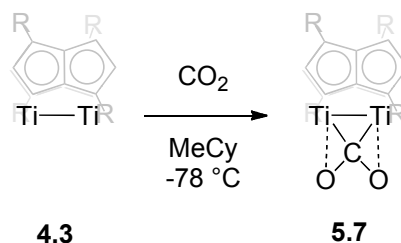
The molecular structure of this pyridine adduct (Figure 5.11) shows pentalene binding through only five of eight carbons of the aromatic ligand. The range of Ti–C distances is 2.283(2)–2.407(2) Å, with an average value of 2.338(2) Å. The average metal-centroid distance is 1.9949(9) Å and the average ring slippage (Δ)¹²⁴ value of 0.046(2) Å is small enough that pentalene may be essentially considered as an η^5 -ligand. This results in a double zwitterionic structure, with a formal positive charge on each Ti(IV) centre and a negative charge on the noncoordinated part of the pentalene ligand. This unusual binding mode has previously been observed by Jonas *et al.* in the mononuclear complexes $(\eta^5\text{-Pn})\text{MCp}^*$ (M = Cr, Co and Rh), and $\text{Li}_2[\text{Zr}(\eta^5\text{-Pn})\text{Me}_2]$.¹²⁵⁻¹²⁷ However no crystallographic data have been reported for any of the latter, which precludes any structural comparison with **5.6**. The C–C bond lengths of both the coordinated and uncoordinated 5-membered rings in **5.6** (which range from 1.393(4)–1.455(4) Å) are comparable to those found in the anti-bimetallic complex $[\text{YbCp}^*(\text{THF})]_2(\mu\text{:}\eta^5\text{:}\eta^5\text{-Pn}^\dagger)$ (which range from 1.401(8)–1.457(1) Å), in which both 5-membered rings are fully coordinated and aromatic.¹²⁸ The ¹H NMR spectrum of **5.6** in C₆D₆ is consistent with the unsolvated complex **5.5** and free pyridine, however the spectrum in pyridine-*d*₅ is broad and unresolved, even at 235 K, possibly indicative of rapid exchange between free and bound pyridine.

The di-carbonyl compound, **5.2**, was separated from the room temperature CO₂ reaction mixture by TMS₂O extraction and isolated in 92% yield with respect to the reaction stoichiometry in Scheme 5.13. The reaction of **4.3** with CO₂ marks the first reported example of small molecule activation by a bis(pentalene) double-sandwich complex,¹²⁹ and may be considered as the result of a 2e[−] reduction per CO₂ driven by the oxidative cleavage of the Ti=Ti double bond to give the Ti(IV) bis(oxo) complex, **5.5**. As a first approximation of the mechanism it was assumed that the concomitantly formed CO rapidly reacts with remaining **4.3** to afford the di-carbonyl complex, **5.2**.

5.3.2 Synthesis and characterisation of $(\mu\text{:}\eta^5\text{:}\eta^5\text{-Pn}^\dagger)_2\text{Ti}_2(\text{CO}_2)$ (**5.7**).

In order to investigate the mechanistic pathway for the reductive deoxygenation, the reaction of **4.3** with one equivalent of either ¹²CO₂ or ¹³CO₂ was carried out in methylcyclohexane-*d*₁₄ at -78 °C. This resulted in a colour change from deep red to a dark green solution, which accompanied quantitative conversion to an intermediate

species (**5.7**) observed by low temperature spectroscopic measurements, which had not been previously detected in the room temperature reaction.



Scheme 5.15 Synthesis of low temperature CO₂ intermediate **5.7**.

The ¹H NMR spectrum of **5.7** at -30 °C showed four sharp doublets in the aromatic region consistent with a diamagnetic complex that exhibits C₂ molecular symmetry on the NMR timescale, while the ¹³C{¹H} spectrum showed a singlet at 219 ppm with no further labeled ¹³C signals. *In situ* IR studies of **5.7** at -65 °C showed distinct bands at 1678 and 1236 cm⁻¹, and these IR bands shifted to 1637 and 1217 cm⁻¹ respectively in the isotopically labeled ¹³C-**5.7**. By analogy with monomeric titanium CO₂ complex Cp₂Ti(CO₂)(PMe₃) studied in depth by Mascetti *et al.*^{91,92} the IR bands at 1678 and 1236 cm⁻¹ in **5.7** are assigned to an asymmetric and symmetric ν(OCO) stretch respectively of the CO₂ ligand, with a C-coordinated bonding mode. The reactivity of **5.7** allows for spectroscopic elucidation only at low temperatures, and all attempts to isolate crystalline samples of this intermediate proved unsuccessful.

Geometry optimisation of the model system Pn₂Ti₂(CO₂) gave a structure with C_{2v} symmetry with a bent CO₂ group bound symmetrically between the two Ti atoms (Figure 5.13). The calculated wavenumbers for the CO₂ group are 1669 cm⁻¹ for the asymmetric stretch and 1214 cm⁻¹ for the symmetric stretch, which are in good agreement with the experimental results. A good match between the metal-metal bonding orbitals and the π-anti-bonding LUMO of CO₂ results in stabilisation of the metal electrons and binding of the substrate. A metal-metal bond is retained between the two Ti atoms consistent with the calculated Ti–Ti distance of 2.41 Å.

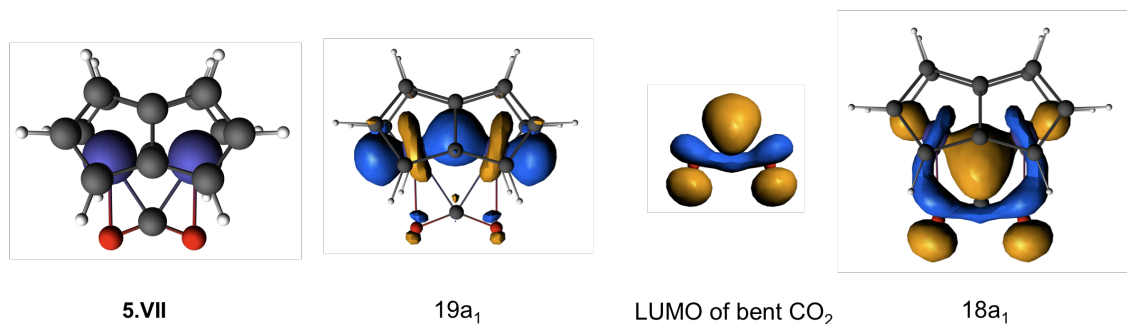


Figure 5.13 Calculated structure of **5.VII**, and schematic drawing of its HOMO (19a₁), the LUMO of bent CO₂ and bonding orbital 18a₁.¹²¹

CO₂ has been observed to bind to dinuclear metal sites with three different bonding modes (Figure 5.14)^{74,130-132} and the proposed $\mu:\eta^2,\eta^2$ - coordination geometry has only recently been structurally authenticated by X-ray crystallography in an *N*-heterocyclic carbene (NHC) nickel(0) dimer, [(IPr)Ni]₂(μ -CO)($\mu:\eta^2,\eta^2$ -CO₂), (IPr = 1,3-bis-(2,6-diisopropylphenyl)imidazol-2-ylidene) by Sadighi *et al.*¹³³

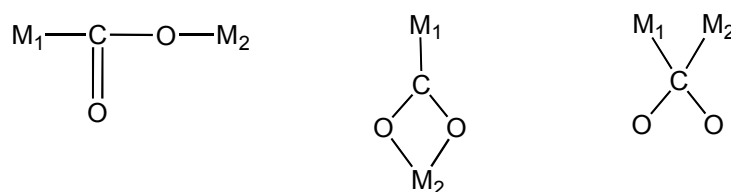
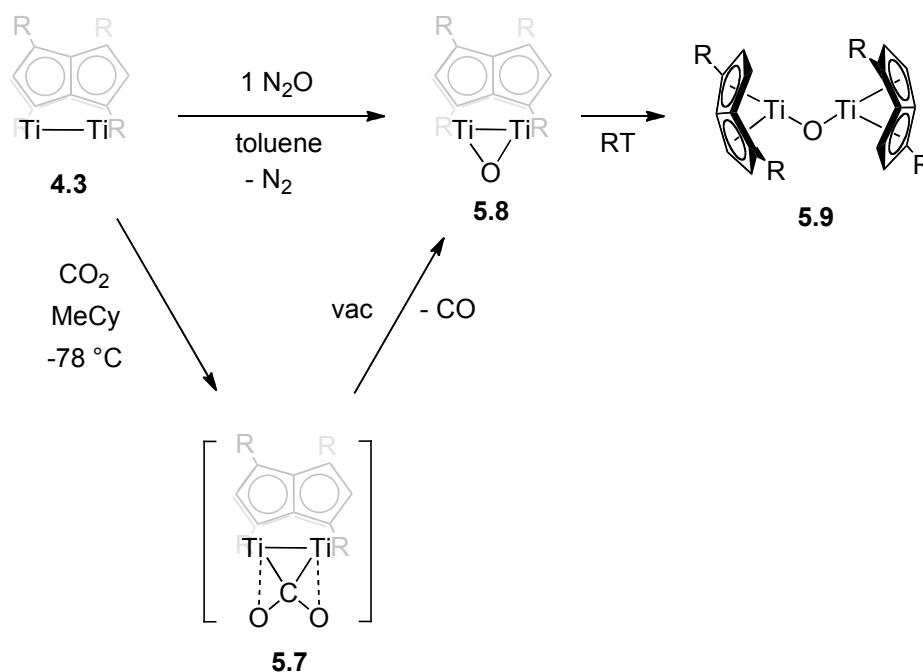


Figure 5.14 Crystallographically characterised bonding modes of CO₂ in bimetallic complexes.

5.3.3 Synthesis and characterisation of mono(μ -oxo) complexes **5.8** and **5.9**

The red mono-oxo complex **5.8** was isolated by allowing methylcyclohexane solutions of **5.7** to warm from -78 °C to room temperature under dynamic vacuum, or alternatively, by the slow addition of one equivalent of N₂O to **4.3** *via* Toepler line (Scheme 5.16).



Scheme 5.16 Synthesis of **5.8** and **5.9**. R = SiⁱPr₃.

The ¹H NMR spectrum of **5.8** shows four sharp doublets in the aromatic region, consistent with a diamagnetic complex with C₂ symmetry. Elemental analysis and mass spectrometry measurements support the proposed formulation.

The molecular structure determined by single crystal XRD reveals a 'dimetallo-epoxide' structure (Figure 5.15), with an oxo ligand symmetrically bridging two formally Ti(III) centres. The molecule possesses a 2-fold improper rotation axis (*S*₂) passing through the μ-O ligand and the midpoint of the Ti–Ti bond, which results in one half of the dimer being generated by symmetry. The Pn[†] ligands are less tightly bound to the Ti₂ core of **5.8** relative to **4.3**, and show the largest average Ti–C and Ti–centroid distances of all the double-sandwich derivatives structurally characterised in this work. Interestingly, the ring slippage parameter (*Δ* = 0.15) and twist angle between the Pn[†] ligands and the di-metal unit (26.6(5)°) also have the largest value of all of these structures. These observations in the solid state structure may be construed as a 'snap shot' of the Pn[†] rings as they move across the Ti₂ core from a bridging (η⁵,η⁵-) bonding mode in **5.8** towards a capping (η⁸-) mode in structural isomer **5.9** (*vide infra*).

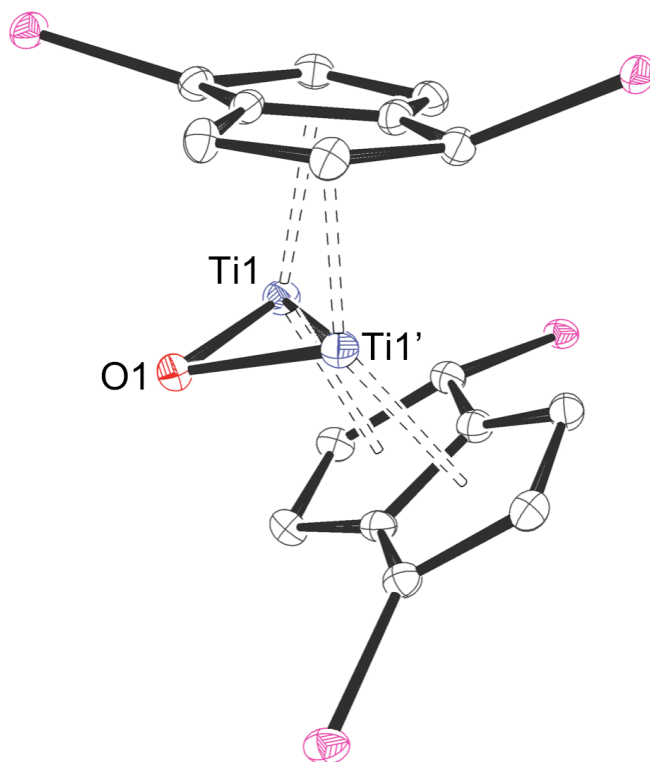


Figure 5.15 ORTEP (30% probability) diagram of **5.8**. Hydrogen atoms and ⁱPr groups omitted for clarity. Primed atoms are generated by symmetry.

Table 5.5 Selected distances (Å), angles (°) and parameters (defined in Figure 5.7) for **5.8**. Ct1, Ct2 and Ct1', Ct2' are the η^5, η^5 -centroids of the Pn1 and Pn1' rings respectively.

Parameter	5.8	Parameter	5.8
Ti1–Ti1'	2.3991(7)	Ti1–O1–Ti1'	80.28(8)
Ti1–O1	1.8607(15)	O1–Ti1–Ti1'	49.86(4)
Ti–Ct ^a	2.133(10)	Ct1–Ti1–Ct2'	139.722(12)
Ti–C _{ring} ^a	2.4548(19)	Fold angle	0.15(13)
Δ ^a	0.150(19)	Twist angle	26.6(5)

^aAverage values.

Complex **5.8** is thermally sensitive, and allowing a red C₆D₆ solution to stand for 12 hours at room temperature led to the precipitation of green crystals of **5.9**. Elemental analysis and mass spectrometry measurements identified **5.9** as a mono-oxo complex, isomeric with **5.8**. X-ray crystallography established the connectivity of the atoms in **5.9** as a μ -O dimer in which the Ti–Ti bond has been cleaved and the pentalene ligands bind in an η^8 -fashion to each formally Ti(III) centre (Figure 5.16). However, problems with the data set precluded accurate refinement of metric parameters ($R_1 = 13.8\%$). Examination of the raw intensity data revealed that the crystal used in the data collection was twinned, and despite several recrystallisations of **5.9**, single crystals of a higher quality could not be obtained.

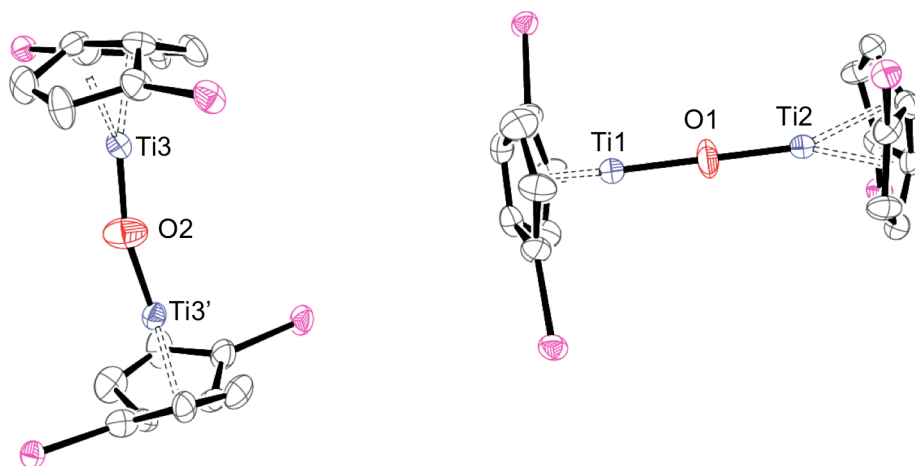


Figure 5.16 Partially refined molecular structure of **5.9** (thermal ellipsoids at 30%), showing two crystallographically independent molecules in the asymmetric unit.

Hydrogen atoms and ¹Pr groups omitted for clarity.

In the ¹H NMR spectrum of **5.9** in THF-*d*₈ solution only broad signals were observed, and the effective magnetic moment determined by the Evans method^{134,135} was 1.73 μ_B per Ti, a value consistent with one unpaired electron per metal centre. EPR spectroscopy of **5.8** was complicated by its extreme sensitivity both in the solid state and THF solution, and its poor solubility in more innocent solvents such as hexane or toluene. The X-band EPR spectrum of a frozen 2-methyltetrahydrofuran solution at 120 K (see Appendix A2) shows a broad principal feature centered at 3095 G assigned to a decomposition product, and a rhombic signal centered at 3374 G, for which an average

g -value of 1.967 is calculated. The latter features may be tentatively assigned to the $\Delta M_S = 1$ transitions of the Ti(III)–O–Ti(III) system **5.8**, however the expected features at half magnetic field for the $\Delta M_S = 2$ transitions of an electronic triplet state were not observed.

DFT calculations on $\text{Pn}_2\text{Ti}_2\text{O}$ with a double-sandwich structure found a local minimum with C_{2v} symmetry, **5.VIII**.¹²¹ The structure of $[(\eta^8\text{-Pn})\text{Ti}]_2\text{O}$ was optimised with both a singlet (**5.IXs**) and a triplet (**5.IXt**) ground state (see appendix A2 for calculated structures and MOs). The energies of all three structures are close and the most stable is both method and temperature dependent (Table 5.6). ADF has the double-sandwich structure the most stable. Gaussian estimates the energy (using the self-consistent field method, SCF) of the sandwich structure to be the lowest, however the free energy at 298 K gives the triplet η^8 -coordinated structure to be the most stable. This in agreement with experiment as the sandwich structure of the mono-oxo complex **5.8** converts to the triplet state **5.9** at room temperature.

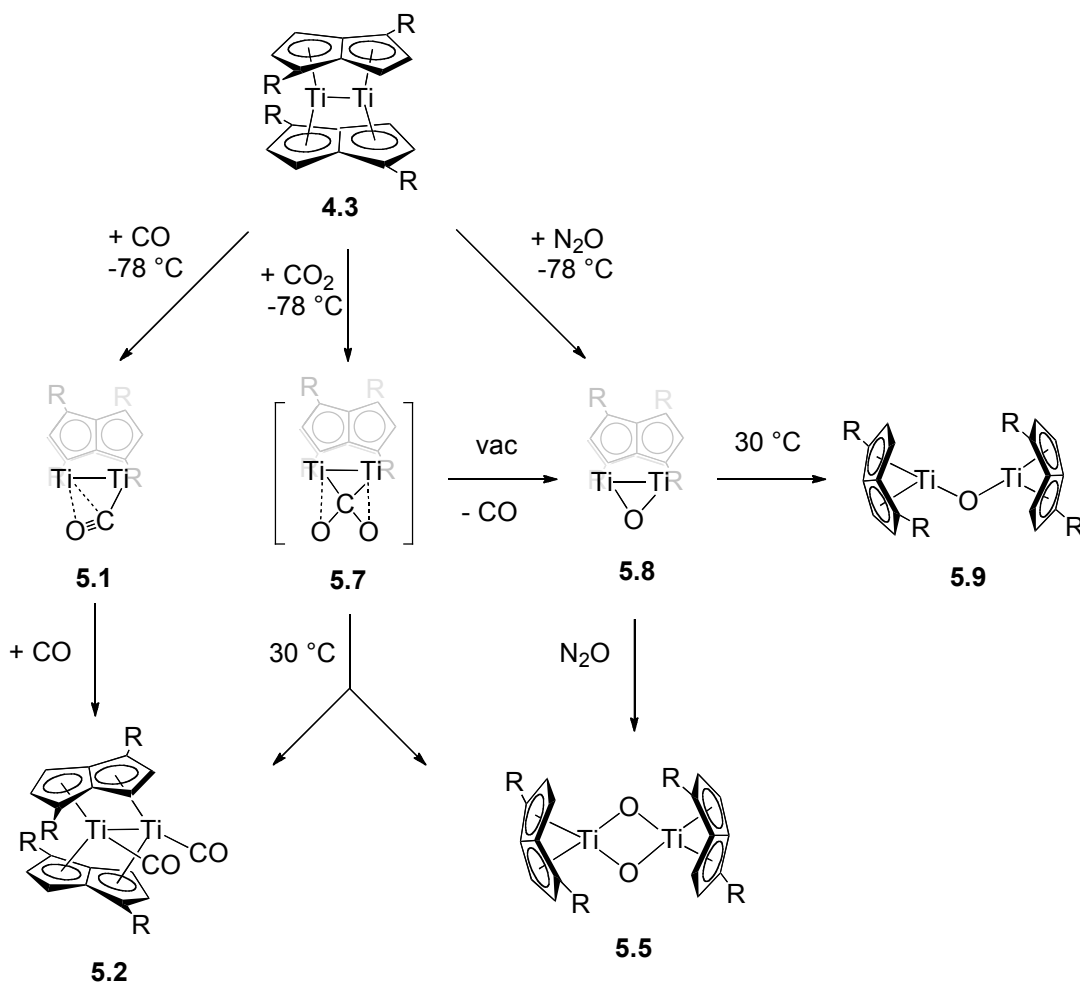
Table 5.6 Ti–O–Ti angles ($^\circ$) and relative energies (kcal mol^{-1}) of structures found for $\text{Pn}_2\text{Ti}_2\text{O}$.¹²¹ ADF values are in normal font and Gaussian values are given in *italics*.

Structure	Ti–O–Ti	$\Delta E(\text{SCF})$	ΔH_{298}^0	ΔG_{298}^0
5.VIII	79, 79	0, 0	0, 0	0, 2
5.IXt	133, 180	12, 4	13, 3	8, 0
5.IXs	103, 100	12, 19	13, 21	10, 20

5.3.4 Mechanistic investigation of reaction of **4.3** with CO_2

Reaction of **4.3** with CO_2 when carried out at low temperatures (between $-90\text{ }^\circ\text{C}$ and $-30\text{ }^\circ\text{C}$) leads to the quantitative formation of CO_2 adduct **5.7**. When solutions of **5.7** were allowed to reach room temperature a colour change from green to brown was observed and the coordinated CO_2 molecule is reduced quantitatively over a period of minutes, to give a bis(oxo) bridged dimer **5.5** and the di-carbonyl complex **5.2**. ^1H NMR spectra measured during the course of this reaction showed additional transient species, of which mono-oxo **5.8** and mono-carbonyl **5.1** were identified by

comparison with the spectra of independently synthesised samples (Scheme 5.17). With characterisation of these complexes in hand together with their calculated structures, a combined experimental and computational study was undertaken to probe the mechanism for the reaction of **4.3** with CO₂.



Scheme 5.17 Summary of reactivity of **4.3** with CO, CO₂ and N₂O.

As a preliminary study to track the course of these intermediates and determine their role in the reaction mechanism, the decomposition of **5.7** at temperatures above 10 °C was monitored by *in situ* IR and NMR spectroscopy.

The rate of decomposition of **5.7** was such that it could be conveniently followed by ¹H NMR spectroscopy. In a typical experiment, a 0.028 M solution of **4.3** in methylcyclohexane-*d*₁₄ at -78 °C (in the presence of ferrocene as an internal standard) was treated with one equivalent of CO₂ and shaken over 60 mins until complete

conversion to dark green **5.7** was observed. The reaction mixture was then placed in a pre-warmed NMR probe, allowed to thermally equilibrate and the conversion of reactants to products was measured over time. Plots of concentration vs time at 30 °C (Figure 5.17) follow a first order exponential decay.

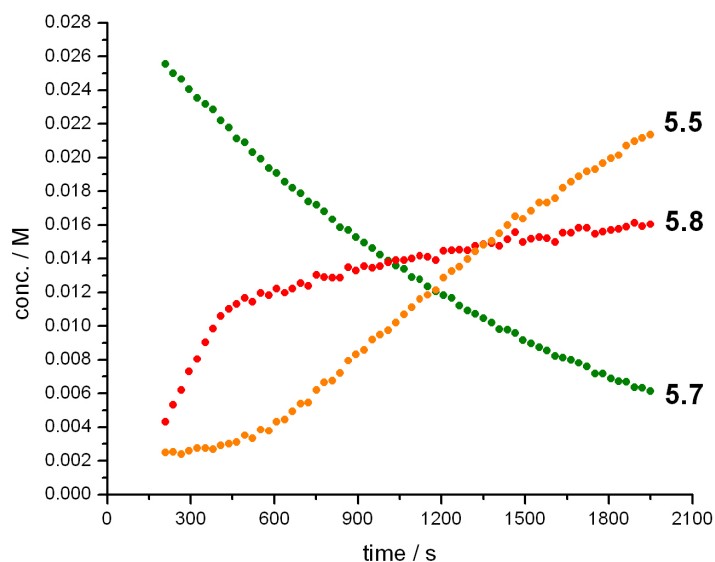


Figure 5.17 Concentration vs time curve for the decomposition of **5.7** to oxo products **5.8** and **5.5** at 30 °C, monitored by ^1H NMR.

In the initial stages of reaction at 30 °C the disappearance of **5.7** is accompanied by the appearance of **5.8**. The rate of increase of **5.8** slows after 200 s with the appearance of **5.5** as the final oxo product. However, the partial precipitation of **5.5** from methylcyclohexane- d_{14} solution does not permit reliable integrations and prohibits reliable determination of rate constants based on the appearance of the products.

A possible reaction pathway was modeled by DFT, which encompasses the intermediates that have been detected experimentally.¹²¹ The free energy profile is shown in Figure 5.18. The two computation methods (ADF and Gaussian) differ quantitatively but overall the energy profiles are similar. Binding of CO_2 to form the symmetrically bridged adduct is energetically favorable. The route to intermediate $\text{Pn}_2\text{Ti}_2\text{O}(\text{CO})$ (**INT**) passes through transition state TS1 with an energy which is thermally accessible at room temperature (22, 13, kcal mol⁻¹). Loss of CO from **INT** to form **5.VIII** is endoenergetic but the products lie below the energy of the previous

transition state. Disproportionation of **5.VIII** to reform **4.III** and **5.V** is just viable ($-2, 0$ kcal mol $^{-1}$) but is driven by coordination of the liberated CO to form **5.I** ($-31, -33$ kcal mol $^{-1}$). Further CO then forms the di-carbonyl, **5.II**.

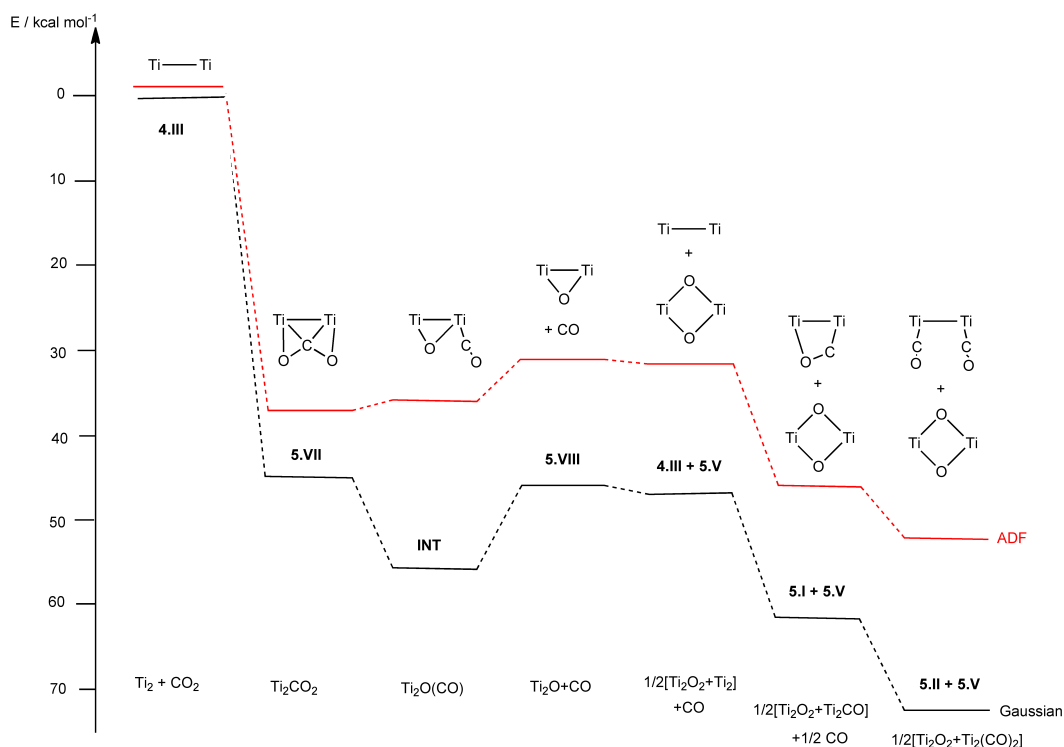


Figure 5.18 Energy profile for the proposed formation and decomposition of **5.VII**.¹²¹

Preliminary trials on an NMR scale to observe the proposed mono(μ -oxo) mono-carbonyl intermediate by reaction of ^{13}C -**5.1** with 1 equivalent of N_2O , or **5.8** with 1 equivalent of ^{13}CO , were inconclusive. The $^{13}\text{C}\{^1\text{H}\}$ NMR spectra were complex in each case, with the di-carbonyl complex ^{13}C -**5.2** identified as the major labelled product after warming to room temperature. ^1H NMR spectra confirmed the presence of di-oxo **5.5** in each case, which is a thermodynamic sink in the reaction of **4.3** with CO_2 , due to the formation of strong Ti–O bonds. This prompted an investigation into **4.3** with heteroallenes such as CS_2 as model molecules for CO_2 with the view to producing more stable and potentially isolable products. The results of these studies are discussed in chapter six.

5.4 Experimental Details for Chapter Five

5.4.1 Synthesis of $(\mu:\eta^5, \eta^5\text{-Pn}^\dagger)_2\text{Ti}_2(\text{CO})$ (**5.1**).

An ampoule charged with **4.3** (50 mg, 0.054 mmol) and toluene (0.5 mL) was cooled to -78 °C and the headspace evacuated. CO gas (0.9 mol eq., 0.050 mmol) was admitted slowly to the mixture with vigorous stirring, resulting in a colour change from deep red to purple. After warming to room temperature the volatiles were removed *in vacuo* to afford a crude purple solid that was recrystallised from pentane (1 mL) at -35 °C.

Total yield: 32 mg (62% with respect to **4.3**).

Alternatively, exposing a methylcyclohexane- d_{14} solution of **4.3** to 0.9 eq. ^{13}CO *via* Toepler pump yields the labeled product, ^{13}C -**5.1**.

^1H NMR (methylcyclohexane- d_{14} , 399.5 MHz, 303 K): δ_{H} 7.69 (1H, apparent t, $^3J_{\text{HH}} = 3.2$ Hz, Pn *H*), 7.10 (1H, d, $^3J_{\text{HH}} = 3.2$ Hz, Pn *H*), 6.62 (1H, d, $^3J_{\text{HH}} = 3.5$ Hz, Pn *H*), 6.34 (1H, d, $^3J_{\text{HH}} = 3.5$ Hz, Pn *H*), 6.30 (2H, d, $^3J_{\text{HH}} = 3.2$ Hz, Pn *H*), 6.22 (2H, d, $^3J_{\text{HH}} = 3.6$ Hz, Pn *H*), 5.74 (1H, d, $^3J_{\text{HH}} = 3.5$ Hz, Pn *H*), 5.62 (1H, d, $^3J_{\text{HH}} = 3.2$ Hz, Pn *H*), 1.62-1.25 (12H, overlapping m, ^iPr CH), 1.25-0.83 (72H, overlapping m, ^iPr CH₃).

$^{13}\text{C}\{^1\text{H}\}$ NMR (methylcyclohexane- d_{14} , 100.5 MHz, 303 K): δ_{C} 295.1 (s, CO), 136.8 (Pn C), 132.5 (Pn C), 132.4 (Pn C), 129.1 (Pn C), 127.7 (Pn C), 125.1 (Pn C), 124.9 (Pn C), 115.1 (Pn C), 108.2 (Pn C), 104.7 (Pn C), 103.2 (Pn C), 101.5 (Pn C), 99.75 (Pn C), 95.08 (Pn C), 93.16 (Pn C), 89.87 (Pn C), 20.94 (^iPr CH₃), 20.84 (^iPr CH₃), 20.79 (^iPr CH₃), 20.64 (^iPr CH₃), 20.62 (^iPr CH₃), 20.37 (^iPr CH₃), 20.36 (^iPr CH₃), 20.13 (^iPr CH₃), 15.14 (^iPr CH), 15.12 (^iPr CH), 14.45 (^iPr CH), 14.22 (^iPr CH).

$^{29}\text{Si}\{^1\text{H}\}$ NMR (methylcyclohexane- d_{14} , 79.4 MHz, 303 K): δ_{Si} 3.40 (s), 2.88 (d, $J_{\text{SiC}} = 1.2$ Hz), 2.40 (s), 2.22 (s).

EI-MS: $m/z = 924$ (100%), $[\text{M} - \text{CO}]^+$, 882 (10%), $[\text{M} - \text{CO} - ^i\text{Pr}]^+$.

Anal. found (calcd. for C₅₃H₉₂Si₄Ti₂): C, 66.78 (66.77); H, 9.81 (9.73) %.

IR (NaCl): **5.1** 1655 (br, ν CO); ^{13}C -**5.1** 1616 (br, ν ^{13}CO) cm⁻¹.

Crystal data for **5.1**: C₅₃H₉₃OSi₄Ti₂, $M_r = 954.43$, monoclinic, space group $C 2/c$, brown plate, $a = 23.4629(16)$ Å, $b = 11.6983(8)$ Å, $c = 39.655(3)$ Å, $\alpha = 90^\circ$, $\beta = 92.283(2)^\circ$,

$\gamma = 90^\circ$, $V = 10875.7(13) \text{ \AA}^3$, $T = 100 \text{ K}$, $Z = 8$, $R_{\text{int}} = 0.0541$, $\lambda_{\text{Mo}}(\text{K}\alpha) = 0.71075 \text{ \AA}$, $\theta_{\text{max}} = 27.485^\circ$, $R_1 [I > 2\sigma(I)] = 0.0411$, $wR_2 (\text{all data}) = 0.1107$, $\text{Goof} = 1.021$.

5.4.2 Synthesis of $(\mu:\eta^5, \eta^5\text{-Pn}^\dagger)_2\text{Ti}_2(\text{CO})_2$ (**5.2**).

A freeze-thaw degassed solution of **4.3** (63 mg, 0.068 mmol) in pentane (5 mL), kept under static vacuum, was exposed to ^{12}CO gas (1 atm) at -78°C before warming to room temperature. Shortly after gas addition the solution appeared orange-brown in colour. The reaction mixture was freeze-thaw degassed, and exposed to an argon atmosphere which resulted in a colour change to green-brown. Storage of this solution at -35°C afforded brown crystals of **5.2** which were isolated by decantation and dried *in vacuo*.

Total yield: 26 mg (39% with respect to **4.3**).

Alternatively, exposing a C_6D_6 solution of **4.3** to 2 eq. ^{13}CO *via* Toepler pump, yields the labeled product ^{13}C -**5.2**.

^1H NMR (C_6D_6 , 399.5 MHz, 303 K): δ_{H} 7.59 (2H, d, $^3J_{\text{HH}} = 3.1 \text{ Hz}$, Pn *H*), 7.51 (2H, d, $^3J_{\text{HH}} = 3.3 \text{ Hz}$, Pn *H*), 5.12 (2H, d, $^3J_{\text{HH}} = 3.3 \text{ Hz}$, Pn *H*), 4.72 (2H, d, $^3J_{\text{HH}} = 3.3 \text{ Hz}$, Pn *H*), 1.68 (6H, m, ^iPr *CH*), 1.41 (6H, m, ^iPr *CH*), 1.33 (18H, d, $^3J_{\text{HH}} = 7.4 \text{ Hz}$, ^iPr CH_3), 1.19 (18H, d, $^3J_{\text{HH}} = 7.3 \text{ Hz}$, ^iPr CH_3), 1.15 (18H, d, $^3J_{\text{HH}} = 7.4 \text{ Hz}$, ^iPr CH_3), 0.93 (18H, d, $^3J_{\text{HH}} = 7.4 \text{ Hz}$, ^iPr CH_3).

$^{13}\text{C}\{^1\text{H}\}$ NMR (C_6D_6 , 100.5 MHz, 303 K): δ_{C} 231.6 (CO), 122.8 (Pn C), 122.1 (Pn C), 121.9 (Pn C), 105.7 (Pn C), 103.0 (Pn C), 90.2 (Pn C), 85.0 (Pn C), 20.1 (^iPr CH_3), 20.0 (^iPr CH_3), 19.8 (^iPr CH_3), 19.5 (^iPr CH_3), 14.1 (^iPr *CH*), 12.8 (^iPr *CH*).

$^{29}\text{Si}\{^1\text{H}\}$ NMR (C_6D_6 , 79.4 MHz, 303 K): δ_{Si} 3.69, 2.85.

EI-MS: $m/z = 923$ (100%), $[\text{M} - 2\text{CO}]^+$.

Anal. found (calcd. for $\text{C}_{54}\text{H}_{92}\text{O}_2\text{Si}_4\text{Ti}_2$): C, 65.99 (66.09); H, 9.49 (9.45) %.

IR (NaCl): **5.2** 1987 (s, ν CO), 1910 (w, ν CO); ^{13}C -**5.3** 1942 (s, ν ^{13}CO), 1868 (w, ν ^{13}CO) cm^{-1} .

IR (methylcyclohexane, 26°C): **5.2** 1991 (s, ν CO), 1910 (w, ν CO); ^{13}C -**5.3** 1948 (s, ν ^{13}CO), 1867 (w, ν ^{13}CO) cm^{-1} .

Crystal data for **5.2**: $C_{54}H_{92}O_2Si_4Ti_2$, $M_r = 981.44$, monoclinic, space group $P2_1/n$, brown plate, $a = 12.894(3)$ Å, $b = 22.342(5)$ Å, $c = 19.113(4)$ Å, $\alpha = 90^\circ$, $\beta = 92.18(3)^\circ$, $\gamma = 90^\circ$, $V = 5502.1(19)$ Å³, $T = 100$ K, $Z = 4$, $R_{int} = 0.1018$, $\lambda_{Mo}(K\alpha) = 0.71073$ Å, $\theta_{max} = 27.483^\circ$, $R_1 [I > 2\sigma(I)] = 0.0766$, wR_2 (all data) = 0.2278, $Goof = 1.067$.

5.4.3 Synthesis of $(\mu:\eta^5, \eta^5\text{-Pn}^\dagger)_2Ti_2(CO)_3$ (**5.3**).

To a degassed solution of **5.2** (10 mg, 0.0108 mmol) in methylcyclohexane- d_{14} (0.5 mL) at -78°C was added ^{13}CO (0.85 bar). Warming of the mixture resulted in a colour change from green-brown to orange-brown.

NMR yield: quantitative with respect to **5.2**.

^1H NMR (methylcyclohexane- d_{14} , 399.5 MHz, 303 K): δ_{H} 7.31 (2H, d, $^3J_{\text{HH}} = 2.9$ Hz, Pn H), 7.22 (2H, br s, $\Delta\nu_{1/2} = 10$ Hz, Pn H), 5.10 (2H, d, $^3J_{\text{HH}} = 2.8$ Hz, Pn H), 4.96 (2H, d, $^3J_{\text{HH}} = 3.0$ Hz, Pn H), 1.59 (6H, m, $^i\text{Pr CH}$), 1.43 (6H, m, $^i\text{Pr CH}$), 1.20 (18H, d, $^3J_{\text{HH}} = 7.4$ Hz, $^i\text{Pr CH}_3$), 1.17 (18H, d, $^3J_{\text{HH}} = 7.4$ Hz, $^i\text{Pr CH}_3$), 1.08 (18H, d, $^3J_{\text{HH}} = 7.4$ Hz, $^i\text{Pr CH}_3$), 0.93 (18H, d, $^3J_{\text{HH}} = 7.4$ Hz, $^i\text{Pr CH}_3$). ^1H NMR (methylcyclohexane- d_{14} , 399.5 MHz, 193 K): δ_{H} 7.00 (2H, s, Pn H), 6.00 (2H, s, Pn H), 5.47 (2H, s, Pn H), 5.29 (2H, s, Pn H), 1.60 (6H, s, $^i\text{Pr CH}$), 1.44 (6H, s, $^i\text{Pr CH}$), 1.26 - 1.08 (36H, overlapping m, $^i\text{Pr CH}_3$), 1.02 (18H, s, $^i\text{Pr CH}_3$), 0.84 (18H, s, $^i\text{Pr CH}_3$).

$^{13}\text{C}\{^1\text{H}\}$ NMR (methylcyclohexane- d_{14} , 100.5 MHz, 303 K): δ_{C} 232.1 (br, $\Delta\nu_{1/2} = 190$ Hz, CO), 128.3 (Pn C), 123.3 (Pn C), 123.0 (Pn C), 122.8 (Pn C), 106.3 (Pn C), 103.9 (Pn C), 91.3 (Pn C), 86.2 (Pn C), 21.0 ($^i\text{Pr CH}_3$), 20.9 ($^i\text{Pr CH}_3$), 20.8 ($^i\text{Pr CH}_3$), 20.4 ($^i\text{Pr CH}_3$), 15.3 ($^i\text{Pr CH}$), 13.9 ($^i\text{Pr CH}$). $^{13}\text{C}\{^1\text{H}\}$ NMR (methylcyclohexane- d_{14} , 100.5 MHz, 193 K): δ_{C} 267.8 (CO), 256.7 (CO), 185.9 (free CO), 128.6 (Pn C), 119.0 (Pn C), 115.1 (Pn C), 114.5 (Pn C), 100.3 (Pn C), 96.2 (Pn C), 91.6 (Pn C), 90.5 (Pn C), 21.2 ($^i\text{Pr CH}_3$), 21.0 ($^i\text{Pr CH}_3$), 20.9 ($^i\text{Pr CH}_3$), 15.4 ($^i\text{Pr CH}$), 13.5 ($^i\text{Pr CH}$).

$^{29}\text{Si}\{^1\text{H}\}$ NMR (methylcyclohexane- d_{14} , 79.4 MHz, 303 K): δ_{Si} 3.59, 3.09.

Anal. found (calcd. for $C_{55}H_{92}O_3Si_4Ti_2$): C, 65.53 (65.44); H, 9.27 (9.19) %.

IR (methylcyclohexane, -65°C): **5.3** 1991 (w, ν CO), 1910 (s, ν CO); ^{13}C -**5.3** 1948 (w, $\nu^{13}\text{CO}$), 1867 (s, $\nu^{13}\text{CO}$) cm^{-1} .

5.4.4 Synthesis of $(\mu:\eta^5, \eta^5\text{-Pn}^+)_2\text{Ti}_2(\mu:\eta^2\text{-CNMe})$ (**5.4**).

A solution of MeNC (32 μL , 3.1 M in toluene- d_8 , 0.099 mmol) was added dropwise to a solution of **4.3** (46 mg, 0.050 mmol) in pentane (1.5 mL) at -35°C . Following addition, the purple mixture was allowed to warm to room temperature and stir for 20 min. The resultant solution was filtered and concentrated to *ca.* 0.5 mL and after cooling to -35°C deposited dark red crystals that were isolated by decantation and dried *in vacuo*.

Total yield: 39 mg (81% with respect to **4.3**).

^1H NMR (toluene- d_8 , 399.5 MHz, 303 K): δ_{H} 7.70 (1H, d, $^3J_{\text{HH}} = 3.4$ Hz, Pn *H*), 7.25 (1H, d, $^3J_{\text{HH}} = 3.0$ Hz, Pn *H*), 6.55 (1H, d, $^3J_{\text{HH}} = 3.2$ Hz, Pn *H*), 6.19 (1H, d, $^3J_{\text{HH}} = 3.3$ Hz, Pn *H*), 6.01 (1H, d, $^3J_{\text{HH}} = 2.9$ Hz, Pn *H*), 5.96 (1H, d, $^3J_{\text{HH}} = 3.2$ Hz, Pn *H*), 5.89 (1H, d, $^3J_{\text{HH}} = 3.5$ Hz, Pn *H*), 5.77 (1H, d, $^3J_{\text{HH}} = 3.4$ Hz, Pn *H*), 3.25 (3H, s, CNCH₃), 1.48 (6H, m, ^iPr CH), 1.31 (6H, m, ^iPr CH), 1.19 (9H, d, $^3J_{\text{HH}} = 6.4$ Hz, ^iPr CH₃), 1.18 (9H, d, $^3J_{\text{HH}} = 7.1$ Hz, ^iPr CH₃), 1.17 (9H, d, $^3J_{\text{HH}} = 6.9$ Hz, ^iPr CH₃), 1.13 (9H, d, $^3J_{\text{HH}} = 7.3$ Hz, ^iPr CH₃), 1.06 (9H, d, $^3J_{\text{HH}} = 7.5$ Hz, ^iPr CH₃), 1.03 (9H, d, $^3J_{\text{HH}} = 7.3$ Hz, ^iPr CH₃), 0.99 (9H, d, $^3J_{\text{HH}} = 6.6$ Hz, ^iPr CH₃), 0.97 (9H, d, $^3J_{\text{HH}} = 7.0$ Hz, ^iPr CH₃).

$^{13}\text{C}\{^1\text{H}\}$ NMR (toluene- d_8 , 100.5 MHz, 303 K): δ_{C} 289.2 (CNCH₃), 132.5 (Pn C), 132.2 (Pn C), 130.5 (Pn C), 126.2 (Pn C), 126.0 (Pn C), 123.2 (Pn C), 111.1 (Pn C), 107.5 (Pn C), 107.0 (Pn C), 106.3 (Pn C), 106.2 (Pn C), 94.78 (Pn C), 94.25 (Pn C), 91.44 (Pn C), 90.81 (Pn C), 44.65 (CNCH₃), 20.46 (^iPr CH₃), 20.40 (^iPr CH₃), 20.35 (^iPr CH₃), 20.27 (^iPr CH₃), 20.19 (br, overlapping m, ^iPr CH₃), 20.09 (^iPr CH₃), 19.91 (^iPr CH₃), 14.67 (^iPr CH), 14.50 (^iPr CH), 13.91 (^iPr CH), 13.44 (^iPr CH).

$^{29}\text{Si}\{^1\text{H}\}$ NMR (toluene- d_8 , 79.4 MHz, 303 K): δ_{Si} 7.92, 7.26, 7.23, 6.25.

EI-MS: $m/z = 967$ (25%), $[\text{M}]^+$; 952 (10%), $[\text{M} - \text{Me}]^+$, 926 (100%), $[\text{M} - \text{MeNC}]^+$.

Anal. found (calcd. for C₅₄H₉₅NSi₄Ti₂): C, 66.99 (67.11); H, 10.03 (9.91) %.

IR (NaCl): 1642 (ν_{CN}) cm^{-1} .

Crystal data for **5.4**: C₅₄H₉₅NSi₄Ti₂, $M_r = 966.41$, monoclinic, space group $P2_1/n$, dark red plate, $a = 12.8717(9)$ Å, $b = 22.7580(16)$ Å, $c = 18.8770(13)$ Å, $\alpha = \gamma = 90^\circ$, $\beta = 91.730(2)^\circ$, $V = 5527.2(7)$ Å³, $T = 100$ K, $Z = 4$, $R_{\text{int}} = 0.161$, $\lambda_{\text{Mo}}(\text{K}\alpha) = 0.71075$ Å, $\theta_{\text{max}} = 25.0^\circ$, $R_1 [I > 2\sigma(I)] = 0.0805$, wR_2 (all data) = 0.2503, $\text{GooF} = 1.004$.

5.4.5 Synthesis of $[(\eta^8\text{-Pn}^{\dagger})\text{Ti}(\mu\text{-O})]_2$ (**5.5**).

An ampoule charged with **4.3** (163.5 mg, 0.177 mmol) and toluene (3 mL) was cooled to -78 °C and the headspace evacuated. N₂O gas (0.37 mmol) was admitted and the reaction mixture was allowed to warm to room temperature, resulting in a colour change from deep red to yellow-brown. After stirring for 1 h a yellow precipitate formed which was taken back into solution by heating the mixture to 100 °C. The hot solution was filtered and the filtrate stripped to dryness, affording a yellow microcrystalline solid, which was treated with pentane (3 mL) and dried *in vacuo*.

Total yield: 152 mg (90% with respect to **4.3**).

¹H NMR (C₆D₆, 399.5 MHz, 303 K): δ_{H} 6.51 (4H, d, ³J_{HH} = 3.3 Hz, Pn H), 5.76 (4H, d, ³J_{HH} = 3.3 Hz, Pn H), 1.26 (12H, m, ⁱPr CH), 1.18 (36H, d, ³J_{HH} = 7.1 Hz, ⁱPr CH₃), 1.12 (36H, d, ³J_{HH} = 7.2 Hz, ⁱPr CH₃).

¹³C{¹H} NMR (C₆D₆, 100.5 MHz, 303 K): δ_{C} 149.4 (Pn C), 129.9 (Pn C), 113.6 (Pn C), 112.6 (Pn C), 19.4 (ⁱPr CH₃), 19.2 (ⁱPr CH₃), 12.1 (ⁱPr CH).

²⁹Si{¹H} NMR (C₆D₆, 79.4 MHz, 303 K): δ_{Si} -0.34.

EI-MS: m/z = 956 (100%), [M]⁺; 913 (25%), [M - ⁱPr₃]⁺.

Anal. found (calcd. for C₅₂H₉₂O₂Si₄Ti₂): C, 65.49 (65.24); H, 9.39 (9.69) %.

Partially refined crystal data for **5.5**: C₅₂H₉₂O₂Si₄Ti₂, M_r = 957.36, triclinic, space group *P*-1, orange plate, a = 15.6612(11) Å, b = 15.6500(11) Å, c = 22.1257(16) Å, α = 88.156(8)°, β = 88.188(8)°, γ = 89.885(8)°, V = 5417.4(6) Å³ T = 100 K, Z = 4, R_{int} = 0.094, $\lambda_{\text{Mo}}(\text{K}\alpha)$ = 0.71075 Å, θ_{max} = 24.7°, R_1 [$I > 2\sigma(I)$] = 0.205, wR_2 (all data) = 0.526, Goof = 1.942.

5.4.6 Synthesis of $[(\eta^5\text{-Pn}^{\dagger})\text{Ti}(\mu\text{-O})(\text{py})]_2$ (**5.6**).

A frozen, degassed solution of **4.3** (52 mg, 0.056 mmol) in hexane (1.5 mL) was exposed to N₂O gas (0.11 mmol) and allowed warm to room temperature. After thawing and stirring for 1 h the reaction mixture appeared as a yellow-brown solution with yellow precipitate, characteristic of **5.5**. An excess of pyridine (0.4 mL) was added dropwise until the precipitate fully dissolved, giving a green solution, which was filtered and concentrated to *ca.* 1 mL. Storage of this solution at -35 °C afforded red

crystals of **5.6**, which were isolated by decantation. Total yield: 30 mg (48% with respect to **4.3**). **5.6** is prone to solvent loss and reforms **5.5** in the absence of excess pyridine, as confirmed by spectroscopic and analytical data.

^1H NMR (pyridine- d_5 , 399.5 MHz, 303 K): δ_{H} 6.38 (2H, br d, Pn H), 6.33 (2H, br d, Pn H), 1.36 (6H, br m, ^iPr CH), 1.29 (6H, br m, ^iPr CH), 1.21 (18H, br d, ^iPr CH₃), 1.16 (18H, br d, ^iPr CH₃), 1.15 (18H, br d, ^iPr CH₃), 1.13 (18H, br d, ^iPr CH₃).

$^{13}\text{C}\{^1\text{H}\}$ NMR (pyridine- d_5 , 100.5 MHz, 303 K): δ_{C} 140.7 (Pn C), 132.4 (Pn C), 111.8 (Pn C), 110.9 (Pn C), 20.05 (^iPr CH₃), 13.05 (^iPr CH).

$^{29}\text{Si}\{^1\text{H}\}$ NMR (pyridine- d_5 , 79.4 MHz, 303 K): resonances could not be identified.

EI-MS: m/z = 953-959 (principal peak 955, 100%), $[\text{M} - \text{py}]^+$; 910-915 (principal peak 912, 25%), $[\text{M} - \text{py} - ^i\text{Pr}_3]^+$.

Anal. found (calcd. for $\text{C}_{52}\text{H}_{92}\text{O}_2\text{Si}_4\text{Ti}_2$ = **5.6** - py): C, 65.14 (65.24); H, 9.81 (9.69); N <0.1 (0.00) %.

Crystal data for **5.6**.(C₅H₅N): $\text{C}_{67}\text{H}_{107}\text{N}_3\text{O}_2\text{Si}_4\text{Ti}_2$, M_r = 1194.71, triclinic, space group $P-1$, red block, a = 13.7134(6) Å, b = 16.0497(6) Å, c = 18.5403(6) Å, α = 85.689(3)°, β = 86.517(3)°, γ = 66.630(4)°, V = 3733.1(3) Å³, T = 173 K, Z = 2, R_{int} = 0.0654, $\lambda_{\text{Cu}}(\text{K}\alpha)$ = 1.54184 Å, θ_{max} = 71.480°, $R_1 [I > 2\sigma(I)]$ = 0.0562, wR_2 = 0.1626, Goof = 0.999.

5.4.7 Synthesis of $(\mu:\eta^5, \eta^5\text{-Pn}^{\dagger})_2\text{Ti}_2(\text{CO}_2)$ (**5.7**).

A J. Young NMR tube was charged with **4.3** (16 mg, 0.017 mmol) and methylcyclohexane- d_{14} (0.5 mL). The solution was cooled to -78 °C, the headspace evacuated, and CO₂ (0.017 mmol) admitted. The tube was briefly shaken and a colour change from deep red to dark green was observed. NMR spectra were immediately measured, with the probe pre-cooled to -30 °C. Alternatively, using $^{13}\text{CO}_2$ in the method above yields the labeled product, ^{13}C -**5.7**.

NMR yield: quantitative with respect to **4.3**.

^1H NMR (methylcyclohexane- d_{14} , 399.5 MHz, 243 K): δ_{H} 5.98 (2H, d, $^3J_{\text{HH}}$ = 3.6 Hz, Pn H), 5.83 (2H, d, $^3J_{\text{HH}}$ = 2.9 Hz, Pn H), 5.66 (2H, d, $^3J_{\text{HH}}$ = 2.8 Hz, Pn H), 5.37 (2H, d, $^3J_{\text{HH}}$ = 3.6 Hz, Pn H), 0.69 (6H, dt, $^3J_{\text{HH}}$ = 7.4, 14.9 Hz, ^iPr CH), 0.57 (6H, dt, $^3J_{\text{HH}}$ = 7.4, 14.7 Hz, ^iPr CH), 0.34 (18H, d, $^3J_{\text{HH}}$ = 7.3 Hz, ^iPr CH₃), 0.31 (18H, d,

$^3J_{\text{HH}} = 7.5 \text{ Hz}$, $^1\text{Pr CH}_3$), 0.20 (18H, d, $^3J_{\text{HH}} = 7.4 \text{ Hz}$, $^1\text{Pr CH}_3$), 0.16 (18H, d, $^3J_{\text{HH}} = 7.4 \text{ Hz}$, $^1\text{Pr CH}_3$).

$^{13}\text{C}\{^1\text{H}\}$ NMR (methylcyclohexane- d_{14} , 100.5 MHz, 243 K, selected data): δ_{C} 219 (s, CO_2).

$^{29}\text{Si}\{^1\text{H}\}$ NMR (methylcyclohexane- d_{14} , 79.4 MHz, 243 K): δ_{Si} 2.12, 1.88.

IR (methylcyclohexane, -65°C): **5.7** 1678 ($\nu_{\text{asym OCO}}$), 1236 ($\nu_{\text{sym OCO}}$); ^{13}C -**5.7** 1637 ($\nu_{\text{asym O}^{13}\text{CO}}$), 1217 ($\nu_{\text{sym O}^{13}\text{CO}}$) cm^{-1} .

5.4.8 Synthesis of $(\mu:\eta^5, \eta^5\text{-Pn}^\dagger)_2\text{Ti}_2(\mu\text{-O})$ (**5.8**).

METHOD A: A J. Young NMR tube was charged with **4.3** (17 mg, 0.018 mmol) and C_6D_6 (0.6 mL). The solution was frozen at -78°C , the headspace evacuated, and N_2O (0.016 mmol) admitted. The tube was warmed to room temperature and a colour change to bright red was observed as the solution thawed.

NMR yield: 68% with respect to **4.3**.

METHOD B: An ampoule charged with **4.3** (78.5 mg, 0.0848 mmol) and methylcyclohexane (5 mL) was cooled to -78°C and the headspace evacuated. CO_2 gas (1 atm) was admitted, resulting in a colour change from deep red to dark green. The ampoule was placed under reduced pressure then removed from the -78°C bath. The solvent was slowly removed *in vacuo* as the reaction mixture warmed to room temperature, giving a crude red residue. Recrystallisation from toluene (1 mL) at -35°C afforded **5.8** as a red microcrystalline solid.

Total yield: 66.3 mg (83% with respect to **4.3**).

Subsequent recrystallisation from a concentrated toluene/pentane solution at -35°C afforded X-ray quality crystals.

^1H NMR (C_6D_6 , 399.5 MHz, 303 K, selected data): δ_{H} 7.86 (2H, d, $^3J_{\text{HH}} = 3.3 \text{ Hz}$, Pn *H*), 6.78 (2H, d, $^3J_{\text{HH}} = 3.2 \text{ Hz}$, Pn *H*), 6.45 (2H, d, $^3J_{\text{HH}} = 3.2 \text{ Hz}$, Pn *H*), 6.39 (2H, d, $^3J_{\text{HH}} = 3.2 \text{ Hz}$, Pn *H*), 1.55 (6H, m, $^1\text{Pr CH}$), 1.26 (6H, m, $^1\text{Pr CH}$), 1.13 (18H, d, $^3J_{\text{HH}} = 7.2 \text{ Hz}$, $^1\text{Pr CH}_3$), 1.10 (18H, d, $^3J_{\text{HH}} = 7.4 \text{ Hz}$, $^1\text{Pr CH}_3$), 1.01 (18H, d, $^3J_{\text{HH}} = 7.4 \text{ Hz}$, $^1\text{Pr CH}_3$), 0.96 (18H, d, $^3J_{\text{HH}} = 7.4 \text{ Hz}$, $^1\text{Pr CH}_3$).

$^{13}\text{C}\{^1\text{H}\}$ NMR (C_6D_6 , 100.5 MHz, 303 K, selected data): δ_{C} 134.2 (Pn C), 133.4 (Pn C), 132.6 (Pn C), 114.9 (Pn C), 111.3 (Pn C), 108.1 (Pn C), 102.2 (Pn C), 99.47 (Pn C),

19.94 (ⁱPr CH), 19.89 (ⁱPr CH), 19.39 (ⁱPr CH₃), 19.35 (ⁱPr CH₃), 14.11 (ⁱPr CH), 12.97 (ⁱPr CH).

²⁹Si{¹H} NMR (C₆D₆, 303 K): δ_{Si} 2.39, 1.01.

EI-MS: m/z = 941 (100%), [M]⁺.

Anal. found (calcd. for C₅₂H₉₂O₁Si₄Ti₂): C, 66.21 (66.35); H, 9.70 (9.85) %.

Crystal data for **5.8**: C₅₂H₉₂O₁Si₄Ti₂, M_r = 941.41, monoclinic, space group $C 2/c$, bronze block, a = 24.0505(8) Å, b = 11.2805(5) Å, c = 22.8005(14) Å, $\alpha = \gamma = 90^\circ$, $\beta = 120.421(6)^\circ$, V = 5334.2(5) Å³, T = 173 K, Z = 4, R_{int} = 0.0344, $\lambda_{\text{Mo}}(\text{K}\alpha)$ = 0.71073 Å, θ_{max} = 28.617°, $R_1 [I > 2\sigma(I)]$ = 0.0433, wR_2 (all data) = 0.1241, Goof = 1.049.

5.4.9 Synthesis of $[(\eta^8\text{-Pn}^\dagger)\text{Ti}]_2(\mu\text{-O})$ (**5.9**).

Storage of a C₆D₆ solution of **5.8** (6.6 μmol) overnight at room temperature afforded green crystals of **5.9** which were isolated by decantation, washed with cold pentane (1 mL, -35 °C) and dried *in vacuo*.

Total yield = 2.0 mg, 32% with respect to **5.8**.

¹H NMR (toluene-*d*₈, 399.5 MHz, 303 K): δ_H 4.09 (br, Δ $\nu_{1/2}$ = 138 Hz, Pn *H*), 4.09 (br, Δ $\nu_{1/2}$ = 138 Hz, Pn *H*), 1.77 (br, Δ $\nu_{1/2}$ = 110 Hz, ⁱPr CH), 1.13 (br, Δ $\nu_{1/2}$ = 106 Hz, ⁱPr CH₃).

¹³C and ²⁹Si NMR resonances were not observed due to the paramagnetic nature of **5.9**.

EPR (2-methyltetrahydrofuran, 120 K, X-band, selected data): g_1 = 1.998, g_2 = 1.983, g_3 = 1.919, g_{iso} = 1.967 (Δ M_S = 1); g = 3.592 (singlet, Δ M_S = 2).

EI-MS: m/z = 941 (100%), [M]⁺.

Anal. found (calcd. for C₅₂H₉₂O₁Si₄Ti₂): C, 66.17 (66.35); H, 9.75 (9.85) %.

Mag. suscep. (Evans method, THF-*d*₈, 303 K): μ_{eff} = 2.45 μ_B per molecule = 1.73 μ_B per Ti.

5.5 References for Chapter Five

1. O. T. Summerscales and F. G. N. Cloke, *Coord. Chem. Rev.*, 2006, **250**, 1122–1140.
2. A. E. Ashley, R. T. Cooper, G. G. Wildgoose, J. C. Green, and D. O'Hare, *J. Am. Chem. Soc.*, 2008, **130**, 15662–15677.
3. O. T. Summerscales, C. J. Rivers, M. J. Taylor, P. B. Hitchcock, J. C. Green, and F. G. N. Cloke, *Organometallics*, 2012, **31**, 8613–8617.
4. M. Kuchta and F. G. N. Cloke, *Organometallics*, 1998, **17**, 1934–1936.
5. F. G. N. Cloke, J. C. Green, and C. N. Jardine, *Organometallics*, 1999, **18**, 1087–1090.
6. A. D. Smith, M.Chem. Dissertation, University of Sussex, 2012.
7. A. F. R. Kilpatrick, J. C. Green, F. G. N. Cloke, and N. Tsoureas, *Chem. Commun.*, 2013, 9434–9436.
8. F. Aubke and C. Wang, *Coord. Chem. Rev.*, 1994, **137**, 483–524.
9. M. L. H. Green and J. A. Timney, in *Organometallic Chemistry: Volume 30*, ed. M. Green, The Royal Society of Chemistry, 2002, vol. 30, pp. 172–188.
10. F. P. Pruchnik, *Organometallic Chemistry of the Transition Elements*, Plenum Press, 1990.
11. H. Werner, *Angew. Chem. Int. Ed. Engl.*, 1990, **29**, 1077–1089.
12. F. A. Cotton, G. Wilkinson, C. A. Murillo, and M. Bochmann, *Advanced Inorganic Chemistry*, Wiley, 6 edn. 1999.
13. J. G. Murray, *J. Am. Chem. Soc.*, 1959, **81**, 752–753.
14. H. Brintzinger and J. E. Bercaw, *J. Am. Chem. Soc.*, 1970, **92**, 6182–6185.
15. S. I. Troyanov, H. Antropiusová, and K. Mach, *J. Organomet. Chem.*, 1992, **427**, 49–55.
16. F. Calderazzo, J. J. Salzmänn, and P. Mosimann, *Inorg. Chim. Acta*, 1967, **1**, 65–67.
17. H. Alt and M. D. Rausch, *J. Am. Chem. Soc.*, 1974, **96**, 5936–5937.
18. B. Demersemann, G. Bouquet, and M. Bigorgne, *J. Organomet. Chem.*, 1975, **101**, C24–C26.
19. G. Fachinetti, G. Fochi, and C. Floriani, *J. Chem. Soc., Chem. Commun.*, 1976, 230.
20. J. L. Atwood, K. E. Stone, H. G. Alt, D. C. Hrnčir, and M. D. Rausch, *J. Organomet. Chem.*, 1977, **132**, 367–375.
21. C. Floriani and G. Fachinetti, *J. Chem. Soc., Dalton Trans.*, 1973, 1954–1957.
22. G. Fachinetti, G. Fochi, and C. Floriani, *J. Organomet. Chem.*, 1973, **57**, C51–C54.
23. G. Fachinetti and C. Floriani, *J. Chem. Soc., Dalton Trans.*, 1974, 2433–2436.
24. G. Fachinetti and C. Floriani, *J. Chem. Soc., Chem. Commun.*, 1974, 66.
25. G. Fachinetti, C. Floriani, and H. Stoeckli-Evans, *J. Chem. Soc., Dalton Trans.*, 1977, 2297–2302.
26. G. Fachinetti, C. Floriani, F. Marchetti, and M. Mellini, *J. Chem. Soc., Dalton Trans.*, 1978, 1398.
27. B. E. Kahn and R. D. Rieke, *Chem. Rev.*, 1988, **88**, 733–745.
28. R. Schobert, F. Maaref, and S. Dürr, *Synlett*, 1995, **1995**, 83–84.
29. W. B. Tolman, Ed., *Activation of Small Molecules: Organometallic and Bioinorganic Perspectives*, Wiley VCH, 2007.
30. R. Choukroun, C. Lorber, C. Lepetit, and B. Donnadieu, *Organometallics*, 2003, **22**, 1995–1997.

31. J. C. Huffman, J. G. Stone, W. C. Krusell, and K. G. Caulton, *J. Am. Chem. Soc.*, 1977, **99**, 5829–5831.
32. N. M. West, A. J. Miller, J. A. Labinger, and J. E. Bercaw, *Coord. Chem. Rev.*, 2011, **255**, 881–898.
33. P. Biloen and W. Sachtler, *Adv. Catal.*, 1981, **30**, 165–216.
34. M. E. Dry, *Catalysis Today*, 2002, **71**, 227–241.
35. H. Schulz, *Applied Catalysis A: General*, 1999, **186**, 3–12.
36. W. A. Herrmann, *Angew. Chem. Int. Ed. Engl.*, 1982, **21**, 117–130.
37. J. M. Manriquez, D. R. McAlister, R. D. Sanner, and J. E. Bercaw, *J. Am. Chem. Soc.*, 1976, **98**, 6733–6735.
38. J. M. Manriquez, D. R. McAlister, R. D. Sanner, and J. E. Bercaw, *J. Am. Chem. Soc.*, 1978, **100**, 2716–2724.
39. P. Berno, C. Floriani, A. Chiesi-Villa, and C. Guastini, *J. Chem. Soc., Chem. Commun.*, 1991, 109–110.
40. C. J. Curtis and R. C. Haltiwanger, *Organometallics*, 1991, **10**, 3220–3226.
41. M. D. Fryzuk, M. Mylvaganam, M. J. Zaworotko, and L. R. MacGillivray, *Organometallics*, 1996, **15**, 1134–1138.
42. P. T. Wolczanski and J. E. Bercaw, *Acc. Chem. Res.*, 1980, **13**, 121–127.
43. C. C. Cummins, G. D. Van Duyne, C. P. Schaller, and P. T. Wolczanski, *Organometallics*, 1991, **10**, 164–170.
44. C. C. Cummins, C. P. Schaller, G. D. Van Duyne, P. T. Wolczanski, A. W. E. Chan, and R. Hoffmann, *J. Am. Chem. Soc.*, 1991, **113**, 2985–2994.
45. M. Horáček, V. Kupfer, U. Thewalt, P. Štěpnička, M. Polášek, and K. Mach, *J. Organomet. Chem.*, 1999, **584**, 286–292.
46. M. H. Chisholm and C. B. Hollandsworth, in *Multiple bonds between metal atoms*, eds. F. A. Cotton, C. A. Murillo, and R. A. Walton, Clarendon Press, 3rd edn. 2005, pp. 203–250.
47. M. H. Chisholm, F. A. Cotton, M. W. Extine, and R. L. Kelly, *J. Am. Chem. Soc.*, 1979, **101**, 7645–7650.
48. M. H. Chisholm, D. M. Hoffman, and J. C. Huffman, *Organometallics*, 1985, **4**, 986–993.
49. M. H. Chisholm, C. E. Hammond, V. J. Johnston, W. E. Streib, and J. C. Huffman, *J. Am. Chem. Soc.*, 1992, **114**, 7056–7065.
50. R. L. Miller, P. T. Wolczanski, and A. L. Rheingold, *J. Am. Chem. Soc.*, 1993, **115**, 10422–10423.
51. M. A. Mironov, in *Isocyanide Chemistry: Applications in Synthesis and Material Science*, ed. V. Nenajdenko, Wiley VCH, 2012, pp. 35–74.
52. L. B. Kool, M. D. Rausch, H. G. Alt, H. E. Engelhardt, and M. Herberhold, *J. Organomet. Chem.*, 1986, **317**, C38–C40.
53. T. Cuenca, R. Gómez, P. Gómez-Sal, and P. Royo, *J. Organomet. Chem.*, 1993, **454**, 105–111.
54. W. Frömberg and G. Erker, *J. Organomet. Chem.*, 1985, **280**, 355–363.
55. P. T. Wolczanski and J. E. Bercaw, *J. Am. Chem. Soc.*, 1979, **101**, 6450–6452.
56. R. A. Walton, *ACS Symp. Ser.*, 1981, **155**, 207.
57. D. D. Klendworth, W. W. Welters, and R. A. Walton, *Organometallics*, 1982, **1**, 336–343.
58. C. J. Cameron, S. M. Tetrack, and R. A. Walton, *Organometallics*, 1984, **3**, 240–247.
59. M. H. Chisholm, J. F. Corning, K. Folting, J. C. Huffman, A. L. Ratermann, I. P. Rothwell, and W. E. Streib, *Inorg. Chem.*, 1984, **23**, 1037–1042.

60. F. A. Cotton, C. A. Murillo, and R. A. Walton, *Multiple Bonds Between Metal Atoms*, Clarendon Press, 3rd edn. 2005.
61. M. H. Chisholm, D. L. Clark, D. Ho, and J. C. Huffman, *Organometallics*, 1987, **6**, 1532–1542.
62. E. M. Carnahan, J. D. Protasiewicz, and S. J. Lippard, *Acc. Chem. Res.*, 1993, **26**, 90–97.
63. F. Takei, K. Yanai, K. Onitsuka, and S. Takahashi, *Angew. Chem. Int. Ed. Engl.*, 1996, **35**, 1554–1556.
64. T. J. Deming and B. M. Novak, *J. Am. Chem. Soc.*, 1993, **115**, 9101–9111.
65. J. Shen, G. P. A. Yap, and K. H. Theopold, *J. Am. Chem. Soc.*, 2014, **136**, 3382–3384.
66. M. Ma, A. Stasch, and C. Jones, *Chem.–Eur. J.*, 2012, **18**, 10669–10676.
67. IPCC, *Climate change 2013: The physical science basis*, Working Group I Contribution to the Fifth Assessment Report of the Intergovernmental Panel on Climate Change, Summary for Policymakers, 2013.
68. M. Aresta, *Carbon Dioxide as Chemical Feedstock*, Wiley, 2010.
69. T. Sakakura, J.-C. Choi, and H. Yasuda, *Chem. Rev.*, 2007, **107**, 2365–2387.
70. H. Arakawa, M. Aresta, J. N. Armor, M. A. Barteau, E. J. Beckman, A. T. Bell, J. E. Bercaw, C. Creutz, E. Dinjus, D. A. Dixon, K. Domen, D. L. DuBois, J. Eckert, E. Fujita, D. H. Gibson, undefined author, D. W. Goodman, J. Keller, G. J. Kubas, H. H. Kung, J. E. Lyons, L. E. Manzer, T. J. Marks, K. Morokuma, K. M. Nicholas, R. Periana, L. Que, J. Rostrup-Nielson, W. M. H. Sachtler, L. D. Schmidt, A. Sen, G. A. Somorjai, P. C. Stair, B. R. Stults, and W. Tumas, *Chem. Rev.*, 2001, **101**, 953–996.
71. M. Cokoja, C. Bruckmeier, B. Rieger, W. A. Herrmann, and F. E. Kühn, *Angew. Chem. Int. Ed. Engl.*, 2011, **50**, 8510–8537.
72. X. Yin and J. R. Moss, *Coord. Chem. Rev.*, 1999, **181**, 27–59.
73. W. Leitner, *Coord. Chem. Rev.*, 1996, **153**, 257–284.
74. D. H. Gibson, *Chem. Rev.*, 1996, **96**, 2063–2096.
75. Z. Lu, Y. Wang, J. Liu, Y.-J. Lin, Z. H. Li, and H. Wang, *Organometallics*, 2013, **32**, 6753–6758.
76. A. Ashley and D. O'Hare, in *Topics in Current Chemistry*, eds. G. Erker and D. W. Stephan, Springer Berlin Heidelberg, 2013, vol. 334, pp. 191–217.
77. C. M. Mömming, E. Otten, G. Kehr, R. Fröhlich, S. Grimme, D. W. Stephan, and G. Erker, *Angew. Chem. Int. Ed. Engl.*, 2009, **48**, 6643–6646.
78. W. J. Evans, J. M. Perotti, J. C. Brady, and J. W. Ziller, *J. Am. Chem. Soc.*, 2003, **125**, 5204–5212.
79. W. J. Evans, C. A. Seibel, and J. W. Ziller, *Inorg. Chem.*, 1998, **37**, 770–776.
80. O. P. Lam and K. Meyer, *Polyhedron*, 2012, **32**, 1–9.
81. B. M. Gardner and S. T. Liddle, *Eur. J. Inorg. Chem.*, 2013, 3753–3770.
82. H. S. La Pierre and K. Meyer, Wiley, 2014, vol. 58, pp. 303–416.
83. J.-C. Berthet, J.-F. Le Maréchal, M. Nierlich, M. Lance, J. Vigner, and M. Ephritikhine, *J. Organomet. Chem.*, 1991, **408**, 335–341.
84. J. G. Brennan, R. A. Andersen, and A. Zalkin, *Inorg. Chem.*, 1986, **25**, 1761–1765.
85. L. Castro, S. Labouille, D. R. Kindra, J. W. Ziller, F. Nief, W. J. Evans, and L. Maron, *Chem.–Eur. J.*, 2012, **18**, 7886–7895.
86. L. Castro, O. P. Lam, S. C. Bart, K. Meyer, and L. Maron, *Organometallics*, 2010, **29**, 5504–5510.
87. L. Castro and L. Maron, *Chem.–Eur. J.*, 2012, **18**, 6610–6615.

88. N. Tsoureas, L. Castro, A. F. R. Kilpatrick, L. Maron, and F. G. N. Cloke, *Chem. Sci.*, 2014, **5**, 3777–3788.
89. P. J. Chirik, *Organometallics*, 2010, **29**, 1500–1517.
90. P. J. Chirik and M. W. Bouwkamp, in *Comprehensive Organometallic Chemistry III*, eds. D. M. P. Mingos and R. H. Crabtree, Elsevier, Oxford, 2007, pp. 243–279.
91. H. G. Alt, K.-H. Schwind, and M. D. Rausch, *J. Organomet. Chem.*, 1987, **321**, C9–C12.
92. C. Jegat, M. Fouassier, M. Tranquille, and J. Mascetti, *Inorg. Chem.*, 1991, **30**, 1529–1536.
93. B. Demerseman, R. Mah, and P. H. Dixneuf, *J. Chem. Soc., Chem. Commun.*, 1984, 1394–1396.
94. V. V. Burlakov, A. V. Polyakov, A. I. Yanovsky, Y. T. Struchkov, V. B. Shur, M. E. Vol'pin, U. Rosenthal, and H. Görls, *J. Organomet. Chem.*, 1994, **476**, 197–206.
95. C. Lefeber, A. Ohff, A. Tillack, W. Baumann, R. Kempe, V. V. Burlakov, U. Rosenthal, and H. Görls, *J. Organomet. Chem.*, 1995, **501**, 179–188.
96. V. V. Burlakov, A. I. Yanovsky, Y. T. Struchkov, U. Rosenthal, A. Spannenberg, R. Kempe, O. G. Ellert, and V. B. Shur, *J. Organomet. Chem.*, 1997, **542**, 105–112.
97. G. Fachinetti, C. Floriani, A. Chiesi-Villa, and C. Guastini, *J. Am. Chem. Soc.*, 1979, **101**, 1767–1775.
98. F. Bottomley, I. J. B. Lin, and M. Mukaida, *J. Am. Chem. Soc.*, 1980, **102**, 5238–5242.
99. V. V. Burlakov, F. M. Dolgushin, A. I. Yanovsky, Y. T. Struchkov, V. B. Shur, U. Rosenthal, and U. Thewalt, *J. Organomet. Chem.*, 1996, **522**, 241–247.
100. D. Santamaría, J. Cano, P. Royo, M. E. G. Mosquera, T. Cuenca, L. M. Frutos, and O. Castaño, *Angew. Chem. Int. Ed. Engl.*, 2005, **44**, 5828–5830.
101. H.-O. Fröhlich and H. Schreer, *Z. Chem.*, 1983, **23**, 348–349.
102. R. Lalrempuia, A. Stasch, and C. Jones, *Chem. Sci.*, 2013, **4**, 4383.
103. A. Noor, S. Qayyum, T. Bauer, S. Schwarz, B. Weber, and R. Kempe, *Chem. Commun.*, 2014, doi:10.1039–C4CC05071A.
104. P. J. Fischer, V. G. Young Jr, and J. E. Ellis, *Chem. Commun.*, 1997, 1249–1250.
105. D. G. Dick, Z. Hou, and D. W. Stephan, *Organometallics*, 1992, **11**, 2378–2382.
106. R. D. Barr, M. Green, J. A. K. Howard, T. B. Marder, I. Moore, and F. G. A. Stone, *J. Chem. Soc., Chem. Commun.*, 1983, 746–748.
107. M. R. Awang, R. D. Barr, M. Green, J. A. K. Howard, T. B. Marder, and F. G. A. Stone, *J. Chem. Soc., Dalton Trans.*, 1985, 2009.
108. G. M. Dawkins, M. Green, K. A. Mead, J.-Y. Salaün, F. G. A. Stone, and P. Woodward, *J. Chem. Soc., Dalton Trans.*, 1983, 527–530.
109. T. E. Hanna, E. Lobkovsky, and P. J. Chirik, *J. Am. Chem. Soc.*, 2004, **126**, 14688–14689.
110. J. A. Timney, *Encyclopedia of Inorganic Chemistry*, 2006.
111. T. E. Hanna, E. Lobkovsky, and P. J. Chirik, *J. Am. Chem. Soc.*, 2006, **128**, 6018–6019.
112. A. K. Brisdon, *Inorganic Spectroscopic Methods*, Oxford University Press, 1998, vol. 62.
113. Y. Yamamoto, *Coord. Chem. Rev.*, 1980, **32**, 193–233.

- 114. S. S. Wreford, M. B. Fischer, J. S. Lee, and E. J. James, *J. Chem. Soc.*, 1981.
- 115. C. P. Horwitz and D. F. Shriver, in *Advances in Organometallic Chemistry*, Academic Press, 1984, vol. 23, pp. 219–305.
- 116. *nist.gov*.
- 117. J. S. Merola, R. A. Gentile, G. B. Ansell, M. Modrick, and S. Zentz, *Organometallics*, 1982, **1**, 1731–1733.
- 118. D. M. Hamilton, W. S. Willis, and G. D. Stucky, *J. Am. Chem. Soc.*, 1981, **103**, 4255–4256.
- 119. R. Ramozzi, N. Chéron, B. Braïda, P. C. Hiberty, and P. Fleurat-Lessard, *New J. Chem.*, 2012, **36**, 1137.
- 120. H. Lindemann and L. Wiegrebe, *Berichte der Deutschen Chemischen Gesellschaft (A and B Series)*, 1930, **63**, 1650–1657.
- 121. J. C. Green, A. F. R. Kilpatrick, and F. G. N. Cloke, *Manuscript in progress*.
- 122. E. L. Muettert, and J. Stein, *Chem. Rev.*, 1979, **79**, 479–490.
- 123. M. R. Smith III, P. T. Matsunaga, and R. A. Andersen, *J. Am. Chem. Soc.*, 1993, **115**, 7049–7050.
- 124. J. W. Faller, R. H. Crabtree, and A. Habib, *Organometallics*, 1985, **4**, 929–935.
- 125. K. Jonas and K. R. Porschke, *224th ACS National Meeting*, 2002.
- 126. K. Jonas, *Report for the Period of January 2000 - December 2001*, Max-Planck-Institut für Kohlenforschung, 2002.
- 127. K. Jonas, *Report for the Period of January 2002 - December 2004*, Max-Planck-Institut für Kohlenforschung, 2005.
- 128. O. T. Summerscales, S. C. Jones, F. G. N. Cloke, and P. B. Hitchcock, *Organometallics*, 2009, **28**, 5896–5908.
- 129. A. F. R. Kilpatrick and F. G. N. Cloke, *Chem. Commun.*, 2014, **50**, 2769–2771.
- 130. D. H. Gibson, M. Ye, and J. F. Richardson, *J. Am. Chem. Soc.*, 1992, **114**, 9716–9717.
- 131. D. H. Gibson, J. M. Mehta, M. Ye, J. F. Richardson, and M. S. Mashuta, *Organometallics*, 1994, **13**, 1070–1072.
- 132. M. Aresta and A. Dibenedetto, *Dalton Trans.*, 2007, 2975.
- 133. C. H. Lee, D. S. Laitar, P. Mueller, and J. P. Sadighi, *J. Am. Chem. Soc.*, 2007, **129**, 13802–13803.
- 134. J. Evans, *J. Chem. Soc.*, 1959, 2003–2005.
- 135. E. M. Schubert, *J. Chem. Educ.*, 1992, **69**, 62.

6 CHAPTER SIX: Reactivity of $(\mu:\eta^5, \eta^5\text{-Pn}^\dagger)_2\text{Ti}_2$ with Heteroallenes and E–E Bonds

6.1 Introduction

"There is the implicit conviction, or perhaps the hope, that through the study of related molecules (e.g. CS₂ and COS) on comparable transition-metal systems, some understanding of the reaction chemistry of these molecules and perhaps of CO₂ will be forthcoming."

J. A. Ibers. Centenary Lecture delivered at Queen's College, Belfast, 27 April 1981.¹

$(\mu:\eta^5, \eta^5\text{-Pn}^\dagger)_2\text{Ti}_2$ (**4.3**) shows exceptional reactivity amongst di-metal bis(pentalene) double sandwich complexes,²⁻⁹ including multiple adduct formation with carbon monoxide and reductive activation of carbon dioxide.¹⁰ Mechanistic studies show that **4.3** binds CO₂ at low temperatures, however, this adduct is thermally unstable and upon warming to room temperature reaction of the coordinated molecule occurs. Investigations in the reactivity of **4.3** with heteroallenes and other organic substrates containing heteroatoms (E) were undertaken a view to forming more stable adducts and exploring the scope for reductive transformations at the $[\text{Ti}_2]^{4+}$ core.

Heteroallenes are unsaturated molecules of general formula X=Y=Z where at least one of the functional atoms X, Y or Z is a heteroatom, most commonly N, O, S or P. These molecules are commonly used to model the reactivity of CO₂,¹¹ however the reactivity of heteroallenes can be strongly influenced by the electronegativity of the functional atoms and the electronic effects of the attached substituents.¹² Examples of the reactivity of the heteroallenes and organic molecules containing heteroatoms relevant to the current study will be briefly summarised.

6.1.1 Carbon disulfide and carbonyl sulfide

CS₂ is a versatile ligand and its coordination chemistry with transition metals is generally more extensive than that of CO₂.^{1,13-16} M–CS₂ complexes have a greater stability relative to that of M–CO₂ complexes, which tend to undergo further conversion

via insertion into M–E bonds,¹⁷ or metal-promoted C=O bond cleavage.^{18,19} Transition metal CS₂ complexes are also more stable in comparison to those of COS,^{16,20} due to the stronger C=S double bond of CS₂ (Table 6.1). Hence COS can function as a good sulfur transfer agent in the presence of a thiophilic metal complex, such as those of the early transition metals²¹ or f-block metals.²²

Table 6.1 Selected properties of CO₂, CS₂ and COS.

	CO ₂	CS ₂	COS	ref
Point group	$D_{\infty h}$	$D_{\infty h}$	$C_{\infty v}$	23
Bond length (Å)	1.162 (C–O)	1.554 (C–S)	1.160 (C–O) 1.560 (C–S)	24
Bond energy (eV)	5.453	4.463	3.12 (OC–S) 6.81 (O–CS)	25,26
IR data (cm ^{–1})	2349 677	1535 397	2062 859 520	27

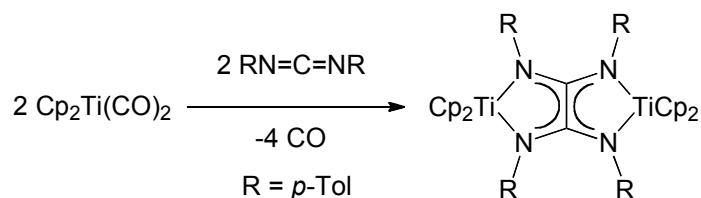
Simple carbon disulfide adducts of titanium have been prepared by the reaction of Cp₂Ti(PMe₃)₂ and Cp₂Ti(η³-allyl)₂ with CS₂ to afford Cp₂Ti(η²-CS₂)(PMe₃)²⁸ and Cp₂Ti(η²-CS₂)²⁹ respectively. These compounds precluded structural characterisation, however a ‘side-on’ coordination mode of CS₂ was proposed on the basis of IR spectroscopy. The observed ν(CS) IR bands at *ca.* 1100 cm^{–1} are considerably lower than that of free CS₂ (1535 cm^{–1}),²⁷ suggesting a reduction in the C–S bond order.

The reaction of Cp₂Ti(CO)₂ with neat CS₂ results in ‘head to head’ reductive coupling to give diamagnetic [Cp₂Ti]₂(μ-η²:η²-C₂S₄) in high yield. In contrast, the [C₂O₄]^{2–} and [C₂(NR)₄]^{2–} bridged titanocene analogues are paramagnetic and consistent with two non-interacting Ti(III) centres.^{30,31} On the basis of magnetic data, electrochemical and XRD studies, the C₂S₄ moiety was classed as a strong electron acceptor, with a formal oxidation state intermediate between the tetrathiooxalate [C₂S₄]^{2–} and the ethylenetetrathiolate [C₂S₄]^{4–} extremes. Such electron delocalising abilities of [C₂S₄]^{n–}

ligands have subsequently been applied in materials chemistry as the conducting units in multimetallic complexes.³²⁻³⁴

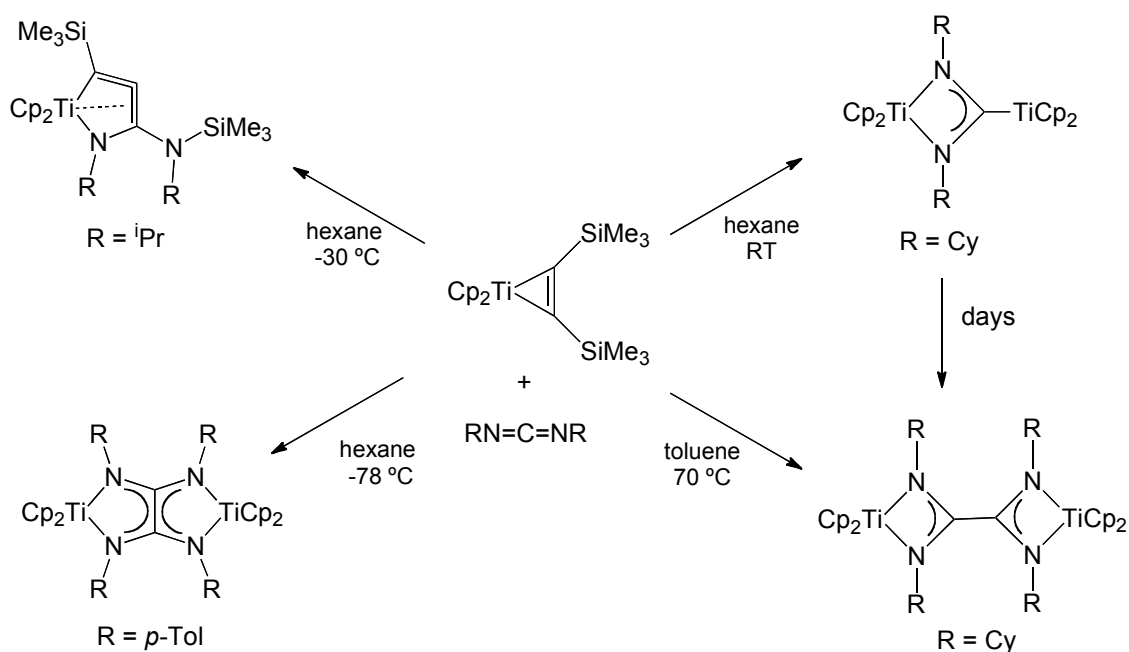
6.1.2 Carbodiimides

Carbodiimides ($X = Z = \text{NR}$, $Y = \text{C}$) have been widely studied as model molecules for the reductive transformations of CO_2 ,³⁵⁻³⁷ and have shown particularly varied reactivity with low valent titanium complexes.^{38,39} For example, Floriani *et al.* reported the reductive coupling of 1,3-*N,N'*-di-*p*-tolylcarbodiimide (*p*-TCD) by $\text{Cp}_2\text{Ti}(\text{CO})_2$ to the delocalised $\eta^2:\eta^2$ -tetra-*p*-tolylloxalylamidine $[\text{C}_2(\text{NR})_4]^{2-}$ ligand, bridging two Ti(III) centres (Scheme 6.1).^{40,41}



Scheme 6.1 Reductive coupling of carbodiimide by a Ti(II) complex.^{40,41}

Recent studies by Rosenthal *et al.* using titanocene(II) alkyne complexes with a variety of different RNCNR' substrates have resulted in insertion, isomerisation, or C–C coupling of the applied carbodiimide depending on the substituents R and R', to form unusual mono-, di-, and tetranuclear Ti(III) complexes.⁴² Theoretical analysis by these researchers suggested a four-membered heterometallacycloallene as a likely intermediate in these reactions.⁴³ However, attempts at isolation of this mononuclear carbene-like species failed, and instead reductive coupling or complexation with another titanocene fragment occurred, yielding bimetallic complexes.⁴⁴



Scheme 6.2 Carbodiimide reactivity with a Ti(II) alkyne complex.⁴²

The tungsten(III) alkoxide dimers, $\text{W}_2(\text{OR})_6$ ($\text{R} = \text{iBu}$ and CMe_2CF_3), form stable 1:1 adducts with $\text{R}'\text{NCNR}'$ ($\text{R}' = p\text{-Tol}$, Cy , iPr) in which the bridging carbodiimide lies parallel to the $\text{M}-\text{M}$ axis in a $\mu:\eta^2, \eta^2$ - fashion (Figure 6.1, left).⁴⁵⁻⁴⁷ As an illustrative example, the X-ray structure of $\text{W}_2(\text{O}^t\text{Bu})_6(\mu\text{-}\{p\text{-Tol}\}\text{NCN}\{p\text{-Tol}\})$ shows a longer $\text{M}-\text{M}$ distance ($2.482(1) \text{ \AA}$) in comparison to $\text{W}_2(\text{O}^t\text{Bu})_6$ (av. $2.332(1) \text{ \AA}$)⁴⁸ and its 4-methylpyridine adduct $\text{W}_2(\text{O}^t\text{Bu})_6(4\text{-Me-py})_2$ ($2.397(1) \text{ \AA}$).⁴⁷ The deviation of the carbodiimide CNCNC chain from linearity (angle $\text{N}-\text{C}-\text{N} = 154.0(2)^\circ$) is consistent with a partially reduced carbodiimide ligand. A simplified bonding picture was proposed involving a combination of the heteroallene π -system (both bonding and non-bonding components, occupied by 4 electrons) with two singly occupied d-orbitals previously involved in $\text{M}-\text{M}$ π -bonding (Figure 6.1, right).⁴⁵ This description results in a three-centre two-electron bond extending over the two W atoms and the central C atom, and two $\text{W}-\text{N}$ single bonds, consistent with the short $\text{M}-\text{C}$ and $\text{M}-\text{N}$ and distances observed experimentally. Fenske-Hall calculations on the related allene adduct, $[\text{W}_2(\text{OH})_6(\text{C}_3\text{H}_4)]$, also show extensive mixing of $\text{W}(\text{d}\pi)-\text{W}(\text{d}\pi)$ and allene $p\pi$ orbitals in the HOMO.⁴⁹

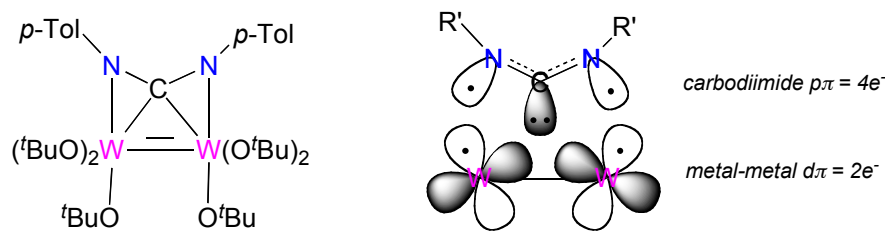


Figure 6.1 Simplified bonding description of W_2 carbodiimide adducts.⁴⁵

In contrast to the facile insertion chemistry reported for $W_2(OR)_6$ complexes with CO_2 and isocyanates,^{50,51} the carbodiimide adducts showed no further reactivity with excess carbodiimide or at elevated temperatures, and failed to react with other substrates ($PhNCO$, PMe_3 , LiO^tBu , LiO^iPr , CO or CO_2) which was attributed to the bulky nature of the diimide.⁴⁶

6.1.3 Organic Isocyanates

Organic isocyanates, $RN=C=O$, have also been studied as reagents for modeling the reactivity of CO_2 , since the introduction of an amido (RN) group results in polarization of the double bonds and thus increased reactivity.⁵² Floriani *et al.* reported the conversion of phenylisocyanate into the diphenylurelyene(2-) ligand, which was found coordinated in three different ways to one or more Ti centres (Figure 6.2).⁵³

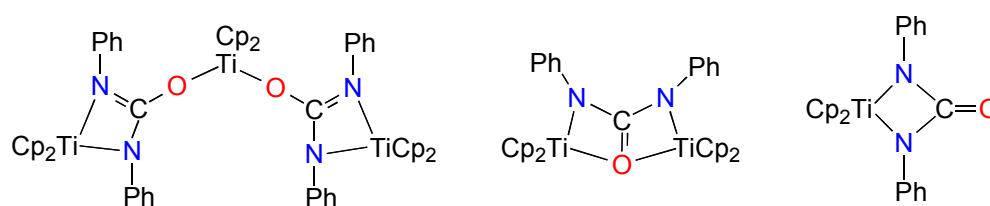
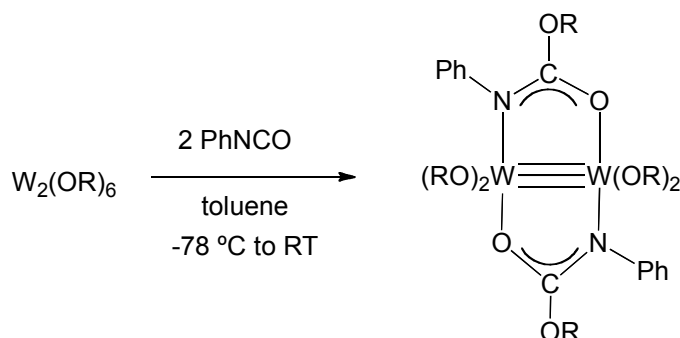


Figure 6.2 Coordination modes of $[(PhN)_2CO]^{2-}$ to titanocene moieties, formed from reductive coupling of $PhNCO$ by $Cp_2Ti(CO)_2$.⁵³

In 1985 Cotton *et al.* reported the structure of M–M bonded di-tungsten complex $W_2(O^tBu)_6(\mu-OCNPh)$, in which the isocyanate behaves as a side-on bridging ligand across the M_2 core, in a very similar manner to the carbodiimide adduct $W_2(O^tBu)_6(\mu-C(NR)_2)$.^{45,46} Complex $W_2(O^tBu)_6(\mu-OCNPh)$ was identified as the low-temperature

intermediate in the reaction of $W_2(O^tBu)_6$ with two equivalents of $PhNCO$,⁵¹ which yielded $W_2(O^tBu)_4[\mu-PhNC(O)O^tBu]_2$ after warming to room temperature (Scheme 6.3). The formation of the monanionic carbamato ester ligand is postulated to proceed *via* a nucleophile-induced migratory insertion of the coordinated alkoxide ligand.⁵⁴



Scheme 6.3 Reaction of phenyl isocyanate with a W(III) alkoxide dimer.^{51,54}

More recently Jones *et al.* have used the β -diketiminate coordinated Mg(I) dimers $(L)_2Mg_2$ ($L = [(ArN^tBu)_2CH_2]$) to facilitate the reductive C–C coupling of *tert*-butyl isocyanate. The Mg(I) dimer with $Ar = 2,6\text{-}^iPr_2C_6H_3$ (= Dip) reacts with two equivalents of tBuNCO to give an *N,N'*-di-*tert*-butyl-oxalamide(2-) coupled product, with an unprecedented *N,O/O,O'* ligation to two $Mg(L)$ fragments (Figure 6.3, left).⁵⁵ The same bridging $[O_2C_2N_2^tBu_2]^{2-}$ moiety is formed in the reaction of tBuNCO with the $Ar = 2,4,6\text{-}Me_3C_6H_2$ (= Mes) complex, however it exhibits delocalisation over its NCO units and coordinates two $Mg(L)$ fragments in an *N,N'/O,O'*-mode (Figure 6.3, right).⁵⁶ These researchers reasoned that the different ligating modes was due to sterics, since the $(L)Mg$ moiety with $Ar = Mes$ and allows for closer approach of the bulky N^tBu units in an *N,N'*-chelate ring, which is disfavoured for the comparatively larger $Ar = Dip$ complex.

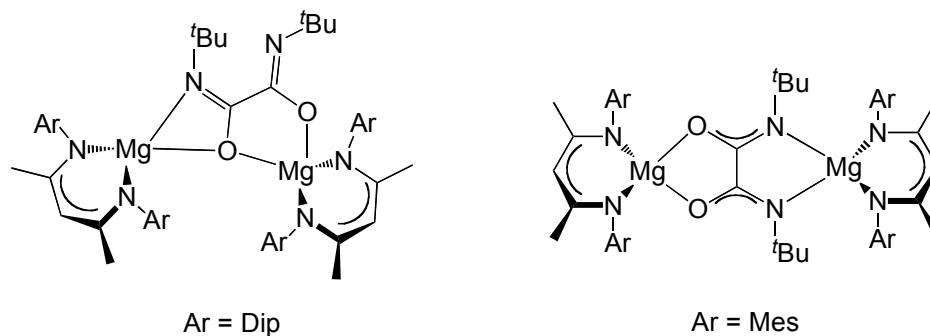


Figure 6.3 Coordination modes of $[O_2C_2N_2^tBu_2]^{2-}$ ligand to $Mg(II)$ moieties.^{55,56}

6.1.4 Homonuclear E–E bonds; Organic dichalcogenides and azobenzene

Organic dichalcogenides, R_2E_2 ($E = S, Se, Te$; $R = \text{alkyl or aryl}$) are commonly employed as redox active substrates with low valent metal complexes including those of early transition metals.⁵⁷⁻⁵⁹ Other examples include lanthanides $Yb(II)$ ^{60,61} and $Sm(II)$,^{62,63} and more recently $U(III)$ ⁶⁴ and low-valent Th .⁶⁵ With highly reducing metal complexes E–E bond cleavage of the dichalcogenide routinely occurs to yield a complex bearing the respective chalcogenoate $(RE)^-$ ligands (Equation 6.1).

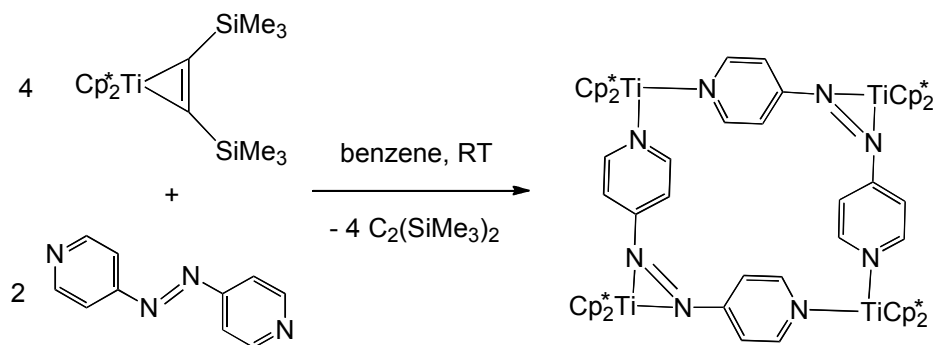


As part of their extensive investigations into the reactions of early d-block metallocenes,⁶⁶ Floriani *et al.* reported in 1974 the oxidative addition of organic disulfides to $Cp_2Ti(CO)_2$, yielding Ti(IV) dithiolate complexes $Cp_2Ti(SR)_2$.⁵⁷ Song *et al.* have extended this chemistry by treatment of an *in situ* generated ‘ Cp_2Ti ’ synthon with organic diselenides to afford Ti(IV) alkyl and aryl diselenolate complexes, $Cp_2Ti(SeR)_2$, in high yields.⁵⁹ While the first example of a tellurolate congener, $Cp_2Ti(TePh)_2$, also dates back to 1974,⁶⁷ complexes of this type remain very rare and are typically synthesised by salt metathesis routes from the corresponding titanocene(IV) dichloride with organotellurolate Li or MgBr salts.⁶⁸⁻⁷⁰ More recently Reid *et al.* have shown titanocene(IV) complexes with di(selenolate) ligands $Cp_2Ti(SeR)_2$ to be suitable as precursors for single source low pressure chemical vapour deposition (CVD) of $TiSe_2$ thin films,⁷¹ which are attracting great attention for their intriguing electronic properties^{72,73} and application in 2D inorganic materials.⁷⁴⁻⁷⁶

Diphenylchalcogenides present easily reducible ‘test cases’ for E–E bond activation, however the formal potential of the $Ph_2E_2/2(EPh)^-$ couple is system dependent and cannot be rationalised straightforwardly. For example irreversible reduction potentials for Ph_2S_2 and Ph_2Se_2 were measured at -1.6 and -0.9 V respectively vs $Ag/AgNO_3$ in $DME/[^nBu_4N][ClO_4]$,⁷⁷ and irreversible Ph_2Te_2 reduction has been observed at -1.06 V vs SCE in $CH_2Cl_2/[^nBu_4N][ClO_4]$.⁷⁸ However subsequent studies by Ludvík *et al.* have shown that Ph_2Se_2 and Ph_2Te_2 react with mercury electrodes, which may lead to erroneous formal potentials (E°) being quoted.⁷⁹

The redox chemistry of azobenzene, $PhN=NPh$, with low-valent metal complexes has been widely studied.⁸⁰ Floriani *et al.* reported the synthesis of a *cis*-azobenzene adduct of titanocene, $Cp_2Ti(\eta^2-N_2Ph_2)$, by the reaction of $Cp_2Ti(CO)_2$ with Ph_2N_2 .^{81,82}

Subsequent *ab initio* MO calculations suggest this diamagnetic complex is best described as a 1,2-diphenylhydrazido(2-) ligand and a formally Ti(IV) centre.⁸³ Recent work by Beckhaus *et al.* has utilised this preference for *cis*-azo ligation to titanocene fragments to synthesise supramolecular squares (Scheme 6.4).⁸⁴



Scheme 6.4 Synthesis of supramolecular squares by *cis*-azo ligation to decamethyltitanocene units.⁸⁴

The reaction of the Ti(III) complex CpTiCl_2 with azobenzene formed a dimeric complex, $[(\text{CpTiCl})_2(\mu\text{-PhN})(\mu\text{-Ph}_2\text{N}_2)]$, which features both a bridging 1,2-diphenylhydrazido(2-) and a bridging phenylimido(2-) ligand (Figure 6.4), the latter resulting from $\text{N}=\text{N}$ bond cleavage promoted by Ti(III).⁸⁵

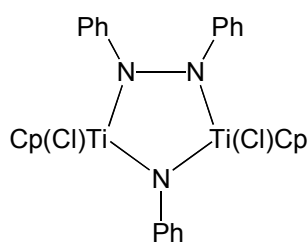
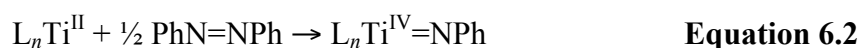


Figure 6.4

There are also several examples of azobenzene reduction and cleavage leading to terminal phenylimido complexes in Ti chemistry,⁸⁶⁻⁹⁰ which constitutes a four-electron process per azobenzene (Equation 6.2).



Azobenzene is known to undergo two one-electron reductions in non-aqueous solvents such as acetonitrile, pyridine, and dimethylformamide, with E° values in the ranges -1.35 to -1.41 V and -1.75 to -2.03 V vs SCE depending on the solvent.⁹¹ Given the high reducing potential for the $[\text{Ti}_2]^{5+}/[\text{Ti}_2]^{4+}$ couple ($E_{1/2} = -2.50$ V vs $\text{FeCp}_2^{+/0}$ or -1.94 V vs SCE)⁹² it is reasonable that **4.3** should be able to reduce azobenzene to both the monoanion and the dianion.

6.2 Reactivity of **4.3** with Heteroallenes

6.2.1 Synthesis and characterisation of $(\mu:\eta^5, \eta^5\text{-Pn}^\dagger)_2\text{Ti}_2(\mu:\eta^2, \eta^2\text{-CS}_2)$ (**6.1**)

Given the transient nature of the intermediates identified in the reaction of **4.3** with CO_2 , the reactivity with CS_2 as a model molecule was explored. Treatment of a pentane solution of **4.3** with CS_2 at -35 °C, gave a dark green solution upon warming to room temperature. Subsequent work-up and cooling to -35 °C produced a red microcrystalline solid in 62% yield, which was identified by spectroscopic and analytical methods as **6.1**. Crystals suitable for X-ray studies were grown from Et_2O solution and the molecular structure (Figure 6.5) reveals a bent CS_2 molecule in a $\mu:\eta^2, \eta^2$ - binding mode between two Ti centres.

The CS_2 ligand in **6.1** is bent with an S–C–S angle of $137.4(3)^\circ$ while the C–S bond lengths (av. $1.657(4)$ Å) are longer than the C–S bond length of free CS_2 (1.554 Å).²⁴ The double-sandwich structure remains intact, with an elongated Ti–Ti distance ($2.4432(10)$ Å) with respect to **4.3** ($2.399(2)$ Å), and a smaller angle between the pentalene rings and the Ti_2 unit (av. $\text{Ct–Ti–Ct} = 138.02(9)^\circ$), giving a more open sandwich structure. The ring slippage parameters for each metal ($\Delta_{\text{Ti1}} = 0.145, 0.092$; $\Delta_{\text{Ti2}} = 0.138, 0.082$) indicate differential bonding to each side of the pentalene ligand. This feature has been observed to a greater extent in the permethylpentalene complex $(\mu\text{-}\eta^5, \eta^3\text{-Pn}^*)_2\text{Co}_2$ ($\Delta_{\text{Co}} = 0.367, 0.089$), in which the Co centres are too far apart (2.491 Å) to support a metal-metal bond.⁷ The distance between the Ti and S atoms (av. $2.497(16)$ Å) is larger than the sum of their covalent radii (0.239 Å),⁹³ however there is an interaction in place.

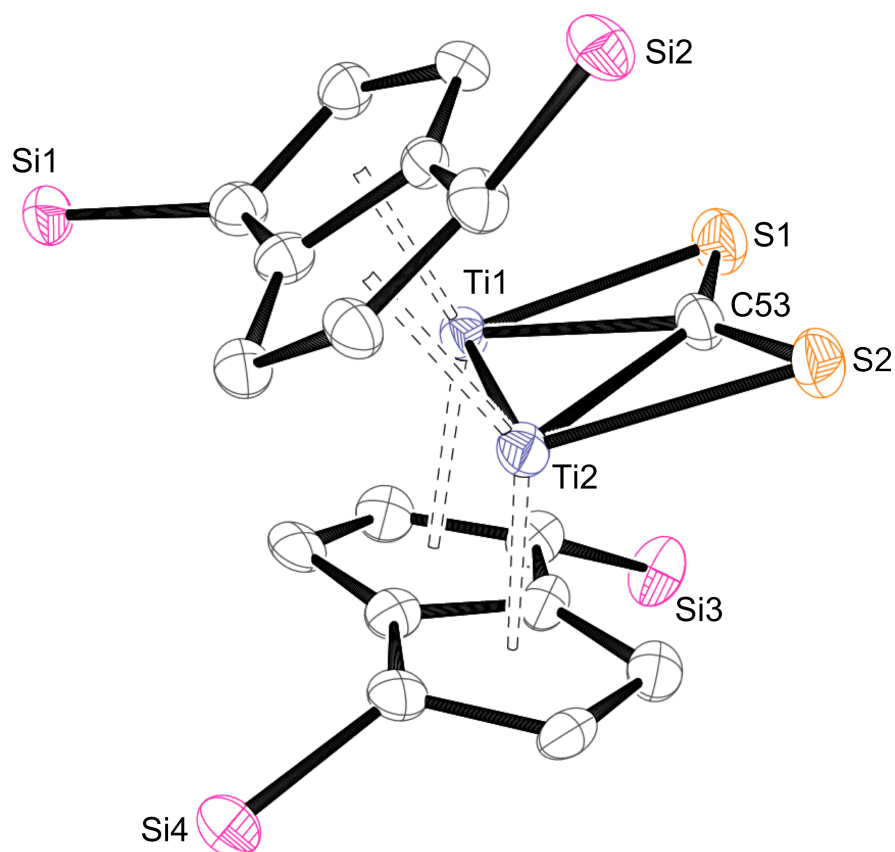


Figure 6.5 ORTEP (50% probability) diagram of **6.1**. H atoms and ⁱPr groups omitted for clarity.

Table 6.2 Selected distances (Å), angles (°) and parameters for **6.1**. Ct denotes the η⁵-centroid of the Pn ring.

Parameter	6.1	Parameter	6.1
Ti1–Ti2	2.4432(10)	Ti–Ct ^a	2.104(13)
Ti1–C53	2.230(4)	Ti–C _{ring} ^a	2.428(4)
Ti2–C53	2.245(4)	∠ ^a	0.114(4)
Ti1–S1	2.4915(16)	S1–C53–S2	137.4(3)
Ti2–S2	2.5032(15)	Ti1–C53–Ti2	66.18(13)
C53–S1	1.649(4)	Ct–Ti–Ct ^a	138.02(9)
C53–S2	1.664(4)	Twist angle	20.8(2)

^aAverage values.

Geometry optimisation of $\text{Pn}_2\text{Ti}_2\text{CS}_2$ resulted in structure **6.I** (Figure 6.6),⁹⁴ which is in good agreement with the experimental structure. The calculated MOs show that one Ti–Ti bonding orbital ($19a_1$) remains intact, which is also the case for the CO_2 adduct **5.VII**. However the CS_2 bonding orbital ($18a_1$) is more delocalised and multicentred than in **5.VII**, consistent with sulfur acting as a better donor to the proximal titanium atoms.

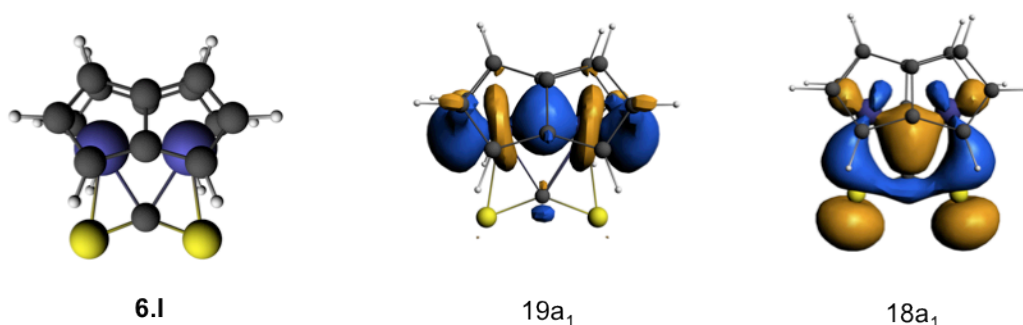


Figure 6.6 Calculated structure of **6.I** and its Ti–Ti bonding orbital ($19a_1$) and $\text{Ti}_2\text{--CS}_2$ bonding orbital ($18a_1$).⁹⁴

The solution IR spectrum of **6.1** shows a band at 1104 cm^{-1} which, compared to the asymmetric stretch of free CS_2 (1535 cm^{-1}),²⁷ is consistent with a sulfur bound CS_2 moiety. This is in fair agreement with the stretching vibration for model system **6.I** (1079 cm^{-1}) calculated by DFT methods.⁹⁴ Precedent for this type of CS_2 coordination involving both C=S π -bonds is limited to a single example, of a dinuclear Cu(I) complex, recently reported by Limberg *et al.*⁹⁵ However in this complex the mean plane of the CS_2 atoms is twisted (49.1°) with respect to the M–C–M mean plane, whereas for **6.1** it is near parallel (3.1°). The solid state structure of **6.1** provides supporting evidence for the doubly bridging CO_2 ligand in **5.7**, as modeled by calculated structure **5.VII** (Section 5.3.2). However **6.1** is stable at room temperature and does not decompose even upon heating at $100\text{ }^\circ\text{C}$, in stark contrast to CO_2 adduct **5.7** which decomposes above $-30\text{ }^\circ\text{C}$ to give μ -oxo complexes with concomitant liberation of carbon monoxide. This may be explained by the relative stability of CO compared with CS ($\Delta_f H_{298\text{ K}}^0 = -110.5$ and 276.5 kJ mol^{-1} respectively)^{96,97} and the driving force for

Ti–O bond formation ($\Delta_{\text{bond}}H^0_{298\text{ K}} = 672.4 \pm 9.2 \text{ kJ mol}^{-1}$) relative to Ti–S ($\Delta_{\text{bond}}H^0_{298\text{ K}} = 418 \pm 3 \text{ kJ mol}^{-1}$).⁹⁸

6.2.2 Reactivity studies with COS

The notable difference in the reactivity of CS₂ versus CO₂ with **4.3**, prompted a study with COS. Reaction of **4.3** with one equivalent of COS at -78 °C in methylcyclohexane-*d*₁₄ produced a metastable adduct (**6.2**) that shows a ¹H NMR spectrum consistent with the loss of C₂ molecular symmetry, as opposed to that of the C₂ symmetric species **5.7** and **6.1**. The ¹³C{¹H} NMR spectrum of **6.2** shows a singlet at 282 ppm, a value intermediate between the CO₂ and CS₂ analogues (219 and 356 ppm respectively). *In situ* IR spectroscopy at -65 °C shows a band at 1498 cm⁻¹ which is tentatively assigned to the ν(CO) stretch of coordinated COS, and is in good agreement with the stretching vibration for model system **6.II** (1487 cm⁻¹) calculated by DFT methods (Figure 6.7, left).⁹⁴

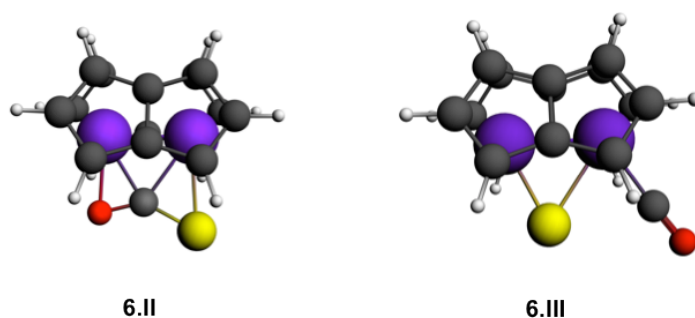


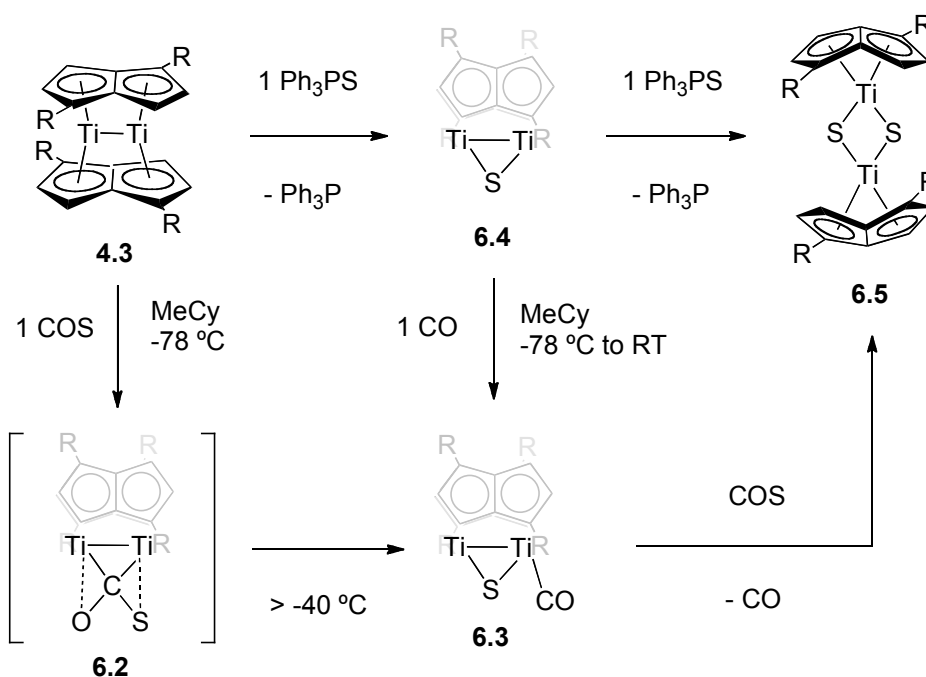
Figure 6.7 Calculated structures for Pn₂Ti₂(COS) and Pn₂Ti₂(S)(CO).⁹⁴

However the COS adduct **6.2** proved to be more thermally unstable than that of CO₂ (**5.7**), and the coordinated molecule undergoes scission to a mono(μ-S) mono(CO) species **6.3**, in 41% conversion by ¹H NMR at -40 °C. Intermediate **6.3** was independently prepared by reaction of mono(μ-S) complex **6.4** with one equivalent of CO; **6.4** itself was readily synthesised by the reaction of **4.3** with Ph₃PS (Scheme 6.5), and fully characterised by spectroscopic and analytical methods (*vide infra*).

The mono(μ-S) mono(CO) intermediate **6.3** precluded isolation in the solid state but was characterised by spectroscopic methods. *In situ* IR spectroscopy shows a broad band at 2011 cm⁻¹, in the expected region for a terminal CO ligand, that shifts to 1966 cm⁻¹ in the isotopically labeled ¹³C-**6.3**. The ¹H NMR spectrum of **6.3** consists of four doublets in the aromatic region, indicative of chemically equivalent Pn[†] rings on

the NMR timescale. This can be attributed to a fluxional process involving intramolecular exchange of CO between the two Ti centres in a similar manner to tri-carbonyl species **5.3** which also shows an averaged NMR structure of C_2 symmetry.

In the presence of excess of COS, green solutions of **6.3** decompose within hours at room temperature to give a brown solution (Scheme 6.5). ^1H NMR spectroscopy of the brown solution showed near quantitative conversion to the bis(μ -sulfide) bridged dimer $[(\eta^8\text{-Pn}^\dagger)\text{Ti}(\mu\text{-S})]_2$ (**6.5**) as the sole Ti-containing product, in contrast to the decomposition of CO_2 adduct **5.7** which also gives di-carbonyl complex **5.2**. The reasons for this difference in product outcomes is unclear, since **6.3** does not show sufficient lifetime to be isolated free from other the products in this complex reaction sequence, and has not been structurally verified by X-ray crystallography. The related oxo-species, $\text{Pn}_2\text{Ti}_2(\text{O})(\text{CO})$, was implicated in the DFT modelled pathway of the CO_2 reaction, but was not observed by *in situ* IR or NMR spectroscopy experiments.



Scheme 6.5 Reactivity of **4.3** with COS and Ph_3PS . $R = \text{Si}^i\text{Pr}_3$.

6.2.3 Synthesis and characterisation of $(\mu:\eta^5, \eta^5\text{-Pn}^\dagger)_2\text{Ti}_2(\mu\text{-S})$ (**6.4**)

Synthesis of compound **6.4** was achieved by reaction of **4.3** with one equivalent of Ph_3PS in toluene (Scheme 6.5), which following work-up, was isolated as red crystals in 52% yield. The mass spectrum for mono-sulfide **6.4** shows the expected molecular ion ($m/z = 957$), together with peaks corresponding to di-sulfide **6.5** ($m/z = 989$) and $(\text{Pn}^\dagger)_2\text{Ti}$ ($m/z = 877$), suggesting ligand redistribution occurs under EI-MS conditions. However the proposed formulation of **6.4** is consistent with (^1H , ^{13}C , ^{29}Si) NMR and elemental analysis data, and was ultimately confirmed by a single crystal XRD study. The molecular structure of **6.4** (Figure 6.8) shows the sulfide ligand bridging two Ti centres in a three-membered ring, akin to mono(μ -oxo) complex **5.8**. The Ti–Ti bond is considerably longer in **6.4** than **5.8** (2.4880(8) and 2.3991(7) Å respectively), and the larger bridging chalcogen atom is bonded at a greater distance from the Ti_2 core (av. Ti–S = 2.3728(8) cf. Ti–O = 1.8607(15) Å) with a more acute Ti–E–Ti angle ($62.68(4)^\circ$ and $80.28(8)^\circ$ respectively). However smaller values of Ti–Ct, ring slippage (Δ) and the twist angle for **6.4** reflect that the Pn^\dagger ligands are more tightly bound compared with **5.8** and this may explain the relative stability of this mono(μ -S) complex.

This triangular M–S–M structural motif is common amongst binuclear complexes with thiolato bridges, but is unique in titanocene mono-sulfide chemistry. For example $[\text{Cp}^*\text{Ti}]_2(\mu\text{-S})$ is a green paramagnetic complex with Ti...Ti separation of 4.7069(7) Å and a Ti–S–Ti angle of $174.37(4)^\circ$.⁹⁹ The lack of a bonding (or an antiferromagnetic coupling) interaction between the two d^1 centres in $[\text{Cp}^*\text{Ti}]_2(\mu\text{-S})$ gives rise to a electronic triplet state. In contrast, both **6.4** and **6.3** are diamagnetic.

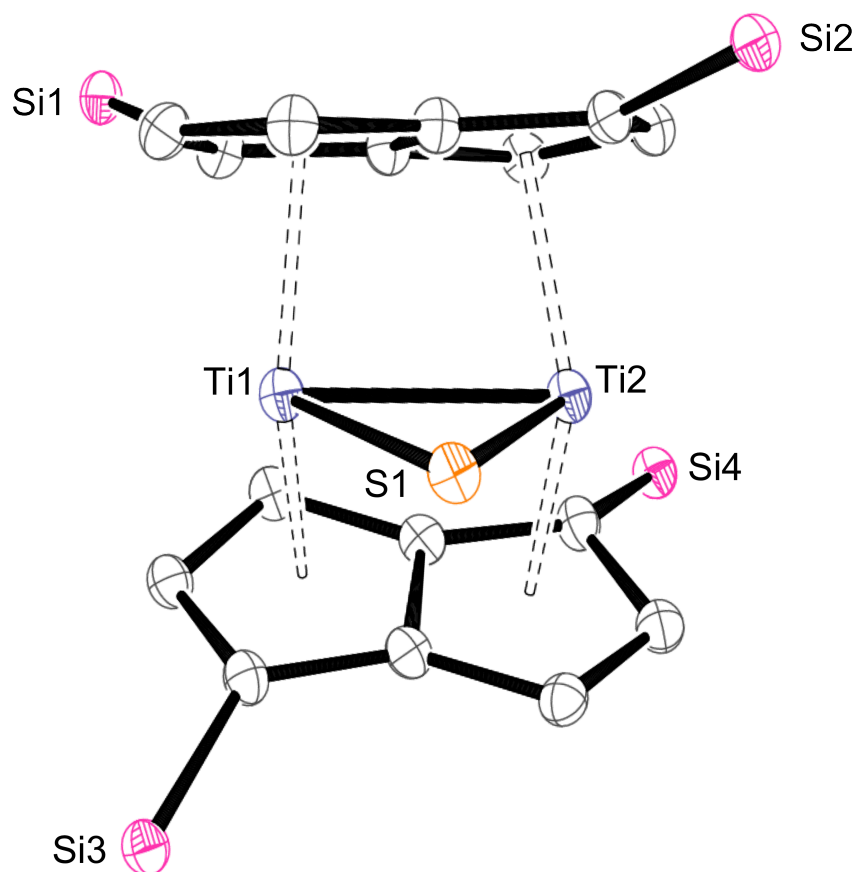


Figure 6.8 ORTEP (30% probability) diagram of **6.4**. H atoms and ⁱPr groups omitted.

Table 6.3 Selected interatomic distances (Å), angles (°) and parameters for **6.4**.
Ct denotes the η^5 -centroid of the Pn ring.

Parameter	6.4	Parameter	6.4
Ti1–Ti2	2.4880(8)	Ti1–S1–Ti2	62.68(4)
Ti1–S1	2.3728(8)	S1–Ti1–Ti2	58.72(3)
Ti–Ct ^a	2.1088(13)	Ct–Ti–Ct ^a	137.11(5)
Ti–C _{ring} ^a	2.436(2)	Fold angle	3.86(8)
Δ ^a	0.135(2)	Twist angle	20.28(15)

^a Average values.

6.2.4 Synthesis and characterisation of $[(\eta^8\text{-Pn}^\dagger)\text{Ti}(\mu\text{-S})]_2$ (**6.5**).

The bis(μ -sulfide) complex (**6.5**) was independently synthesised by the reaction of **4.3** with two equivalents of Ph_3PS in toluene (Scheme 6.5), and isolated in 80% yield. NMR spectroscopy, mass spectrometry and elemental analysis confirmed the identity and purity of the product. Single crystals suitable for X-ray diffraction analysis were grown from a saturated Et_2O solution at -35°C , and its molecular structure is depicted in Figure 6.9 with important structural parameters listed in Table 6.4. Complex **6.5** crystallises in the tetragonal space group $P4_2/nbc$ and is highly symmetrical; the asymmetric unit contains one quarter-molecule of the constituent dimer, giving rise to a Ti_2S_2 unit which makes a regular ring which has a perfectly planar diamond core (torsion angle $\text{Ti1-S1-Ti1'-S1}' = 0^\circ$). However there is significant asymmetry in the Ti-S bond lengths (2.2238(16) and 2.4227(16) Å). The Ti-S-Ti angle is relatively acute ($84.92(6)^\circ$), yet the Ti...Ti distance is considerably longer than in the bis(μ -oxo) congener (2.7376(6) Å).¹⁰ The relative orientation of the η^8 -pentalene ligands (as defined by the angles between the two bridgehead C-C vectors) is $21.1(5)^\circ$.

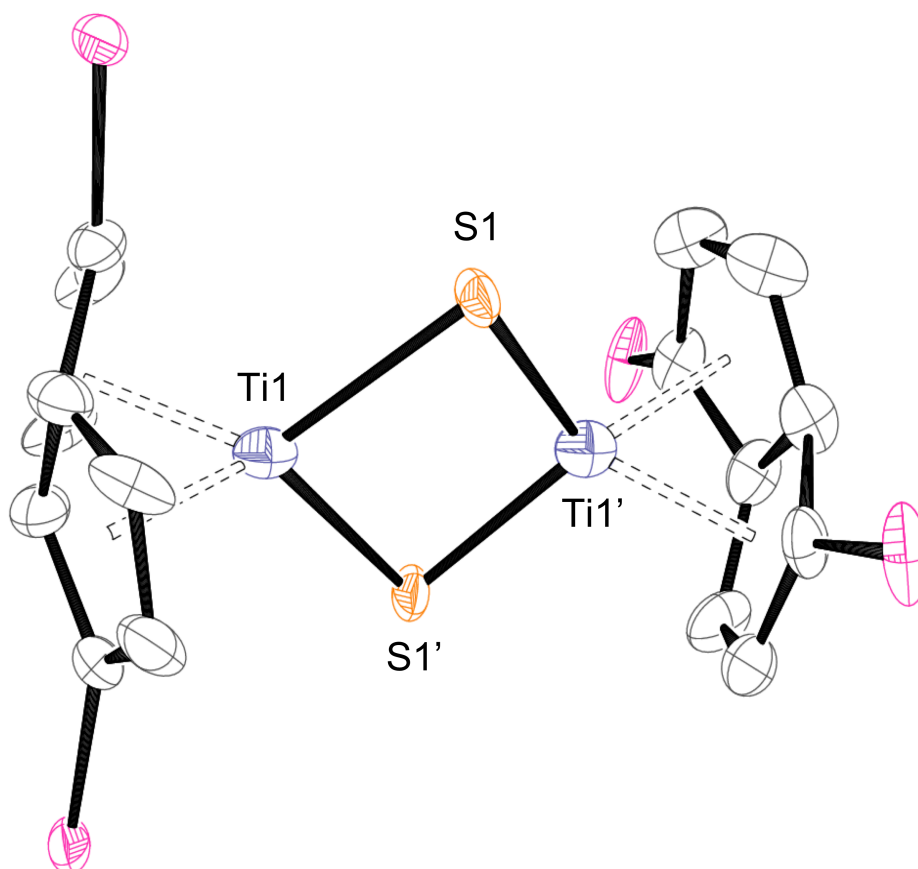


Figure 6.9 ORTEP (30% probability) diagram of **6.5**. H atoms and ⁱPr groups omitted for clarity. Ct1 and Ct1' are the η^5, η^5 -centroids of the Pn ring.

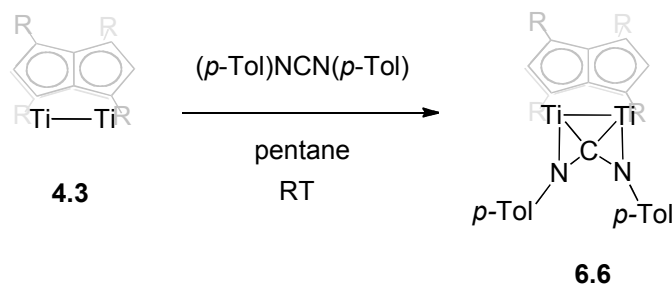
Table 6.4 Selected interatomic distances (Å) and angles (°) for **6.5**. Ct denotes the η^5 -centroid of the Pn ring.

Parameter	6.5	Parameter	6.5
Ti1··Ti1'	3.1402(6)	Ti1–S1–Ti1'	84.92(6)
Ti1–S1	2.2238(16)	Ct1–Ti–Ct1'	57.09(9)
Ti1–S1'	2.4227(16)	Twist angle	21.1(5)
Ti–Ct ^a	1.9470(18)	Fold angle	17.30(12)
Ti–C _{ring} ^a	2.326(4)	Hinge Angle	1.4(4)

^a Average values

6.2.5 Synthesis and characterisation of $(\mu:\eta^5, \eta^5\text{-Pn}^\dagger)_2\text{Ti}_2(\mu\text{-C}\{N(4\text{-C}_6\text{H}_4\text{CH}_3)\}_2)$ (**6.6**)

Addition of one equivalent of 1,3-*N,N'*-di-*p*-tolylcarbodiimide (*p*-TCD) to a solution of **4.3** in pentane resulted in a colour change to brown-green. Subsequent work-up and recrystallisation from SiMe_4 afforded bronze crystals in good yield (92%), which were identified as compound **6.6** (Scheme 6.6).



Scheme 6.6 Synthesis of carbodiimide adduct **6.6**. R = Si^iPr_3 .

Elemental analysis and mass spectrometry (EI) were consistent with the formation of a 1:1 carbodiimide adduct. The ^1H NMR spectrum of **6.6** shows four sharp doublets assigned to the Pn^\dagger ring protons, typical of a diamagnetic C_2 -symmetric double-sandwich complex in solution. The $^{13}\text{C}\{^1\text{H}\}$ spectrum shows a singlet at 181.9 ppm, which is assigned to the carbodiimide central carbon atom.

Single crystal XRD studies unambiguously confirmed the molecular structure of **6.6** in the solid state, which agrees with solution NMR spectroscopic data. The molecular structure (Figure 6.10) shows a bent *p*-TCD ligand in a $\mu:\eta^2, \eta^2$ - binding mode between two Ti centres forming a dimetallocyclopropane-type motif with a Ti–C–Ti angle of $68.2(2)^\circ$. In a similar fashion to the μ -oxo **5.8**, the molecule possesses a 2-fold rotoinversion axis (S_2) passing through the carbodiimide carbon (C53) the midpoint of the Ti–Ti bond, which results in one half of the dimer being generated by symmetry.

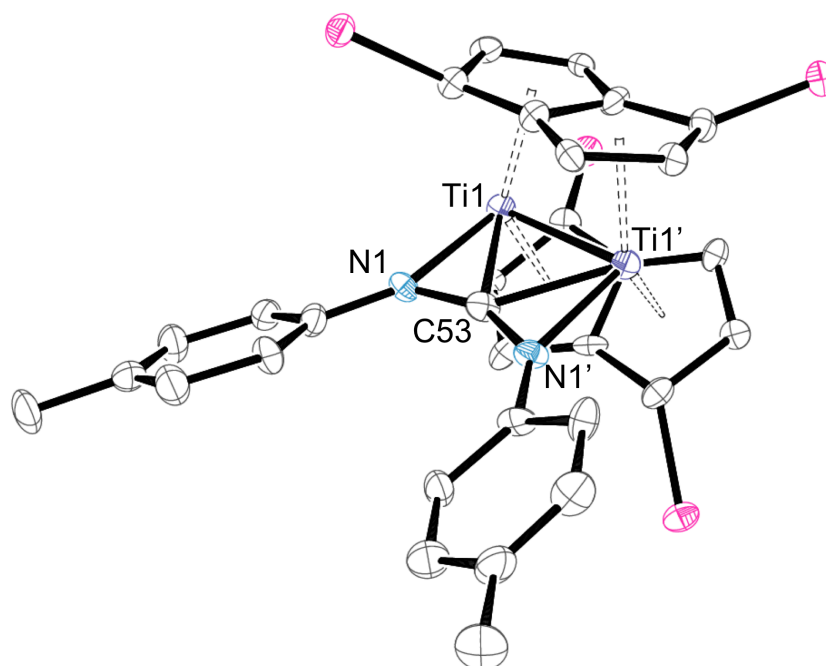


Figure 6.10 ORTEP (30% probability) diagram of **6.6**. H atoms and ⁱPr groups omitted for clarity. Primed atoms are generated by symmetry.

Table 6.5 Selected distances (Å), angles (°) and parameters for **6.6**. Ct denotes the η^5 -centroid of the Pn ring.

Parameter	6.6	Parameter	6.6
Ti1–Ti1'	2.4374(8)	Ti1–C53–Ti1'	68.13(7)
Ti1–C53	2.176(2)	C53–Ti1–Ti1'	55.94(4)
Ti1–N1	2.1159(15)	Ti1–C53–N1	69.87(9)
C53–N1	1.3004(15)	N1–C53–N1'	152.2(2)
Ti–Ct ^a	2.1218	Ct1–Ti1–Ct2	137.83(4)
Ti–C _{ring} ^a	2.419(2)	Twist angle	22.5(3)
Δ ^a	0.034(2)	Hinge angle	3.8(2)
Pn C–C _{ring} ^a	1.459(3)	Fold angle	4.59(10)
<i>p</i> -Tol C–C _{ring} ^a	1.390(3)		

^aAverage values.

The distance of each Ti atom **6.6** to the carbodiimide central carbon atom is 2.176(2) Å, in the range of a Ti–C single bond ($\sum r_{\text{cov}} = 2.11$ Å),¹⁰⁰ and comparable with that found in Rosenthal's carbene-like dinuclear Ti(III) complex, $[\text{Cp}_2\text{Ti}(\mu\text{-}\kappa^2\text{:}\eta^1\text{-}\{\text{Cy}\}\text{NCN}\{\text{Cy}\})\text{TiCp}_2]$, (2.199(4) Å) (Section 6.1.2, Scheme 6.2).⁴⁴ Indeed, the Ti–C distance in **6.6** is comparable with the shorter Ti–C_{carbene} distances in titanium complexes with NHC ligands reported to date, which range from 2.160(3)¹⁰¹ to 2.212 Å,¹⁰² however it is significantly longer than those for titanium Schrock carbene complexes. Examples of this class include terminal alkylidene complexes, which have very short Ti=C bonds (*ca.* 1.830 Å),^{103–106} and bridging alkylidene complexes,^{107–111} most famously the Tebbe reagent $[\text{Cp}_2\text{Ti}(\mu\text{-Cl})(\mu\text{-CH}_2)\text{AlMe}_2]$,^{112–115} which has a Ti–C_{carbene} distance of 2.095(5) Å.¹¹²

The Ti–N distance of 2.1159(15) Å, while in the range of a Ti–N single bond ($\sum r_{\text{cov}} = 2.07$ Å),¹⁰⁰ is notably longer than those of titanocene(III) amides such as $\text{Cp}^*_2\text{Ti}(\text{NRH})$ (1.9555(5) Å R = Me,¹¹⁶ Å, 1.944(2) R = H,¹¹⁷) as these complexes have an additional π -bonding interaction from the N lone pair. However this value is shorter than in $\text{Cp}^*_2\text{Ti}(\text{NMePh})$ (2.157(5) Å),¹¹⁸ where the Ti–amide bond lacks its π -constituent due to steric congestion. The metrics of the TiNC unit in **6.6** are best compared with those found in monomeric titanocene(III) η^2 -aminoacyl complexes, for example $\text{Cp}_2\text{Ti}(\eta^2\text{-}\{\text{Ph}\}\text{CN}\{\text{Xyl}\})$ ¹¹⁹ and $[\text{Cp}_2\text{Ti}(\eta^2\text{-}\{\text{Me}\}\text{CN}\{\text{Bu}\})][\text{BPh}_4]$ (Ti–C = 2.096(4) and 2.080(6) Å; Ti–N = 2.149(7) and 2.125(5) Å respectively). **6.6** features a more acute Ti–C–N angle (69.87(9)°) than in these η^2 -aminoacyl complexes presumably due to further conjugation at the carbodiimide central carbon atom to the second half of the dimer.

The carbodiimide moiety in **6.6** is bent with a N–C–N angle of 152.2(2)° and the C–N bond lengths of 1.3004(15) Å are consistent with the partial loss of the cumulene structure of the free substrate upon complexation. For comparison, in the free carbodiimide, the N=C=N angle is 170.4(4)° and the C–N bond lengths are 1.223(5) and 1.204(4) Å.¹²⁰ This is reflected in the IR spectrum of **6.6** which shows a $\nu(\text{NCN})$ asymmetric stretching vibration at 1659 cm^{–1}, a value significantly lower than that of *p*-TCD ($\nu_{\text{NCN}} = 2139$ cm^{–1}).¹²¹ The molecular structure of **6.6** is reminiscent of carbodiimide adducts of M–M bonded di-tungsten complexes $\text{W}_2(\text{O}^t\text{Bu})_6$ and $\text{W}_2(\text{OCMe}_2\text{CF}_3)$,^{45,47} which have been structurally characterised.

Compound **6.6** is thermally robust, with no change observed by ^1H NMR spectroscopy after heating at 100 °C in methylcyclohexane- d_{14} for 4 days. This may be attributed to the kinetic stability imparted on the carbenic carbon atom, which is a potential reactive site, but is somewhat buried in the ‘cleft’ provided by Ti_2 double-sandwich structure. Additional steric protection is provided by the *para*-tolyl substituents on the bound carbodiimide and hence the approach of a second molecule is severely hindered.

6.2.6 *Synthesis and characterisation of $[(\eta^8\text{-Pn}^\dagger)\text{Ti}]_2(\mu\text{-}\kappa^2\text{:}\kappa^2\text{-O}_2\text{CNPh})$ (**6.7**)*

Slow addition of PhNCO to a pentane solution of **4.3** at -35 °C resulted in a green-brown solution upon warming to room temperature, which after concentration and cooling to -35 °C, deposited green crystals suitable for X-ray diffraction analysis. The molecular structure (Figure 6.11) revealed not the anticipated PhNCO adduct but complex **6.7** in which the double-sandwich structure has been cleaved and an unusual phenyl-carbonimidate ligand bridges two formally Ti(III) centres. Complex **6.7** was further characterised by mass spectrometry, elemental analysis and shows a characteristic IR band at ν 1564 cm^{-1} , assigned to the aromatic C=C stretch of the phenyl group. In the ^1H NMR spectrum of **6.7** in THF- d_8 solution only broad signals were observed, and the effective magnetic moment determined by the Evans method was 1.3 μ_{B} per Ti, which is less than the spin-only value for a Ti^{3+} ion (1.73 μ_{B}). SQUID and EPR studies were not possible due to the small amount of material isolated from the reaction with PhNCO.

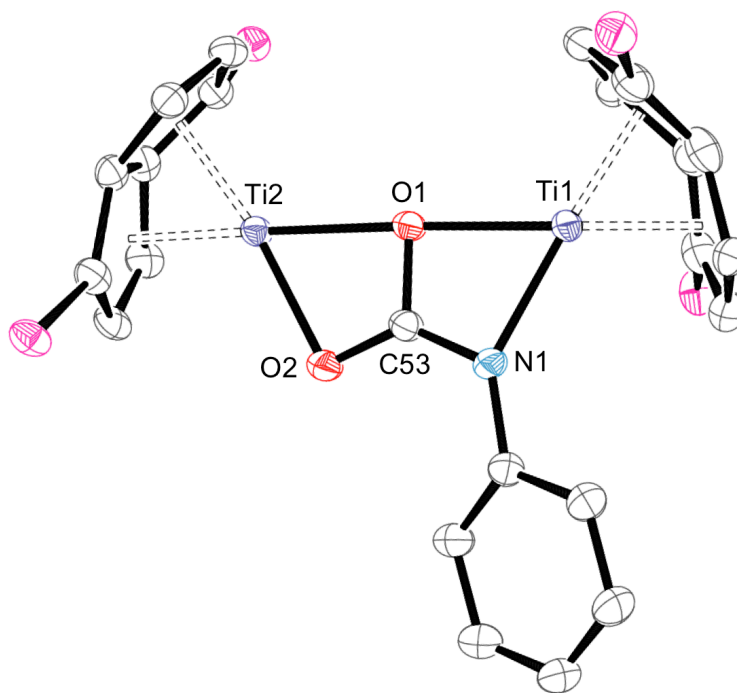


Figure 6.11 ORTEP (30% probability) diagram of **6.7**. H atoms and ⁱPr groups omitted.

Table 6.6 Selected distances (Å), angles (°) and parameters for **6.7**.

Ct denotes the η^5 -centroid of the Pn ring.

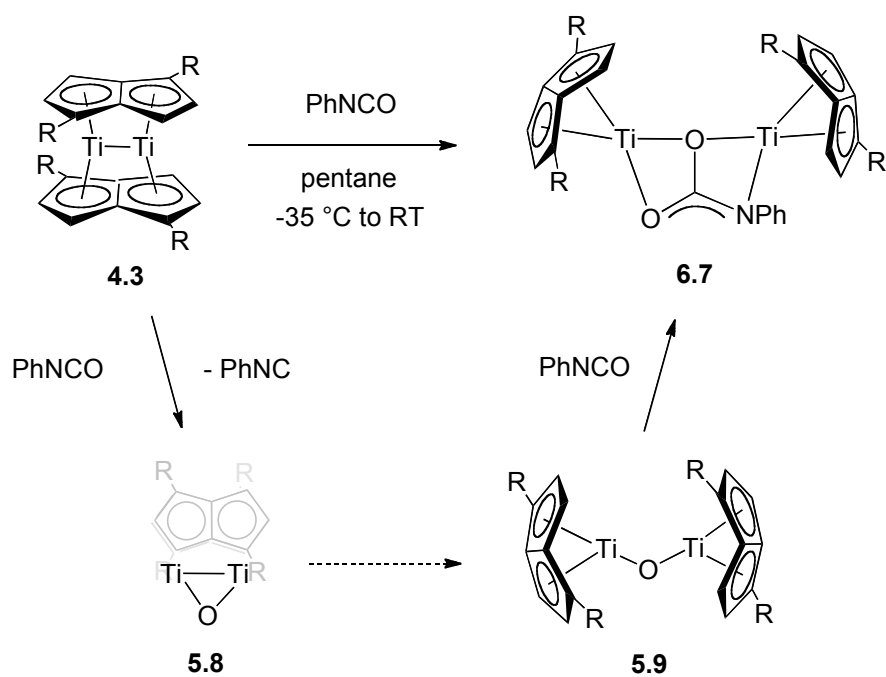
Distance	6.7	Angle	6.7
Ti1...Ti2	4.3011(11)	Ti1–O1–Ti2	176.44(12)
Ti1–O1	2.145(2)	O1–Ti1–N1	62.90(9)
Ti2–O1	2.146(2)	O1–Ti2–O2	63.10(9)
Ti1–N1	2.124(3)	O1–C53–N1	113.4(3)
Ti2–O2	2.081(3)	O1–C53–O2	114.8(3)
C53–O1	1.350(4)	O2–C53–N1	131.7(3)
C53–O2	1.275(4)	Ct–Ti–Ct ^a	57.32(9)
C53–N1	1.314(4)	Fold angle ^a	35.1(3)
Ti–Ct ^a	1.9354(18)	Hinge Angle ^a	3.2(6)
Ti–C _{ring} ^a	2.325(5)		

^a average values

The C–O distances about the central carbon atom of the bridging ligand are between the range of lengths for a C(sp²)–O single and double bond (1.293–1.407 Å and 1.187–1.255 Å respectively);¹²² furthermore, the C–N distance also lies between the C(sp²)–N single and double bond range (1.279–1.329 Å and 1.321–1.416 Å respectively).^{122,123} The NCO₂ core is planar and the sum of its angles are 360°. These results indicate the delocalisation of negative charge over the bidentate phenyl-carbonimidate ligand. Other examples of this ligand in the Cambridge Structural Database (CSD) are limited to a single report by Zhou *et al.*,¹²⁴ which details a series of lanthanide(III) complexes, [Cp₂Ln(THF)]₂(μ-κ²:κ²-O₂CNPh) (Ln = Y, Er, Yb), showing similar metrics about the [PhNCO₂]²⁻ bridge. These complexes were prepared from the lanthanocene(III) hydroxides [Cp₂Ln(μ-OH)(THF)]₂ and PhNCO followed by reaction with the corresponding Cp₃Ln. In contrast a redox reaction has clearly taken place between **4.3** and PhNCO to afford **6.7**.

The yield was 40% with respect to **4.3** and PhNCO, however based on the formula of **6.7** with two oxygens atoms in the bimetallic product, it follows that the reaction stoichiometry requires two equivalents of PhNCO per dimer. The mechanism for this unexpected transformation is unclear, but is postulated to proceed *via* O-atom transfer from PhNCO to give the mono(μ-oxo) complex **5.8**, which is known to be thermally unstable with respect to the more open triplet structure **5.9**. The second step involves nucleophilic attack of the μ-O ligand at the carbon atom of a second PhNCO molecule, a position which is generally nucleophilic.¹²⁵

Further studies are needed to establish how general this Ti-mediated isocyanate to carbonimidate transformation is. However, it is remarkable that the reaction **4.3** with PhNCO is kinetically stabilised at a carbonimidate-bridged Ti(III)–Ti(III) complex, in contrast to the heteroallenes CO₂ and COS which give oxo- and sulfido-bridged Ti(IV)–Ti(IV) products respectively.

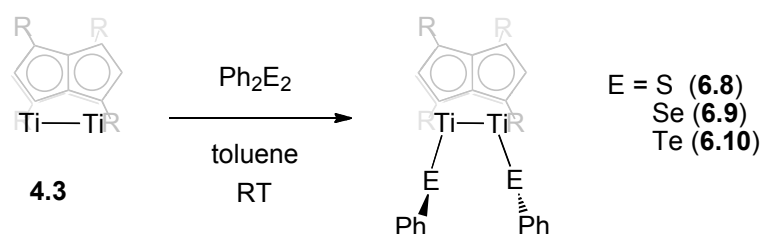


Scheme 6.7 Synthetic route to **6.7** ($R = \text{Si}^i\text{Pr}_3$), via postulated intermediates.

6.3 Reactivity of 4.3 with Homonuclear E–E Bonds

6.3.1 Synthesis and characterisation of $(\mu\text{-}\eta^5, \eta^5\text{-Pn}^\dagger)_2[\text{Ti}(\text{EPh})]_2$, for $\text{E} = \text{S}$ (**6.8**), Se (**6.9**) and Te (**6.10**).

When deep red solutions of **4.3** in toluene were treated with one equivalent of Ph_2E_2 reagent ($\text{R} = \text{S}, \text{Se}$ and Te) an immediate colour change from deep red to red-brown was observed. Subsequent work-up and recrystallisation from pentane furnished the respective di-phenylchalcogenoate complexes $(\mu\text{-}\eta^5, \eta^5\text{-Pn}^\dagger)_2[\text{Ti}(\text{EPh})]_2$, for $\text{E} = \text{S}$ (**6.8**), Se (**6.9**) and Te (**6.10**) as analytically pure brown solids (Scheme 6.8).



Scheme 6.8 Synthesis of di-phenylchalcogenoate complexes. $\text{R} = \text{Si}^i\text{Pr}_3$.

EI-MS showed a parent ion or a common fragment ($[\text{M} - \text{Ph}]^+$ or $[\text{M} - ^i\text{Pr}]^+$) for each complex. Solid state IR for **6.9** and **6.10** showed essentially identical spectra with a sharp band at *ca.* 1570 cm^{-1} assigned to the aromatic $\text{C}=\text{C}$ stretch of the phenyl group. In contrast **6.8** shows a broad IR band at 1620 cm^{-1} . ^1H NMR spectroscopy showed very similar spectra for **6.8**, **6.9** and **6.10**, consisting of seven sharp signals in the aromatic region; three of which were assigned to the *o*, *m*, and *p*-H of the two equivalent Ph groups with integration (ratio 2:2:1 respectively) and multiplicity as expected (d, t and t respectively); four doublet signals of equal intensity were assigned to the Pn^\dagger ring protons in a double-sandwich structure with C_2 symmetry on the NMR timescale. Multinuclear (^{13}C , ^{29}Si) NMR spectra were consistent with this interpretation. The $^{77}\text{Se}\{^1\text{H}\}$ and $^{125}\text{Te}\{^1\text{H}\}$ NMR of **6.9** and **6.10** respectively showed one singlet signal at δ_{Se} 511 and δ_{Te} 418 respectively. These chemical shifts are relatively upfield in comparison with those of known titanium selenolate and tellurolate complexes, for which $^{77}\text{Se}\{^1\text{H}\}$ and $^{125}\text{Te}\{^1\text{H}\}$ NMR spectroscopic data have been provided (Table 6.7). This may be correlated with the $\text{Ti(III)}\text{--Ti(III)}$ oxidation state in **6.9** and **6.10**,

which renders the chalcogenoate ligand more shielded with respect to monomeric d^0 Ti(IV) complexes. However the $(RE)^+$ ligands in these literature examples have very different electronic properties, so firm comparisons cannot be made. Known Ti(III) selenolate and tellurolates such as $Cp_2Ti^{III}[TeSi(SiMe_3)_3]PMe_3$ ⁶⁹ precluded NMR characterisation due to their paramagnetic nature.

Table 6.7 Solution $^{77}Se\{^1H\}$ and $^{125}Te\{^1H\}$ NMR data for **6.9** and **6.10** and related titanium selenolate and telluroate complexes.

Compound	δ	solvent	ref
6.9	511	cyclohexane- d_{12}	this work
$Cp_2Ti(\underline{Se}Ph)_2$	847	n/a	126
$Cp_2Ti(o-\underline{Se}_2C_6H_4)$	982	n/a	126
$Cp_2Ti(\underline{Se}Me)_2$	914.2	CD_2Cl_2/CH_2Cl_2	71
$Ti[\underline{Se}Si(SiMe_3)_3]_4$	865	C_6D_6	127
$Ti[\underline{Se}Si(SiMe_3)_3]_3(CH_2Ph)$	828	C_6D_6	127
$Ti[\underline{Se}Si(SiMe_3)_3]_2(OEt)_2$	416	C_6D_6	127
6.10	418	cyclohexane- d_{12}	this work
$Cp_2Ti[\underline{Te}Si(SiMe_3)_3]_2$	810	C_6D_6	70
$Cp'_2Ti[\underline{Te}Si(SiMe_3)_3]_2$	783	C_6D_6	70
$Cp_2Ti(\underline{Te}SiPh_3)_2$	709	C_6D_6	128
$Cp'_2Ti(\underline{Te}SiPh_3)_2$	659	C_6D_6	128

This work has shown that the $(Pn^+)_2Ti_2$ double-sandwich motif can incorporate both terminal and bridging ligands, and titanium thiolates complexes with terminal and bridging bonding modes are well known.¹²⁹ Assuming that the mechanism for oxidative

addition of Ph_2E_2 occurs exclusively at one face of complex **4.3**, two possible C_2 symmetric structures for **6.8**, **6.9** and **6.10** are possible (Figure 6.12).

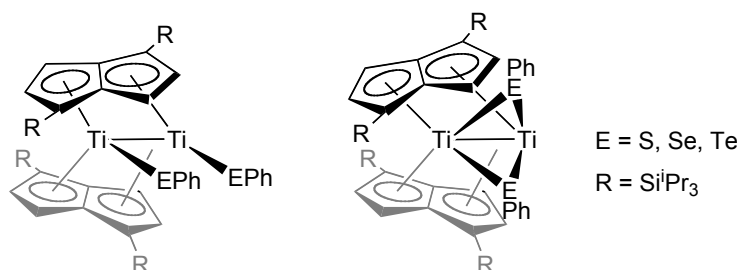


Figure 6.12 Possible structures of di-phenylchalcogenoate complexes.

Spectroscopic and analytical data alone were not sufficient to distinguish between a terminal or bridging mode for the chalcogenolate ligands, so an XRD study was carried out. Selenolate complex **6.9** was recrystallised from SiMe_4 , however the X-ray data collected for the crystals were weak at high angle, and suffered from a highly disordered solvent molecule which could not be modelled adequately. Therefore the X-ray data for **6.9** precluded accurate refinement of metric parameters, and only basic connectivity was established (see appendix A2). Gratifyingly, an Et_2O solution of thiolate complex **6.8** and a SiMe_4 solution of telluroate complex **6.10** each provided single crystals which were of sufficient quality for structural determination by XRD. The general structural feature common to **6.8**, **6.9** and **6.10** is the double-sandwich motif with terminal di-chalcogenoate ligands pointing out of one face, and the Ph groups pointing in opposite directions to minimise steric repulsions with the Si^iPr_3 substituents on this face. The molecular structure of **6.10** is depicted in Figure 6.13 as a typical example and selected structural parameters for this complex are included in Table 6.8.

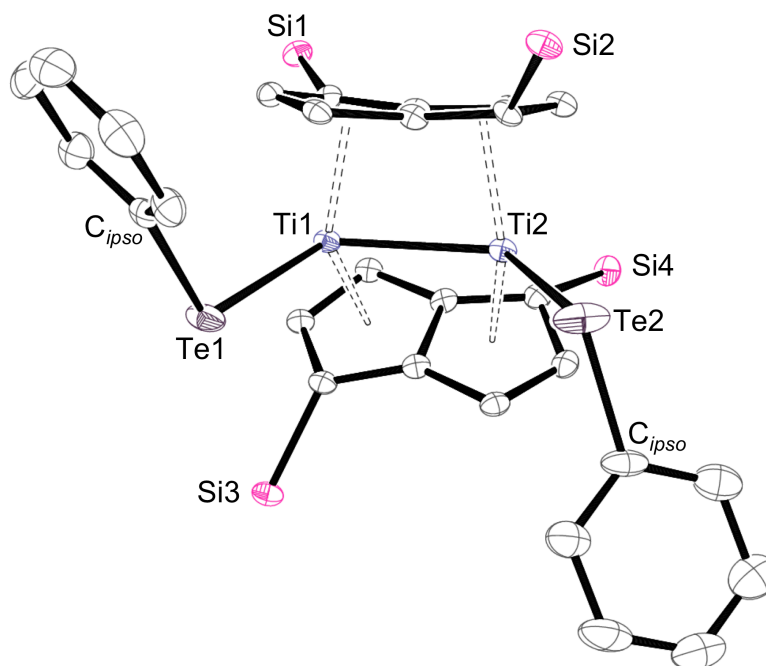


Figure 6.13 Displacement ellipsoid plot (30% probability) of **6.10**. H atoms and ⁱPr groups omitted for clarity.

Table 6.8 Selected interatomic distances (Å), angles (°) and parameters for **6.10**.
Ct denotes the η⁵-centroids of the Pn ring.

Parameter	6.10	Parameter	6.10
Ti1–Ti2	2.6530(9)	Ti–Ti–Te ^a	120.69(3)
Ti1–Te1	2.6809(7)	Ti–Te–C _{ipso} ^a	112.65(13)
Ti2–Te2	2.6922(7)	C _{ipso} –Te–Te–C _{ipso}	140.73(18)
Ti–Ct ^a	2.0807(17)	Te–Ti–Ti–Te	7.01(5)
Ti–C _{ring} ^a	2.411(4)	Ct–Ti–Ct ^a	135.14(7)
Δ ^a	0.115(4)	Twist angle	17.4(3)
Pn C–C _{ring} ^a	1.438(2)	Hinge angle	5.4(4)
Ph C–C _{ring} ^a	1.384(4)	Fold angle	11.0(2)

^aAverage values.

The most noteworthy structural feature is the longer Ti–Ti distance for **6.10** (2.6530(9) Å) with respect to the starting compound **4.3** (2.399(2) Å), consistent with the loss of two electrons from the M–M bonding HOMO of **4.3** upon oxidative addition of Ph₂Te₂. Indeed, the intermetallic distance is significantly longer than in the mono(μ-O) and mono(μ-S) complexes, **5.8** and **6.4** (2.3991(7) and 2.4682(8) Å respectively), and the (tri-*tert*-butylsilyl)imido complex [(*t*-Bu₃SiNH)Ti]₂(μ-NSi^{*t*}Bu)₂ (2.442(1) Å)¹³⁰ which was the only example found in the CSD of a metal-metal bond between two formally Ti(III) centres.

The Ti–Te distances for **6.10** (av. 2.6866(7) Å) lie between the sum of their single and double bond covalent radii (2.72 and 2.45 Å respectively),⁹³ and are comparatively short relative to those of previously determined tellurolate complexes of Ti(III), Cp₂Ti[TeSi(SiMe₃)₃]PMe₃ (2.8955(30) Å), Cp₂Ti(TeSnPh₃) (2.8681(18) Å)⁷⁰ and even of Ti(IV), Cp₂Ti[TeSi(SiMe₃)₃]₂ (2.788(1) Å).⁷⁰ This suggests a possible π-bonding interaction between titanium and tellurium in **6.10**, an effect which has been invoked in the permethyltitanocene(III) telluride complex [Cp*Ti]₂(μ-Te),¹³¹ which shows an average Ti–Te distance of 2.702(3) Å.

The angle between the Ti–Te vectors (61.7°) reflects the extent to which the large Te atoms are pointing away from each other, in comparison with the di-carbonyl complex **5.2** in which the Ti–C_{CO} vectors are near parallel (9.8°). The phenyl substituents on the tellurolate ligands point away from one another (C_{*ipso*}–Te–Te–C_{*ipso*} = 140.7°) to minimise steric repulsions, in comparison to **5.2** in which back bonding to the CO π* orbitals constrains the two ligands to a near parallel arrangement (O–C–C–O = 140.7°).

Terminal chalcogenolate ligands act as 1 electron donors (X-function in the Green *et al.* counting scheme)¹³² meaning **6.8**, **6.9** and **6.10** are formally 17 VE per Ti, with diamagnetic behaviour which may be explained by a M–M single bond. However antiferromagnetic coupling between Ti(III) centres could also be mediated through the pentalene ligand, as described in chapter one.

It was then of interest to investigate the potential for a four electron oxidation of **4.3** to give 18 VE per Ti centre, and the effect this would have on the double-sandwich structure. Azobenzene was selected as a substrate, given its ability to undergo both 2 and 4 electron redox reactions with low valent metal complexes.

6.3.2 Synthesis and characterisation of $[(\eta^8\text{-Pn}^\dagger)\text{Ti}]_2(\mu\text{-NPh})_2$ (**6.11**).

Addition of one equivalent of azobenzene to a toluene solution of **4.3** resulted in a colour change to dark red. Removal of the solvent and recrystallisation from hexane furnished red crystals of $[(\eta^8\text{-Pn}^\dagger)\text{Ti}]_2(\mu\text{-NPh})_2$ (**6.11**), isolated in 70% yield. Elemental analysis and EI-MS data support the proposed formulation. Solution phase NMR spectroscopy data are consistent with a C_{2v} symmetric structure; the ^1H spectrum contains two signals assigned to the Pn^\dagger ring protons, reminiscent of the ^1H spectrum of bis(μ -oxo) compound **5.5**, and three further signals in the aromatic region assigned to the two equivalent Ph groups.

XRD analysis of single crystals of **6.11** revealed two phenylimido ligands bridging two formally Ti(IV) centres, forming a Ti_2N_2 heterocyclic ring (Figure 6.14). The coordination geometry of both titanium atoms is distorted tetrahedral. The Ti...Ti distance of 2.8935(5) Å is not unusually short for a bimetallic Ti(IV) complex, and similar distances have been observed in related species.^{85,133-135} The bridging region of the complex is asymmetric, such that the Ti–N bond lengths are different, ranging from 1.9830(17) Å to 1.9536(17) Å. Asymmetrically bridging imido ligands have previously been observed for several different transition-metal complexes, and Nugent *et al.* have ascribed this effect to an increase in π -donation to the metal centre.¹³⁵ However, these researchers suggested that a substantial distortion of the M–N bond lengths in four-coordinate Group 4 $[\text{M}_2(\mu\text{-NR})_2]$ -containing complexes is not expected on electronic grounds. Hence, it is postulated that the difference in the Ti–N bond lengths in **6.11** is sterically induced by the asymmetric disposition of the Pn^\dagger ligands with respect to the $[\text{Ti}_2(\mu\text{-NPh})_2]$ unit. The reaction can be considered a $4e^-$ reduction per azobenzene molecule driven by the oxidative cleavage of the Ti–Ti double bond to give the di-Ti(IV) bis(μ -NPh) complex.

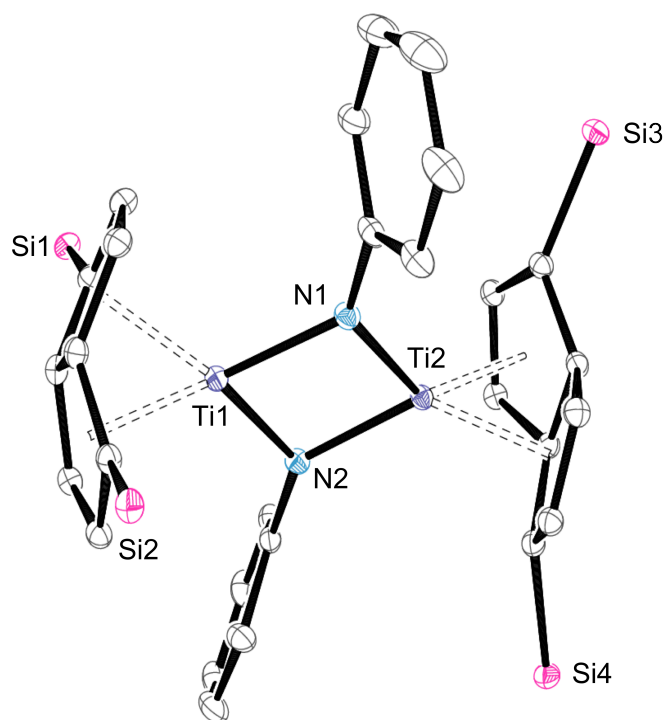


Figure 6.14 ORTEP (30% probability) diagram of **6.11**.

H atoms and ⁱPr groups omitted for clarity.

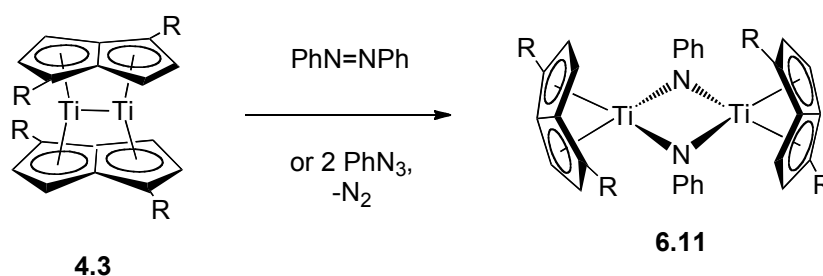
Table 6.9 Selected interatomic distances (Å), angles (°) and parameters for **6.11**.

Ct denotes the η^5 -centroid of the Pn ring.

Parameter	6.11	Parameter	6.11
Ti1···Ti2	2.8935(5)	Ph C–C _{ring} ^a	1.401(3)
Ti1–N1	1.9799(17)	Ti1–N1–Ti2	94.47(7)
Ti1–N2	1.9614(17)	Ti1–N1–Ti2	94.61(7)
Ti2–N1	1.9536(17)	Ct–Ti–Ct ^a	56.57(4)
Ti2–N2	1.9536(17)	Twist angle	32.30(15)
Ti–Ct ^a	1.9975(10)	Fold angle ^a	32.6(3)
Ti–C _{ring} ^a	2.384(2)	Hinge Angle	1.3(2)
Pn C–C _{ring} ^a	1.443(3)		

^a average values

Organic azides (RN_3) are common reagents for the transfer of a nitrene (RN) group to a metal complex, upon loss of N_2 , and presented an alternative synthetic route to **6.11**. Addition of 1 equivalent of azidobenzene (PhN_3) to a solution of **4.3** in C_6D_6 resulted in a rapid colour change to red and the effervescence of dinitrogen. ^1H NMR spectroscopy showed two sets of characteristic Pn ring signals corresponding to **6.11** and unreacted **4.3** in approximately equal ratio. Addition of a further 1 equivalent of PhN_3 showed complete conversion to **6.11**.



Scheme 6.10 Summary of synthetic routes to **6.11**. $\text{R} = \text{Si}^i\text{Pr}_3$.

Metal-driven reductive transformations of organic azides to imido complexes are well known for titanium,^{136,137} uranium,¹³⁸⁻¹⁴¹ and late transition metals.¹⁴² However with Ti mononuclear *terminal*-imido complexes are typically formed. The reaction of **4.3** with PhN_3 can be considered a $2e^-$ redox process per organoazide. The imido/nitrene $[\text{PhN}]^{2-}$ fragment produced is isolobal with O^{2-} , and hence this reaction parallels that of **4.3** with N_2O to give bis(μ -oxo) complex **5.5**.¹⁴³ It is of interest to explore the scope of this reaction using different organic azides, as a method to install RN fragments into the double sandwich structure, with a view to forming a *mono*(imido) complex given their precedent for C–H bond activation with group 4 metals.¹⁴⁴ However due to time restraints this work was not completed in the current study and warrants further investigation.

6.4 Conclusions on Reactivity of **4.3**

The reactivity of **4.3** with heteroallenes provides useful insight into that with CO_2 . The thermally stable CS_2 and carbodiimide adducts **6.1** and **6.6** show symmetrical binding to the Ti_2 unit that is supporting evidence for the doubly bridging CO_2 ligand in **5.7**.

The reactivity observed with COS is even more capricious than that with CO₂ but some parallels can be made. The asymmetric COS molecule undergoes scission at low temperatures, forming a mono(μ -S) mono(CO) species **6.3** which has sufficient stability for spectroscopic elucidation. A mono(μ -O) mono(CO) counterpart was implicated in the CO₂ reaction pathway, but was not observed experimentally. However by extension to the mono(μ -S) and mono(μ -O) complexes **6.4** and **5.8**, a stability trend may be invoked. Comparisons of their structures reveals more extreme ligand-metal distances in the di-metalloepoxide such that **5.8** may be construed as a 'snapshot' of the change in Pn[†] bonding from double-sandwich (μ - η^5 : η^5) to umbrella-mode (η^8). This is the process which accompanies the metal-metal bond cleavage of **5.8** to the yield **5.9** at room temperature, and also its ultimate fate in the CO₂ reaction, to yield the bis(μ -O) **5.5**. Mono(μ -S) mono(CO) species **6.3** was also found to open up to the η^8 -Pn[†] capped structure, giving bis(μ -S) **6.5**, but only in the presence of excess COS.

The reaction of **4.3** with PhNCO to give unusual phenyl-carbonimide bridged **6.7** shows that heteroallene reactions can be kinetically stabilised at the Ti(III)–Ti(III) stage, however further studies are required to fully rationalise this transformation. It would also be of great interest in the design of any potential catalytic cycle to investigate whether Ti(III)–Ti(III) complexes such as **6.7** can be reduced back to **4.3** (chemically or electrochemically) with concomitant removal of the bridging ligand. This would also help to clarify the proposed disproportionation step in the CO₂ mechanism.

The reactivity with dichalogenides and azobenzene shows **4.3** can act as a 2e[−] and 4e[−] reductant respectively. These reactions were clean and essentially quantitative, giving diamagnetic products which were straightforwardly identified by ¹H NMR spectroscopy. Hence, these studies provide a blueprint for more predictable redox transformations at [Ti₂]⁴⁺, which are consistent with the electrode potential measured at −2.5 V vs FeCp₂⁺⁰. In future work these investigations may be extended to higher energy homonuclear E–E bonds (e.g. P–P or Si–Si), and more even more inert molecules such as dinitrogen. The introduction of different substituents on the pentalene rings around [Ti₂]⁴⁺ would enable structure-activity relationships to be made, for example additional steric stabilisation may lead to more controlled reactivity with CO₂.

The reactivity of **4.3** has invited obvious comparisons with the titanocene(II) fragment explored by Floriani and others, and also the electron rich di-tungsten hexaalkoxide

complexes of Cotton, Chisholm and co-workers. The chemistry of titanium-titanium multiple bonds remains relatively underexplored and it is hoped that future work on double-sandwich complexes will provide further interesting examples of small molecule activation, and potentially more useful product outcomes.

6.5 Experimental Details for Chapter Six

6.5.1 Synthesis of $(\mu:\eta^5, \eta^5\text{-Pn}^\dagger)_2\text{Ti}_2(\mu:\eta^2, \eta^2\text{-CS}_2)$ (**6.1**).

To a solution of **4.3** (58 mg, 0.058 mmol) in pentane (2 mL) at -35 °C was added CS₂ (14 µL, 0.23 mmol) *via* microsyringe. The resultant dark green mixture was allowed to warm to room temperature and stir for 3 h. Filtration followed by cooling to -35 °C afforded red microcrystals which were isolated by decantation and dried *in vacuo*.

Total yield: 36 mg (62% with respect to **4.3**).

Recrystallisation from a saturated Et₂O (1 mL) solution at -35 °C afforded dark red crystals suitable for X-ray diffraction studies.

¹H NMR (toluene-*d*₈, 399.5 MHz, 303 K): δ_H 7.30 (2H, ³J_{HH} = 3.0 Hz, Pn *H*), 6.35 (2H, ³J_{HH} = 3.0 Hz, Pn *H*), 6.25 (2H, ³J_{HH} = 3.5 Hz, Pn *H*), 5.85 (2H, ³J_{HH} = 3.5 Hz, Pn *H*), 1.48 (6H, m, ⁱPr *CH*), 1.42 (6H, m, ⁱPr *CH*), 1.15 (18H, d, ³J_{HH} = 7.4 Hz, ⁱPr *CH*₃), 1.13 (18H, d, ³J_{HH} = 7.5 Hz, ⁱPr *CH*₃), 1.05 (18H, d, ³J_{HH} = 7.4 Hz, ⁱPr *CH*₃), 1.01 (18H, d, ³J_{HH} = 7.5 Hz, ⁱPr *CH*₃).

¹³C{¹H} NMR (toluene-*d*₈, 100.5 MHz, 303 K): δ_C 355.5 (CS₂), 133.4 (Pn *C*), 132.4 (Pn *C*), 127.1 (Pn *C*), 107.6 (Pn *C*), 105.5 (Pn *C*), 95.1 (Pn *C*), 20.37 (ⁱPr *CH*₃), 20.21 (ⁱPr *CH*₃), 19.82 (ⁱPr *CH*₃), 14.73 (ⁱPr *CH*), 12.93 (ⁱPr *CH*).

²⁹Si{¹H} NMR (toluene-*d*₈, 79.4 MHz, 303 K): δ_{Si} 7.65, 7.39.

EI-MS: *m/z* = 1002 (65%), [M]⁺, 960 (30%), [M - ⁱPr]⁺.

Anal. found (calcd. for C₅₂H₉₂S₂Si₄Ti₂): C, 63.49 (63.56); H, 9.26 (9.26) %.

IR (methylcyclohexane, 26 °C): 1104 (ν_{asym} SCS) cm⁻¹.

Crystal data for **6.1**: C₅₃H₉₂S₂Si₄Ti₂, *M_r* = 1000.53, triclinic, space group *P*-*I*, dark red block, *a* = 14.1432(8) Å, *b* = 14.1716(7) Å, *c* = 18.3870(9) Å, α = 88.928(4)°, β = 69.270(5)°, γ = 65.223(5)° *V* = 3092.8(3) Å³, *T* = 173 K, *Z* = 2, *R*_{int} = 0.0957,

$\lambda_{\text{Mo}}(\text{K}\alpha) = 0.71073 \text{ \AA}$, $\theta_{\text{max}} = 24.713^\circ$, $R_1 [I > 2\sigma(I)] = 0.0596$, $wR_2 (\text{all data}) = 0.1682$, $\text{GooF} = 0.954$.

6.5.2 Synthesis of $(\mu:\eta^5, \eta^5\text{-Pn}^\dagger)_2\text{Ti}_2(\text{COS})$ (**6.2**).

A J. Young NMR tube was charged with **4.3** (20 mg, 0.022 mmol) and methylcyclohexane- d_{14} (0.6 mL). The solution was cooled to -78°C , the headspace evacuated, and COS (0.048 mmol) admitted. The tube was briefly shaken and a colour change from deep red to green was observed. NMR spectra were immediately measured, with the probe pre-cooled to -30°C .

NMR yield: 45% with respect to **4.3**.

^1H NMR (methylcyclohexane- d_{14} , 399.5 MHz, 243 K, selected data): δ_{H} 7.00 (1H, d, $^3J_{\text{HH}} = 3.0 \text{ Hz}$, Pn H), 6.96 (1H, d, $^3J_{\text{HH}} = 3.0 \text{ Hz}$, Pn H), 6.72 (1H, d, $^3J_{\text{HH}} = 3.7 \text{ Hz}$, Pn H), 6.45 (1H, d, $^3J_{\text{HH}} = 3.0 \text{ Hz}$, Pn H), 6.43 (1H, d, $^3J_{\text{HH}} = 3.6 \text{ Hz}$, Pn H), 6.31 (1H, d, $^3J_{\text{HH}} = 3.7 \text{ Hz}$, Pn H), 6.09 (1H, d, $^3J_{\text{HH}} = 3.7 \text{ Hz}$, Pn H), 1.79-1.44 (12H, overlapping m, $^i\text{Pr CH}$), 1.34-1.02 (72H, overlapping m, $^i\text{Pr CH}_3$). One Pn H signal was not resolved due to coincidental overlap with **6.5** signals.

$^{13}\text{C}\{^1\text{H}\}$ NMR (methylcyclohexane- d_{14} , 100.5 MHz, 243 K, selected data): δ_{C} 283 (s, COS).

$^{29}\text{Si}\{^1\text{H}\}$ NMR (methylcyclohexane- d_{14} , 79.4 MHz, 243 K, selected data): δ_{Si} 2.48, 2.07, 1.73, 1.08.

IR (NaCl): 1493 ($\nu_{\text{asym SCO}}$) cm^{-1} .

IR (methylcyclohexane, -65°C): 1498 ($\nu_{\text{asym SCO}}$) cm^{-1} .

6.5.3 Synthesis of $(\mu:\eta^5, \eta^5\text{-Pn}^\dagger)_2\text{Ti}_2(\mu\text{-S})(\text{CO})$ (**6.3**).

METHOD A: A J. Young NMR tube charged with **4.3** (16 mg, 0.017 mmol) and toluene- d_8 (0.65 mL) at -78°C was degassed and COS gas (0.015 mmol) slowly admitted. The reaction mixture was briefly shaken, resulting in a colour change from deep red to green, and was allowed to warm to room temperature over a period of 2 h.

NMR yield: 47% with respect to **4.3**.

METHOD B: An ampoule charged with **6.4** (0.028 mmol) and toluene-*d*₈ (0.7 mL) was cooled to -78 °C and the headspace evacuated. ¹³CO gas (0.025 mmol) was admitted slowly to the stirred mixture, resulting in a colour change from red to green. After warming to room temperature the solution was decanted into a J. Young tube and ¹³C-**6.3** was identified by its NMR and IR spectra.

NMR yield: 75% with respect to **4.3**.

Alternatively, exposing a solution of **6.4** to 0.9 mol eq. CO *via* Toepler pump yields primarily the unlabeled product **6.3**.

¹H NMR (toluene-*d*₈, 399.5 MHz, 303 K, selected data): δ_H 7.81 (2H, d, ³J_{HH} = 2.9 Hz, Pn *H*), 6.09 (br, Δν_{1/2} = 13 Hz, Pn *H*), 5.75 (2H, d, ³J_{HH} = 2.9 Hz, Pn *H*), 5.38 (2H, d, ³J_{HH} = 2.7 Hz, Pn *H*), 1.62-1.24 (12H, overlapping m, ⁱPr *CH*), 1.22-0.96 (72H, overlapping m, ⁱPr *CH*₃).

¹³C{¹H} NMR (toluene-*d*₈, 100.5 MHz, 303 K, selected data): δ_C 247 (br, Δν_{1/2} = 110 Hz, CO).

²⁹Si{¹H} NMR (toluene-*d*₈, 79.4 MHz, 303 K, selected data): δ_{Si} 2.56, 1.46.

IR (methylcyclohexane, -65 °C): **6.3** 2011 (br, νCO); ¹³C-**6.3** 1966 (br, ν¹³CO) cm⁻¹.

6.5.4 Synthesis of (μ:η⁵,η⁵-Pn[†])₂Ti₂(μ-*S*) (**6.4**).

A solution of Ph₃PS (56 mg, 0.19 mmol) in toluene (3 mL) was added dropwise to a stirred solution of **4.3** (177 mg, 0.191 mmol) in pentane (3 mL) at -35 °C. The resultant red mixture was allowed to warm to room temperature, stirred for 30 min and then stripped to dryness. A red residue was obtained which was placed under high vacuum (*ca.* 10⁻⁶ mbar), heated at 75 °C for 1 h, and then 100 °C for 2 h to ensure complete sublimation of a white crystalline solid, presumably Ph₃P. The residue was extracted with pentane (3 x 2 mL), filtered, and allowed to concentrate to *ca.* 3 mL. Cooling of this solution to -35 °C afforded red crystals of **6.4** suitable for X-ray diffraction studies.

Total yield: 95 mg (52% with respect to **4.3**).

¹H NMR (C₆D₆, 399.5 MHz, 303 K): δ_H 9.25 (2H, d, ³J_{HH} = 3.4 Hz, Pn *H*), 7.06 (2H, d, ³J_{HH} = 3.2 Hz, Pn *H*), 6.10 (2H, d, ³J_{HH} = 3.1 Hz, Pn *H*), 5.96 (2H, d, ³J_{HH} = 3.4 Hz, Pn *H*), 2.01 (6H, m, ⁱPr *CH*), 1.35 (6H, m, ⁱPr *CH*), 1.17 (18H, d, ³J_{HH} = 7.5 Hz, ⁱPr *CH*₃),

1.13 (18H, d, $^3J_{\text{HH}} = 7.3$ Hz, $^i\text{Pr CH}_3$), 0.98 (18H, d, $^3J_{\text{HH}} = 7.5$ Hz, $^i\text{Pr CH}_3$), 0.60 (18H, d, $^3J_{\text{HH}} = 7.5$ Hz, $^i\text{Pr CH}_3$).

$^{13}\text{C}\{^1\text{H}\}$ NMR (C_6D_6 , 100.5 MHz, 303 K): δ_{C} 141.7 (Pn C), 132.5 (Pn C), 130.0 (Pn C), 123.0 (Pn C), 118.6 (Pn C), 115.3 (Pn C), 113.2 (Pn C), 98.53 (Pn C), 19.50 ($^i\text{Pr CH}_3$), 19.41 ($^i\text{Pr CH}_3$), 19.14 ($^i\text{Pr CH}_3$), 18.89 ($^i\text{Pr CH}_3$), 13.72 ($^i\text{Pr CH}$), 13.15 ($^i\text{Pr CH}$).

$^{29}\text{Si}\{^1\text{H}\}$ NMR (C_6D_6 , 79.4 MHz, 303 K): δ_{Si} 2.20, 1.82.

EI-MS: $m/z = 989$ (60%) $[\text{M} + \text{S}]^+$; 956-959 (principal peak 957, 20%), $[\text{M}]^+$; 877 (100%), $[\text{M} - \text{Ti} - \text{S}]^+$.

Anal. found (calcd. for $\text{C}_{52}\text{H}_{92}\text{SSi}_4\text{Ti}_2$): C, 65.33 (65.23); H, 9.61 (9.69) %.

Crystal data for **6.4**: $\text{C}_{52}\text{H}_{92}\text{SSi}_4\text{Ti}_2$, $M_r = 957.47$, triclinic, space group $P-1$, red block, $a = 11.283(2)$ Å, $b = 12.867(3)$ Å, $c = 21.651(4)$ Å, $\alpha = 99.66(3)^\circ$, $\beta = 91.04(3)^\circ$, $\gamma = 115.71(3)^\circ$, $V = 2777.2(12)$ Å³, $T = 100$ K, $Z = 2$, $R_{\text{int}} = 0.0578$, $\lambda_{\text{Mo}}(\text{K}\alpha) = 0.71073$ Å, $\theta_{\text{max}} = 27.542^\circ$, $R_1 [I > 2\sigma(I)] = 0.0455$, wR_2 (all data) = 0.1238, $\text{Goof} = 0.983$.

6.5.5 Synthesis of $[(\eta^8\text{-Pn}^{\dagger})\text{Ti}(\mu\text{-S})]_2$ (**6.5**).

METHOD A: An ampoule containing a solution of **4.3** (141 mg, 0.152 mmol) in benzene (2 mL), frozen at -35°C , was degassed and fitted with a balloon containing COS gas (1 atm). The solution was allowed to warm to room temperature and, shortly after thawing, appeared green in colour. After stirring for 30 mins at room temperature a colour change to red-brown was observed. The reaction mixture was frozen and lyophilised and a spectroscopically pure red-brown solid was isolated.

Total yield: 145 mg (96% with respect to **4.3**).

METHOD B: To an ampoule containing **4.3** (100 mg, 0.108 mmol) and Ph_3PS (64 mg, 0.216 mmol) was added toluene (2 mL). After 4 h of stirring at room temperature the red-brown mixture was stripped to dryness, extracted with Et_2O (2 x 5 mL), filtered, and the solvent removed *in vacuo*. A brown solid was obtained which was placed under high vacuum (*ca.* 10^{-6} mbar) and heated at 60°C for 2.5 h, 75°C for 1 h, and finally 100°C for 30 min to ensure complete sublimation of a white crystalline solid, presumably Ph_3P . The residue was extracted with Et_2O (2 x 5 mL), filtered, and allowed to

concentrate to *ca.* 4 mL. Cooling of this solution to -35 °C afforded red crystals suitable for X-ray diffraction studies.

Total yield: 86 mg (80% with respect to **4.3**).

^1H NMR (C_6D_6 , 399.5 MHz, 303 K): δ_{H} 6.59 (4H, d, $^3J_{\text{HH}} = 3.3$ Hz, Pn H), 5.92 (4H, d, $^3J_{\text{HH}} = 3.2$ Hz, Pn H), 1.31 (12H, m, ^iPr CH), 1.19 (36H, d, $^3J_{\text{HH}} = 7.3$ Hz, ^iPr CH₃), 1.14 (36H, d, $^3J_{\text{HH}} = 7.3$ Hz, ^iPr CH₃).

$^{13}\text{C}\{^1\text{H}\}$ NMR (C_6D_6 , 100.5 MHz, 303 K): δ_{C} 148.9 (Pn C), 130.0 (Pn C), 115.2 (Pn C), 113.9 (Pn C), 19.66 (^iPr CH₃), 19.50 (^iPr CH₃), 12.31 (^iPr CH).

$^{29}\text{Si}\{^1\text{H}\}$ NMR (C_6D_6 , 79.4 MHz, 303 K): δ_{Si} -0.15.

EI-MS: $m/z = 989$ (100%), $[\text{M}]^+$; 946 (50%), $[\text{M} - ^i\text{Pr}]^+$.

Anal. found (calcd. for $\text{C}_{52}\text{H}_{92}\text{S}_2\text{Si}_4\text{Ti}_2$): C, 63.20 (63.12); H, 9.44 (9.37) %.

Crystal data for **6.5**: $\text{C}_{52}\text{H}_{92}\text{S}_2\text{Si}_4\text{Ti}_2$, $M_r = 989.53$, tetragonal, space group $P4_2/nbc$, red rod, $a = b = 15.714(2)$ Å, $c = 24.660(5)$ Å, $\alpha = \beta = \gamma = 90^\circ$, $V = 6089(2)$ Å³, $T = 100$ K, $Z = 4$, $R_{\text{int}} = 0.0887$, $\lambda_{\text{Mo}}(\text{K}\alpha) = 0.71073$ Å, $\theta_{\text{max}} = 27.460^\circ$, $R_1 [I > 2\sigma(I)] = 0.0864$, wR_2 (all data) = 0.1786, $\text{Goof} = 1.280$.

6.5.6 Synthesis of $(\mu\text{:}\eta^5, \eta^5\text{-Pn}^+)_2\text{Ti}_2(\mu\text{-C}\{N(4\text{-C}_6\text{H}_4\text{CH}_3)\}_2)$ (**6.6**).

Solid 1,3-*N,N'*-di-*p*-tolylcarbodiimide (13 mg, 0.057 mmol) was added slowly to a solution of **4.3** (53 mg, 0.057 mmol) in pentane (2 mL) at room temperature, resulting in a colour change from deep red to brown-green. The solvent was removed by slow evaporation at ambient pressure and the brown residue was redissolved in SiMe_4 (1 mL). Cooling this solution to -35 °C produced bronze crystals that were isolated by decantation and dried *in vacuo*.

Total yield: 60 mg (92% with respect to **4.3**).

^1H NMR (C_6D_6 , 399.5 MHz, 303 K): δ_{H} 7.35 (2H, d, $^3J_{\text{HH}} = 3.0$ Hz, Pn H), 7.09 (4H, t, $^3J_{\text{HH}} = 8.0$ Hz, *o*-4- $\text{C}_6\text{H}_4\text{Me}$), 6.95 (4H, t, $^3J_{\text{HH}} = 8.2$ Hz, Ph *m*-4- $\text{C}_6\text{H}_4\text{Me}$), 6.73 (2H, d, $^3J_{\text{HH}} = 3.6$ Hz, Pn H), 6.53 (2H, d, $^3J_{\text{HH}} = 3.1$ Hz, Pn H), 6.19 (2H, d, $^3J_{\text{HH}} = 3.6$ Hz, Pn H), 2.16 (2H, s, 4- $\text{C}_6\text{H}_4\text{CH}_3$), 1.57 (6H, m, ^iPr CH), 1.23 (18H, d, $^3J_{\text{HH}} = 7.4$ Hz, ^iPr CH₃), 1.11 (18H, d, $^3J_{\text{HH}} = 7.5$ Hz, ^iPr CH₃), 1.08 (18H, d, $^3J_{\text{HH}} = 7.4$ Hz, ^iPr CH₃),

0.96 (18H, d, $^3J_{\text{HH}} = 7.4$ Hz, $^i\text{Pr CH}_3$). One $^i\text{Pr CH}$ multiplet signal was not resolved due to coincidental overlap with $^i\text{Pr CH}_3$ doublet signal at δ_{H} 1.23.

$^{13}\text{C}\{^1\text{H}\}$ NMR (C_6D_6 , 100.5 MHz, 303 K): δ_{C} 181.9 ($\text{C}\{\text{NTol}\}_2$), 146.3 (*i*-4- $\text{C}_6\text{H}_4\text{Me}$), 133.0 (Pn bridgehead C), 132.3 (*p*-4- $\text{C}_6\text{H}_4\text{Me}$), 131.4 (Pn CH), 128.9 (*o*-4- $\text{C}_6\text{H}_4\text{Me}$), 125.8 (*m*-4- $\text{C}_6\text{H}_4\text{Me}$), 124.7 (Pn CH), 117.6 (Pn CH), 108.6 (Pn CH), 98.01 (Pn C-Si), 93.27 (Pn C-Si), 20.99 (4- $\text{C}_6\text{H}_4\text{CH}_3$), 20.10 ($^i\text{Pr CH}_3$), 20.06 ($^i\text{Pr CH}_3$), 20.01 ($^i\text{Pr CH}_3$), 19.80 ($^i\text{Pr CH}_3$), 14.27, ($^i\text{Pr CH}$), 12.77 ($^i\text{Pr CH}$).

$^{29}\text{Si}\{^1\text{H}\}$ NMR (C_6D_6 , 79.4 MHz, 303 K): δ_{Si} 2.44, 2.28.

EI-MS: $m/z = 1144$ -1149 (principal peak 1146, 20%), $[\text{M}]^+$; 1027-1032 (principal peak 1029, 100%), $[\text{M} - \text{CN}(\text{C}_6\text{H}_4\text{CH}_3)]^+$.

Anal. found (calcd. for $\text{C}_{67}\text{H}_{106}\text{N}_2\text{Si}_4\text{Ti}_2$): C, 69.87 (70.12); H, 9.42 (9.31); N, 2.48 (2.44) %.

IR (NaCl): 1659 ($\nu_{\text{asym}} \text{NCN}$), 1599 (ν aromatic C=C), 1318 ($\nu_{\text{sym}} \text{NCN}$) cm^{-1} .

Crystal data for **6.6**: $\text{C}_{67}\text{H}_{106}\text{N}_2\text{Si}_4\text{Ti}_2$, $M_r = 1147.69$, monoclinic, space group $C 2/c$, bronze block, $a = 25.872(5)$ Å, $b = 15.032(3)$ Å, $c = 19.626(4)$ Å, $\alpha = \gamma = 90^\circ$, $\beta = 121.30(3)^\circ$, $V = 6522(3)$ Å³, $T = 150$ K, $Z = 4$, $R_{\text{int}} = 0.0546$, $\lambda_{\text{Mo}}(\text{K}\alpha) = 0.71073$ Å, $\theta_{\text{max}} = 27.564^\circ$, $R_1 [I > 2\sigma(I)] = 0.0476$, wR_2 (all data) = 0.1301, $\text{Goof} = 1.062$.

6.5.7 Synthesis of $[(\eta^8\text{-Pn}^{\dagger})\text{Ti}]_2(\mu\text{-}\kappa^2\text{:}\kappa^2\text{-O}_2\text{CNPh})$ (**6.7**).

To a solution of **4.3** (70 mg, 0.076 mmol) in pentane (1 mL) was added a solution of PhNCO (9 mg, 0.076 mmol) in pentane (2 mL), dropwise at -35°C . A colour change to brown-green occurred and the mixture was allowed to warm to room temperature, stirred for 10 min and then filtered. The filtrate was concentrated to *ca.* 1 mL and after cooling to -35°C , deposited pale green crystals that were isolated by decantation and dried *in vacuo*.

Total yield: 32 mg (40% with respect to **4.3**).

^1H NMR ($\text{THF-}d_8$, 399.5 MHz, 303 K): δ_{H} 7.25 (br, $\Delta\nu_{1/2} = 65$ Hz, Pn H), 5.96 (br, $\Delta\nu_{1/2} = 57$ Hz, Pn H), 1.77 (br, $\Delta\nu_{1/2} = 110$ Hz, $^i\text{Pr CH}$), 1.37 (br, $\Delta\nu_{1/2} = 280$ Hz, $^i\text{Pr CH}_3$).

^{13}C and ^{29}Si NMR resonances were not observed due to the paramagnetic nature of **6.7**.

EI-MS: m/z = 1059-1062 (principal peak 1060, 15%), $[M]^+$; 1031-1035 (principal peak 1032, 20%), $[M - CO]^+$; 955-961 (principal peak 957, 100%), $[M - PhNC]^+$.

Anal. found (calcd. for $C_{59}H_{97}NO_2Si_4Ti_2$): C, 66.73 (66.82); H, 9.09 (9.22); N, 1.36 (1.32) %.

IR (NaCl): 1564 (ν aromatic C=C) cm^{-1} .

Crystal data for **6.7**: $C_{59}H_{97}NO_2Si_4Ti_2$, M_r = 1060.53, triclinic, space group $P-1$, green rod, a = 13.0980(9) Å, b = 13.2073(9) Å, c = 18.7778(13) Å, α = 75.122(2)°, β = 77.239(2)°, γ = 79.896(2)°, V = 3037.5(4) Å³, T = 150 K, Z = 2, R_{int} = 0.0891, $\lambda_{Mo}(K\alpha)$ = 0.71075 Å, θ_{max} = 27.463°, $R_1 [I > 2\sigma(I)]$ = 0.0857, wR_2 = 0.2416, $Goof$ = 0.984.

6.5.8 Synthesis of $(\mu:\eta^5, \eta^5-Pn^+)_2[Ti(SPh)]_2$ (**6.8**).

Solid PhSSPh (21 mg, 0.096 mmol) was added slowly to a stirring solution of **4.3** (89 mg, 0.096 mmol) in toluene (2 mL) at room temperature, resulting in a colour change from deep red to red-brown. The solvent was removed under reduced pressure and the products were extracted with pentane (3 mL) and filtered. The red-brown filtrate was concentrated to *ca.* 1 mL and after cooling to -35 °C, deposited brown crystals that were isolated by decantation and dried *in vacuo*.

Total yield: 82 mg (75% with respect to **4.3**).

¹H NMR (C_6D_6 , 399.5 MHz, 303 K): δ_H 8.34 (2H, d, $^3J_{HH}$ = 3.2 Hz, Pn *H*), 7.65 (4H, d, $^3J_{HH}$ = 7.2 Hz, Ph *o-H*), 7.37 (2H, d, $^3J_{HH}$ = 3.3 Hz, Pn *H*), 7.24 (4H, t, $^3J_{HH}$ = 7.7 Hz, Ph *m-H*), 7.02 (2H, t, $^3J_{HH}$ = 7.4 Hz, Ph *p-H*), 5.60 (2H, d, $^3J_{HH}$ = 3.1 Hz, Pn *H*), 5.23 (2H, d, $^3J_{HH}$ = 3.3 Hz, Pn *H*), 1.72 (6H, m, ⁱPr CH), 1.64 (6H, m, ⁱPr CH), 1.27 (18H, d, $^3J_{HH}$ = 7.4 Hz, ⁱPr CH₃), 1.17 (18H, d, $^3J_{HH}$ = 7.4 Hz, ⁱPr CH₃), 1.11 (18H, d, $^3J_{HH}$ = 7.5 Hz, ⁱPr CH₃), 0.97 (18H, d, $^3J_{HH}$ = 7.5 Hz, ⁱPr CH₃).

¹³C{¹H} NMR (C_6D_6 , 100.5 MHz, 303 K): δ_C 152.7 (Ph *i-C*), 142.0 (Pn C), 137.9 (Pn CH), 132.1 (Ph *o-C*), 128.6 (Ph *m-C*), 127.2 (Pn CH), 126.3 (Pn CH), 125.4 (Ph *p-C*), 117.2 (Pn C), 111.2 (Pn CH), 91.90 (Pn C), 20.45 (ⁱPr CH₃), 20.34 (ⁱPr CH₃), 20.05 (ⁱPr CH₃), 19.92 (ⁱPr CH₃), 14.41 (ⁱPr CH), 13.19 (ⁱPr CH).

²⁹Si{¹H} NMR (C_6D_6 , 79.4 MHz, 303 K): δ_{Si} 4.21, 3.09.

EI-MS: m/z = 1142-1147 (principal peak 1143, 30%), $[M]^+$; 1063-1069 (principal peak 1065, 100%), $[M - Ph]^+$.

Anal. found (calcd. for $C_{64}H_{102}S_2Si_4Ti_2$): C, 67.13 (67.12); H, 9.14 (8.99) %.

IR (NaCl): 1620 (br, ν aromatic C=C) cm^{-1} .

Crystal data for **6.8**: $C_{64}H_{102}S_2Si_4Ti_2$, M_r = 1143.73, triclinic, space group $P-1$, dark red block, a = 14.3166(6) Å, b = 15.1682(5) Å, c = 20.1061(9) Å, α = 93.573(3)°, β = 108.624(4)°, γ = 105.973(3)°, V = 3923.4(3) Å³, T = 173 K, Z = 2, R_{int} = 0.0538, $\lambda_{Mo}(K\alpha)$ = 0.71073 Å, θ_{max} = 25.0°, $R_1 [I > 2\sigma(I)]$ = 0.0728, wR_2 (all data) = 0.2015, $Goof$ = 1.079.

6.5.9 Synthesis of $(\mu:\eta^5, \eta^5-Pn^{\dagger})_2[Ti(SePh)]_2$ (**6.9**).

To a solution of **4.3** (92 mg, 0.099 mmol) in toluene (1 mL) was added a solution of PhSeSePh (31 mg, 0.099 mmol) in toluene (2 mL), dropwise at room temperature. A colour change from deep red to brown was observed and the mixture was allowed to stir for 30 min. The solvent was removed under reduced pressure and the products were extracted with pentane (4 mL) and filtered. The red-brown filtrate was concentrated to *ca.* 2 mL and after cooling to -35 °C, deposited red-brown crystals that were isolated by decantation and dried *in vacuo*.

Total yield: 106 mg (86% with respect to **4.3**). Subsequent recrystallisation from Et₂O at -35 °C afforded X-ray quality crystals.

¹H NMR (cyclohexane-*d*₁₂, 399.5 MHz, 303 K): δ_H 8.08 (2H, d, $^3J_{HH}$ = 3.2 Hz, Pn *H*), 7.40 (4H, d, $^3J_{HH}$ = 7.0 Hz, Ph *o-H*), 7.27 (2H, d, $^3J_{HH}$ = 3.3 Hz, Pn *H*), 7.11 (4H, t, $^3J_{HH}$ = 7.3 Hz, Ph *m-H*), 7.04 (2H, t, $^3J_{HH}$ = 7.3 Hz, Ph *p-H*), 5.37 (2H, d, $^3J_{HH}$ = 3.1 Hz, Pn *H*), 5.04 (2H, d, $^3J_{HH}$ = 3.2 Hz, Pn *H*), 1.69-1.58 (12H, overlapping m, ⁱPr *CH*), 1.26 (18H, d, $^3J_{HH}$ = 7.4 Hz, ⁱPr *CH*₃), 1.05 (18H, d, $^3J_{HH}$ = 7.4 Hz, ⁱPr *CH*₃), 0.97 (18H, d, $^3J_{HH}$ = 7.5 Hz, ⁱPr *CH*₃), 0.92 (18H, d, $^3J_{HH}$ = 7.5 Hz, ⁱPr *CH*₃).

¹³C{¹H} NMR (cyclohexane-*d*₁₂, 100.5 MHz, 303 K): δ_C 145.5 (Ph *i-C*), 141.9 (Pn *C*), 136.9 (Pn *CH*), 135.2 (Ph *o-C*), 128.7 (Ph *m-C*), 128.6 (Pn *CH*), 127.5 (Pn *CH*), 125.8 (Ph *p-C*), 115.7 (Pn *C*), 111.3 (Pn *CH*), 91.07 (Pn *C*), 20.68 (ⁱPr *CH*₃), 20.62 (ⁱPr *CH*₃), 20.30 (ⁱPr *CH*₃), 20.21 (ⁱPr *CH*₃), 15.00 (ⁱPr *CH*), 13.95 (ⁱPr *CH*).

$^{77}\text{Se}\{^1\text{H}\}$ NMR (cyclohexane- d_{12} , 76.21 MHz, 303 K): δ_{Se} 511.

$^{29}\text{Si}\{^1\text{H}\}$ NMR (cyclohexane- d_{12} , 100.5 MHz, 303 K): δ_{Si} 4.88, 2.77.

EI-MS: $m/z = 1237$ (60%), $[\text{M}]^+$.

Anal. found (calcd. for $\text{C}_{64}\text{H}_{102}\text{Se}_2\text{Si}_4\text{Ti}_2$): C, 61.97 (62.12); H, 8.35 (8.31) %.

IR (NaCl): 1575 (sh, ν aromatic C=C) cm^{-1} .

Unrefined crystal data for **6.9** from pentane solution: $\text{C}_{64}\text{H}_{102}\text{Se}_2\text{Si}_4\text{Ti}_2$, $M_r = 1237.53$, triclinic, space group $P-1$, dark red block, $a = 14.4267(7)$ Å, $b = 15.2429(8)$ Å, $c = 20.0970(14)$ Å, $\alpha = 93.221(5)^\circ$, $\beta = 107.934(5)^\circ$, $\gamma = 106.739(5)^\circ$, $V = 3975.3(4)$ Å³.

Partially refined crystal data for **6.9** from SiMe_4 solution: $\text{C}_{64}\text{H}_{102}\text{Se}_2\text{Si}_4\text{Ti}_2$, $M_r = 1237.53$, monoclinic, space group $P 2_1/c$, dark orange block, $a = 18.0739(13)$ Å, $b = 15.7855(7)$ Å, $c = 25.7705(17)$ Å, $\alpha = \gamma = 90^\circ$, $\beta = 102.416(7)^\circ$, $V = 7180.5(8)$ Å³, $T = 173$ K, $Z = 4$, $R_{\text{int}} = 0.0734$, $\lambda_{\text{Mo}}(\text{K}\alpha) = 0.71073$ Å, $\theta_{\text{max}} = 22.499^\circ$, $R_1 [I > 2\sigma(I)] = 0.0882$, wR_2 (all data) = 0.2492, $\text{Goof} = 1.155$.

6.5.10 Synthesis of $(\mu:\eta^5, \eta^5\text{-Pn}^\dagger)_2[\text{Ti}(\text{TePh})]_2$ (**6.10**).

To a solution of **4.3** (88.5 mg, 0.0956 mmol) in toluene (2 mL) was added a solution of PhTeTePh (39.1 mg, 0.0956 mmol) in toluene (2 mL), dropwise at room temperature. A colour change from deep red to dark brown was observed and the mixture was allowed to stir for 30 min. The solvent was removed under reduced pressure and the products were extracted with pentane (4 mL) and filtered. The red-brown filtrate was concentrated to *ca.* 1 mL and after cooling to -35°C , deposited dark brown crystals that were isolated by decantation and dried *in vacuo*.

Total yield: 90 mg (71% with respect to **4.3**).

^1H NMR (cyclohexane- d_{12} , 499.9 MHz, 303 K): δ_{H} 7.95 (2H, d, $^3J_{\text{HH}} = 3.0$ Hz, Pn H), 7.90 (2H, d, $^3J_{\text{HH}} = 3.1$ Hz, Pn H), 7.74 (4H, dd, $J = 2.8, 6.2$ Hz, Ph *o*- H), 7.20-7.16 (6H, overlapping m, Ph *m*- and *p*- H), 5.44 (2H, d, $^3J_{\text{HH}} = 2.9$ Hz, Pn H), 5.31 (2H, d, $^3J_{\text{HH}} = 3.1$ Hz, Pn H), 1.69 (6H, m, $^i\text{Pr CH}$), 1.54 (6H, m, $^i\text{Pr CH}$), 1.23 (18H, d, $^3J_{\text{HH}} = 7.3$ Hz, $^i\text{Pr CH}_3$), 1.04-0.96 (32H, overlapping m, $^i\text{Pr CH}_3$), 0.90 (18H, d, $^3J_{\text{HH}} = 7.5$ Hz, $^i\text{Pr CH}_3$).

$^{13}\text{C}\{^1\text{H}\}$ NMR (cyclohexane- d_{12} , 125.7 MHz, 303 K): δ_{C} 141.5 (Ph *o*-C), 139.5 (Pn C), 133.9 (Pn CH), 129.2 (Pn CH), 129.0 (Ph C), 127.1 (Ph C), 126.7 (Pn C), 122.2 (Pn C), 112.4 (Pn CH), 111.0 (Pn C), 92.80 (Pn C), 20.79 (^iPr CH₃), 20.77 (^iPr CH₃), 20.26 (^iPr CH₃), 20.13 (^iPr CH₃), 15.01 - 14.90 (overlapping m, ^iPr CH).

$^{29}\text{Si}\{^1\text{H}\}$ NMR (cyclohexane- d_{12} , 303 K): δ_{Si} 5.20, 2.74.

$^{125}\text{Te}\{^1\text{H}\}$ NMR (cyclohexane- d_{12} , 126.04 MHz, 303 K): δ_{Te} 418.

EI-MS: m/z = 1303-1312 (principal peak 1307, 50%), $[\text{M} - \text{CMe}]^+$; 1174-1183 (principal peak 1179, 80%), $[\text{M} - ^i\text{Pr}]^+$.

Anal. found (calcd. for $\text{C}_{64}\text{H}_{102}\text{Te}_2\text{Si}_4\text{Ti}_2$): C, 57.60 (57.59); H, 7.69 (7.70) %.

IR (NaCl): 2193, 2092, 1572 (sh, ν aromatic C=C) cm^{-1} .

Crystal data for **6.10**: $\text{C}_{64}\text{H}_{102}\text{Si}_4\text{Te}_2\text{Ti}_2$, M_r = 1334.81, monoclinic, space group $P 2_1/c$, dark orange block, a = 18.1208(3) Å, b = 16.1056(3) Å, c = 25.6467(5) Å, $\alpha = \gamma = 90^\circ$, β = 101.708(2)°, V = 7329.2(2) Å³, T = 173 K, Z = 4, R_{int} = 0.052, $\lambda_{\text{Cu}}(\text{K}\alpha)$ = 1.54184 Å, θ_{max} = 71.263°, $R_1 [I > 2\sigma(I)]$ = 0.0578, wR_2 = 0.1658, Goof = 1.064.

6.5.11 Synthesis of $[(\eta^8\text{-Pn}^+)\text{Ti}]_2(\mu\text{-NPh})_2$ (**6.11**).

METHOD A: To a solution of **4.3** (87 mg, 0.094 mmol) in toluene (2 mL) was added a solution of azobenzene (17 mg, 0.094 mmol) in toluene (2 mL), dropwise at room temperature. A colour change to dark red was observed and the mixture was allowed to stir for 30 min. The solvent was removed under reduced pressure and the products were extracted with hexane (2 mL) and filtered. The red filtrate was concentrated to *ca.* 1 mL and after cooling to -35 °C, deposited red crystals that were isolated by decantation and dried *in vacuo*.

Total yield: 73 mg (70% with respect to **4.3**).

METHOD B: To a solution of **4.3** (15 mg, 0.016 mmol) in pentane (3 mL) at -35 °C was added azidobenzene (32 μL , 0.016 mmol, 0.5 M soln in Me-THF), dropwise. Effervescence and a colour change to red was observed, and the reaction mixture was allowed to warm to room temperature and stir for 10 mins. The solvent was removed *in vacuo* and ^1H NMR spectroscopy showed *ca.* 50% conversion of **4.3** to **6.11**. Addition

of further azidobenzene (32 μL , 0.016 mmol, 0.5 M soln in Me-THF) to the reaction mixture furnished **6.11** in essentially quantitative yield.

^1H NMR (C_6D_6 , 399.5 MHz, 303 K): δ_{H} 6.98 (4H, t, $^3J_{\text{HH}} = 7.8$ Hz, Ph *m*-H), 6.71 (4H, d, $^3J_{\text{HH}} = 3.2$ Hz, Pn *H*), 6.62 (2H, t, $^3J_{\text{HH}} = 7.3$ Hz, Ph *p*-H), 6.42 (4H, d, $^3J_{\text{HH}} = 7.3$ Hz, Ph *o*-H), 5.22 (4H, d, $^3J_{\text{HH}} = 3.2$ Hz, Pn *H*), 1.15 (36H, d, $^3J_{\text{HH}} = 7.5$ Hz, ^iPr CH_3), 1.13 (36H, d, $^3J_{\text{HH}} = 7.6$ Hz, ^iPr CH_3), 0.93 (12H, m, ^iPr CH).

$^{13}\text{C}\{^1\text{H}\}$ NMR (C_6D_6 , 100.5 MHz, 303 K): δ_{C} 167.3 (Ph *i*-C), 149.0 (Pn bridgehead C), 134.0 (Pn CH), 127.3 (Ph *m*-C), 120.6 (Ph *p*-C), 119.8 (Ph *o*-C), 114.4 (Pn CH), 111.4 (Pn C-Si), 20.01 (^iPr CH_3), 19.87 (^iPr CH_3), 12.78 (^iPr CH).

$^{29}\text{Si}\{^1\text{H}\}$ NMR (C_6D_6 , 100.5 MHz, 303 K): δ_{Si} 0.61.

EI-MS: $m/z = 1104$ – 1111 (principal peak 1107, 100%), $[\text{M}]^+$; 1030 – 1034 (principal peak 1032, 30%), $[\text{M} - \text{Ph}]^+$.

Anal. found (calcd. for $\text{C}_{64}\text{H}_{102}\text{N}_2\text{Si}_4\text{Ti}_2$): C, 67.13 (67.12); H, 9.14 (8.99) %.

IR (NaCl): 1581 (ν aromatic C=C) cm^{-1} .

Crystal data for **6.11**. $\frac{1}{2}(\text{C}_6\text{H}_{14})$: $\text{C}_{67}\text{H}_{109}\text{N}_2\text{Si}_4\text{Ti}_2$, $M_r = 1150.72$, monoclinic, space group $C 2/c$, dark red plate, $a = 15.3653(11)$ Å, $b = 23.5936(17)$ Å, $c = 37.7380(3)$ Å, $\alpha = \gamma = 90^\circ$, $\beta = 99.890(5)^\circ$, $V = 13477.6(14)$ Å³, $T = 100$ K, $Z = 8$, $R_{\text{int}} = 0.0491$, $\lambda_{\text{Mo}}(\text{K}\alpha) = 0.71075$ Å, $\theta_{\text{max}} = 27.464^\circ$, $R_1 [I > 2\sigma(I)] = 0.0476$, wR_2 (all data) = 0.1291, $\text{Goof} = 1.018$.

6.6 References for Chapter Six

1. J. A. Ibers, *Chem. Soc. Rev.*, 1982, **11**, 57–73.
2. T. J. Katz and N. Acton, *J. Am. Chem. Soc.*, 1972, **94**, 3281–3283.
3. T. J. Katz, N. Acton, and J. McGinnis, *J. Am. Chem. Soc.*, 1972, **94**, 6205–6206.
4. M. Kuchta and F. G. N. Cloke, *Organometallics*, 1998, **17**, 1934–1936.
5. G. Balazs, F. G. N. Cloke, A. Harrison, P. B. Hitchcock, J. Green, and O. T. Summerscales, *Chem. Commun.*, 2007, 873–875.
6. G. Balazs, F. G. N. Cloke, L. Gagliardi, J. C. Green, A. Harrison, P. B. Hitchcock, A. R. M. Shahi, and O. T. Summerscales, *Organometallics*, 2008, **27**, 2013–2020.
7. A. E. Ashley, R. T. Cooper, G. G. Wildgoose, J. C. Green, and D. O'Hare, *J. Am. Chem. Soc.*, 2008, **130**, 15662–15677.
8. O. T. Summerscales, C. J. Rivers, M. J. Taylor, P. B. Hitchcock, J. C. Green, and F. G. N. Cloke, *Organometallics*, 2012, **31**, 8613–8617.

9. A. F. R. Kilpatrick, J. C. Green, F. G. N. Cloke, and N. Tsoureas, *Chem. Commun.*, 2013, 9434–9436.
10. A. F. R. Kilpatrick and F. G. N. Cloke, *Chem. Commun.*, 2014, **50**, 2769–2771.
11. H. Werner, *Coord. Chem. Rev.*, 1982, **43**, 165–185.
12. W. Reichen, *Chem. Rev.*, 1978, **78**, 569–588.
13. I. S. Butler and A. E. Fenster, *J. Organomet. Chem.*, 1974, **66**, 161–194.
14. P. V. Yaneff, *Coord. Chem. Rev.*, 1977, **23**, 183–220.
15. H. Werner, M. Ebner, W. Bertleff, and U. Schubert, *Organometallics*, 1983, **2**, 891–895.
16. K. K. Pandey, *Coord. Chem. Rev.*, 1997, **140**, 37–114.
17. M. Aresta and A. Dibenedetto, *Dalton Trans.*, 2007, 2975.
18. J. Mascetti, F. Galan, and I. Papai, *Coord. Chem. Rev.*, 1999, **190–192**, 557–576.
19. I. Castro-Rodriguez and K. Meyer, *J. Am. Chem. Soc.*, 2005, **127**, 11242–11243.
20. K. K. Pandey and H. L. Nigam, *Rev. Inorg. Chem.*, 1984, **6**, 69–94.
21. S. Gambarotta, M. L. Fiallo, and C. Floriani, *Inorg. Chem.*, 1984, **23**, 3532–3537.
22. J. G. Brennan, R. A. Andersen, and A. Zalkin, *Inorg. Chem.*, 1986, **25**, 1756–1760.
23. F. A. Cotton, *Chemical Applications of Group Theory*, Wiley, 3rd edn. 2008.
24. G. Herzberg, *Molecular Spectra and Molecular Structure. Vol. 3. Electronic Spectra and Electronic Structure of Polyatomic Molecules*, Van Nostrand-Reinhold, 1966, vol. 3.
25. P. C. Cross and L. O. Brockway, *J. Chem. Phys.*, 1935, **3**, 821.
26. I. L. Karle and J. Karle, *J. Chem. Phys.*, 1949, **17**, 1057.
27. K. Nakamoto, *Infrared and Raman Spectra of Inorganic and Coordination Compounds, Part A*, Wiley, 6 edn. 2009.
28. H. G. Alt, K.-H. Schwind, and M. D. Rausch, *J. Organomet. Chem.*, 1987, **321**, C9–C12.
29. E. Klei, J. H. Teuben, H. J. de Liefde Meijer, and E. J. Kwak, *J. Organomet. Chem.*, 1982, **224**, 327–339.
30. F. Bottomley, I. Lin, and P. S. White, *J. Organomet. Chem.*, 1981, **212**, 341–349.
31. L. C. Francesconi, D. R. Corbin, A. W. Clauss, D. N. Hendrickson, and G. D. Stucky, *Inorg. Chem.*, 1981, **20**, 2059–2069.
32. A. E. Pullen, S. Zeltner, R.-M. Olk, E. Hoyer, K. A. Abboud, and J. R. Reynolds, *Inorg. Chem.*, 1996, **35**, 4420–4426.
33. A. E. Pullen, S. Zeltner, R.-M. Olk, E. Hoyer, K. A. Abboud, and J. R. Reynolds, *Inorg. Chem.*, 1997, **36**, 4163–4171.
34. K. Kubo, A. Nakao, H. M. Yamamoto, and R. Kato, *J. Am. Chem. Soc.*, 2006, **128**, 12358–12359.
35. M. Pasquali, S. Gambarotta, C. Floriani, A. Chiesi-Villa, and C. Guastini, *Inorg. Chem.*, 1981, **20**, 165–171.
36. S. P. Green, C. Jones, and A. Stasch, *Science*, 2007, **318**, 1754–1757.
37. W. J. Evans, J. R. Walensky, J. W. Ziller, and A. L. Rheingold, *Organometallics*, 2009, **28**, 3350–3357.
38. M. Bottrill, P. D. Gavens, and J. McMeeking, in *Comprehensive Organometallic Chemistry*, eds. G. Wilkinson, F. G. A. Stone, and E. W. Abel, Pergamon Press, 1982, vol. 3.

39. P. J. Chirik and M. W. Bouwkamp, in *Comprehensive Organometallic Chemistry III*, eds. D. M. P. Mingos and R. H. Crabtree, Elsevier, Oxford, 2007, pp. 243–279.
40. M. Pasquali, C. Floriani, A. Chiesi-Villa, and C. Guastini, *J. Am. Chem. Soc.*, 1979, **101**, 4740–4742.
41. M. Pasquali, C. Floriani, A. Chiesi-Villa, and C. Guastini, *Inorg. Chem.*, 1981, **20**, 349–355.
42. M. Haehnel, M. Ruhmann, O. Theilmann, S. Roy, T. Beweries, P. Arndt, A. Spannenberg, A. Villinger, E. D. Jemmis, A. Schulz, and U. Rosenthal, *J. Am. Chem. Soc.*, 2012, **134**, 15979–15991.
43. S. Roy, E. D. Jemmis, A. Schulz, T. Beweries, and U. Rosenthal, *Angew. Chem. Int. Ed. Engl.*, 2012, **51**, 5347–5350.
44. O. Theilmann, M. Ruhmann, A. Villinger, A. Schulz, W. W. Seidel, K. Kaleta, T. Beweries, P. Arndt, and U. Rosenthal, *Angew. Chem. Int. Ed. Engl.*, 2010, **49**, 9282–9285.
45. F. A. Cotton, W. Schwotzer, and E. S. Shamshoum, *Organometallics*, 1985, **4**, 461–465.
46. F. A. Cotton and E. S. Shamshoum, *Polyhedron*, 1985, **4**, 1727–1734.
47. T. A. Budzichowski, M. H. Chisholm, K. Folting, and J. C. Huffman, *Polyhedron*, 1998, **17**, 857–867.
48. M. H. Chisholm, J. C. Gallucci, and C. B. Hollandsworth, *Polyhedron*, 2006, **25**, 827–833.
49. R. H. Cayton, S. T. Chacon, M. H. Chisholm, M. J. Hampden-Smith, J. C. Huffman, K. Folting, P. D. Ellis, and B. A. Huggins, *Angew. Chem. Int. Ed. Engl.*, 1989, **28**, 1523–1525.
50. M. H. Chisholm, F. A. Cotton, M. W. Extine, and B. R. Stults, *Inorg. Chem.*, 1977, **16**, 603–611.
51. M. H. Chisholm, F. A. Cotton, K. Folting, J. C. Huffman, A. L. Ratermann, and E. S. Shamshoum, *Inorg. Chem.*, 1984, **23**, 4423–4427.
52. P. Braunstein and D. Nobel, *Chem. Rev.*, 1989, **89**, 1927–1945.
53. G. Fachinetti, C. Biran, C. Floriani, A. Chiesi-Villa, and C. Guastini, *J. Chem. Soc., Dalton Trans.*, 1979, 792–800.
54. F. A. Cotton and E. S. Shamshoum, *J. Am. Chem. Soc.*, 1985, **107**, 4662–4667.
55. S. J. Bonyhady, S. P. Green, C. Jones, S. Nembenna, and A. Stasch, *Angew. Chem. Int. Ed. Engl.*, 2009, **48**, 2973–2977.
56. S. J. Bonyhady, C. Jones, S. Nembenna, A. Stasch, A. J. Edwards, and G. J. McIntyre, *Chem.–Eur. J.*, 2009, **16**, 938–955.
57. G. Fachinetti and C. Floriani, *J. Chem. Soc., Dalton Trans.*, 1974, 2433–2436.
58. W. A. Howard, T. M. Trnka, and G. Parkin, *Inorg. Chem.*, 1995, **34**, 5900–5909.
59. L.-C. Song, C. Han, Q.-M. Hu, and Z.-P. Zhang, *Inorg. Chim. Acta*, 2004, **357**, 2199–2204.
60. D. J. Berg, R. A. Andersen, and A. Zalkin, *Organometallics*, 1988, **7**, 1858–1863.
61. M. Wedler, A. Recknagel, J. W. Gilje, and M. Nottmeyer, *J. Organomet. Chem.*, 1992, **426**, 295–306.
62. A. Recknagel, M. Nottmeyer, D. Stalke, and U. Pieper, *J. Organomet. Chem.*, 1991, **411**, 347–356.
63. W. J. Evans, K. A. Miller, D. S. Lee, and J. W. Ziller, *Inorg. Chem.*, 2005, **44**, 4326–4332.

64. W. J. Evans, K. A. Miller, S. A. Kozimor, J. W. Ziller, A. G. DiPasquale, and A. L. Rheingold, *Organometallics*, 2007, **26**, 3568–3576.
65. W. Ren, G. Zi, and M. D. Walter, *Organometallics*, 2012, **31**, 672–679.
66. C. Floriani and G. Fachinetti, *J. Chem. Soc., Chem. Commun.*, 1972, 790.
67. M. Sato and T. Yoshida, *J. Organomet. Chem.*, 1974, **67**, 395–399.
68. H. Köpf and T. Klapötke, *J. Chem. Soc., Chem. Commun.*, 1986, 1192.
69. V. Christou and J. Arnold, *J. Am. Chem. Soc.*, 1992, **114**, 6240–6242.
70. V. Christou, S. P. Wuller, and J. Arnold, *J. Am. Chem. Soc.*, 1993, **115**, 10545–10552.
71. A. L. Hector, W. Levason, G. Reid, S. D. Reid, and M. Webster, *Chem. Mater.*, 2008, **20**, 5100–5106.
72. E. Morosan, H. W. Zandbergen, B. S. Dennis, J. W. G. Bos, Y. Onose, T. Klimczuk, A. P. Ramirez, N. P. Ong, and R. J. Cava, *Nat. Phys.*, 2006, **2**, 544–550.
73. J. Rasch, T. Stemmler, B. Müller, L. Dudy, and R. Manzke, *Phys. Rev. Lett.*, 2008, **101**, 237602.
74. T. Li, Y.-H. Liu, S. Porter, and J. E. Goldberger, *Chem. Mater.*, 2013, **25**, 1477–1479.
75. M. Chhowalla, H. S. Shin, G. Eda, L. J. Li, and K. P. Loh, *Nat. Chem.*, 2013, **5**, 263–275.
76. S. L. Benjamin, C. H. K. de Groot, C. Gurnani, A. L. Hector, R. Huang, K. Ignatyev, W. Levason, S. J. Pearce, F. Thomas, and G. Reid, *Chem. Mater.*, 2013, **25**, 4719–4724.
77. R. E. Dessy, P. M. Weissman, and R. L. Pohl, *J. Am. Chem. Soc.*, 1966, **88**, 5117–5121.
78. Y. Lifman and M. Albeck, *Electrochim. Acta*, 1984, **29**, 95–98.
79. J. Ludvík and B. Nygård, *Electrochim. Acta*, 1996, **41**, 1661–1665.
80. D. Sutton, *Chem. Rev.*, 1993, **93**, 995–1022.
81. G. Fachinetti, G. Fochi, and C. Floriani, *J. Organomet. Chem.*, 1973, **57**, C51–C54.
82. J. Bart, I. W. Bassi, G. F. Cerruti, and M. Calcaterra, *Gazz. Chim. Ital.*, 1980, **110**, 423–442.
83. G. Fochi, C. Floriani, J. Bart, and G. Giunchi, *J. Chem. Soc., Dalton Trans.*, 1983, 1515–1521.
84. O. Theilmann, W. Saak, D. Haase, and R. Beckhaus, *Organometallics*, 2009, **28**, 2799–2807.
85. S. Gambarotta, C. Floriani, A. Chiesi-Villa, and C. Guastini, *J. Am. Chem. Soc.*, 1983, **105**, 7295–7301.
86. J. E. Hill, R. D. Profilet, P. E. Fanwick, and I. P. Rothwell, *Angew. Chem. Int. Ed. Engl.*, 1990, **29**, 664–665.
87. J. E. Hill, P. E. Fanwick, and I. P. Rothwell, *Inorg. Chem.*, 1991, **30**, 1143–1144.
88. R. Duchateau, A. J. Williams, S. Gambarotta, and M. Y. Chiang, *Inorg. Chem.*, 1991, **30**, 4863–4866.
89. S. D. Gray, J. L. Thorman, L. M. Berreau, and L. K. Woo, *Inorg. Chem.*, 1997, **36**, 278–283.
90. S. D. Gray, J. L. Thorman, V. A. Adamian, K. M. Kadish, and L. K. Woo, *Inorg. Chem.*, 1998, **37**, 1–4.
91. F. G. Thomas and K. G. Boto, in *The Chemistry of the Hydrazo, Azo and Azoxy Groups*, ed. S. Patai, Wiley, 1975.

92. N. G. Connelly and W. E. Geiger, *Chem. Rev.*, 1996, **96**, 877–910.
93. P. Pykkö and M. Atsumi, *Chem.–Eur. J.*, 2009, **15**, 186–197.
94. J. C. Green, A. F. R. Kilpatrick, and F. G. N. Cloke, *Manuscript in progress*.
95. P. Haack, C. Limberg, T. Tietz, and R. Metzinger, *Chem. Commun.*, 2011, **47**, 6374–6376.
96. J. H. D. Eland and J. Berkowitz, *J. Chem. Phys.*, 1979, **70**, 5151.
97. J. D. Cox, D. D. Wagman, and V. A. Medvedev, *CODATA Key Values for Thermodynamics*, Hemisphere, New York, 1989.
98. D. R. Lide, Ed., *CRC Handbook of Chemistry and Physics*, CRC press, 80 edn. 1999.
99. J. Pinkas, I. Císařová, M. Horáček, J. Kubišta, and K. Mach, *Organometallics*, 2011, **30**, 1034–1045.
100. P. Pykkö and M. Atsumi, *Chem.–Eur. J.*, 2009, **15**, 12770–12779.
101. C. Romain, L. Brelot, S. Bellemin-Laponnaz, and S. Dagorne, *Organometallics*, 2010, **29**, 1191–1198.
102. J. Li, C. Schulzke, S. Merkel, H. W. Roesky, P. P. Samuel, A. Döring, and D. Stalke, *Z. Anorg. Allg. Chem.*, 2010, **636**, 511–514.
103. R. Baumann, R. Stumpf, W. M. Davis, L.-C. Liang, and R. R. Schrock, *J. Am. Chem. Soc.*, 1999, **121**, 7822–7836.
104. R. R. Schrock, *Chem. Rev.*, 2002, **102**, 145–179.
105. D. J. Mindiola, B. C. Bailey, and F. Basuli, *Eur. J. Inorg. Chem.*, 2006, **2006**, 3135–3146.
106. D. Adhikari, F. Basuli, J. H. Orlando, X. Gao, J. C. Huffman, M. Pink, and D. J. Mindiola, *Organometallics*, 2009, **28**, 4115–4125.
107. J. W. Park, P. B. Mackenzie, W. P. Schaefer, and R. H. Grubbs, *J. Am. Chem. Soc.*, 1986, **108**, 6402–6404.
108. F. Ozawa, J. W. Park, P. B. Mackenzie, W. P. Schaefer, L. M. Henling, and R. H. Grubbs, *J. Am. Chem. Soc.*, 1989, **111**, 1319–1327.
109. C. Krüger, R. Mynott, C. Siedenbiedel, L. Stehling, and G. Wilke, *Angew. Chem. Int. Ed. Engl.*, 1991, **30**, 1668–1670.
110. L. Scoles, R. Minhas, R. Duchateau, J. Jubbe, and S. Gambarotta, *Organometallics*, 1994, **13**, 4978–4983.
111. P. N. Riley, P. E. Fanwick, and I. P. Rothwell, *J. Chem. Soc., Dalton Trans.*, 2001, 181–186.
112. R. Thompson, E. Nakamaru-Ogiso, C.-H. Chen, M. Pink, and D. J. Mindiola, *Organometallics*, 2014, **33**, 429–432.
113. F. N. Tebbe, G. W. Parshall, and G. S. Reddy, *J. Am. Chem. Soc.*, 1978, **100**, 3611–3613.
114. F. N. Tebbe, G. W. Parshall, and D. W. Ovenall, *J. Am. Chem. Soc.*, 1979, **101**, 5074–5075.
115. T. R. Howard, J. B. Lee, and R. H. Grubbs, *J. Am. Chem. Soc.*, 1980, **102**, 6876–6878.
116. W. W. Lukens, M. R. Smith, and R. A. Andersen, *J. Am. Chem. Soc.*, 1996, **118**, 1719–1728.
117. E. Brady, J. R. Telford, G. Mitchell, and W. Lukens, *Acta Crystallogr., Sect. C: Cryst. Struct. Commun.*, 1995, **51**, 558–560.
118. J. Feldman and J. C. Calabrese, *J. Chem. Soc., Chem. Commun.*, 1991, 1042–1044.
119. E. J. M. De Boer and J. H. Teuben, *J. Organomet. Chem.*, 1979, **166**, 193–198.
120. A. T. Vincent and P. J. Wheatley, *J. Chem. Soc., Perkin Trans. 2*, 1972, 687.

121. W. Darwish, E. Seikel, R. Käsmarker, K. Harms, and J. Sundermeyer, *Dalton Trans.*, 2011, **40**, 1787–1794.
122. F. H. Allen, O. Kennard, D. G. Watson, and L. Brammer, *J. Chem. Soc., Perkin Trans. 2*, 1987, S1–S19.
123. W. J. Evans, C. H. Fujimoto, and J. W. Ziller, *Organometallics*, 2001, **20**, 4529–4536.
124. C. Zhang, R. Liu, J. Zhang, Z. Chen, and X. Zhou, *Inorg. Chem.*, 2006, **45**, 5867–5877.
125. S. Patai, *Chemistry of Cyanates and Their Thio Derivatives*, J. Wiley, 1977.
126. T. M. Klapötke, *Phosphorus, Sulfur Silicon Relat. Elem.*, 1989, **41**, 105–111.
127. C. P. Gerlach, V. Christou, and J. Arnold, *Inorg. Chem.*, 1996, **35**, 2758–2766.
128. D. E. Gindelberger and J. Arnold, *Organometallics*, 1994, **13**, 4462–4468.
129. D. W. Stephan and T. T. Nadasdi, *Coord. Chem. Rev.*, 1996, **147**, 147–208.
130. C. C. Cummins, C. P. Schaller, G. D. Van Duyne, P. T. Wolczanski, A. W. E. Chan, and R. Hoffmann, *J. Am. Chem. Soc.*, 1991, **113**, 2985–2994.
131. J. M. Fischer, W. E. Piers, L. R. Macgillivray, and M. J. Zaworotko, *Inorg. Chem.*, 1995, **34**, 2499–2500.
132. M. Green, *J. Organomet. Chem.*, 1995, **500**, 127–148.
133. W. J. Grigsby, M. M. Olmstead, and P. P. Power, *J. Organomet. Chem.*, 1996, **513**, 173–180.
134. S. C. Dunn, N. Hazari, A. R. Cowley, J. C. Green, and P. Mountford, *Organometallics*, 2006, **25**, 1755–1770.
135. D. L. Thorn, W. A. Nugent, and R. L. Harlow, *J. Am. Chem. Soc.*, 1981, **103**, 357–363.
136. S. M. Mullins, A. P. Duncan, R. G. Bergman, and J. Arnold, *Inorg. Chem.*, 2001, **40**, 6952–6963.
137. T. E. Hanna, I. Keresztes, E. Lobkovsky, W. H. Bernskoetter, and P. J. Chirik, *Organometallics*, 2004, **23**, 3448–3458.
138. J. G. Brennan and R. A. Andersen, *J. Am. Chem. Soc.*, 1985, **107**, 514–516.
139. A. Zalkin, J. G. Brennan, and R. A. Andersen, *Acta Crystallogr., Sect. C: Cryst. Struct. Commun.*, 1988, **44**, 1553–1554.
140. P. Roussel, R. Boaretto, A. J. Kingsley, N. W. Alcock, and P. Scott, *J. Chem. Soc., Dalton Trans.*, 2002, 1423–1428.
141. I. Castro-Rodriguez, K. Olsen, P. Gantzel, and K. Meyer, *J. Am. Chem. Soc.*, 2003, **125**, 4565–4571.
142. S. Cenini and G. La Monica, *Inorg. Chim. Acta*, 1976, **18**, 279–293.
143. W. A. Nugent and J. M. Mayer, *Metal-Ligand Multiple Bonds*, Wiley, New York, 1988.
144. H. M. Hoyt, F. E. Michael, and R. G. Bergman, *J. Am. Chem. Soc.*, 2004, **126**, 1018–1019.

APPENDIX ONE: EXPERIMENTAL DETAILS

A1.1 General Procedures

The manipulation of air-sensitive compounds and their spectroscopic measurements were undertaken using standard Schlenk techniques¹ under Ar (pureshield) passed through a column containing BASF R3-11(G) catalyst and activated molecular sieves (4 Å), or in a MBraun glovebox under N₂ or Ar (O₂ and H₂O <1 ppm). Nitrogen and argon gases were supplied by BOC Gases UK. All glassware was dried at 160 °C overnight prior to use. Celite was predried in a 200 °C oven and then flame-dried under dynamic vacuum ($<2 \times 10^{-2}$ mbar) prior to use. Filter cannulae equipped with Whatman 25 mm glass microfibre filters were dried in an oven at 160 °C prior to use.

A1.2 Purification of Solvents

Solvents were purified by pre-drying for a minimum of 72 h over sodium wire before refluxing over the appropriate drying agents: Na-K alloy (pentane, Et₂O, petroleum ether 40:60, SiMe₄), K (THF, 1,4-dioxane, methylcyclohexane, hexane, pyridine, *t*-BuOMe), Na (toluene, DME, (Me₃Si)₂O, TMEDA) or CaH₂ (CH₂Cl₂, 1,2-difluorobenzene, PhCF₃, MeCN) under a N₂ atmosphere. Dried solvents were collected, degassed and stored over argon in potassium-mirrored ampoules, except THF, Et₂O, DME, CH₂Cl₂, TMEDA and pyridine, which were stored in ampoules containing activated 4 Å molecular sieves. 1,2-difluorobenzene, PhCF₃ and MeCN were stored in ampoules containing activated 3 Å molecular sieves. All were degassed prior to use.

Deuterated NMR solvents (C₆D₆, toluene-*d*₈, THF-*d*₈, methylcyclohexane-*d*₁₄, pyridine-*d*₅, cyclohexane-*d*₁₄) were obtained from Aldrich and were degassed by three freeze-thaw cycles, dried by refluxing over K for 3 days, vacuum distilled into ampoules and stored under N₂.

A1.3 Instrumentation

A1.3.1 NMR spectroscopy

NMR spectra were measured by the author using Varian VNMRs 400 and 500 MHz spectrometers. The spectra were referenced internally to the residual protic solvent (¹H) or the signals of the solvent (¹³C). ¹¹B, ¹⁹F, ⁷⁷Se, ²⁹Si, ¹²⁵Te, ¹⁷¹Yb NMR spectra were

referenced externally relative to $\text{BF}_3\cdot\text{OEt}_2$, CFCl_3 (10%), Me_2Se , SiMe_4 , Me_2Te (90%), and YbCp^*_2 (in 10% THF/ C_6D_6) respectively.

A1.3.2 EPR spectroscopy

EPR spectroscopy was carried out by Dr S. Sproules and D. Sells from the EPSRC National UK EPR Facility and Service at the University of Manchester. X- and Q-band continuous wave EPR spectra measurements were performed using a Bruker E580 ELEXSYS spectrometer and simulated with the XSophe² suite.

A1.3.3 IR spectroscopy

IR spectra were recorded on a Perkin-Elmer 1600 Fourier Transform spectrometer. Samples were prepared in a glove box as thin films between NaCl plates. *In situ* IR spectroscopy was recorded on a Mettler Toledo ReactIR system, featuring an IR probe inside a gas tight cell attached to a Toepler pump. Background spectra of degassed methycyclohexane solutions of the starting material at $-65\text{ }^\circ\text{C}$ were acquired prior gas addition, allowing the growth of product IR bands to be readily identified. Spectra were acquired every 5 s with a resolution of 4 cm^{-1} .

A1.3.4 Mass spectrometry

Mass spectra were recorded by Dr A. Abdul-Sada at the University of Sussex using a VG Autospec Fisons instrument (electron ionisation at 70 eV).

A1.3.5 Elemental analysis

Elemental analyses for all compounds were carried out by S. Boyer at the Elemental Analysis Service, London Metropolitan University. Additional elemental analyses for compound **4.1** were carried out at the Mikroanalytisches Labor Pascher to determine the chloride percentage in the crude solid. Additional elemental analyses for compounds **2.2**, **2.3**, **4.1** and **4.2** were carried out at the analytical laboratories of the Friedrich-Alexander-University (FAU) Erlangen-Nürnberg on Euro EA 3000, prior to SQUID magnetometry measurements.

A1.3.6 *Magnetic measurements*

Magnetic measurements of polycrystalline samples of **2.2**, **2.3**, **4.1** and **4.2** were carried out by the author (with the assistance of A. C. Schmidt) at FAU Erlangen, using a Quantum Design MPMS-5 SQUID magnetometer at different fields (0.1 - 5 Tesla) and different temperatures (2 - 300 K). Accurately weighed samples (*ca.* 30 mg) were placed into gelatine capsules and then loaded into nonmagnetic plastic straws before being lowered into the cryostat. Samples used for magnetisation measurement were recrystallised multiple times and checked for chemical composition and purity by elemental analysis (**2.2**, **2.3**, **4.2**) and ^1H NMR spectroscopy (**2.3**). Data reproducibility was carefully checked on two independently synthesised and measured samples.

Magnetic measurements of **2.6** were carried out by Dr F. Tuna at the University of Manchester using a Quantum Design MPMS-7 SQUID magnetometer at temperatures in the range 1.8 - 300 K. The polycrystalline samples were transferred to Kel-F capsules in an N_2 glovebox, which were then sealed with an O-ring cap, and the capsules were then placed in plastic straws. One end of the straw was then sealed with a cap, and the other end was sealed with Blu-Tac. The straw was then sealed in a Schlenk tube and taken to the magnetometer. The straw was removed from the Schlenk tube and the Blu-Tac quickly replaced with the carbon fibre rod, and then the sample was quickly transferred to the purged sample space of the cryostat. Values of the magnetic susceptibility were corrected for the underlying diamagnetic increment by using tabulated Pascal constants,³ and the effect of the blank sample holders (gelatin capsule/straw). Analysis of the in-phase and out-of-phase magnetic susceptibility data for **2.6** was carried out by Dr T. Pugh at the University of Manchester using the CCFIT software program by N. F. Chilton.⁴

Solution phase magnetic susceptibility were determined using the Evans method, and measured on the Varian VNMRS 400 MHz spectrometer. Samples were allowed 15 min to thermally equilibrate at the given probe temperature which was calibrated with a methanol thermometer. The solvent density at the given temperature was factored in to the magnetic susceptibility calculation.^{5,6}

A1.3.7 Cyclic voltammetry

Cyclic voltammetry studies were carried out by the author using a BASi Epsilon-EC potentiostat under computer control. iR drop was compensated by the feedback method. CV experiments were performed in an Ar glovebox using a three-electrode configuration with a Au disc (2.0 mm²) or glassy carbon disc (7.0 mm²) as the working electrode, a Pt wire as the counter electrode and a Ag wire as the pseudoreference electrode. Sample solutions were prepared by dissolving the analyte (*ca.* 5 mM) in THF (1.0 cm³) followed by addition of a supporting electrolyte [ⁿBu₄N][B(C₆F₅)] or [ⁿBu₄N][PF₆]. The reported mid-peak potentials are referenced internally to that of the FeCp₂⁺⁰ redox couple, which was measured by adding ferrocene (*ca.* 1 mg) to the sample solution.

A1.3.8 X-ray crystallography

Single crystal XRD data for **2.3**, **3.2**, **4.1**, **4.2**, **4.3**, **4.4**, **4.5**, **5.1**, **5.2**, **5.4**, **5.5**, **5.9**, **6.4**, **6.5**, **6.7**, **6.8**, **6.9** and **6.11** were collected by the UK National Crystallography Service (NCS),⁷ at the University of Southampton on a Rigaku FR-E+ Ultra High Flux diffractometer ($\lambda_{\text{Mo(K}\alpha)}$) equipped with VariMax VHF optics and a Saturn 724+ CCD area detector. The data were collected at 100 or 150 K using an Oxford Cryosystems Cobra low temperature device. An empirical absorption correction was carried out using the MULTI-SCAN program.^{8,9} Single crystal XRD data for **6.6** were collected by the NCS at the Diamond Light Source using synchrotron radiation ($\lambda_{\text{Mo(K}\alpha)}$). An empirical absorption correction was carried out using the 'DTABSCOR' program. Data collected by the NCS were processed using CrystalClear-SM Expert 3.1 b18,¹⁰ and unit cell parameters were refined against all data. Single crystal XRD data for **2.1**, **2.2**, **2.4**, **2.5**, **2.6**, **2.7**, **2.8**, **3.1**, **3.3**, **3.4**, **3.5**, **3.6**, **4.7**, **5.6**, **5.8**, **6.1**, **6.8** and **6.10** were collected at the University of Sussex on a Enraf-Nonius CAD4 diffractometer with graphite-monochromated ($\lambda_{\text{Mo(K}\alpha)}$) radiation or an Agilent Technologies Xcalibur Gemini ultra diffractometer ($\lambda_{\text{Mo(K}\alpha)}$ or $\lambda_{\text{Cu(K}\alpha)}$ source) equipped with a Eos CCD area detector. The data were collected at 173 K using an Oxford Cryosystems Cobra low temperature device. Data were processed using KappaCCD software or CrysAlisPro (version 1.171.36.32),¹¹ and unit cell parameters were refined against all data. An empirical absorption correction was carried out using the MULTI-SCAN program.^{8,9}

Structures **2.2**, **2.3**, **2.4**, **2.5**, **2.6**, **2.7**, **2.8**, **4.2**, **4.4**, **4.5**, **4.7**, **5.1**, **5.2**, **5.4**, **5.5**, **5.6**, **5.8**, **5.9**, **6.1**, **6.4**, **6.5**, **6.6**, **6.7**, **6.8**, **6.9**, **6.10** and **6.11** were solved by the author, with Drs S. M. Roe, N. Tsoureas and B. M. Day gratefully acknowledged for their patience, advice and assistance with crystallography. Structures **2.3**, **3.1** and **3.2** were solved by Dr M. P. Coles. Structures **2.1**, **3.3**, **3.4**, **3.5**, **3.6** and **4.3** were solved by Dr N. Tsoureas. All structures were solved using SHELXL-2013,¹² DIRDIF-2008¹³ or SUPERFLIP¹⁴ and refined on F_o^2 by full-matrix least-squares refinements using SHELXL-2013.¹² Solutions and refinements were performed using the OLEX2¹⁵ or WinGX¹⁶ packages and software packages within. All non-hydrogen atoms were refined with anisotropic displacement parameters except **2.7** where the carbon atoms of a disordered Cp* ligand were left isotropic. All hydrogen atoms were refined using a riding model. Disordered solvent molecules in **5.6**, **6.1**, **6.4**, **6.5**, **6.8**, **6.9** and **6.10** could not be modelled properly; therefore, this disorder was treated by using the SQUEEZE¹⁷ routine in PLATON.¹⁸ Disordered solvent molecules in **6.4** were treated using the "solvent mask" routine in OLEX2,¹⁵ which resulted in improved refinement indices relative to SQUEEZE so these data have also been included in appendix A2.

A1.3.9 DFT calculations

Density functional calculations were carried out by Prof J. C. Green at the University of Oxford using two computational methods. One employed the Amsterdam Density Functional package (version ADF2012.01).¹⁹ The Slater-type orbital (STO) basis sets were of triple- ζ quality augmented with a one polarization function (ADF basis TZP). Core electrons were frozen (C 1s; Ti 2p) in the model of the electronic configuration for each atom. The local density approximation (LDA) by Vosko, Wilk and Nusair (VWN)²⁰ was used together with the exchange correlation corrections of Becke and Perdew (BP86).^{21,22} The other used Gaussian (version 09 revision A.02)²³ with the B3LYP functional and SDD basis sets. In both sets of calculations tight optimisation conditions were used and frequency calculations were used to confirm stationary points. Using the ADF code, molecules were subjected to fragment analyses where the MOs of fragments, with the same geometry as they possess in the molecules, were used as the basis set for a full molecular calculation.

A1.4 Commercially Supplied Reagents

The following materials were purchased from Aldrich and used as received: 1,3-*N,N'*-di-*p*-tolylcarbodiimide, azidobenzene (0.5 M solution in Me-THF), [FeCp₂][BF₄], [ⁿBu₄N][PF₆] (electrochemical grade), SiⁱPrOTf, SmI₂(THF)₂ (*ca.* 0.1 M solution in THF), C₃H₅MgCl (2.0 M solution in THF). The following materials were purchased from Aldrich and purified or dried prior to use,²⁴ and stored under an inert atmosphere: CS₂, Fe(acac)₂, PhNCO, Ph₃PS. Potassium metal was purchased as lumps from Fischer Scientific, which were washed with hexane and taken into an Ar glovebox and the oxide layer carefully removed with a scalpel. COT was purchased from Alfa, stored in the dark over 4 Å molecular sieves, and vacuum transferred prior to use. Solutions of ⁿBuLi (*ca.* 2.5 M in hexanes) were supplied by Acros Organics and titrated to determine the exact molarity. Isocyanides MeNC and ^tBuNC were kindly donated by colleagues and were stored over 4 Å sieves and degassed before use. The gases used were of very high purity - CO (99.999%) and CO₂ (99.99%) - supplied by Union Carbide, and used in combination with a high-purity regulator. N₂O (puriss >99.998%) was supplied by Fluka and added *via* Toepler line. Isotopically enriched gases ¹³CO (99.7%) and ¹³CO₂ (99%) were supplied by Euriso-top and Cambridge Isotopes respectively, and added *via* Toepler line. Reagents KC₈, Bu₂Mg, Hg, KH, [ⁿBu₄N][B(C₆F₅)], Cp*₂UCl₂, [K]₂COT[†], [FeCp*₂][B(C₆F₅)], YbI₂, YbI₃, EuI₂, YCl₃, ScCl₃ were kindly donated by F. G. N. Cloke and co-workers. The reagents COS (97% Aldrich), Ph₂S₂, Ph₂Se₂, Ph₂Te₂ (Acros) and azobenzene (Aldrich) were kindly donated by Prof K. Meyer during the author's "Short Term Scientific Mission" to FAU Erlangen-Nürnberg in February 2014, funded by COST Action.

A1.5 Synthesis of Starting Materials

KCp*,²⁵ NaCp*,²⁵ [Et₃NH][BPh₄],²⁶ Cp*₂Yb(OEt₂)₂,²⁷ Cp*₂Sm(THF)₂,²⁸ Cp*₂Sm,²⁹ Cp*₂Yb, Cp*₂Eu,²⁹ Cp*Sm(BPh₄), Cp*Yb(BPh₄),³⁰ Cp*Eu(BPh₄),³¹ Cp*₂UMe₂,³² Cp*₂U(BPh₄),³³ KNH₂, [Li(DME)_x]Pn, Pn[†]H₂, [K]₂Pn[†],³⁴ [K]Pn[†]H,³⁵ Cp*FeCl(TMEDA),³⁶ KBn,³⁷ [Cp*Ln(μ-I){THF}₂]₂ (Ln = Yb, Sm),³⁸ (Pn[†])₂V₂,³⁹ TiCl₃(THF)₃,⁴⁰ UI₃,⁴¹ and TlI₃⁴² were synthesised according to published procedures. DyCl₃ was prepared by dehydration of DyCl₃·6H₂O with excess Me₃SiCl in refluxing heptane over 3 d. FeCl₂(THF)_x⁴³ was sent for elemental analysis to determine the amount of coordinated THF, and the data obtained best fit to a value of *x* = 1.1.

A1.6 References for Appendix One

1. D. F. Shriver, *The Manipulation of Air-Sensitive Compounds*, Wiley-Interscience, 2nd edn. 1986.
2. G. R. Hanson, K. E. Gates, C. J. Noble, M. Griffin, A. Mitchell, and S. Benson, *J. Inorg. Biochem.*, 2004, **98**, 903–916.
3. G. A. Bain and J. F. Berry, *J. Chem. Educ.*, 2008, **85**, 532.
4. N. F. Chilton, *CCFIT*.
5. E. W. Washburn, *International Critical Tables*, McGraw-Hill, New York, 1929, vol. 3.
6. D. Ostfeld and I. A. Cohen, *J. Chem. Educ.*, 1972, **49**, 829.
7. S. J. Coles and P. A. Gale, *Chem. Sci.*, 2012, **3**, 683–689.
8. R. H. Blessing and D. A. Langs, *J. Appl. Crystallogr.*, 1987, **20**, 427–428.
9. R. H. Blessing, *Acta Crystallogr., A, Found. Crystallogr.*, 1995, **51**, 33–38.
10. Rigaku, *CrystalClear*, 2011.
11. Agilent Technologies, *CrysAlisPro 1.171.36.32*, 2011.
12. G. M. Sheldrick, *Acta Crystallogr., A, Found. Crystallogr.*, 2008, **64**, 112–122.
13. P. T. Beurskens, G. Beurskens, R. Gelder, J. M. M. Smits, S. Garcia-Granda, and R. O. Gould, 2008.
14. L. Palatinus and G. Chapuis, *J. Appl. Crystallogr.*, 2007, **40**, 786–790.
15. O. V. Dolomanov, L. J. Bourhis, R. J. Gildea, J. A. K. Howard, and H. Puschmann, *J. Appl. Crystallogr.*, 2009, **42**, 339–341.
16. L. J. Farrugia, *J. Appl. Crystallogr.*, 1999, **32**, 837–838.
17. P. van der Sluis and A. L. Spek, *Acta Crystallogr., A, Found. Crystallogr.*, 1990, **46**, 194–201.
18. A. L. Spek, *J. Appl. Crystallogr.*, 2003, **36**, 7–13.
19. SCM, *Amsterdam Density Functional, ADF*, 2006.
20. S. H. Vosko, L. Wilk, and M. Nusair, *Can. J. Phys.*, 1980.
21. A. Becke, *Phys. Rev., A*, 1988, **38**, 3098–3100.
22. J. P. Perdew, *Phys. Rev. B*, 1986, **33**, 8800.
23. M. Frisch, G. W. Trucks, H. B. Schlegel, G. E. Scuseria, M. A. Robb, J. R. Cheeseman, G. Scalmani, V. Barone, B. Mennucci, G. A. Petersson, others, *Inc., Wallingford, CT*, 2009, 270, 271.
24. D. Perrin and W. Armarego, *Purification of Laboratory Chemicals*, Pergamon Press, 1988.
25. G. Rabe, H. W. Roesky, D. Stalke, F. Pauer, and G. M. Sheldrick, *J. Organomet. Chem.*, 1991, **403**, 11–19.
26. N. M. Kuuloja, T. M. Kylvälä, J. E. Tois, R. E. Sjöholm, and R. G. Franzén, *Synth. Commun.*, 2011, **41**, 1052–1063.
27. T. D. Tilley, J. M. Boncella, D. J. Berg, C. J. Burns, and R. A. Andersen, *Inorg. Synth.*, 1990, **27**, 146.
28. W. J. Evans, L. A. Hughes, and T. P. Hanusa, *J. Am. Chem. Soc.*, 1984, **106**, 4270–4272.
29. W. J. Evans, L. A. Hughes, and T. P. Hanusa, *Organometallics*, 1986, **5**, 1285–1291.
30. W. J. Evans, T. M. Champagne, and J. W. Ziller, *Organometallics*, 2007, **26**, 1204–1211.
31. W. J. Evans, J. R. Walensky, F. Furche, A. G. DiPasquale, and A. L. Rheingold, *Organometallics*, 2009, **28**, 6073–6078.
32. P. J. Fagan, J. M. Manriquez, E. A. Maatta, A. M. Seyam, and T. J. Marks, *J. Am.*

- Chem. Soc.*, 1981, **103**, 6650–6667.
33. W. J. Evans, G. W. Nyce, K. J. Forrestal, and J. W. Ziller, *Organometallics*, 2002, **21**, 1050–1055.
 34. F. G. N. Cloke, M. C. Kuchta, R. M. Harker, P. B. Hitchcock, and J. S. Parry, *Organometallics*, 2000, **19**, 5795–5798.
 35. O. T. Summerscales and F. G. N. Cloke, *Coord. Chem. Rev.*, 2006, **250**, 1122–1140.
 36. K. Jonas, P. Klusmann, and R. Goddard, *Z. Naturforsch. B*, 1995, **50**, 394–404.
 37. M. Schlosser and J. R. Hartmann, *Angew. Chem. Int. Ed. Engl.*, 1973, **12**, 508–509.
 38. W. J. Evans, J. W. Grate, H. W. Choi, I. Bloom, W. E. Hunter, and J. L. Atwood, *J. Am. Chem. Soc.*, 1985, **107**, 941–946.
 39. A. D. Smith, M.Chem. Dissertation, University of Sussex, 2012.
 40. L. E. Manzer, *Inorg. Synth.*, 1982, **21**, 135.
 41. F. G. N. Cloke and P. B. Hitchcock, *J. Am. Chem. Soc.*, 2002, **124**, 9352–9353.
 42. J. D. Corbett, *Inorg. Synth.*, 1983, **22**, 31.
 43. P. Kovacic and N. O. Brace, *J. Am. Chem. Soc.*, 1954, **76**, 5491–5494.